Addis Ababa University

Research and Graduate Programs

Department of Chemistry

Preparation, Characterization and Application of Chemically Modified Glassy Carbon Electrodes for Square Wave Voltammetric Determination of Selected Pharmaceutical Drugs

By

Birhanu Mekassa Wolde

Supervisors: Dr. Merid Tessema

Prof. B. S. Chandravanshi

May, 2018

Abstract

In this thesis, various types of simple, scalable and low cost chemically modified electrodes were successfully developed for the sensitive and selective determination of some commonly and widely used pharmaceutical drugs. First, a simple and fast modification of conventional bare glassy carbon electrode (GCE) with poly(L-aspartic acid) was performed by electropolymerization of L-aspartic acid (L-Asp) using cyclic voltammetry for the determination of ibuprofen (IBP). The poly(L-Asp)/GCE was characterized by cyclic voltammetry (CV), electrochemical impedance spectroscopy (EIS) and electroactive surface area (ESA) measurements. The cyclic voltammetric and square wave voltammetric study of IBP in 0.25 M acetate buffer solution (ABS) at pH 4 showed an obvious electrocatalytic effect towards IBP oxidation, which resulted in a higher current response and a negative shift in the peak potential at the polymer film modified electrode compared to the bare GCE. Under the optimized conditions, a linear calibration curve was obtained using square wave voltammetry (SWV) at the poly(L-Asp)/GCE in the range of 1 to 150 µM with a limit of detection (LOD, $3S_b/m$) and a limit of quantification (LOQ, $10S_b/m$) of 0.22 and 0.74 µM, respectively. Next, a poly(L-aspartic acid)/functionalized multi-walled carbon nanotubes composite modified glassy carbon electrode, P(L-Asp)/f-MWCNTs/GCE, was prepared for the simultaneous determination of caffeine (CF) and theophylline (TP) using SWV. The electrode preserves and combines the properties of the individual modifiers synergistically. A significant enhancement in the peak current response of CF and TP were observed accompanied with a negative shift in peak potentials at the composite modified electrode compared to the bare electrode. The prepared electrode exhibited excellent SWV responses towards the simultaneous determination of CF and TP in the range of 1–150 and 0.1–50 µM with a limit of detection of 0.28 and 0.02 µM, respectively. Similarly, a sensitive poly(L-aspartic acid)/electrochemically reduced graphene oxide modified GCE, P(L-Asp)/ERGO/GCE, was developed for epinephrine (EP) determination by electrochemical reduction of GO drop coated on GCE in 2 mM L-aspartic acid by CV in pH 6 phosphate buffer solution (PBS) which gives rise to in situ polymerization of L-aspartic acid on the electrochemically reduced graphene oxide. Raman, FTIR and UV spectroscopies were used to characterize GO, ERGO, P(L-Asp) and P(L-Asp)/ERGO composite. The electrochemical response of P(L-Asp)/ERGO/GCE towards EP determination was characterized by EIS, CV and

ESA measurements. The CV results showed a significant enhancement in the peak current response accompanied with a negative shift in the peak potential for EP at the composite modified electrode. The prepared P(L-Asp)/ERGO/GCE exhibited excellent SWV response towards EP determination in the range of 0.1–110 µM with LOD and LOQ of 0.025 and 0.083 µM, respectively. The method was further validated by UV assay and the obtained results confirmed the applicability of the developed method for routine analysis. Lastly, a new GCE modified with electrochemically reduced graphene oxide decorated with nickel nanoparticles (NiNPs/ERGO/GCE) was developed by electrodeposition. TEM, SEM, EDS, SAED, EIS, CV and SWV were used for the characterization of the synthesized GO, NiNPs and the prepared novel platform, NiNPs/ERGO/GCE. The as prepared platform was used for the determination of diclofenac (DIC) and ethambutol (ETB). A significant enhancement in the peak current response for DIC and ETB was observed at the composite modified electrode compared to the unmodified electrode. The composite modified electrode demonstrated excellent SWV response towards the determination of both DIC and ETB in the working range of 0.25–125 µM and 0.05–100 µM with LOD of 0.09 and 0.023, respectively. Generally, all the developed sensors were validated successfully for real sample analysis in pharmaceutical formulation and human urine samples with good recovery results. The proposed sensors also displayed good repeatability, reproducibility, long-term stability and selectivity towards potential interferents and are promising materials for electrochemical sensing of similar drugs and biologically active compounds in real samples.

Acknowledgments

First and foremost I would like to thank and praise the almighty God for giving me the strength and endurance throughout my PhD study to carry out my work. I bow my head in reverence before Him for blessing my life in all my activities.

I would like to express my deepest and sincere gratitude to my supervisors, Dr. Merid Tessema and Prof. B. S. Chandravanshi for their unreserved and continuous encouragement, excellent guidance, advice, invaluable suggestions and discussions throughout this endeavor, which nurtured a lot of confidence in me. Their support in providing and facilitating the necessary materials for my research work were tremendous. I also thank them immensely for their critical comments during the courses, seminars, manuscript preparations and thesis write-up. I was privileged to enjoy their fatherly consultation, warm approach and treatment throughout my study.

My appreciation goes to Prof. Priscilla Baker for hosting and supervising me in her lab as an exchange student and providing all the chemicals, apparatus and instrumentation required. I was lucky enough to spend some time at the Sensor Lab, Department of Chemistry, University of the Western Cape, South Africa. I am very grateful for her cooperation and invaluable guidance during my stay. I am also thankful to Sensor lab staff members and all PhD and MSc students.

I am highly indebted to Dr. Ahmed Mustefa for his special treatment, continuous motivation and encouragement starting from the write up of the proposal. I am also thankful to Dr. Ahmed for his timely support as Head of the Department of Chemistry in arranging the necessary materials throughout my study and facilitating my travel to South Africa.

My appreciation goes to Dr. Solomon Mehretie for providing me with lab materials and constructive criticism during seminar presentations and progress report. I would like to acknowledge Dr. Negussie Negash for his unreserved constant encouragement and invaluable advice throughout my study. Moreover, I am very grateful for his critical comments and positive criticism. I owe my sincere gratitude to Dr. Weldegebriel Yohannes for his friendly approach, moral support and motivation and positive comments on my research work. I am thankful to all

the academic and technical staff members of the Chemistry Department of Addis Ababa University.

My heartfelt special thanks and appreciation goes to Dr. Tesfaye Waryo, his wife Mrs. Tsion and their daughter Lensa who have provided me with pleasant atmosphere during my stay in South Africa. I will always remember their kindness and treatment that made me feel at home.

My sincere gratitude goes to my previous lab mate and colleague Dr. Molla Tefera whose genuine support and guidance at the beginning of the lab work was very critical and immense. My appreciation also goes to Dr. Dessie Tibebe for his continuous support and friendship. I express my sincere gratitude to Dr. Solomon Legese for his friendship and invaluable discussions. I would like to show my gratitude to PhD students of the analytical chemistry stream particularly: Asamene Embiale, Tesfu Hailu, Teshoma Tolcha and Bisratwongel Tegegne whose discussions and friendships were socially invaluable in my study. All PhD students in the Department of Chemistry are kindly acknowledged for sharing resources and also for the discussions, affection and companionship we had together during this long journey. All my friends who have contributed in one way or another in my journey are kindheartedly acknowledged.

I am greatly indebted to my parents and families for their intensification of the whole spectrum of my life. Their guidance, support and unconditional love are a lot in my life career.

I am thankful to the Department of Chemistry, Addis Ababa University, for giving me the scholarship, providing the financial support and laboratory facilities to pursue my PhD study.

Last but not least, I would like to acknowledge Wachemo University, Hossana, Ethiopia, for sponsoring me and additional support for my study.

Table of Contents

List of Figures

List of Tables

List of Abbreviations

AA	Ascorbic acid
ABS	Acetate buffer solution
BRB	Britton–Robinson buffer
CE	Capillary electrophoresis
CF	Caffeine
CMEs	Chemically modified electrodes
CNTs	Carbon nanotubes
CoNPs	Cobalt nanoparticles
CPs	Conductive polymers
CVD	Chemical vapor deposition
CV	Cyclic voltammetry
DIC	Diclofenac
DPV	Differential pulse voltammetry
EDS	Energy dispersive spectroscopy
EIS	Electrochemical impedance spectroscopy
EP	Epinephrine
ERGO	Electrochemically reduced graphene oxide
ETB	Ethambutol
f-MWCNTs	Functionalized multiwall carbon nanotubes
FTIR	Fourier transform infrared spectroscopy
GCE	Glassy carbon electrode
GC	Gas chromatography
GO	Graphene oxide
HPLC-MS	High performance liquid chromatography coupled with mass spectroscopy
HRSEM	High resolution scanning electron microscope
HRTEM	High resolution transmission electron microscope
IBP	Ibuprofen
L-Asp	L-Aspartic acid
LOD	Limit of detection

LOQ	Limit of quantification
LSV	Linear sweep voltammetry
MNPs	Metal nanoparticles
MWCNTs	Multiwall carbon nanotubes
NiNPs	Nickel nanoparticles
NSAIDs	Non-steroidal anti-inflammatory drugs
PBS	Phosphate buffer solution
P(L-Asp)	Poly(L-Aspartic acid)
RSD	Relative standard deviations
SAED	Selected-area electron diffraction
SCE	Saturated calomel electrode
SEM	Scanning electron microscope
SWCNTs	Single wall carbon nanotubes
SWV	Square wave voltammetry
TEM	Transmission electron microscopy
TP	Theophylline
UA	Uric acid
UV-Vis	Ultraviolet-Visible

1. Introduction

Improvement of life quality is one of the most important objectives of the global research efforts. Naturally, the quality of life is closely related to a better control of diseases, drug and food quality and safety, and last but not least, the quality of our environment. However, the number of chemicals used in clinical, agricultural, food and other applications has been steadily increasing recently. Hence, a sensitive, fast and reliable monitoring methods are required to control key parameters in all these fields [1]. Analytical scientists are concerned with reliable means for detecting these compounds. Although many advances have been made in this area in recent years, much is yet to be accomplished. Thus, there is a high demand for new analytical methods with better precision, accuracy, sensitivity and selectivity. These methods must not be prohibitively expensive and, ideally, should be adapted for measurement in the field [2].

A large number of instrumental techniques such as UV-Visible and infrared spectrophotometry, atomic absorption spectrophotometry, flame photometry, fluorimetry, mass spectrometry and chromatography, etc. are available for analytical chemists. In general, these methods provide reproducible results with high sensitivity and good selectivity. However, all these analytical techniques require expensive and sophisticated instruments and exhaustive sample preparation before measurement which may be time consuming and inconvenient. In this regard, electrochemical sensors are a viable and alternative option as they do not have such requirements. They provide accurate, reproducible, fast and often selective determination of various chemical species. Moreover, the technique could be non-destructive, adaptable to small sample volumes and to on-line monitoring due to these merits. Therefore, the utilization of chemical sensors is being increasingly realized in medicinal, food, agricultural, environmental and industrial fields [3].

1.1. Electroanalytical Methods

Electroanalytical methods are among the most powerful and popular techniques used in analytical chemistry [4]. They are vital tools in almost every chemical and biochemical research laboratory [5]. The measurement of electrical quantities, such as current, potential and charge, and their correlation with the chemical characteristics of a sample is the basis of electrochemical

methods of analysis. Electrochemical processes occur at the electrode solution interface and therefore a small amount of molecules present in the bulk solution contributes to the oxidation/reduction process at the electrode surface to generate the electrical response [6]. Thus, the interest in developing electrochemical-sensing devices for use in environmental monitoring, clinical assays, or process control is growing rapidly. Electrochemical sensors satisfy many of the requirements for such tasks particularly owing to their inherent specificity, rapid response, sensitivity, and simplicity of preparation for the determination of organic molecules, including drugs and related molecules in pharmaceutical dosage forms and biological fluids [7].

1.2. Electrochemical Sensors

Electroanalytical methods are widely used in scientific studies and in monitoring of industrial materials, pharmaceutical compounds, biological samples, and the environment [8]. Electrochemical sensors represent the most rapidly growing class of chemical sensors. A chemical sensor can be defined as a device that provides continuous information about its environment. Ideally, a chemical sensor provides a certain type of response directly related to the quantity of a specific chemical species. All chemical sensors consist of a transducer, which transforms the response into a detectable signal on modern instrumentation. They can be classified according to the property to be determined as: electrical, optical, mass or thermal sensors and they are designed to detect and respond to an analyte in the gaseous, liquid or solid state. Compared to optical, mass and thermal sensors, electrochemical sensors are especially attractive because of their remarkable detection ability, experimental simplicity and low cost. They have a leading position among the presently available sensors that have reached the commercial stage and which have found a vast range of important applications in the fields of clinical, industrial, environmental and agricultural analyses [9].

1.3. Classification of Electrochemical Sensors

Electrochemical sensors are classified into three main types: potentiometric, voltammetric/ amperometric and conductometric. Potentiometric sensors are based on measuring the potential of an electrochemical cell without drawing appreciable current. Voltammetric sensors are

based on the measurement of the current flowing through the working electrode dipped in a solution containing electro-active compounds, while a potential scanning is imposed on it. It measures the current-potential behavior at an electrode surface. In voltammetric sensors, the potential is varied in some systematic manner to cause oxidation or reduction of the electroactive chemical species at the electrode. The resulting current is proportional to the concentration of the oxidized/reduced electroactive species [3, 10].

Amperometric sensors exploit the use of applied potential between a reference and a working electrode, to cause the oxidation or reduction of an electroactive species to measure the resulting current. They are based on the measurement of current at a fixed operating potential. If this potential is conveniently chosen, then the magnitude of the current is directly proportional to concentration. This current is the result of electrochemical oxidation or reduction of the electroactive compound. Additionally, if steady state convection is employed, as in flowing streams and the concentration of electroactive species is uniform, then a constant current is measured [3, 9, 11]. Conductometric sensors involve the measurement of conductivity at a series of frequencies. On the other hand, coulometry involves the measurement of the quantity of electricity needed to convert the analyte quantitatively to a different oxidation state [9, 11].

2. Electrode Materials for Electrochemical Determination of Drugs

The performance of the voltammetric procedure strongly depends on the working-electrode material. The working electrode should provide high signal-to-noise characteristics, as well as a reproducible response. Thus, its selection depends primarily on two factors: the redox behavior of the target analyte and the background current over the potential region required for the measurement. Other considerations include the potential window, electrical conductivity, surface reproducibility, mechanical properties, cost, availability, and toxicity. A range of materials have found application as working electrodes for electroanalysis. The most popular ones include mercury, carbon and noble metal electrodes (particularly platinum and gold) [9, 10].

However, many compounds that are biologically and environmentally important show no response within a potential window at bare electrodes or necessitate overpotential. Thus, direct electrochemical detection usually requires high potential for such compounds. This can produce large background current, resulting in inferior detection limits. Besides, passivation and/or deactivation of the electrode surface, due to adsorption of macromolecules (e.g. proteins and surfactants) or reaction products, greatly affect the stability of the electrode response. Furthermore, coexisting components, which may be present in concentrations much larger than the analytes, may severely interfere with the determination of trace analytes which necessitates complicated sample pretreatments to eliminate or separate interfering components [12].

A promising route to overcome the above problems is manipulating the chemical nature of the electrode based on tailoring of the electrode surface–the application of chemically modified electrodes (CMEs). Thus, chemical modification of an electrode surface with various conductive or semiconductive substrates have attracted considerable interest over the past decades as researchers attempted to exert more direct control over the chemical nature of an electrode surface, aimed to tailor the electrode to meet specific applications. By deliberately incorporating specific chemical groupings or "microstructures" on conventional electrode surfaces, it is possible to control and devise the electrode surface to acquire the chemical properties of the attached substrate materials. This appealing concept of rational molecular design of electrode surfaces has played considerable success and stimulated much research. Consequently, CMEs

offer not only easily variable redox characteristics but also the possibility of adjustable physical and chemical properties (such as charge, polarity, chirality, permeability) [12, 13].

The beauty of electrochemical techniques is to utilize a tailor made chemically modified electrodes (CME) for sensitive and selective analytical applications. CMEs possess a conductive and semiconductive substrate modified with electroactive thin films, monolayers, or thick coatings of selected monomolecular, multimolecular, ionic, or polymeric film of a chemical modifier. The modified electrodes are fabricated for a particular application which is not possible with a bare conductive electrode. To prepare CME, most often a thin film of selected chemical is either bound or coated onto the electrode surface to endow desirable properties of the film in rationally and chemically designed manners. These modifications involve irreversible adsorption, self-assembled layers, covalent bonding, electropolymerization, and others, which may result in enhanced electron transfer kinetics. A variety of substrates such as carbon nanotubes (CNTs), graphene, metal nanoparticles (MNPs), polymer films, metalloporphyrins, composites, etc are used for the modification of electrode surfaces [14-16]. Thus, CMEs have been widely studied and extensively used for the determination of numerous electroactive components including pharmaceutical analysis [17]. In the present study various substrates such as conducting polymer and composites of polymer–carbon nanotubes, polymer–graphene and graphene–metal nanoparticles were proposed for electrode modifications and applications.

2.1.1. Carbon Nanotubes

Carbon nanotubes (CNTs), discovered by Iijima, are an interesting class of nanomaterials offering high electrical conductivity, high surface area, significant mechanical strength and good chemical stability. CNTs constitute a new structure of graphitic carbon consisting of one or several concentric tubules each with a helically wound hexagonal honeycomb lattice and can be divided into multi-wall carbon nanotubes (MWCNTs) and single wall carbon nanotubes (SWCNTs) according to the carbon atom layers in the wall of the nanotubes [18-21]. Figure 1 depicts the structures of SWCNTs and MWCNTs. Electrochemical sensors based on carbon nanotubes (CNTs) represent a new and interesting alternative for quantification of different analytes. These materials have attracted enormous interest because of their unique structural,

mechanical, electronic, and chemical properties. Some of these properties include high chemical and thermal stability, high elasticity, high tensile strength and, in some instances, metallic conductivity. The subtle electronic properties suggest that CNTs have the capability of promoting electron transfer reactions and improving sensitivity in electrochemistry, and thus they are widely used as electrodes. CNT modified electrodes have been proved to have excellent electroanalytical properties, such as wide potential window, low background current, low detection limits, high sensitivities, reduction of over potentials, and resistance to surface fouling. There are reports that reveal that CNT modified electrodes have shown electrocatalytic behavior with excellent performance in the study of a number of biological species [7, 22-24].

However, poor solubility of CNT in most solvents is currently a major barrier for developing CNT-based devices. The challenge of solubilizing CNT can be addressed through their covalent modification or noncovalent functionalization. In particular, "wrapping", of CNT with polymeric chains can be useful for improving their solubility without impairing their physical properties. Thus, the fabrication of conducting polymer-carbon nanotubes (CP/CNTs) composites has gained much interest recently because of their unique chemical and electrochemical properties. It has been demonstrated that CP/CNTs composites possess special properties of each of the constituents with a synergistic effect. Addition of MWCNTs to a polymer also results in a significant increase in the mechanical properties of the polymer and enhances its electrical properties by facilitating the charge-transfer processes between these two components [25].

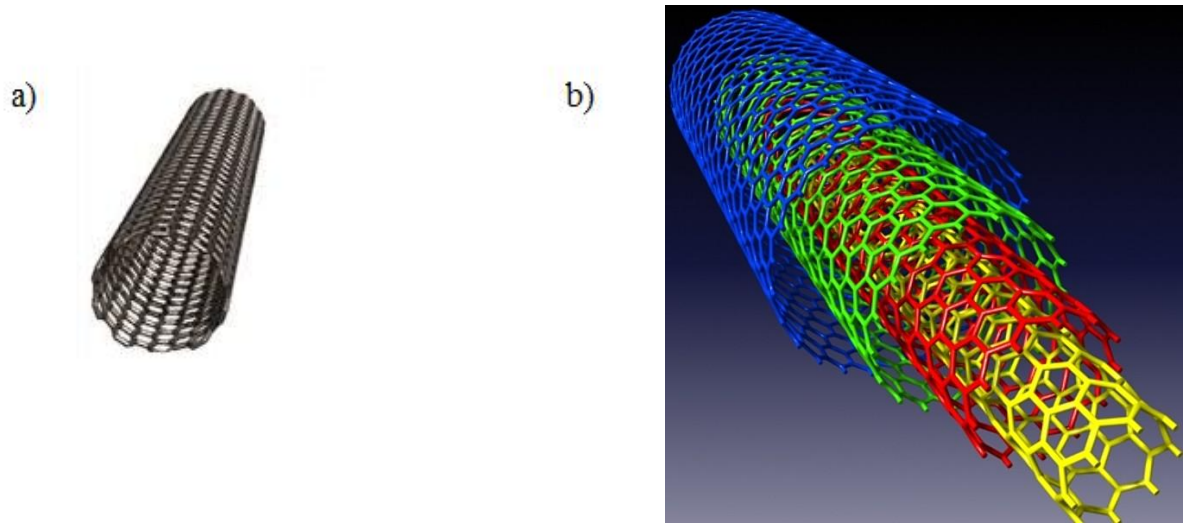

Figure 1. Chemical structure of a) SWCNTs and b) MWCNTs

2.1.2. Polymer Films

Organic conjugated polymers (conducting polymers) are mainly organic compounds that have an extended π-orbital system, through which electrons can move from one end of the polymer to the other. Common classes of organic conductive polymers include poly(acetylene)s, poly(pyrrole)s, poly(thiophene)s, poly(terthiophene)s, poly(aniline)s, poly(fluorine)s, poly(3-alkylthiophene)s, polytetrathiafulvalenes, polynapthalenes, poly(*p*-phenylene sulfide)s, poly(*p*-phenylene vinylene)s, poly(L-aspartic acid), etc [3, 26]. Conducting polymer films are attractive for sensor applications because their electronic and electrochemical properties are highly sensitive to molecular interactions, which provide excellent signal transduction for molecular detection [27]. One of the most striking properties of conducting polymers is their ability to catalyze some electrode reactions. A thin layer of a polymer film, deposited onto the surface of a substrate electrode, can enhance the kinetics of electrode processes [28-33]. Polymer-modified electrodes (PMEs) prepared by electropolymerization have received extensive interest in the detection of analytes because of their selectivity, sensitivity and homogeneity in electrochemical deposition, strong adherence to an electrode surface and chemical stability of the film [25, 27].

Recently, there has been a growing interest in the synthesis, characterization, properties, mechanisms and fabrication of conducting polymer films. L-aspartic acid is an amino acid that contains two carboxyl groups (-COOH) and one amino group ($-NH_2$). It can feasibly be electro-

polymerized on the surface of a glassy carbon electrode by cyclic voltammetry to form poly(L-aspartic acid), P(L-Asp). The P(L-Asp) film modified electrode prevents possible loss of the materials from the electrode surface, improves the oxidation currents of analytes and the anti-interferential ability of the sensor [34, 35]. The polymer film possesses a three-dimensional (3D) spatial structure and offers much available potential energy, making it possible to react in 3D space. Compared with chemically polymerized systems, electrochemically prepared conducting polymers are more stable in air and their physicochemical properties are not easily changed by an external stimulus. Hence, electrochemically deposited polymer films have attracted lots of attention and numerous studies have been reported [36].

2.1.3. Graphene

Graphene, an allotrope of elemental carbon, has been considered as a novel material in recent times by scientific researchers ever since its discovery in 2004 [37]. It is one of the basic building blocks of the carbon family with one atom thick layer of sp^2 hybridized carbon atoms in a closely packed honeycomb two-dimensional (2D) lattice. Graphene has recently attracted enormous attention in the construction of electrochemical sensors and biosensors due to its novel properties. Owing to its unique physicochemical properties, the profound application of graphene and graphene-based materials is being observed in the field of nanotechnology, sensors, catalysis and biosensors. Graphene is the most recently reported carbon nanomaterials which exhibit fascinating properties, such as a large surface area, zero band gap, high elasticity, tensile strength, electron mobility and thermal conductivity. The remarkable physicochemical properties include a high surface area of 2630 $m^2\ g^{-1}$, an excellent mechanical strength of 1100 GPa, an outstanding electrical conductivity of 1738 $S\ m^{-1}$, exceptional thermal conductivity of 5000 $W\ m^{-1}\ K^{-1}$ and the provision of a broad spectrum for functionalization. This broad spectrum for functionalization explains the capability of graphene and graphene-based materials to absorb a variety of biomolecules through either electrostatic or π–π stacking interactions in the field of (bio)sensors. Also, the high density edge defects in graphene play a role in the heterogeneous electron transfer process for an observable signal. These unique electrical and optical properties of graphene facilitate its use in the field of (bio)sensors [38-40].

Various strategies have been reported in the literature for the fabrication of graphene such as chemical vapor deposition (CVD), micromechanical and ultrasonication assisted exfoliations of graphite, unzipping of CNTs and reduction of graphene oxide (GO). However, the technique based on GO reduction is well-suited for mass production due to its simplicity and low material cost [37]. Among the various preparation methods of graphene for chemical modification of electrodes, direct electrodeposition of reduced graphene oxide on a glassy carbon electrode has been reported to be an efficient method, providing some unique advantages, such as simplicity to prepare, green, fast and with easy control over the amount of deposited graphene [41].

Graphene oxide (GO), as an important derivative of graphene, possesses many significant functional groups, that are responsible for its hydrophilicity and dispersibility, excellent film forming capability and controllable electronic properties, except for the distinctive structural features and unique electronic conductivity possessed by graphene [42]. Hummers' method is the most common route for the synthesis of graphene oxide from graphite, Scheme 1. The use of graphene oxide for electrode modification is done in various ways either by reducing graphene oxide or by functionalization of graphene oxide with various other components, such as enzymes, polymers, organic molecules, inorganic complexes, metallic and metallic oxides nanostructures, ionic liquids, etc. Graphene oxide has also been used for various applications in solar cells, supercapacitors, electrochemical sensors, biosensors, etc. The widest application of graphene oxide is in the electrochemical and biosensor areas. Graphene-based nanostructured materials provide a template for electrodes and a high electroactive surface area due to the presence of carboxylic groups [39].

Graphene-based nanocomposites, such as graphene-metal nanoparticle hybrids, that combine unique properties of graphene and the catalytic activity of metal nanoparticles with a synergistic effect, have attracted extensive attention in electrochemical sensor fields. These outstanding properties of graphene-metal nanoparticle composites have shown a considerable prospect for the fabrication of a high performance electrochemical (bio)sensor [43].

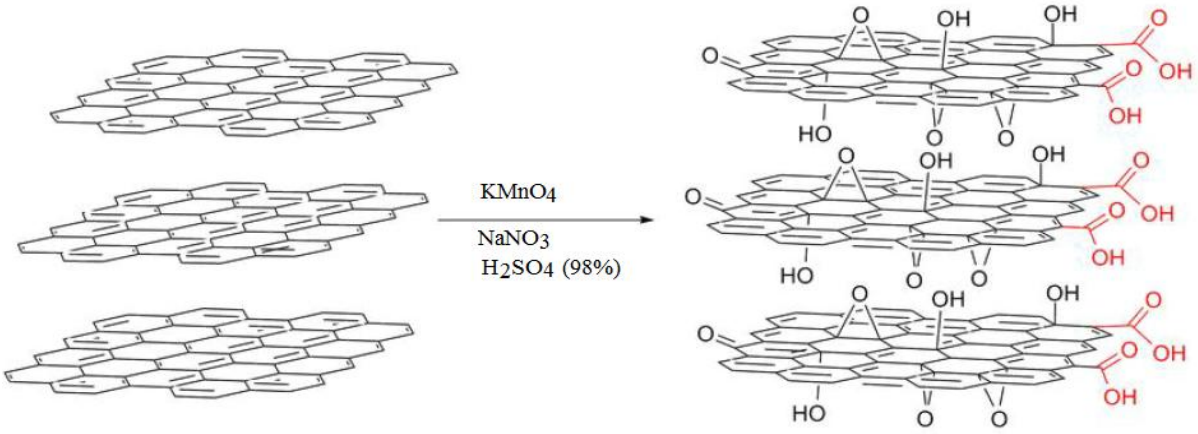

Scheme 1. The synthesis of GO by Hummers' method

2.1.4. Metal Nanoparticles

Nanotechnology has recently become one of the most exciting forefront fields in analytical chemistry. A wide variety of nanomaterials, especially nanoparticles with different properties have found broad application in various analytical methods. Due to their small size (normally in the range of 1–100 nm), nanoparticles exhibit unique chemical, physical and electronic properties that are different from those of bulk materials, and can be used to construct novel and improved sensing devices; in particular, electrochemical sensors and biosensors. Many types of nanoparticles of different sizes and compositions are now available, which facilitate their application in electroanalysis [44]. The development of nanomaterials for biological detection, sensing, and catalytic applications has been an active and interesting field of research in recent years. Very recently, the use of mediating nanomaterials for electrode surface modification is a hot topic owing to large specific surface area, excellent conductivity and electrocatalytic activity. Nanomaterials can be directly used as electrode materials or as catalytic labels for the amplified electrochemical detection. Different metallic nanoparticles (MNPs) have gained increasing attention due to their unique physical and chemical properties at nanoscale, which differ substantially from those of both the bulk material and single atoms. Generally, metal nanoparticles have excellent conductivity and catalytic properties, which make them suitable for acting as "electronic wires" that enhances the electron transfer between redox centers and electrode surfaces, and as catalysts to increase electrochemical reactions. Hence, the synthesis and characterization of metal nanoparticles (MNPs) has attracted great interest to scientists and

technologists during recent years [44-46]. Many studies focus on tuning the electronic and optical properties of metal nanostructures by varying their sizes and shapes or by combining them with other nanomaterials, from which significant synergistic effects can develop [44]. Owing to the numerous unique physical, chemical and biological properties of the nanomaterials and their nanocomposites, a significant effort has been devoted on the development of the synthetic strategies for highly controllable size, shape, surface charge and physicochemical characteristics over the last few decades. The main paths employed for the production of nanomaterials include physical strategy (such as physical vapor deposition and laser ablation), chemical strategy (such as chemical vapor deposition, sol-gel processes, thermal decomposition and hydrothermal methods), electrochemical (such as anodic oxidation and electrodeposition) and photochemical strategy (such as photodeposition) [47, 48].

Metallic nanomaterials play key roles in the design of electrochemical sensor and biosensor platforms due to the unique size and shape dependent physical, chemical and electrochemical properties. Metal nanoparticles based electrochemical sensor platforms provide a strong potential for enhancing both sensitivity and selectivity via tuned signal amplifications [44, 47]. However, a major drawback, which still limits the wider application of MNPs, is insufficient stability of MNPs, exemplified by their pronounced tendency to aggregate [49]. Moreover, the electrochemical applications of MNPs (e.g., in sensor and biosensor) are based on the use of noble metals such as Au, Ag and Pt due to their well-known electrocatalytic properties. The main problem associated with the use of these metals is their high cost and scarcity which limits the wider use and commercial application. Hence, one of the most important challenges is decreasing the loading of noble metal in the synthesis of MNPs without impairing the performance of the nanocatalysts. The use of relatively cheaper MNPs is another alternative option. Transition metal nanoparticles such as Ni, Co, Fe, Zn, Cu, etc have attracted extensive interest as an alternative solution due to their low cost and easy availability and have also proven to show outstanding performances for electroanalytical applications [46, 50, 51].

2.1.5. Nanocomposite Materials

A nanocomposite is a mixture of two or more materials producing a new material with at least one dimension in the nano range. The materials constituting nanocomposites are mixed in such a way that the resulting material exhibits ‘‘averaged” properties between the two. The assembly of the two materials is done in such a way that the composite exhibits better properties such as catalytic, thermal stability and adsorption properties, etc. than the individual materials as a result of the synergistic effect. Mostly, composite materials are composed of two phases, the discontinuous (reinforcing material) and the continuous (matrix). On the basis of properties, nanocomposites are classified into two broad categories as functional materials (based on electrical, magnetic and optical properties) and structural materials (based on their mechanical properties). The applications of nanocomposites is growing at a faster rate and are widely used in (bio)sensors, medicine, engineering, drug delivery, anti-corrosion barrier protection and UV protection gels, etc [52].

Composite modified electrodes have received great attention in the last decade due to their wide applications in analytical chemistry as chemical and biosensors. Preparation of composite electrodes by incorporation of metal nanoparticles, graphene, carbon nanotubes (single walled or multiwalled carbon nanotubes) or polymers on the electrode surface can extensively enhance the catalytic activity of the electrodes towards electrochemical behaviors of many biologically important molecules [26]. Recently, a large number of literatures on composite materials of graphene-metal nanoparticles [50, 53-58] graphene-polymer [59-63] and carbon nanotubes-polymer [64-68] were reported for electrochemical sensing applications.

2.2. Chemically Modified Electrodes for Drug Analysis

Drug analysis is one of the most important tools for drug quality control [69]. Recent progress in technology and science has led to the development of several synthetic drugs. It is therefore imperative to develop analytical methods for determination of these drugs both in the quality control manufacturing phase of the pharmaceutical formulations and their determination in the human body [70]. Generally, the scope of drug analysis includes the analytical investigation of bulk-drug materials, the intermediates during their synthesis, products of drug

research, drug formulations, impurities and degradation products of drugs, biological samples containing the drugs and their metabolites to get data that can contribute to the maximal efficacy and maximal safety of drug therapy and the maximal economy of the production of drugs. The efficacy, safety and economy of drug therapy are extremely important issues not only from the point of view of public health, but their financial and political aspects are also immense. As a result, pharmaceutical and biomedical analysis is among the most important branches of applied analytical chemistry. In order to fulfill the rapidly increasing demands with regard to the number and the quality of analytical measurements, great efforts have been made and are being made to apply further developments in the field of analytical chemistry [71].

Determination and quantification of drugs in biological fluids and pharmaceutical samples are also essential in clinical chemistry, toxicological, doping and pharmaceutical investigations. Quantitative analysis of pharmaceuticals is indispensable during various phases of drug development and fabrication stage, to ensure appropriate formulation quality and stability. Other major fields include toxicology testing in pharmacology and in the clinical trial phase for monitoring bio-availability, pharmacokinetics and possible drug abuse. Therefore, the development of simple, sensitive, rapid, and reliable methods for the determination of drugs is of great importance for drug monitoring purposes [7, 17, 72]. Though, historically the analysis of pharmaceuticals has been carried out by spectrophotometry, fluorimetry and liquid or gas chromatographic methods, recent investigations have focused on electrochemical methods [73]. Despite their widespread application and use, little work has been reported on the determination of pharmaceutical drugs by electrochemical and related sensing devices [72]. The electrochemical techniques, especially voltammetry, have gained important attention during recent years. They have been applied widely for the determination of pharmaceutical compounds in dosage forms (tablets, capsules, injections and suspension) and biological samples (urine, blood serum). Various types of pharmaceutical compounds have been analyzed by voltammetric techniques [74]. In particular, voltammetric techniques based on chemically modified electrodes, chemical sensors, have recently attracted much attention in the electrochemical determination of important pharmaceutical drugs [17, 73].

Biosensors, combining a biological recognition element and a suitable transducer, also represent another alternative to chemical sensors for the determination of electroactive biological molecules including pharmaceutical drugs. The biological recognition element of a biosensor interacts selectively with the target analyte(s), assuring the selectivity of the sensors. The transducer converts the biological response resulting from the interaction with the target analyte into a quantifiable signal. The traditional transducers are electrochemical, optical, piezoelectric and thermal. The latest generation affinity biosensors combine the classical measurement principles of piezoelectric and magnetic transducers. The selectivity of the biosensor for the target analyte is mainly determined by the bio-recognition element, whilst the sensitivity of the biosensor is greatly influenced by the transducer. The most widely used biosensors are the enzyme-based amperometric electrodes. However, many enzyme-based amperometric biosensors described in the recent literature still display a few drawbacks when compared to chemical sensors. The most difficult problems to overcome for biosensors application include reduced stability. Enzymes removed from their natural environment tend to rapidly lose their activity and thus limit the lifetime of the sensor. Electrochemical interference due to the complex sample matrices is another limitation. Sample matrices are very complex and thus modifying electrode surfaces in a way that favors exclusively one single electrochemical process is a difficult task. Biocompatibility and bio-fouling are also critical issues in case of in-vivo measurements [1, 12].

In this work, we have proposed the use of poly(L-aspartic acid), poly(L-aspartic acid)/multiwalled carbon nanotubes, poly(L-aspartic acid)/electrochemically reduced graphene oxide and nickel nanoparticles/electrochemically reduced graphene oxide composite modified glassy carbon electrodes for the sensitive and selective voltammetric determinations of selected pharmaceutical drugs (ibuprofen, caffeine, theophylline, epinephrine, diclofenac and ethambutol). These selected drugs are among the most commonly and widely used pharmaceutical drugs. However, excessive and/or continuous consumption of these pharmaceutical drugs have known to cause several health hazards and side effects [17, 36, 71]. Furthermore, the sensitivity, stability, reproducibility and selectivity of most of the electrochemical methods reported so far for the determination of these selected drugs in real samples are not satisfactorily enough. Therefore, the development of sensitive and selective electrochemical sensors with acceptable stability and reproducibility for rapid determinations of

these drugs in pharmaceutical formulations and biological dosage forms is very important in this regard.

2.3. Rationale and Motivation

Pharmaceuticals drugs play an important role in improving human health and promoting well-being. However, to produce the desired effect, they have to be safe, efficacious and of acceptable quality, and have to be used rationally. Therefore, quantitative analysis of pharmaceutical drugs is essential during various phases of drug development and during the fabrication stage, to ensure appropriate formulation, stability and quality. Drug quality monitoring is also important in various locations, including hospital point-of-care settings, by caregivers in non-hospital settings and by patients at home. Other major fields include toxicology testing in pharmacology and in the clinical trial phase for monitoring bio-availability, pharmacokinetics and possible drug abuse.

However, conventional methods for drug quality monitoring and quantification in pharmaceutical formulations and biological fluids are quite expensive, require complicated and tedious sample preparation protocols, need skilled personnel and also not suited for field or onsite measurements. Therefore, simpler, faster and cheaper devices are highly desirable for replacement of time-consuming laboratory-analysis. Considering these aspects, the motive for the current study was thus formulated.

2.4. Objectives

General Objective

The general objective of this research work was to develop simple and low cost electrochemical sensors for sensitive, selective and rapid determination of selected drugs (ibuprofen, caffeine, theophylline, epinephrine, diclofenac and ethambutol) in pharmaceutical formulations and biological fluids using chemically modified glassy carbon electrodes.

Specific Objectives

1. To synthesize graphene oxide and nickel nanoparticles.
2. To modify conventional glassy carbon electrode with poly(L-aspartic acid), poly(L-aspartic acid)/multiwalled carbon nanotubes, poly(L-aspartic acid)/electrochemically reduced graphene oxide and nickel nanoparticles/electrochemically reduced graphene oxide composites.
3. To characterize the synthesized materials and the modified electrodes using high resolution scanning electron microscopy (HRSEM), high resolution transmission electron microscopy (HRTEM), energy dispersive spectroscopy (EDS), Raman spectroscopy, Fourier transform infrared (FTIR) spectroscopy, UV-Vis spectroscopy, cyclic voltammetry (CV) and electrochemical impedance spectroscopy (EIS).
4. To study the catalytic effects of the modified electrodes towards the electrochemical redox reaction of the selected drugs (ibuprofen, caffeine, theophylline, epinephrine, diclofenac and ethambutol).
5. To set the optimum working conditions for the determination of the selected drugs.
6. To establish the analytical performance characteristics (such as linear response range, method detection limit, repeatability, reproducibility, stability) of the developed sensors.
7. To investigate the selectivity of the method towards potentially interfering substances.
8. To investigate the analytical applications of the fabricated electrodes for the quantitative determination of the drugs in real samples such as pharmaceutical formulations and biological fluids (blood and urine).
9. To compare the analytical performance of the developed methods with literature reports.

3. Methodology and Techniques Used in the Study

3.1. Voltammetric Techniques

3.1.1. Electrochemical Cell

Voltammetry refers to a class of electroanalytical techniques that is used to designate the current-voltage measurement obtained at a given electrode. An electrochemical cell consisting of a solution of the analyte of interest, supporting electrolyte and the electrodes is used in voltammetric measurements. A three-electrode system is used in voltammetry, which includes a working electrode, at which the oxidation or reduction process of interest occurs, a reference electrode, such as saturated calomel electrode (SCE) or silver-silver chloride electrode (Ag/AgCl) and an auxiliary or counter electrode, which carries the bulk of the current (instead of reference electrode). Voltammetry functions by measurement of a current response (I) at a working electrode as a function of the applied potential (E) with respect to a reference electrode by means of a potentiostat. When a potential is applied between the working and reference electrodes, the current that is produced passes between the working electrode and a third auxiliary/counter electrode. Platinum wire is often used as the material for the auxiliary electrode [10, 75]. A schematic representation of a typical electrochemical cell set up is given in Figure 2. The most common voltammetric techniques encountered in electroanalytical chemistry and used in the present study are discussed in details in the following sub-sections.

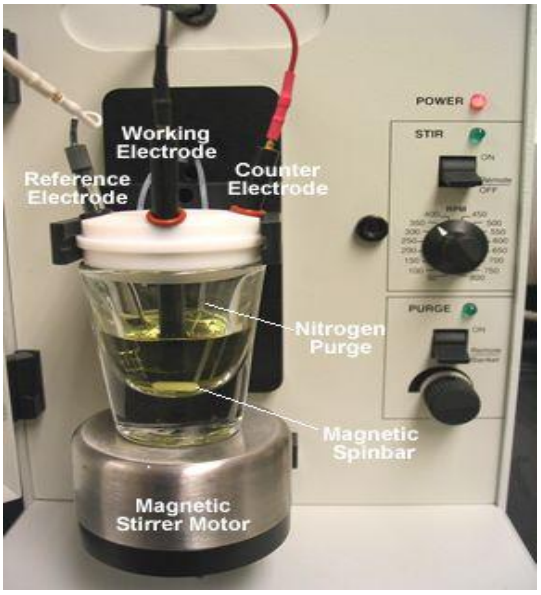

Figure 2. Typical electrochemical cell composed of three electrode system for voltammetry [10]

3.1.2. Cyclic Voltammetry

Cyclic voltammetry (CV) has become an important and widely used electroanalytical technique in many areas of chemistry. It is the most widely used technique for acquiring qualitative information about electrochemical reactions. The power of cyclic voltammetry results from its ability to rapidly provide considerable information on the thermodynamics of redox processes and the kinetics of heterogeneous electron transfer reactions and on coupled chemical reactions or adsorption processes. CV is often the first experiment performed in an electroanalytical study. It offers a rapid location of redox potentials of the electroactive species and a convenient evaluation of the effect of media on the redox process. It is widely used for the study of redox processes, understanding reaction intermediates and obtaining stability of reaction products.

CV is based on varying the applied potential at a working electrode in both forward and reverse directions while monitoring the current. It consists of scanning linearly the potential of a stationary working electrode (in an unstirred solution), using a triangular potential waveform (Figure 3). Depending on the information sought, single or multiple cycles can be used. During the potential sweep, the potentiostat measures the current resulting from the applied potential. The resulting current–potential plot is termed a cyclic voltammogram, Figure 4. The important parameters in a cyclic voltammogram are the peak potentials (E_{pc}, E_{pa}) and peak currents (I_{pc}, I_{pa}) of the cathodic and anodic peaks, respectively. If the electron transfer process is fast when compared to mass transfer (diffusion), the reaction is said to be electrochemically reversible [10, 11, 75]. The peak current for a reversible couple (at 25 ºC) is given by the Randles–Sevcik equation (1).

$$I_p = (2.69 \times 10^5) n^{3/2} A C_o D_R^{1/2} v^{1/2}, \qquad (1)$$

where n is the number of electrons transferred, A the electrode area (cm^2), C_o is the concentration (mol cm^{-3}), D_R the diffusion coefficient (cm^2 s^{-1}), and v the scan rate (V s^{-1}). Accordingly, the current is directly proportional to concentration and increases with the square root of the scan rate. Such dependence on the scan rate is indicative of electrode reaction controlled by mass

transport (semiinfinite linear diffusion). For a simple reversible couple, the reverse-to-forward peak current ratio, I_{rev}/I_{for} is unity and the formal potential is centered between $E_{p,a}$ and $E_{p,c}$:

$$E^{\circ} = \frac{E_{p,a} + E_{p,c}}{2} \qquad (2)$$

The separation between the peak potentials (for a reversible couple) is given by

$$\Delta E_p = E_{p,a} - E_{p,c} = \frac{0.059}{n} V \qquad (3)$$

For an irreversible electrode processes with sluggish electron exchange, the individual peaks are reduced in size and widely separated. Generally, totally irreversible systems are characterized by a shift of the peak potential with the sweep rates:

$$E_p = E^{\circ} - \frac{RT}{\alpha n_a F}[0.78 - \ln \frac{k^{\circ}}{D^{1/2}} + \ln (\frac{\alpha n_a F v}{RT})^{1/2}] \qquad (4)$$

where α is the transfer coefficient and n_a is the number of electrons involved in the charge transfer step. The peak current for an irreversible systems, given by

$$I_p = (2.99 \times 10^5) n(\alpha n_a^{1/2}) A C_o D_R^{1/2} v^{1/2} \qquad (5)$$

For quasi-reversible systems the current is controlled by both the charge transfer and mass transport. Overall, the voltammograms of a quasi-reversible system are more drawn out and exhibit a larger separation in peak potentials compared to a reversible system [10, 11].

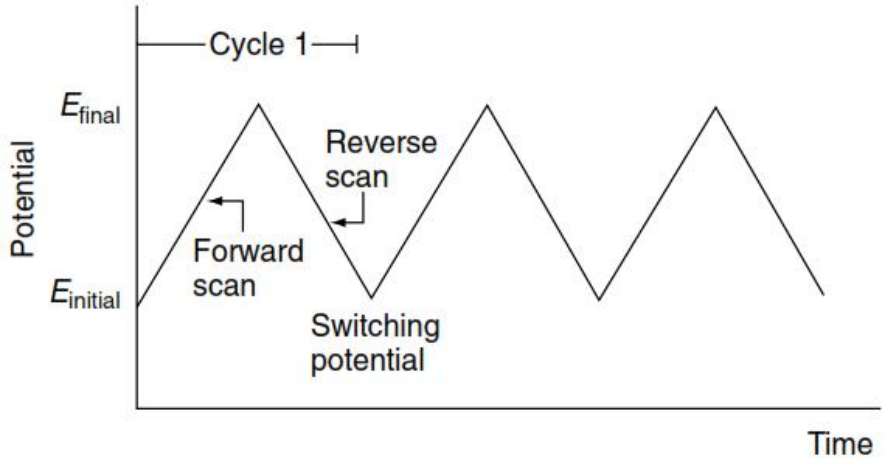

Figure 3. Potential–time excitation signal in a cyclic voltammetric experiment

One of the most important applications of CV is for the qualitative diagnosis of coupled chemical reactions that precede or succeed the redox process of inorganic, organic or

pharmaceutical compounds. It can also be used for understanding the redox mechanisms of many biologically important molecules and pharmaceutically active compounds. The results of CV investigations into the redox mechanism of pharmaceutically active compounds and biomolecules can have profound implications for the understanding of in-vivo redox processes, as in neuroscience, or pharmacological activity [76].

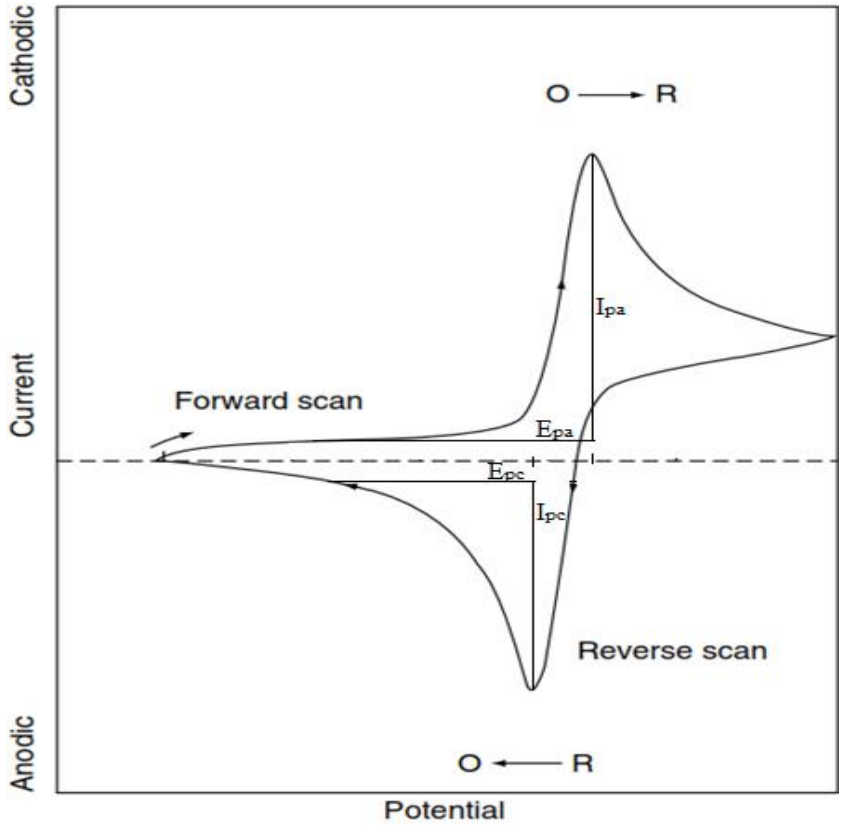

Figure 4. Typical cyclic voltammogram for a reversible: $O + ne^- \leftrightarrow R$, redox process

3.1.3. Square Wave Voltammetry

Pulse voltammetric techniques are aimed at lowering the detection limits of voltammetric measurements. These techniques permit convenient measurements up to 10^{-8} M concentration level. Because of their highly improved performance, modern pulse techniques have largely replaced classical polarography in the analytical laboratory. The various pulse techniques are all based on a sampled current/potential-step experiment. A sequence of such potential steps, each with duration of about 50 milliseconds, is applied onto the working electrode. After the potential is stepped, the charging current decays rapidly (exponentially) to a negligible value, while the

faradaic current decays more slowly. Thus, by sampling the current late in the pulse life, an effective discrimination against the charging current is achieved. The difference between the various pulse voltammetric techniques is the excitation waveform and the current sampling regime [10, 75]. The most common pulse voltammetric techniques include normal pulse voltammetry (NPV), differential pulse voltammetry (DPV), square wave voltammetry (SWV) and staircase voltammetry [6, 8-11].

Square-wave voltammetry (SWV) is a powerful electrochemical technique suitable for analytical application, mechanistic study of electrode processes and electrokinetic measurements. Currently it is considered as one of the most advanced voltammetric techniques, which combines the advantages of pulse techniques (enhanced sensitivity), cyclic voltammetry (insight into the electrode mechanism) and impedance techniques (kinetic information of very fast electrode processes). The modern SWV equipment, incorporated in digital electrochemical instruments, utilizes a combination of a staircase potential modulation and periodic square-shaped potential function, applied at a stationary electrode [77]. Square wave voltammetry is a voltammetric technique in which the excitation signal consists of a symmetrical square-wave pulse of amplitude E_{SW} superimposed on a staircase waveform, where the forward pulse of the square wave coincides with the staircase step, Figure 5. The current is sampled twice during each square-wave cycle, once at the end of the forward pulse (at τ_1) and once at the end of the reverse pulse (at τ_2). The net current, i_{net}, is obtained by taking the difference between the forward and reverse currents (i_{for}–i_{rev}) and is centered on the redox potential. The peak height is directly proportional to the concentration of the electroactive species and direct detection limits as low as 10^{-8} M is possible. Square-wave voltammetry has several advantages. Among these are its excellent sensitivity, the effective rejection/discrimination of charging background currents and speed. This speed, coupled with computer control and signal averaging, allows for experiments to be performed repetitively and increases the signal to noise ratio. Excellent sensitivity results from the fact that the net current is larger than either the forward or reverse components, Figure 6. Comparison between square-wave and differential-pulse voltammetry for reversible and irreversible cases indicated that the square-wave currents are 4 and 3.3 times higher, respectively, than the analogous differential-pulse response [10, 75].

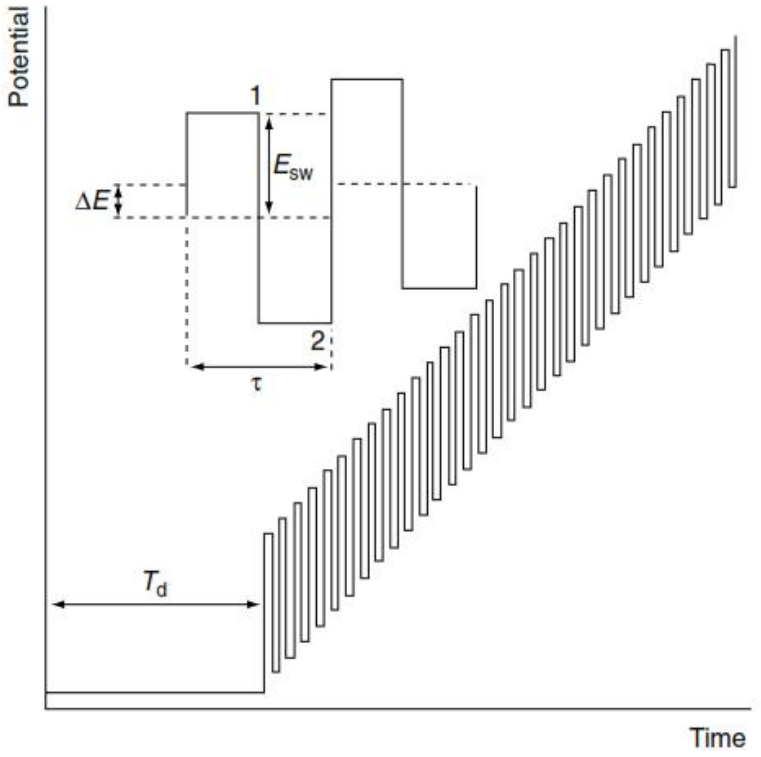

Figure 5. Square-wave waveform showing the amplitude E_{sw}, step height ΔE, square wave period τ, delay time T and current measurement times 1 and 2

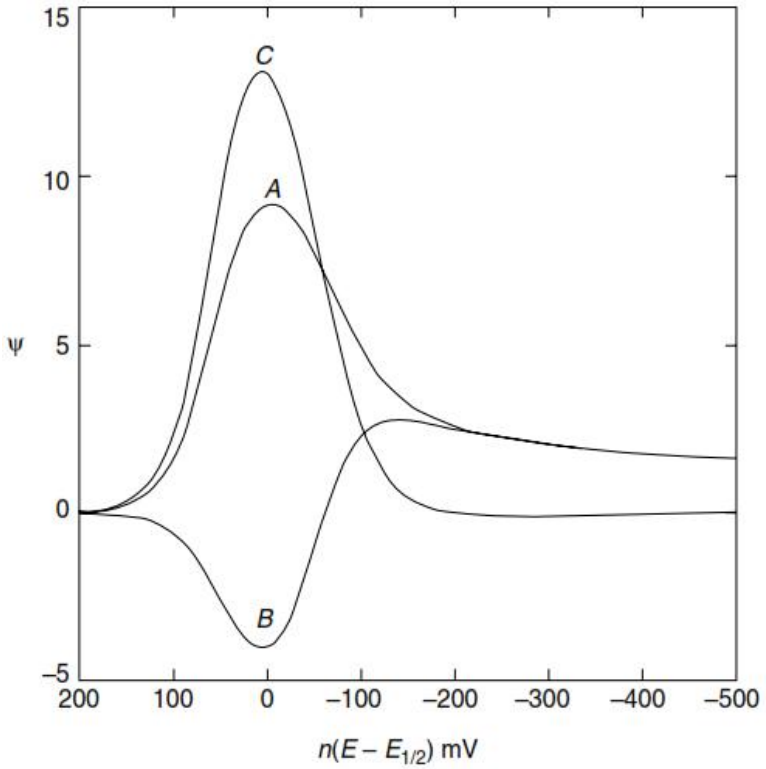

Figure 6. SWV of a reversible reaction (A) forward, (B) reverse and (C) net current

3.2. Electrochemical Impedance Spectroscopy (EIS)

Electrochemical impedance spectroscopy (EIS) is a high precision and frequently used technique for the evaluation of heterogeneous charge-transfer systems and studies of double-layer structure [11, 78]. It is a powerful method of characterizing many of the electrical properties of materials and their interfaces with electronically conducting electrodes [79]. Impedance spectroscopy is an effective technique for probing the features of chemically-modified electrodes (CMEs) and for understanding electrochemical reaction rates. Impedance is a complex resistance encountered when a current flows through a circuit made of combinations of resistors, capacitors, or inductors [10]. The representation of the impedance data can be carried out using (i) Nyquist plot, viz. the imaginary *vs*. real part of the impedance (–Z" *vs*. Z'); (ii) Bode phase angle plot (θ *vs* log ω) and (iii) Bode magnitude plot (|Z| *vs* log ω). However, for estimating the specific capacitances, the variation of the imaginary part of the impedance (-Z") with the reciprocal frequency ($1/f$) is constructed in order to calculate the slope from (6):

$$\frac{d(-Z'')}{d(1/\mathrm{f})} = \frac{1}{2\pi C} \qquad (6)$$

where, f denotes the frequency. By dividing the C value obtained from the above equation by the mass of the deposited species, the specific capacitance per unit mass arises [80]. A typical Nyquist plot for an electrochemical impedance spectroscopy is depicted in Figure 7a.

Although the above equation is satisfactory for estimating the specific capacitance, the power of the EIS will be lost if all the system parameters (double layer capacitance, various resistances, exchange current density, Warburg impedance, etc.) essential for comprehending the electrochemical behavior are not reported. Hence, the construction of appropriate equivalent circuits for deducing the system parameters becomes essential. Thus, electrochemical transformations occurring at the electrode–solution interface can be modeled using components of the electronic equivalent circuit that correspond to the experimental impedance spectra. Particularly useful to model interfacial phenomena is the Randles electronic equivalent-circuit model (Figure 7b). A common feature of most of the circuits is the presence of the ohmic resistance of the electrolyte solution (R_s), the electron transfer resistance or the charge transfer resistance (R_{ct}), Warburg impedance (W) resulting from the diffusion of ions from the bulk solution to the electrode surface and double layer capacitance (C_{dl}) or constant phase elements

(CPE). The impedance of the interface, derived by application of Ohm's law, consists of two parts, a real number Z' and an imaginary one, Z″ [10, 80].

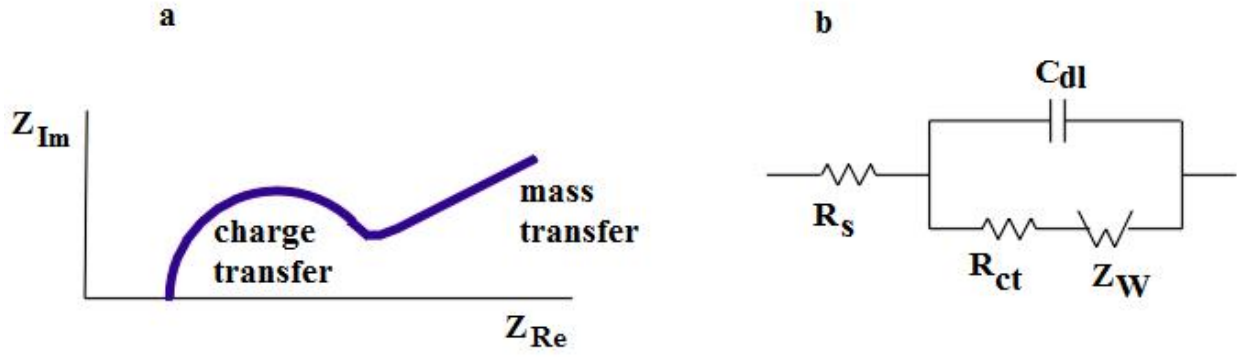

Figure 7. (a) Impedance spectra presented in the form of Nyquist plot for an electrochemical system. Regions of mass-transfer and kinetic control are found at low and high frequencies, respectively; (b) Randles equivalent circuit for electrochemical systems

The measurement of impedance generally involves the application of a small-amplitude perturbing sinusoidal voltage signal (at a ω frequency) to the electrochemical cell and measuring the current response. The resulting faradaic impedance spectrum, known as a Nyquist plot, corresponds to the dependence of the imaginary number on the real number (Figure 7a), and contains extensive information about the electrified interface and the electron transfer reaction. The Nyquist spectra can be used for extracting the electron transfer kinetics and diffusional characteristics. In the case of very fast electron transfer processes the impedance spectrum includes only the linear part, while very slow electron transfer processes are characterized by a large semicircular region. The diameter of the semicircle equals the electron transfer resistance. The intercepts of the semicircle with the Z_{re} axis correspond to those of R_s [10, 81].

The total impedance for the circuit of Figure 7b can be derived from (7),

$$Z_{total} = R_s + \frac{\left(R_{ct} + \left(\sigma/\sqrt{\omega}\right)\right) - \left(j\sigma/\sqrt{\omega}\right)}{\left(1 + \sigma \cdot \sqrt{\omega} C_{dl}\right) + j\left(\omega C_{dl} R_{ct} + \sigma\sqrt{\omega} C_{dl}\right)} \qquad (7)$$

where, σ is the Warburg coefficient, comprising the diffusion coefficient of the species [80].

3.3. Spectroscopic and Microscopic Characterization Techniques

Spectroscopic methods are the most commonly used techniques and continue to enjoy wide popularity [70]. Spectroscopy is the study of the interaction of electromagnetic radiation with matter. Spectroscopic methods can be based on phenomena of emission, absorption, fluorescence or scattering. Different spectroscopic methods are frequently used for the characterization of a wide range of samples of interest. These methods are used for qualitative and quantitative analysis of sample. Some of the spectroscopic methods (e.g. UV–Vis) are used as a screening method since they give tentative identification of a sample and are not specific in nature while other spectroscopic methods (e.g. infrared spectroscopy and mass spectrometry) are used as a confirmatory method as they give the reliable identity of sample and are specific in nature [82].

Microscopy has been equally important to understand both inanimate matter and living objects at their elementary level. It involves the study of objects that are too small to be examined by the unaided eye. Initially, these instruments relied on focusing of visible light, but within the past 60 years other forms of radiation have been used. Of these, electrons have arguably been the most successful, by providing us with direct images down to the atomic level. Therefore, electron microscopy is being used routinely to examine materials of sub-micrometer dimensions. Nanotechnology also makes use of electron beams, both for characterization and fabrication. Nowadays, microscopic techniques such as TEM and SEM are among the most widely used microscopic techniques by engineers and scientists for material characterization [83].

3.3.1. Ultraviolet-Visible (UV-Vis) Spectroscopy

UV-Visible spectroscopy is a mature and well established analytical technique used extensively in many industrial sectors including environmental analysis, pharmaceutical testing, food and beverage production, etc. UV-visible spectroscopy involves the measurement of the absorbance of ultra-violet or visible radiation when light passes through an analayte. When radiation interacts with matter, a number of processes can occur, including reflection, scattering, absorbance, fluorescence/phosphorescence (absorption and emission), and photochemical reaction (absorbance and bond breaking). In general, when measuring UV-visible spectra, we want only absorbance to occur. Absorption of photons of light measures transitions from the

ground state to the excited state. Molecules containing π-electrons or non-bonding electrons (n-electrons) can absorb energy in the form of ultraviolet or visible light to excite their electrons to higher anti-bonding molecular orbitals. The more easily excited the electrons (i.e. lower energy gap between the HOMO and the LUMO), the longer the wavelength of light it can absorb. UV-Vis spectroscopy is an effective technique for both qualitative and quantitative analysis of organic and inorganic compounds. It is routinely used for the quantitative determination of solutions of transition metal ions and highly conjugated organic compounds based on Beer-Lambert law, equation (8), which states that the absorbance of a solution (A) is directly proportional to its concentration (c) and path length (l) when the wavelength of the incidence light remains fixed, and is summarized as [84, 85]:

$$A = Ɛcl \quad (8)$$

where, Ɛ is the molar absorptivity coefficient.

3.3.2. Fourier Transform Infrared Spectroscopy (FTIR)

Infrared (IR) spectroscopy has become almost indispensable in the chemistry laboratory as it is ideally suited for carrying out qualitative and quantitative analysis, particularly of organic compounds [86]. It is a well known analytical technique dealing with the infrared region of the electromagnetic spectrum. IR spectroscopy is a fast, accurate and nondestructive technique that can detect a range of functional groups through the interaction between an infrared radiation and a sample that can be solid, liquid or gaseous [87]. The Fourier transform spectrometers employing an interferometer (FTIR) have almost replaced the other IR spectrophotometers such as dispersive spectrophotometers with a grating monochromator and non-dispersive photometers using a filter or an absorbing gas because of their speed, reliability, signal-to-noise advantage and convenience. FTIR can be used to identify compounds or investigate sample composition and is sensitive to changes in molecular structure. The FTIR radiation encompasses a long range of wavelengths, which consists of other sub-regions: near, middle and far infrared regions. However, most infrared spectroscopic measurements are performed in the mid-infrared region, which covers the spectral region between 400 cm^{-1} and 4000 cm^{-1}. IR measures the frequencies at which the sample absorbs and also the intensities of these absorptions. It exploits the fact that bonds in molecules have specific frequencies at which they rotate or vibrate corresponding to

discrete energy levels (vibrational modes). These resonant frequencies are determined by the shape of the molecular potential energy surfaces, the masses of the atoms and, by the associated vibronic coupling. Since, functional groups are responsible for the absorption of radiation at different frequencies; it is possible to identify the composition of a sample. Infrared spectroscopy is widely used in both research and industry as a simple and reliable technique for quality control. The sensitivity and accuracy of FTIR detectors along with a wide variety of software algorithms have dramatically increased the practical use of infrared for quantitative analysis. It is perhaps the most widely used method of applied spectroscopy [87-89].

3.3.3. Raman Spectroscopy

Raman spectroscopy was named in the honor of its inventor, C.V. Raman, who, along with K.S. Krishnan, published the first paper on this technique. Raman spectroscopy is a versatile method used for qualitative as well as quantitative analysis of a wide range samples. Qualitative analysis can be performed by measuring the frequency of scattered radiations while quantitative analysis can be performed by measuring the intensity of scattered radiations. Raman spectroscopy measures the vibrational motions of a molecule like IR spectroscopy. However, the physical method of observing the vibrations is different from infrared spectroscopy. In Raman spectroscopy one measures the scattering of light whereas IR spectroscopy is based on absorption of photons. Hence, Raman spectroscopy is a scattering technique resulting from Raman Effect, i.e., the frequency of a small fraction of a scattered radiation is different from the frequency of a monochromatic incident radiation. It is based on the inelastic scattering of an incident radiation through its interaction with vibrating molecules. It probes molecular vibrations. In Raman spectroscopy, the sample is illuminated with a monochromatic laser beam which interacts with the molecules of the sample and produces a scattered light. The scattered light having a frequency different from that of the incident light (inelastic scattering) is used to construct a Raman spectrum. Thus, Raman spectra arise due to inelastic collision between an incident monochromatic radiation and the molecules of a sample. Briefly, when a monochromatic radiation strikes a sample, it scatters in all directions after its interaction with sample molecules. Much of this scattered radiation has a frequency which is equal to the frequency of the incident radiation and constitutes Rayleigh scattering. Only a small fraction of

the scattered radiation has a frequency different from the frequency of the incident radiation and constitutes Raman scattering. When the frequency of the incident radiation is higher than the frequency of the scattered radiation, stoke lines appear in the Raman spectrum. But when the frequency of the incident radiation is lower than the frequency of the scattered radiation, anti-stoke lines appear in the Raman spectrum. Scattered radiation is usually measured at right angle to the incident radiation [82, 90].

Raman spectroscopy is a widely used tool for the characterization of carbon products, especially considering the fact that conjugated and carbon-carbon double bonds lead to high Raman intensities [91]. The Raman spectra of all carbon systems show only a few prominent features, no matter the final structure. The spectra appear deceivingly simple: just a couple of very intense bands in the 1000–2000 cm^{-1} region and few other second-order modulations. However, their shape, intensity and positions allow distinguishing the type and property of carbon materials, giving as much information as that obtained by a combination of other lengthy and destructive approaches. The peculiar dispersion of the π electrons in graphene is the fundamental reason why Raman spectroscopy in carbon is always resonant and, thus, a powerful and efficient probe of their electronic properties, not only of their vibrations [92].

Graphene and related materials are routinely examined with Raman spectroscopy. The Raman spectra of graphene materials are simple, containing few peaks, but are unfortunately not so simple to interpret. There are two Raman active modes in a defect-free graphene lattice, viz. E_{2g} (stretching) and A_{1g} (breathing), often assigned to the G- and D-peak, respectively. The assignment of the D and G peaks is straightforward in the "molecular" picture of carbon materials. These bands are present in all poly-aromatic hydrocarbons. The G peak is due to the bond stretching of all pairs of sp^2 atoms in both rings and chains. The D peak is due to the breathing modes of sp^2 atoms in rings [92-94].

3.3.4. Energy Dispersive X-Ray Spectroscopy (EDS)

Energy dispersive X-ray spectroscopy (EDS or EDX) is an analytical technique used for elemental analysis and chemical characterization of a sample. All elements from atomic number

4 (Be) to 92 (U) can be detected in principle, although not all instruments are equipped for 'light' elements (Z < 10). The application of EDS includes material evaluation and identification, contamination identification, spot detection analysis of regions up to 10 cm in diameter, quality control screening, and others. EDS relies on the investigation of a sample through interactions between electromagnetic radiation and matter, analyzing X-rays emitted by the matter in response to being hit with charged particles. Its characterization capabilities are due to in large part to the fundamental principle that each element has a unique atomic structure allowing a unique set of peaks on its electromagnetic emission spectrum. To stimulate the emission of characteristic X-rays from a specimen, a high-energy beam of charged particles (electrons or protons) or a beam of X-rays, is focused onto the sample being studied. The incident beam may excite an electron in an inner shell, ejecting it from the shell while creating an electron hole. An electron from an outer, higher-energy shell then fills the hole, and the difference in energy between the higher-energy shell and the lower energy shell is released in the form of an X-ray, Figure 8. The number and energy of the X-rays emitted from a specimen can be measured by an energy-dispersive spectrometer. As the energies of the X-rays are characteristic of the difference in energy between the two shells and of the atomic structure of the emitting element, EDS allows the elemental composition of the specimen to be measured [95, 96].

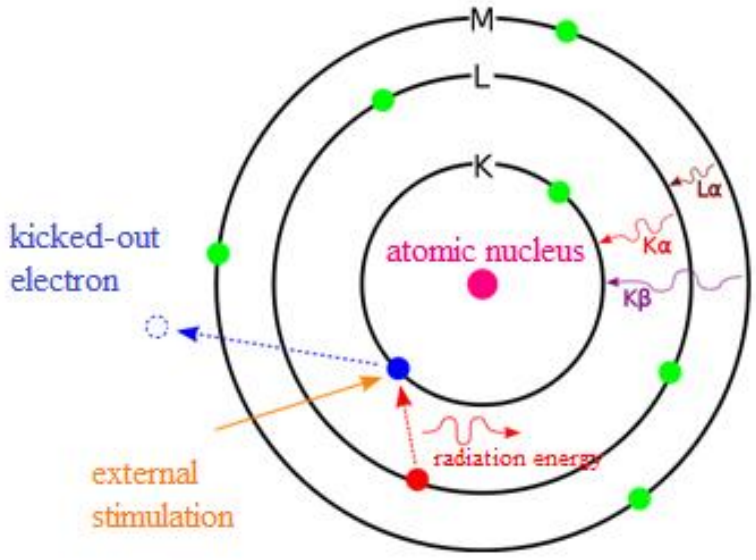

Figure 8. X-ray generation by specific electron jumps

3.3.5. Transmission Electron Microscopy (TEM)

Microscopy plays an important role in the examination of nanomaterials. Light cannot be used to see the nano-world, as its resolution is limited by its own wavelength, so optical microscopes are useless for nanotechnology. Electron microscopes use electrons instead of photons, because electrons have a much shorter wavelength than photons and so allow observing matter with atomic resolution. Generally, there are two types of electron microscopes, transmission electron microscope (TEM) and scanning electron microscope (SEM) [97]. TEM is an imaging technique whereby a beam of electrons is focused onto a specimen causing an enlarged version to appear on a fluorescent screen or layer of photographic film, or to be detected by a sensor such as a CCD camera [98]. In TEM, electrons penetrate an ultra thin specimen, interacting with the specimen as it passes through and are then imaged by appropriate lenses, in broad analogy with the biological light microscope. When electrons are accelerated up to high energy levels, few hundreds keV, and focused on a material, they can scatter or backscatter elastically or inelastically, or produce many interactions, which are sources of different signals such as X-rays, Auger electrons or light. An image is formed from the interaction of the electrons transmitted through the specimen; the image is magnified and focused onto an imaging device [83, 98]. Dropping of dispersed particles onto a TEM grid followed by drying is a common sample preparation strategy used during the investigation of nanomaterials in TEM [99].

TEM has proved invaluable for examining the ultrastructure of metals such as crystalline defects. With a modern TEM it is even possible to image individual atomic planes or columns of atoms. A resolution of 0.2 nm is achieved with modern TEM. This is the typical separation between two atoms in a solid and this resolution is 1,000 times greater than a light microscope and about 500,000 times greater than that of a human eye. Although most modern TEMs use an electron accelerating voltage between 100 kV and 300 kV, a few high-voltage instruments have been constructed with accelerating voltages as high as 3 MV. TEM is capable of displaying magnified images of a thin specimen, typically with a magnification in the range 10^3 to 10^6. In addition, the instrument can be used to produce electron-diffraction patterns, useful for analyzing the properties of a crystalline specimen [83].

3.3.6. Scanning Electron Microscopy (SEM)

The characterization of the morphology of nanoparticles is becoming a task to be performed not only at a transmission electron microscope but also more and more at modern, high-resolution SEMs. A SEM is perhaps the mostly widespread analytical instrument available in analytical laboratories destined to characterize physical properties such as morphology, shape, size or size distribution of materials at the microscale and nanoscale. The performance of a modern high-resolution SEM, in particular its spatial resolution, allows the identification and even accurate morphology characterization of nanoparticles down to below 10 nm [96].

SEM is a technique of electron microscopy that produces high resolution images of a sample surface. It is a powerful microscopic technique in which the image of the sample surface is produced by scanning it with a high-energy beam of electrons in a raster scan pattern. Figure 9 depicts the different type of interactions produced when the incident electron beam strikes the sample specimen. The electrons interact with the atoms that make up the sample producing signals that contain information about the surface topography, composition and other properties of the sample such as electrical conductivity. SEM images have a characteristic three-dimensional appearance and are useful to show the surface structure of the target sample [98]. One limitation of TEM is that, unless the specimen is made very thin, electrons are strongly scattered within the specimen, or even absorbed rather than transmitted. This constraint has provided the incentive to develop electron microscopes that are capable of examining relatively thick (bulk) specimens. In TEM, electrons are indeed reflected" (backscattered) from a bulk specimen. But another possibility is for the incoming (primary) electrons to supply energy to the atomic electrons that are present in a solid, which can then be released as secondary electrons. These electrons are emitted with a range of energies, making it more difficult to focus them into an image by electron lenses. However, there is an alternative mode of image formation that uses a scanning principle: primary electrons are focused into a small-diameter electron probe that is scanned across the specimen, making use of the fact that electrostatic or magnetic fields, applied at right angles to the beam, can be used to change its direction of travel. By scanning simultaneously in two perpendicular directions, a square or rectangular area of a specimen (known as a raster) can be covered and an image of this area can be formed by collecting

secondary electrons from each point on the specimen. In general, the secondary electron mode yields an image with a three-dimensional appearance while the backscattered electron mode yields an image that relates brightness to composition and is thus useful for general phase identification. A modern SEM provides an image resolution typically between 1 nm and 10 nm, not as good as a TEM but much superior to light microscope [83, 95].

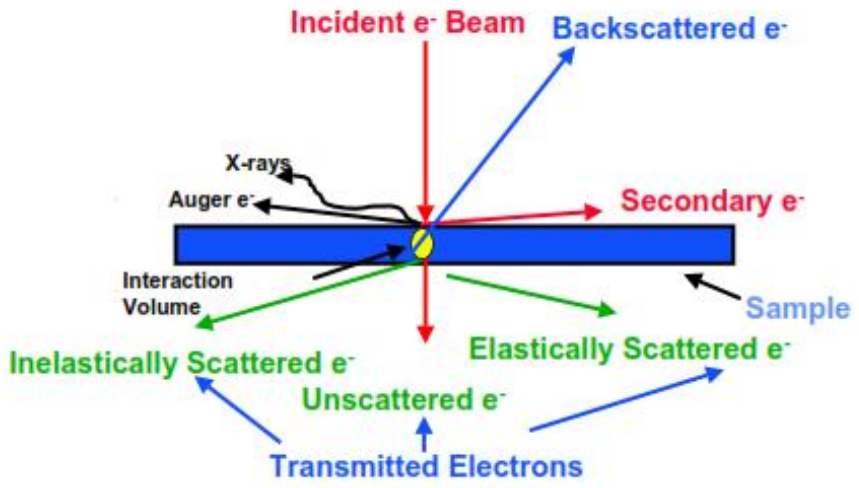

Figure 9. Various signals produced when an incident electron beam enters the specimen

3.3.7. Selected-Area Electron Diffraction (SAED)

In selected-area electron diffraction (SAED), a parallel beam (plane wave travelling in one direction) interacts with the sample. An aperture is used to define the area from which the diffraction pattern from a thin sample is to be recorded. This aperture is typically located in the first image plane below the sample. Typical size of an area studied by SAED is a few hundreds of nanometers. SAED diffraction patterns are either simple spot patterns corresponding to single-crystal diffraction or ring patterns corresponding to powder diffraction from multiple crystals with a variable orientation. Each ring corresponds to atomic planes of different orientation and different interplanar spacing (d spacing). SAED is commonly used for phase identification, determination of structural intergrowth, determination of growth directions, etc. Lattice parameters from SAED have accuracy of about 5%, and due to multiple diffraction, kinematically forbidden reflections are often present [83, 100].

4. Experimental

4.1. Chemicals and Reagents

All the chemicals and reagents used in this study were of analytical grade and used as received without any further purification. Double distilled water and/or ultrapure water from a Milli-pore Mill Q system was used throughout the preparation of solutions. Ibuprofen (≥98%), theophylline (≥99%), caffeine, epinephrine, diclofenac sodium, ethambutol dihydrochloride, ascorbic acid (≥95%), uric acid (99%), acetaminophen (98%), isoniazid, urea, glucose, lactose, magnesium acetate and sodium nitrate, nickel chloride (98%), graphite powder (<20 µm), hydrogen peroxide (30%), sulfuric acid (95-98%), hydrochloric acid (37%), and sodium hydroxide pellets (98%) were obtained from Sigma-Aldrich. Carbon nanotubes, multi-walled (>90% carbon basis), synthesized by chemical vapor deposition (CVD) and graphene oxide, 2 mg mL^{-1}, dispersed in H_2O were purchased from Sigma-Aldrich (USA). L-aspartic acid from Pharmacos Ltd (England) and potassium permanganate (99%, Merck) were used without further purification.

Acetate buffer solution (ABS) of 0.25 M prepared from anhydrous sodium acetate (BDH Chemicals Ltd, England) and acetic acid (≥99.8%, Sigma-Aldrich, Germany) and phosphate buffer solution (PBS) of 0.1 M prepared from Na_2HPO_4 and NaH_2PO_4 were used as supporting electrolytes. Hydrochloric acid (0.1 M) and sodium hydroxide (0.1 M) solutions were used to adjust the pH of the supporting electrolyte to the desired value. $K_3Fe(CN)_6$ (BDH Chemicals Ltd, England) in KCl was used during measuring the electroactive surface area and as a probe for electrochemical impedance spectroscopic measurements (EIS). For real sample analyses, two commercial pharmaceutical brands of ibuprofen formulations (Daehwa, Korean and Cadila, Indian), Panadol extra (GSK Dungarvan, Ireland) containing caffeine (65 mg $tablet^{-1}$) and adrenaline injection (1 mg mL^{-1}) (Greenfield Pharmaceutical, Jiangsu, China) were purchased from a local drug store from Addis Ababa, Ethiopia. Diclofenac sodium (DIC) (labeled 50 mg $tablet^{-1}$) and rifafour e-275 tablets (275 mg $tablet^{-1}$ in ethambutol) were obtained from a local pharmacy in Cape Town, South Africa. Green tea sample (Ethio Agri-CEFT PLC) was purchased from a local super market in Addis Ababa, Ethiopia.

4.2. Apparatus and Instruments

All the electrochemical experiments for the determination of ibuprofen, epinephrine and simultaneous determination of caffeine and theophylline were performed using CHI760D electrochemical workstation (CHInstruments, USA). For the voltammetric determination of diclofenac and ethambutol, PalmSens compact electrochemical interfaces (Palm Instruments BV, The Netherlands) interfaced to a PC were employed. Electrochemical impedance spectroscopic experiments were performed on a CHI760D electrochemical workstation (CH Instruments, Inc., Austin, Texas, USA) and ZAHNER EIS machine (Germany) supported with THALES software. All experiments were carried out using a conventional three electrode system with a bare or modified glassy carbon electrode (GCE, 3 mm in diameter) as a working electrode, a platinum wire as an auxiliary electrode, and a silver/silver chloride (Ag/AgCl, KCl, saturated) as a reference electrode. Hence, all the voltammetric results were reported with respect to Ag/AgCl in this study. Alumina micropolish (1, 0.3, and 0.05 µm) and polishing pads (Buehler, USA) were used for electrode polishing. Electrode cleaning after each polishing of the GCE was carried out in an ultrasonic cleaner (YJ 5120-B, Shanghai, China). The pH measurements were carried out using a pH meter (sensION, SHA Snilu Instruments CO. LTD, China). All electrochemical measurements were made at room temperature (22±2 ^{o}C) under atmospheric conditions (without inert gas bubbling).

LAMBDA 950 UV/Vis/NIR (USA) and Thermo Scientific Nicolet Evolution 100 (Thermo-Electron Corporation, UK) UV-Visible spectrophotometers were used for UV-Vis measurements. Fourier transform infrared, FT-IR, spectra were recorded on powder samples (pellet formed using KBr) using Spectrum 65 FT-IR, (PerkinElmer, USA) and Spectrum Two FT-IR (PerkinElmer, USA) spectrometer. Raman spectroscopy experiments were performed by using the XploRA HORIBA model Edge filter with gratings 600–2400 lines/mm. Backscattering geometry wavelengths were 532 nm and 676 nm. Raman spectrometer was coupled to a confocal microscope (adjustable pinhole) and motorized XYZ Table (0.1 µm steps).

SEM analysis were performed using high resolution scanning electron microscope (AURIGA, Field Emission Gun High resolution scanning electron microscope (FEG HRSEM, Zeiss)),

coupled with Energy Dispersive Spectroscope (EDS) for elemental analysis. Samples were coated for viewing with carbon to enhance the conductivity of the membrane. Screen printed electrodes were employed for the electrodeposition of ERGO and NiNPs/ERGO composite for HRSEM measurement. High resolution transmission electron microscopy (HRTEM, FEI Tecnai G2 F20 X-Twin 200 kV field-emission gun) equipped with energy dispersive X-ray spectrometer (EDS) was used to characterize the synthesized materials. Powder samples were dispersed in ethanol by ultrasonication for about 10 min and one drop of the sample suspension were cast onto transmission electron microscope (TEM) copper grids and left on the grids to evaporate the solvent under a Xenon lamp for 10 min.

4.3. Preparation of Standard Solutions

Stock standard solutions of all the drugs in this study were freshly prepared immediately prior to the experiments in appropriate solvents. Stock solutions of ibuprofen standards were prepared in ethanol. All working standard solutions of ibuprofen were prepared in 0.25 M acetate buffer. During analysis, the pH of sample solutions was maintained at 4 using 0.25 M acetate buffers. Similarly, stock solutions of caffeine and theophylline standards were prepared in double distilled water and all working standard solutions were prepared in 0.1 M PBS.

Standard solution of epinephrine (1 mM) was prepared daily in double distilled water. The working standards were prepared by dilution in 0.1 M PBS (pH 4). Diclofenac solutions were prepared in ultrapure water by ultrasonication for 30 min followed by dilution in 0.1 M PBS (pH 4.0) to get the final working standard solutions. Ethambutol standards were also first dissolved in ultrapure water to get the stock standard solutions. The working standards were then obtained by dilution in 0.1 M PBS pH 7.

4.4. Preparation of Real Samples

4.4.1. Pharmaceutical Formulations

4.4.1.1. Ibuprofen Formulations

Ibuprofen tablet formulations were obtained from a local drug store for real sample analysis. Each tablet contained a dose of 400 mg tablet^{-1} of IBP as a substantial and electrochemically active component of the tablet as certified by the manufacturer in the drug information leaflet. Ten tablets were completely ground to a fine powder and homogenized in a mortar and a weight corresponding to one tablet was dissolved in ethanol using an ultrasonic bath for 30 min. The mixture was filtered through a filter paper to obtain a clear filtrate and then quantitatively transferred into a 100 mL volumetric flask. To obtain final concentrations in the range of the calibration curve, the sample solutions were suitably diluted with the supporting electrolyte.

4.4.1.2. Panadol Extra

Ten tablets of Panadol extra containing caffeine (65 mg tablet^{-1}) were ground into fine powder, mixed and homogenized in agate mortar. The weight equivalent to one tablet was accurately weighed and dissolved in 25 mL double distilled water by ultrasonication for 30 min. Then, the solution was filtered using Whatman filter paper to obtain a clear filtrate and then quantitatively transferred into a 50 mL volumetric flask. To obtain final concentration in the range of the calibration curve, the sample solutions were appropriately diluted with the supporting electrolyte.

4.4.1.3. Adrenaline Injection

Adrenaline injection (1 mg mL^{-1}, ≈ 4.55 mM) was obtained from a local pharmacy and was diluted with the supporting electrolyte to obtain the final concentration in the range of the calibration curve. 5 mL of this solution was taken and transferred to 25 mL volumetric flasks. After spiking with different concentrations of the EP standard, the whole solution was further diluted to the mark using PBS. Finally, the blank, the unknown and the spiked samples were transferred separately into a voltammetric cell to determine EP without further treatment. The

peak current response was measured using SWV under the optimized conditions and the standard addition method was used to determine EP in the real sample. All solutions were kept in a refrigerator at 4 ^{o}C in the dark.

4.4.1.4. Diclofenac Sodium

Five tablets of diclofenac sodium (labeled 50 mg tablet^{-1}) were finely powdered and homogenized using a mortar and pestle. A weight equivalent to one tablet was transferred to a 100 mL volumetric flask and dissolved using ultrapure water by ultrasonication for 30 min. The content of the flask was filtered using a Whatman filter paper to obtain a clear filtrate which was further diluted using the buffer solution to obtain the final concentration within the linear range of the proposed method. The solutions were stored in a refrigerator for further use.

4.4.1.5. Rifafour

Rifafour (rifafour e-275) tablet, a drug that is used to treat tuberculosis, is a combination of four first line drugs: rifampicin (150 mg), isoniazid (75 mg), pyrazinamide (400 mg) and ethambutol (275 mg), typically given at the early stages of tuberculosis. Five tablets of rifafour containing ethambutol as one of the active ingredient were finely powdered, mixed and homogenized thoroughly. Then, a weight equivalent to one tablet was weighed and dissolved in 250 mL ultrapure water by ultrasonication for 30 min. The solution was filtered twice using a Whatman filter paper. Finally, the solution was appropriately diluted to get the final concentration in the linear range of the calibration curve.

4.4.2. Blood Samples

Human blood sample was obtained from a healthy volunteer (with no known health problems and who was not taking the drug under study) at a nearby clinic (Silasie Higher Clinic, Addis Ababa, Ethiopia) by a physician. The blood sample was collected using appropriate vials provided by the clinic and stored in the refrigerator until analysis. About 5 mL fresh blood sample was taken and centrifuged at 1500 rpm for 20 min to remove all precipitating materials. The blank serum sample was prepared by diluting 0.5 mL of the serum to 25 mL with pH 4.5

phosphate buffer [161]. To prepare the spiked samples, 0.5 mL of the serum was transferred to 25 mL volumetric flask containing 10 mL of PBS. After spiking with different concentrations of TP and CF, the mixture solution obtained was diluted to the mark using 0.1 M PBS pH 4.5. Then, the blank and spiked serum samples were transferred to a voltammetric cell to detect TP and CF by the proposed SWV method without any further pretreatment. The standard addition method was used for the determination of TP and CF in all the real samples.

4.4.3. Urine Samples

Human urine sample was obtained from a healthy volunteer in sterilized plastic containers and stored in a refrigerator immediately after collection until analysis. The samples were filtered using Whatman filter paper (0.45 µm pore size) and 5 mL of the sample aliquot was measured and transferred to a 50 mL volumetric flask. Then, an appropriate quantity of the standard drug solutions were added and diluted to the mark with the appropriate working buffer solutions to make the final concentration. The solutions were transferred into a voltammetric cell to be analyzed without any further pretreatment. The standard addition method was used for the determination of drugs in the urine samples.

4.4.4. Green Tea Samples

About 5 g of green tea sample (Ethio Agri-CEFT PLC), purchased from a local super market, was weighed and transferred into 50 mL of boiling water for 30 min to extract TP and CF. After filtration, the filtrate was collected in a 100 mL volumetric flask and diluted to the mark with double distilled water. Before the measurements the filtrate was diluted with the supporting electrolyte by a factor 1:100 (*v/v*).

4.5. Preparation of L-Aspartic Acid Solution

The solution of L-aspartic acid was prepared by dissolving appropriate quantity of L-aspartic acid in distilled water followed by dilution in 0.1 M PBS pH 6 to get a final concentration of 2 mM L-aspartic acid.

4.6. Functionalisation of MWCNTs

MWCNT is hydrophobic in nature and hence difficult to disperse in an aqueous solution to get a homogeneous mixture [101]. In order to obtain a uniform dispersion, strong interactions between the carbon nanotubes and the GC surface and achieve stable and uniform films of MWCNTs on the GCE surface, MWCNTs were functionalized by refluxing in a mixture of 3 M H_2SO_4 and 3 M HNO_3 (3:1 by volume) at 100 ºC for 6 h in a reflux condenser. The functionalisation also helps in removing catalyst impurities present and generates more surface functional groups. The carbon atoms at the edge plane as well as at the defect sites on the basal plane undergo oxidation during acid treatment producing –COOH groups [102]. After cooling slowly to room temperature, the acid treated MWCNTs were washed several times by centrifugation at 3,500 rpm with double distilled water until the filtrate was neutral and then dried at 60 ºC in an oven for 24 h. The functionalized MWCNTs were designated as f-MWCNTs. A uniform dispersion of the functionalized MWCNTs in deionized water was prepared by dispersing 10 mg of f-MWCNTs in 5 mL of water by ultrasonication for 30 min.

4.7. Synthesis of Nickel Nanoparticles (NiNPs)

A 0.5 g of nickel chloride was dissolved in 50 mL ethylene glycol. Then, 5 mL hydrazine monohydrate was added to the above solution followed by addition of 36 mL of 1 M NaOH solution. The whole solution was kept under a magnetic stirrer for 1 h at 60 ºC. After 1 h the reaction was completed and black nickel nanoparticles were formed. The initial green color of the Ni^{2+} solution first turned to blue upon addition of hydrazine monohydrate and sodium hydroxide which was followed by formation of a black color, indicating the formation of Ni nanoparticles. The nanoparticles were collected and washed several times with ethanol and once with acetone and dried overnight in an oven. N_2 gas was continuously bubbled up in the reaction mixture which creates N_2 atmosphere during the reaction. Hence, no extra N_2 gas was required for the synthesis of nickel nanoparticles. The reduction reaction can be expressed as follows [103]:

$$2Ni^{2+} + N_2H_4 + 4OH^- \rightarrow 2Ni\,(s) + N_2 + 4H_2O \qquad (9)$$

4.8. Synthesis of Graphene Oxide (GO)

Graphene oxide was synthesized from graphite powder according to Hummer's method [104], with some necessary modifications. In brief, graphite powder (2 g) and sodium nitrate (1 g) were mixed with sulfuric acid (50 mL) in a dry clean conical flask and stirred at room temperature for 30 min, followed by mixing in an ice bath for 20 min. Potassium permanganate (6 g) was added gradually over 30 min period with constant stirring. The resulting solution was allowed to reach room temperature prior to being placed in a water bath set at 35±5 ºC and stirred for 2 hours. The flask was returned to the ice bath with constant stirring and 150 mL of ultrapure water was added before addition of 10 mL hydrogen peroxide (H_2O_2), until the effervescence ceased. The flask was removed from the ice bath and was left to stir overnight at room temperature. Finally, the solution was centrifuged for 20 min and washed successively three times with 5% HCl followed by three times with ultrapure water. The resulting dark brown product was dried for 72 hours in a vacuum oven at 60 ºC.

4.9. Preparation of Modified Electrodes

4.9.1. Poly(L-Aspartic acid) Modified Glassy Carbon Electrode

The modified electrode was prepared according to literature reports [105-107] with slight modifications of the conditions. Prior to modification, a bare GCE was polished to a mirror-like finish with alumina slurries of 1.0, 0.3 and 0.05 µm successively on Buehler polishing cloth, thoroughly rinsed, and sonicated for 5 min in ethanol and double-distilled water in sequence by ultrasonication to remove residual polishing material from the electrode surface. Then, the electrode was treated by cyclic scanning to stabilize in the potential window of –0.80–0.80 V in 0.1 M H_2SO_4. After each step, the electrode was rinsed with water and ethanol, and dried at room temperature. Using this pre-treated electrode, cyclic voltammetry was performed in pH 6.0 PBS containing 2 mM L-aspartic acid in the potential range of 1.0–1.7 V at a scan rate of 100 mV s^{-1} for 20 cycles to polymerize L-aspartic acid on the electrode. Then, the electrode was rinsed with ethanol, water and 0.1 M PBS (pH 6.0), to remove any physisorbed and unreacted materials from the electrode surface, and then dried at room temperature. The electrode prepared was denoted as P(L-Asp)/GCE and stored in 0.1 M PBS (pH 6.0) at room temperature.

4.9.2. Poly(L-Aspartic Acid)/Functionalized Multi-Walled Carbon Nanotubes Modified Electrode

First, f-MWCNTs modified GCE was fabricated by drop casting 20 µL of f-MWCNTs suspension (following optimized procedure) onto a well polished GCE surface and left to dry in an open air. To prepare the polymer/f-MWCNTs-composite modified electrode, poly(L-aspartic acid) was grown on the f-MWCNTs/GC electrode potentiodynamically by scanning the potential in the range of –1.0–1.7 V at a scan rate of 100 mV s^{-1} for 20 cycles in pH 6.0 PBS containing 2.0 mM L-aspartic acid. The modified electrode was rinsed repeatedly with distilled water and cycled in a monomer free PBS until a stable voltammogram was obtained. The poly(L-Asp)/f-MWCNTs composite film modified GCE was rinsed with distilled water, and then dried at room temperature. The electrode prepared, denoted as P(L-Asp)/f-MWCNTs/GCE, was kept in PBS (pH 6.0) at room temperature prior to use.

4.9.3. Poly(L-Aspartic Acid)/Electrochemically Reduced Graphene Oxide Modified Electrode

To prepare poly(L-aspartic acid)/electrochemically reduced graphene oxide composite modified glassy carbon electrode, (P(L-Asp)/ERGO/GCE), 7.5 µL of GO suspension was coated on a clean GCE surface by drop casting and allowed to dry in an open air. After drying, the GO coated GCE was placed in 2 mM L-aspartic acid monomer solution and the poly(L-aspartic acid) was grown by cyclic scanning in the range of –1.0–1.8 V at a scan rate of 100 mV s^{-1} for 20 cycles in pH 6.0 PBS. The modified electrode was rinsed repeatedly with distilled water and cycled in a monomer free PBS (pH 6.0) until a stable voltammogram is obtained. The P(L-Asp)/ERGO composite film modified GCE was rinsed with distilled water, and then dried at room temperature. For comparison, GO, P(L-Asp) and ERGO modified GC electrodes were prepared similarly.

4.9.4. Nickel Nanoparticles Decorated Electrochemically Reduced Graphene Oxide Modified Electrode

For the preparation of nickel nanoparticles (NiNPs) decorated electrochemically reduced graphene oxide (ERGO) nanocomposite, 10 mg of each synthesized NiNPs and GO was weighed

and dispersed in 10 mL of 0.1 M phosphate buffer solution pH 7 by ultrasonication for 2 h. Then, the GO dispersion decorated with the NiNPs was electrodeposited onto the surface of GCE by cyclic voltammetry in the potential window of –1.5 to 0.3 V for 15 cycles. The reduction peak of GO almost disappears after 12 cycles. Hence, 15 cycle of electrodeposition was taken as the optimum. The electrode obtained was marked as NiNPs/ERGO/GCE. For comparison, ERGO/GCE was prepared by electrodeposition of GO in the same way without NiNPs while NiNPs/GCE was prepared by drop casting of NiNPs dispersion onto GC surface.

5. Results and Discussion

5.1. Square Wave Voltammetric Determination of Ibuprofen at Poly(L-Aspartic acid) Modified Glassy Carbon Electrode

5.1.1. Background

The development of pharmaceuticals has brought a radical change in improving the human health. These pharmaceuticals would serve their purpose only if they are free from impurities and are administered in an appropriate amount [108]. Thus, the analysis of pharmaceuticals is an integral and vital part of the overall drug development process [70]. Ibuprofen (IBP), α-methyl-4-(2-methylpropyl)-benzene acetic acid, Scheme 2, is the third most common non-prescription, non-steroidal anti-inflammatory drug (NSAID) used in reducing inflammation and pain associated with many diseases. It is one of the most potent orally active antipyretic and analgesic drugs used extensively in the treatment of acute and chronic pain, fever, osteoarthritis, dysmenorrhea, rheumatoid arthritis, headaches, migraine, muscle aches, tooth aches, postoperative pain and ankylosing spondylitis and other musculoskeletal disorders. Furthermore, IBP has an anti-platelet effect and is known as a blood-thinning drug. The conventional dose of this NSAID is 600–1200 mg per day [109-116]. IBP is the active ingredient of a variety of oral medicines in tablets, gel pellets and syrup forms that are used worldwide due to their higher efficiency, better tolerability and lower gastrointestinal adverse effects and toxicity than other NSAIDs [117-119].

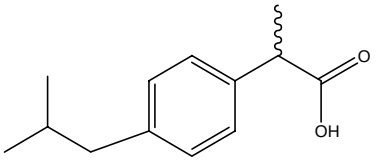

Scheme 2. The chemical structure of ibuprofen

Ibuprofen is rapidly absorbed after orally administered (within 45 to 95 min) and is extensively bound to plasma proteins (99%) with a relatively short elimination half-life (55 to 150 min). It is metabolized by oxidation in the liver to produce two major metabolites: hydroxy-ibuprofen (2-[4-(2-hydroxy-2-methylpropyl)phenyl]propionic acid) and carboxy-ibuprofen (2-[4-(2-carboxypropyl)phenyl]propionic acid). These metabolites, as well as up to 10% of ibuprofen are excreted in urine [120]. Ibuprofen exerts its pharmacologic actions by inhibiting cyclooxygenase

and hence blocks the first step in the production of prostaglandins. High level of ibuprofen inhibits the migration, adherence, swelling as well as aggregation of neutrophils and the discharge of lysosomal enzymes. High doses of ibuprofen, taken constantly for 4 years, significantly slowed the decline of pulmonary function in patients with cystic fibrosis and mild lung disease. It has been shown to delay the progression of lung disease without serious adverse effects in patients with cystic fibrosis. For ibuprofen to achieve the desired inhibitory effect on neurophil activation and migration, peak plasma concentration (C_{max}) of 50 to 100 mg L^{-1} had to be reached. Preliminary study suggests that when ibuprofen concentration is very low, the opposite effect may occur and the influx of neurophils increases. IBP is excreted in the form of various conjugates, e.g. hydroxy-IBP, carboxy-IBP and carboxy-hydratropic acid that causes high acute toxicity. They are also suspected of endocrine disrupting activity in humans and wildlife [120, 121]. Therefore, the determination of IBP in pharmaceutical formulations and biological fluids is of paramount importance.

A number of analytical techniques have been reported in the literature for the determination of ibuprofen in pharmaceutical samples and biological fluids, including chromatographic [109, 110, 113, 122-128], electrophoretic [129-131], spectroscopic [117-119, 132-135] and spectrofluorimetry [136]. Although these methods are sensitive and reliable, almost all are complex and expensive requiring expertise in handling the instruments in addition to time-consuming sample pretreatment steps. Therefore, it is important to develop a simple, cheap, portable instrumentation for direct field applications and user friendly method free from exhaustive sample pretreatment and sophisticated instrumentation [109, 114, 137]. Electroanalytical techniques have played a significant role in the analysis of drugs and pharmaceuticals as they are simple, economical, rapid, selective and sensitive when compared with most of the aforementioned methods. Among the electroanalytical methods, voltammetry coupled with pulse waveform (such as SWV) is considered as a highly sensitive technique with very low detection limit attributed to zero background current [137-139]. A survey of the literature indicates only few reports on the electrochemical determinations of ibuprofen that include: determination of ibuprofen in water using silver-doped zeolite-expanded graphite composite electrode [114], ultrasensitive ibuprofen nanoaptasensor prepared by covalent attachment of aptamer to electrochemically deposited gold nanoparticles on glassy carbon

electrode [115], disposable screen printed graphite electrode for the direct electrochemical determination of ibuprofen in surface water [137], simultaneous determination of paracetamol and ibuprofen in pharmaceutical samples by differential pulse voltammetry using a boron-doped diamond electrode [139], electrochemical oxidation of ibuprofen and its voltammetric determination at a boron-doped diamond electrode [140], electrochemical detection and degradation of ibuprofen from water on multi-walled carbon nanotubes-epoxy composite electrode [141] and silver-functionalized carbon nanofiber composite electrodes for ibuprofen detection [142].

Electrochemical techniques have been widely studied and much interest has been focused on the use of carbon as cheap substrate [143]. However, direct electrochemical detections at conventional bare carbon electrodes usually show drawbacks such as high activation overpotential, slow kinetics, electrode fouling, low selectivity, and poor sensitivity. In this regard, chemically modified electrodes (CMEs) have opened up great possibilities. These electrodes are assembled by means of deliberate and systematic surface modification of an electrode with a variety of redox mediators. These compounds facilitate charge transfer between the electrode and electroactive species in solution at much lower potentials [143, 144]. Polymer-modified electrodes prepared by electropolymerization have received extensive interest in the detection of analytes because of their selectivity, sensitivity, and homogeneity in electrochemical deposition, strong adherence to the electrode surface and high chemical stability [145].

L-aspartic acid, $C_4H_7NO_4$, an amino acid which contains two carboxyl groups (-COOH) and one amino group ($-NH_2$), can be electrochemically polymerized on GCE by cyclic voltammetry and forms a membrane surface rich with negative charge [34]. The application of poly(L-aspartic acid)-modified glassy carbon electrode for the electrochemical determination of some biological molecules like epinephrine [34], dopamine and norepinphrine [105], 2,4-dinitrophenol and 2,5-dinitrophenol [106], hydroquinone and catechol [146], has been reported. The fabrication of a polyaspartic acid modified gold electrode for electrochemical reaction of Cytochrome C [147] and poly(aspartic acid)-nanogold modified electrode for the simultaneous determination of dopamine, ascorbic acid and uric acid [26] have been described. These reports indicated that the polymer film of polyaspartic acid can be easily deposited on the electrode surface by

electrooxidation of its monomer, and the modified electrodes have exhibited excellent electrocatalytic effects towards the compounds reported. Here we report the construction and successful application of P(L-Asp)/GCE for the detection of ibuprofen in pharmaceutical formulations and biological fluids.

5.1.2. Electropolymerization of L-Aspartic Acid on GCE

The P(L-Asp)/GCE modified electrode was prepared according to the procedure described in Section 4.9.1. Figure 10 shows the CV curves for the electropolymerization of L-aspartic acid on the GC electrode in 0.1 M PBS pH 6.0. The oxidation peak current at higher potential region increased with the number of cycles, indicating that a conductive polymer film has been coated on the GC electrode surface. Furthermore, the electrode was rinsed with distilled water and a gray color P(L-Asp) film was observed on the electrode surface which also confirms the formation of an electroconductive polymer on the surface of GCE. According to the literature [26, 105, 107], the L-Asp monomer is oxidized first at a higher positive potential to form α-amino free radicals, and these cation radicals can form carbon–nitrogen links at the carbon electrode surface, and then the P(L-Asp) films are formed (Scheme 3). The effect of the polymer film thickness on the oxidation of IBP was investigated by varying the number of polymerization cycles from 5 to 30 and taking the voltammetric measurements each time. The response of the modified electrode showed a general increase in the oxidation peak currents for IBP with increasing film thickness up to 20 cycles and then remained constant up on increasing the number of cycles indicating saturation of the film growth, Inset of Figure 10. Therefore, 20 cycles of polymerization was taken as the optimum polymer film thickness for subsequent measurements.

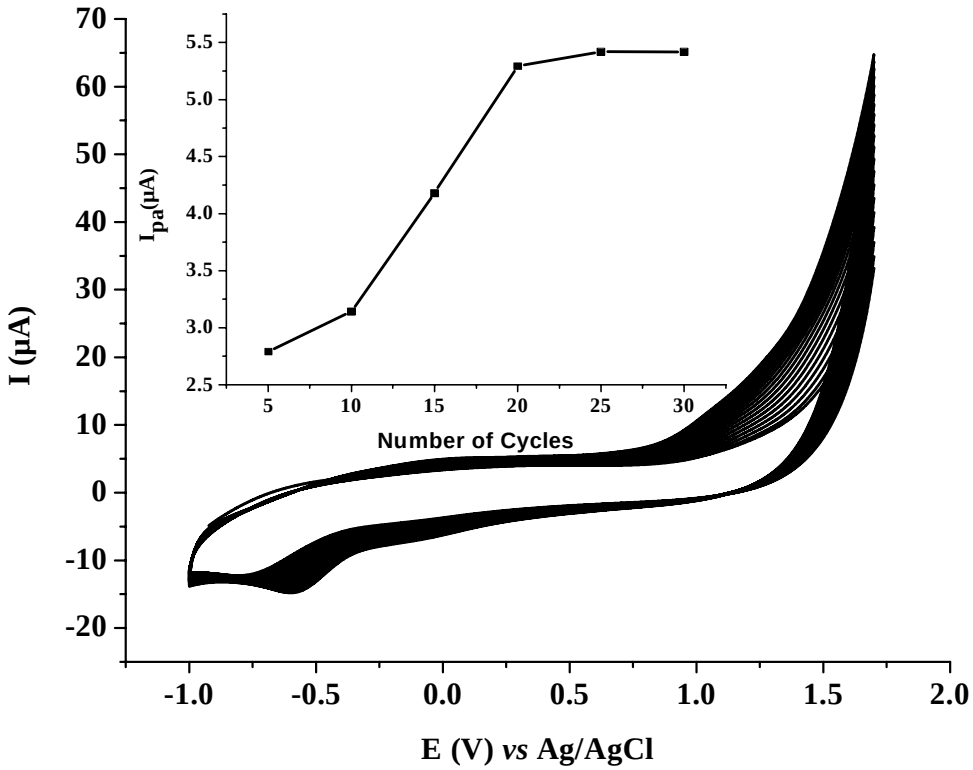

Figure 10. Cyclic voltammetric polymerization of 2 mM L-aspartic acid in 0.1 M PBS (pH 6) supporting electrolyte at GCE between the potentials –1.0 and 1.7 V for 20 cycles at scan rate of 100 mV s^{-1}. Inset: The effect of polymer film thickness on the peak current of 0.1 mM IBP at P(L-Asp)/GCE at scan rate of 100 mV s^{-1}

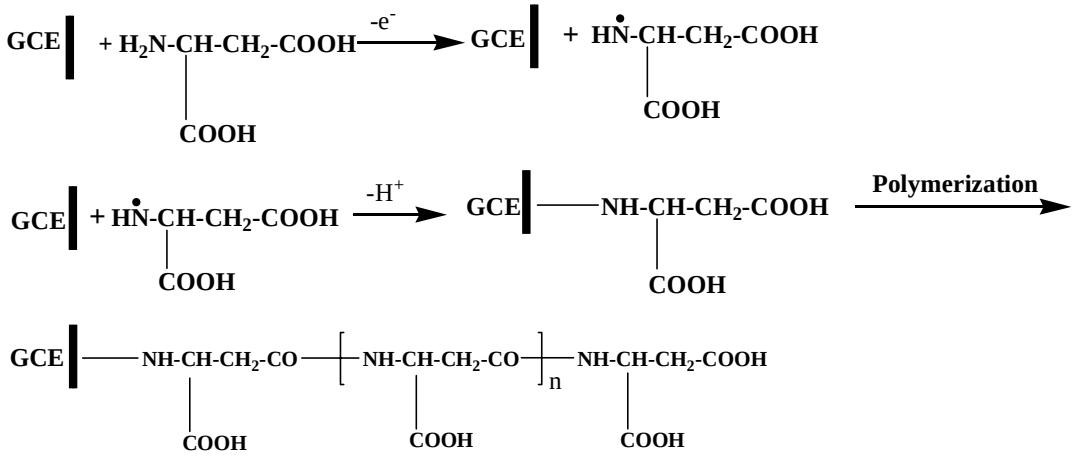

Scheme 3. The electropolymerization of L-aspartic acid on glassy carbon electrode [105,107]

5.1.3. Estimation of the Electroactive Surface Area

Electrode reaction rates and most double layer parameters are extensive quantities and have to be referred to the unit area of the interface. Knowledge of the real surface area of electrodes is therefore needed. Obviously, the electroactive surface area of an electrocatalyst is related with its geometric surface area. Accordingly, the higher the exposed surface, the higher currents are measured across the electrode–solution interface. Nevertheless, the true importance of the electroactive area is that it reveals which portion of the surface remains available to species in solution for the transfer of charge. Strictly speaking, it measures the efficiency of the exposed surface towards the electrocatalytic reaction [148, 149].

In order to investigate whether the prepared P(L-Asp)-modified GCE film could increase the surface area and hence the conductivity of the sensor, the electroactive surface area (A) of the bare GCE and P(L-Asp)-modified glassy carbon electrode were determined by cyclic voltammetry (CV) using 1 mM $K_3Fe(CN)_6$ as a probe at different scan rates. For a reversible process, the Randles-Sevcik formula, equation (1) [69, 150], has been used to calculate the electroactive surface area. For 1 mM $K_3Fe(CN)_6$ in 0.1 M KCl electrolyte, n = 1, $D_R = 7.6 \times 10^{-6}$ $cm^2\ s^{-1}$. Both the anodic and cathodic peak currents of the bare GCE and P(L-Asp)-modified electrode were proportional to the square root of the scan rate. Therefore, with the constant parameters of D_R, C_o and n, we could successfully obtain an approximate value of A according to the Randles-Sevcik equation. From the slope of the plot of I_p versus $v^{1/2}$, the electroactive area was calculated. For the bare GCE, the electroactive surface area of the electrode was found to be 3.36–3.58 mm^2 and, for P(L-Asp)-modified GCE, the surface area was 4.6–5.3 mm^2. Thus, the electroactive surface area after modification, which measures the efficiency of the exposed surface towards the catalytic reaction, was increased by about 37–47% compared to the bare GCE, which provided an evidence for the superior conductivity of P(L-Asp)-film as expected.

5.1.4. Electrochemical Impedance Analysis of P(L-Asp)/GCE

Electrochemical impedance spectroscopy (EIS) is a very versatile and powerful technique for characterizing charge transfer processes taking place at the surface of modified and unmodified electrodes [137]. The semicircle diameter at higher frequencies in the Nyquist plot of EIS can be

used to describe the interfacial properties of the electrode. Its value varies when different substances are adsorbed on the electrode surface. The EIS Nyquist spectra usually include two parts, semicircular and linear, Figure 11A. The semicircular part which is located at higher frequencies represents a charge-transfer-limited process (faradaic process) whereas the linear part positioned at lower frequencies is characteristic of a diffusion-limited process [36, 137].

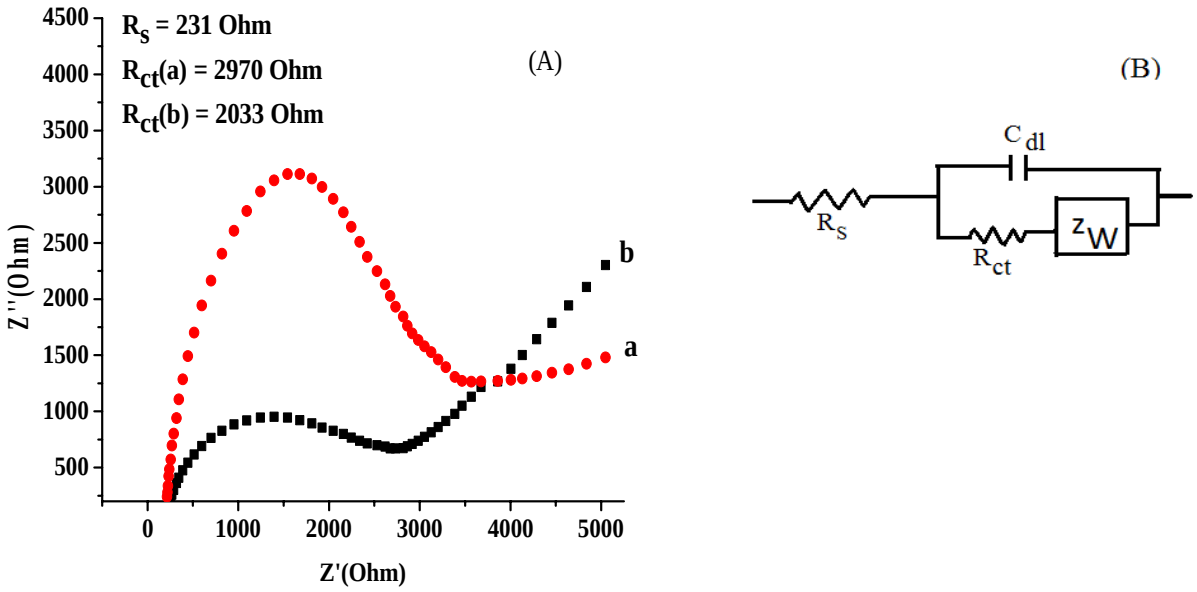

Figure 11. (A) Nyquist plots of EIS obtained at bare GCE (a) and P(L-Asp)/GCE (20 cycles) (b) in 5 mM $Fe(CN)_6^{-3/-4}$ (supporting electrolyte 0.1 M KCl). Frequency: 100 kHz–0.01 Hz; perturbation amplitude: 10 mV. (B) Randles equivalent circuit used for data evaluation

Figure 11A displays the EIS Nyquist spectra of 5 mM $Fe(CN)_6^{-3/-4}$ at bare GCE and P(L-Asp)/GCE in 0.1 M KCl. The EIS results were fitted based on the Randles equivalent circuit shown in Figure 11B. This equivalent circuit consists of the ohmic resistance of the electrolyte solution (R_s), the charge transfer resistance (R_{ct}), the Warburg impedance (Z_w) and the double layer capacitance (C_{dl}). As shown in Figure 11A, the semicircle diameter of the Nyquist plot of the polyaspartic acid modified electrode, which represents the charge transfer resistance (R_{ct}) is about 2033 Ω, is less than that of the bare glassy carbon electrode, 2970 Ω. The higher R_{ct} value of the bare GCE shows a slow charge transfer rate. A lower charge transfer resistance observed for the grafted electrode could be due to the increase of the roughness and the preconcentration of the redox probe on the pinholes of the attached film. Hence, the electron transfer process of

the redox probe is easier and occurs at longer distances when the polymer film is present. These results are also in good agreement with the CV and electroactive surface area measurements and provide evidence for the successful immobilization of P(L-Asp) film on the GCE.

5.1.5. Electrochemical Behavior of IBP

Figure 12 shows the characteristic cyclic voltammograms of 0.1 mM IBP in 0.25 M acetate buffer (pH 4) recorded at bare GCE (b) and P(L-Asp)/GCE (c) in the potential range of 0 V to 1.5 V *vs* Ag/AgCl. The absence of a reduction peak on the reverse scan shows irreversible chemical oxidation of IBP at both bare and modified GCE with peak potentials at around 1.4 V and 1.2 V, respectively. The oxidation signal of IBP at the bare GCE was poor and appeared at a higher potential. Whereas, at the P(L-Asp)/GCE, the oxidation of IBP yielded a very sharp and well defined peak at about 1.2 V (*vs* Ag/AgCl). Moreover, the peak potential shifted to a less positive value by about 200 mV at the P(L-Asp)-modified GCE under the same conditions. As compared to the bare GCE a significant increase in the peak current response was observed which confirms the catalytic role played by the polyaspartic acid film at the modified electrode which facilitates the electron transfer. The good properties of the poly(L-aspartic acid) film are ascribed to its three-dimensional structure and the rich carboxyl groups [105]. Having been polymerized in PBS, poly(L-aspartic acid) formed a conductive polymer film on the electrode surface. Hence, the nitrogen and oxygen atoms in ploy(L-aspartic acid) film may interact with –COOH group of IBP molecule to form hydrogen bonding, which weakened the bond energy of hydroxyl group in IBP and made it easier for IBP to adsorb on the surface of the modified electrode. Thus, the concentration of IBP adsorbed on the electrode surface is increased, and therefore the oxidation signals of IBP were enhanced significantly. Therefore, the rate of electron transfer is accelerated and the current is increased. Moreover, the catalytic effect of the polymer film of P(L-Asp) can be attributed to the increased effective surface area of the P(L-Asp)-modified GCE. The electrochemical behavior of IBP was also investigated using square wave voltammetry (SWV) at both electrodes and similar results were obtained in terms of peak current enhancement and peak potential shifts, Figure 13.

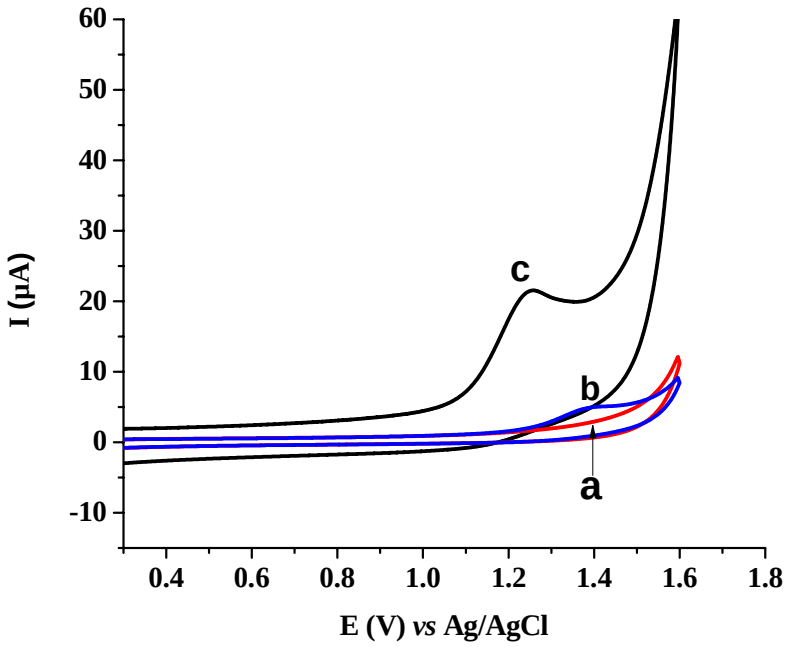

Figure 12. CVs of the supporting electrolyte (a) and 0.1 mM IBP (b, c) at bare GCE (b) and P(L-Asp)/GCE (a, c) in 0.25 M of acetate buffer (pH 4.0) at scan rate of 100 mV s^{-1}

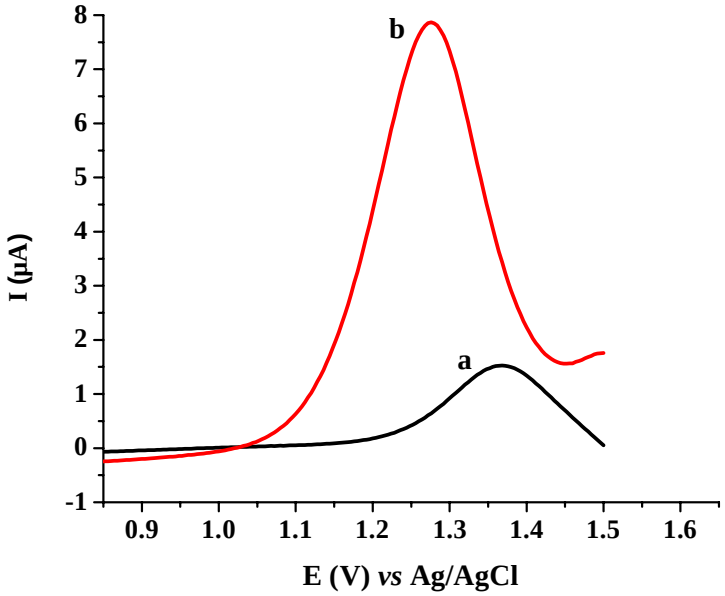

Figure 13. SWVs of 0.1 mM IBP in 0.25 M of acetate buffer (pH 4.0) at bare GCE (a) and P(L-Asp)/GCE (b)

5.1.6. The Effect of pH

The effect of pH on the voltammetric signals for ibuprofen oxidation was investigated in 0.25 M acetate buffer solution (ABS) in the pH range 3.0 to 6.0 using cyclic voltammetry. It was noted that the current response and the peak potential of IBP significantly changed with increasing pH from 3.0 to 6.0 which shows that the oxidation of IBP is pH dependent. As shown in Figure 14, the oxidation peak current of IBP increased with increasing pH from 3.0 to 3.5 and then a gradual decrease in pH was observed from 3.5 to 6.0. A decrease in the peak current response for IBP with increasing pH revealed that the detection of IBP at the P(L-Asp)/GC electrode is feasible only in an acidic medium. Though, the maximum oxidation peak current response was obtained at pH 3.5, pH 4.0 was selected for further study by considering the stability of the peak current response of IBP and effective buffering capacity region of ABS.

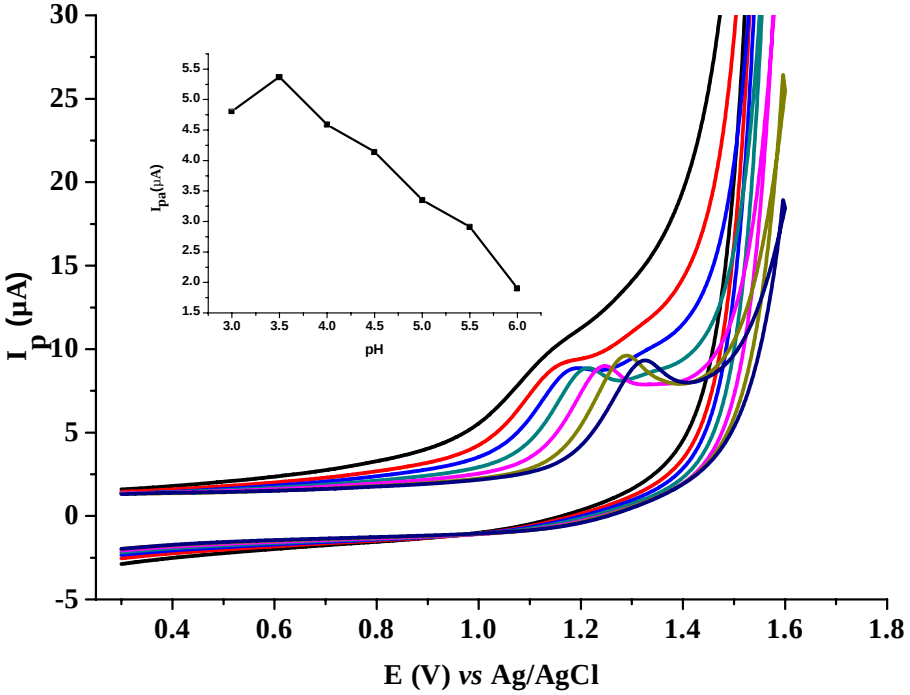

Figure 14. CVs of 50 µM IBP at different pH values (3.0–6.0) at P(L-Asp)/GCE in 0.25 M of acetate buffer at scan rate of 100 mV s^{-1}. Inset: The plot of peak currents *vs* pH

The oxidation peak potential of IBP was also affected by a change in pH (Figure 14). The peak potential shifted negatively with increase in pH value from 3.0 to 6.0. This result suggests the involvement of protons in the electrode process. A linear relationship was observed between the

oxidation peak potential and the pH with a regression equation of: E (V) = –0.062pH + 1.5, R^2 = 0.993, Figure 15. A slope of 62 mV/pH suggests that the electrode process involves the transfer of equal number of protons and electrons. The proposed electrochemical oxidation mechanism of IBP is similar to the one verified for naproxen [114, 139, 151, 152] and its mechanism possibly involves a single-electron transfer *via* radical cation formation that can be stabilized through the formation of resonance structures following decarboxylation reaction, Scheme 4.

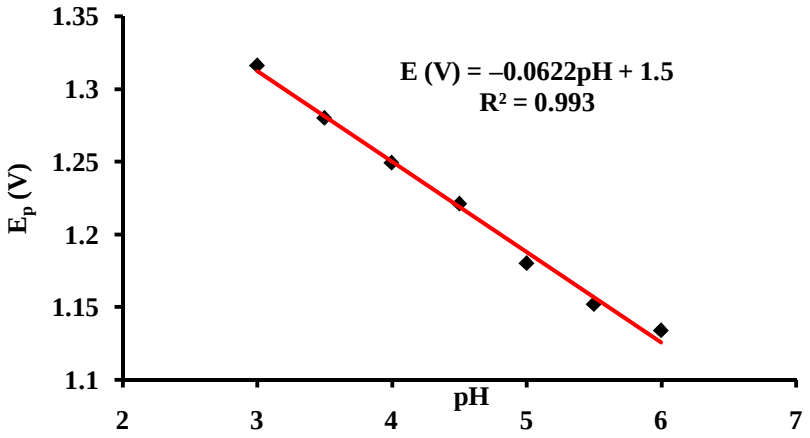

Figure 15. Plot of peak potentials of 50 µM IBP as a function of pH at P(L-Asp)/GCE in 0.25 M of acetate buffer at scan rate of 100 mV s^{-1}

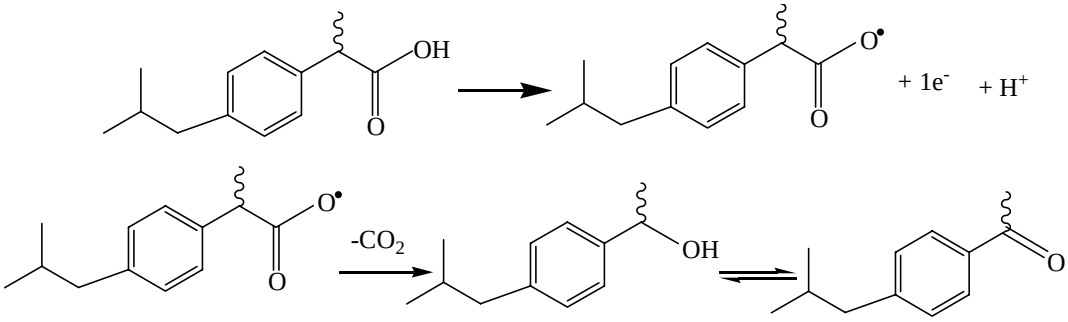

Scheme 4. A proposed mechanism for the oxidation of IBP

5.1.7. The Effect of Scan Rate

The effect of potential scan rate on the oxidation current of ibuprofen was investigated by cyclic voltammetry (Figure 16) in acetate buffer pH 4 containing 50 µM IBP. The plot of the oxidation peak current of ibuprofen *vs* scan rate in the range 25–300 mV s^{-1} (Inset of Figure 16) is linear with a regression equation of: I_{pa} (µA) = 0.0246*v* (mV s^{-1}) + 0.485; with R^2 value of 0.999.

Moreover, the study of log I *vs* log *v*, with a regression equation: log I (µA) = 0.83log *v* – 7.2, R^2 = 0.997 gives the slope value of 0.83 which is closer to 1. Additionally, the peak potential slightly shifted to the positive direction with increasing scan rates. These results suggests that the electrochemical oxidation of IBP at the surface of P(L-Asp)/GCE is predominantly an adsorption controlled irreversible process.

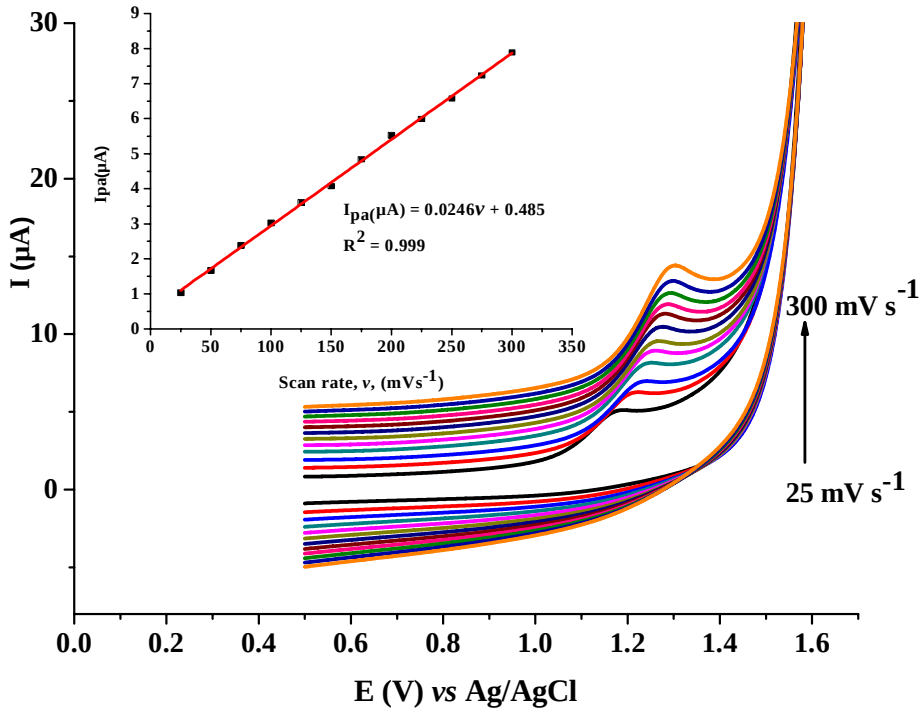

Figure 16. CVs of 50 µM of IBP at P(L-Asp)/GCE at scan rates of 25–300 mV s^{-1} in ABS pH 4. Inset: peak current of ibuprofen *vs* scan rate

5.1.8. The Effect of Accumulation Potential and Time

Since the oxidation of IBP at the surface of P(L-Asp)/GCE is an adsorption controlled process, the effect of accumulation potential and time were studied using SWV. The effect of accumulation potential was studied by varying the accumulation potential from 1.0 to 0.5 V with 60 s accumulation time. However, the peak current response of 0.1 mM IBP was almost unchanged, indicating that the accumulation potential has no significant effect on the oxidation peak current of ibuprofen at the P(L-Asp)-modified GCE. Thus, an open circuit accumulation was employed for subsequent measurements.

The effect of accumulation time was also studied in the range of 0 to 120 s at an open circuit accumulation potential. The peak current increased with accumulation time from 0 to 60 s and reached a maximum value around 60, Figure 17. Upon increasing the accumulation time beyond 60 s the oxidation peak current of IBP remains almost constant. Therefore, an open circuit accumulation time of 60 s was employed for subsequent study in this work.

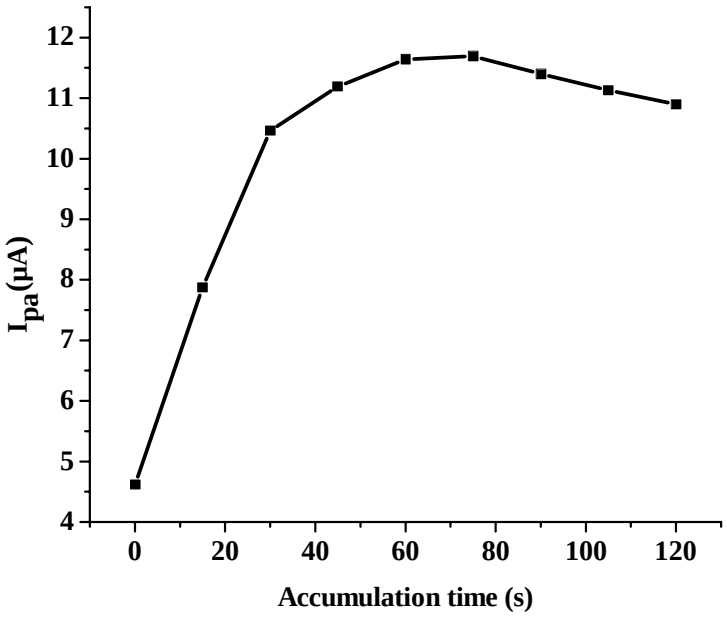

Figure 17. The effect of accumulation time on the oxidation peak current of 0.1 mM IBP at P(L-Asp)/GCE

5.1.9. Optimization of SWV Parameters for IBP Determination

Square wave parameters were evaluated in order to obtain the highest signal for ibuprofen oxidation. The dependence of the peak current on SW parameters was studied in the range of: step potential (1–15 mV); amplitude (10–120 mV) and frequency (10–100 Hz) by keeping two of these parameters at constant value while measuring the other. By considering the optimum signal and good square wave voltammetric peak shape for IBP, the optimized parameters were 4 mV step potential; 25 mV amplitude and 15 Hz frequency.

5.1.10. Determination of IBP

Under the optimum conditions, the square wave voltammetric responses for different concentrations of IBP were recorded in 0.25 M acetate buffer solution pH 4, Figure 18. The anodic peak current is linearly related to IBP concentration in the range of 1 to 150 µM with a regression equation of: I_{pa} (µA) = 0.031C (µM) + 0.15 and R^2 = 0.996 (Figure 18, Inset). The limit of detection, LOD, (*3s/m*) and limit of quantification, LOQ, (*10s/m*), (where *s* is the standard deviation of the blank and *m* is the slope of the calibration curve), were found to be 0.22 µM and 0.74 µM, respectively. These values were compared with similar studies reported in the literature, Table 1. As shown in the table, the analytical performance of the presently modified electrode shows promising result in terms of simultaneously providing higher sensitivity and wider linear range when compared to most of the chemically modified electrodes reported for the determination of IBP (Table 1). Furthermore, the preparation of the P(L-Asp) modified electrode is a one step simple procedure and avoids complicated surface modification steps.

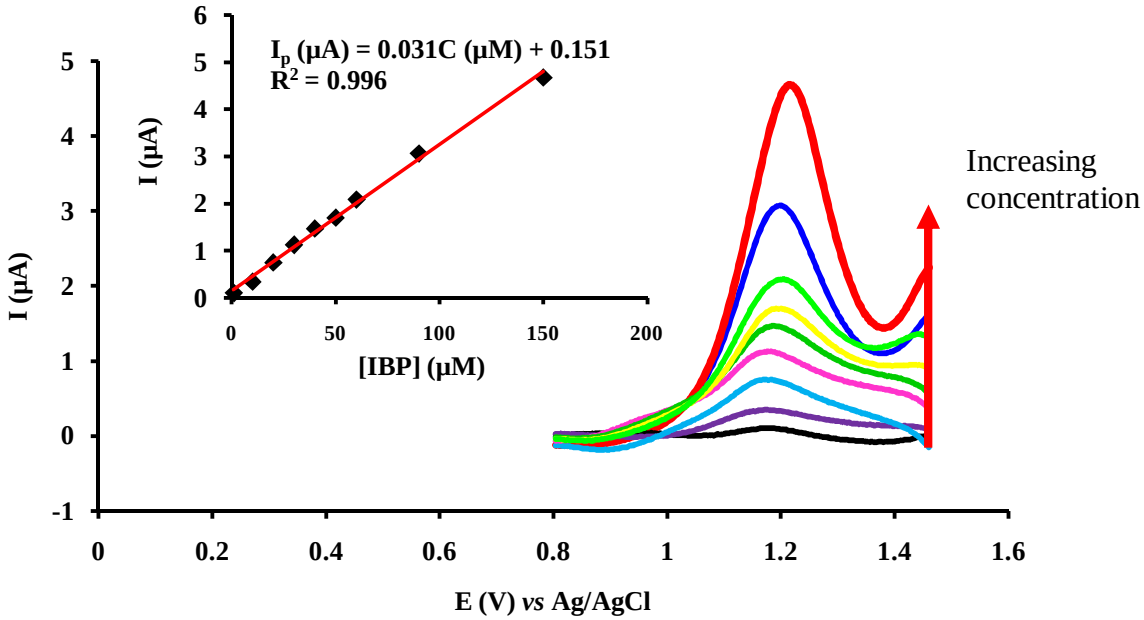

Figure 18. SWVs for varying concentrations of IBP (background subtracted): 1, 10, 20, 30, 40, 50, 60, 90 and 150 µM in 0.25 M ABS pH 4 at P(L-Asp)/GCE. Inset: The corresponding calibration curve of peak current *vs* ibuprofen concentrations

Table 1. Comparison of the proposed method with other electrochemical methods used for the determination of IBP

Electrode	Analyte	Linear range (µM)	LOD (µM)	Method	Real sample	Reference
[a]AgZEG	IBP	4.8–48	0.15	DPV	–	[114]
			0.048	SWV		
[b]Pretreated SPGE	IBP	–	0.4	SWV	Waste and river water	[137]
[c]BDDE	PC & IB	20–400	3.8	DPV	Pharmaceutical formulations	[139]
BDDE	IBP	20–400	5.0	DPV	Pharmaceutical formulations	[140]
[d]AgZMWCNT	IBP	9.7–48.4	0.4	DPV	Tap water	[141]
		9.7–29.1	1.5	SWV		
[e]AgZCNF	IBP	2.4–24	0.043	SWV	–	[142]
P(L-Asp)/GCE	IBP	1–150	0.22	SWV	Pharmaceutical tablet and human urine	[This study]

[a]Ag-doped zeolite-expanded graphite composite electrode; [b]Screen printed graphite electrodes; [c]Boron-doped diamond electrode; [d]Silver-modified zeolite-multi-walled carbon nanotube-epoxy composite electrodes; [e]Silver-functionalized zeolite modified carbon nanofiber-epoxy composite modified electrode.

5.1.11. Repeatability, Reproducibility and Stability of the Modified Electrode

To investigate the repeatability of the electrochemical responses of the P(L-Asp)/GCE for 0.1 mM of IBP in 0.25 M acetate buffer solution, several consecutive measurements were conducted. The relative standard deviation of eight successive measurements was found to be 3.1%, which indicates good repeatability of the electrode. Similarly, the reproducibility of the method was estimated by comparing the peak current responses of three different modified electrodes prepared following similar procedure. A RSD of 4.0% was obtained for the peak current response of 0.1 mM of IBP, showing a very good reproducibility of the developed method. The stability of the modified electrode was also evaluated by measuring the current response for IBP at the P(L-Asp)/GCE daily for one week. After 7 days the electrode retained 91.5% of its original activity which shows good stability of the modified electrode which rules out the possibility of significant fouling and deactivation of the electrode.

5.1.12. Interference Study

The influence of various potentially interfering substances in the determination 0.1 mM of IBP was studied under the optimum conditions. The potentially interfering substances were among those commonly found with IBP in pharmaceutical formulations and/or in biological fluids. The oxidation peak currents of IBP were compared before and after addition of the following potential interferents: ascorbic acid (AA), uric acid (UA), caffeine, glucose, lactose, Mg^{2+} and Na^{+} and the results are shown in Table 2. The percent changes in the peak currents was less than 5% for the studied substances except for caffeine. This indicates that the electrode exhibited no response to a number of potentially interfering ionic and non ionic excipients usually used in the manufacturing of the pharmaceutical formulations or are present in biological fluids. According to the results ascorbic acid (AA), uric acid (UA), glucose, lactose, Mg^{2+} and Na^{+} did not show interference in the determination of IBP, but caffeine showed significant interference, even at equimolar concentrations. This can be attributed to the redox potential of caffeine which overlaps with that of ibuprofen as proved by a magnified peak at the redox potential of IBP. Thus, the separation of caffeine is recommended prior to the electrochemical determination of ibuprofen. Uric acid shows a slight interference when present at concentrations of 10 fold or higher than that of IBP. In general, the P(L-Asp)/GCE has good selectivity and can be used for the determination of IBP without significant interferences.

Table 2. Effect of interferents on the determination of IBP at P(L-Asp)/GCE under the optimum conditions, (average of three determinations)

Interferent	Concentration, µM	Response change (%)
Ascorbic acid (AA)	100	3.3
	1000	4.8
Uric acid (UA)	100	4.3
	1000	26.1
D-Glucose	100	4.4
	1000	2.1
Lactose	100	3.6
	1000	4.7
Mg^{2+}	100	1.6
	1000	3.1
Na^{+}	100	0.14
	1000	0.7

5.1.13. Analytical Application

The practical application of the developed sensor was demonstrated by determining ibuprofen in two commercial pharmaceutical tablet formulations (Korean and Indian brands). The experimentally detected values and the labeled values were compared, Table 3. It was found that the results obtained using the proposed sensor are in good agreement with labeled amounts with RSD ≤ 3%. Therefore, it is recommended that the proposed sensor can be utilized successfully for the determination of IBP in pharmaceutical preparations. Moreover, the accuracy and reliability of the proposed method was checked by spiking the pharmaceutical tablet formulations and human urine samples with appropriate quantity of the standard IBP and calculating the percent recovery values. The samples were prepared according to section 4.4.1.1 and standard addition method was used for the assay of IBP in these samples. The results are shown in Table 3. As can be seen from the table, the recovery results lie between 90.0% and 108%, indicating that the effect of the sample matrix is not significant and hence the P(L-Asp) modified electrode has excellent potential to be used in real sample analysis.

Table 3. Recovery results of the determination of IBP in commercial tablets and urine samples at P(L-Asp)/GCE

Sample	Specified content (mg/tablet)	*Found± %RSD (mg/tablet)	%Detected	Detected (µM)	Added (µM)	*Found± %RSD (µM)	Recovery (%)
IBP-K**	400	391±2	97.7	30.5	60	89.3±2	98.0
					100	127±4	96.4
IBP-I**	400	379±3	94.8	29.4	60	85.7±4	93.8
					100	119 ±4	90.0
Urine					60	62.5±6	104
		–			100	108±3	108

*Average of three determinations; **Korean and Indian*

5.2. Simultaneous Determination of Caffeine and Theophylline Using Square Wave Voltammetry at Poly(L-Aspartic Acid)/Functionalized Multi-Walled Carbon Nanotubes Composite Modified Electrode

5.2.1. Background

Xanthines are purine bases which are known to act as anti-depressants, anti-therapeutic and anti-hyperuraemic agents [153]. Caffeine (1,3,7-trimethylxanthine), theophylline (1,3-dimethylxanthine) and theobromine (3,7-dimethylxanthine), (Scheme 5), are xanthines that are widely found in the human diet. These compounds naturally occur in food products such as tea, coffee, and cocoa beans and, therefore, in the food and beverages made from them [154-159]. They have received increased attention in the food industry because they can cause various physiological effects. Very recently, xanthine derivatives such caffeine and theophylline have been identified as micromolar inhibitors of bacterial family, thereby opening up potential applications for such molecules as fungicides and nematocides, and renewing interest in their use as asthma therapeutics [160].

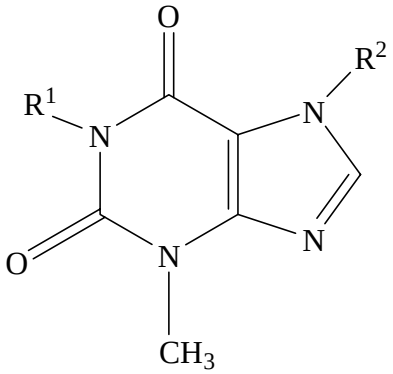

$R^1 = R^2 = CH_3$: Caffeine
$R^1 = CH_3$; R^2 = H: Theophylline
R^1 = H; $R^2 = CH_3$: Theobromine

Scheme 5. The chemical structure of methylated xanthines

Theophylline (TP) and caffeine (CF) are found in a variety of pharmaceutical products and drugs because they possess the following properties: stimulate the central nervous system, induce gastric secretions, and act as a diuretic. Studies have also been done on these alkaloids to assess their antioxidant properties [156, 157]. TP and CF also display multiple pharmacological effects, such as enhancing cognitive function, increasing endurance, and reliving from anxiety. However, excessive intake of such compounds has been associated with several negative side effects ranging from simple tremor and tachycardia to cancer and even death [161].

Theophylline has been widely used for pharmaceutical purposes as a bronchodilator drug in the treatment of asthma and chronic obstructive pulmonary disease due to its cheapness and effectiveness [162]. TP relaxes and opens the air passages to the lungs, making it easier to breathe. This drug is used mainly in solid oral dosage forms, particularly slow release forms, and has a narrow therapeutic index, requiring regular monitoring of serum theophylline concentrations to avoid adverse effects [163]. Caffeine is a psychoactive substance in daily human life and plays an important role in food and drug chemistry. It is probably the most frequently ingested pharmacologically active substance in the world. Caffeine stimulates the central nervous system, cardiac muscle, the respiratory system, and gastric secretion. It is used both recreationally and medically to reduce physical fatigue and restore mental alertness when unusual weakness or drowsiness occurs. However, high amounts of CF can cause trembling, nausea, nervousness and seizures and mutation effects such as inhibition of DNA [164, 165].

Thus, the investigation and determination of theophylline and caffeine not only have clinical significances but can also give beneficial guidance to people's health and life [161]. Since TP and CF usually coexist in real samples, the development of a selective and sensitive method for their simultaneous determination is highly desirable for analytical and diagnostic applications.

Various methods exist for the determination of theophylline and caffeine in different matrices such as food, drinks, clinical samples and pharmaceutical products. The most widely used analytical techniques are mainly chromatography, such as liquid chromatography and gas chromatography with various detectors [166-173], spectroscopy [174-180], and electrochemical methods. Nevertheless, some of these methods, such as chromatography and spectroscopy, are expensive and time-consuming since they require extensive sample pretreatment and cleanup steps. Instead, electrochemical methods are characterized by practical advantages such as operational simplicity, high sensitivity, wide linear range, good stability, low-cost instrumentation, possibility of miniaturization, suitability for real-time detection and less sensitive to matrix effects in comparison with separation and spectral methods [164, 181].

Several articles reported the electrochemical detection of TP and CF at different electrodes [182-186]. However, a key problem encountered is the overlap of the peak potentials of these species

at conventional electrodes with pronounced fouling effect, resulting in poor selectivity and reproducibility. To overcome the above problems, various chemically modified electrodes were used. Recently, chemically modified electrodes (CMEs) have become important electrochemical methods for the determination of biologically important compounds because of their good sensitivity, selectivity and stability [187]. However, only a few reports appeared for the simultaneous determination of CF and TP using CMEs [161, 188-190], including large mesoporous carbon/Nafion modified electrode [161], glassy carbon disk electrode modified with a composite consisting of poly(Alizarin Violet 3B), multiwalled carbon nanotubes and graphene [188] facile fabrication of a novel anisotropic gold nanoparticle–chitosan–ionic liquid/graphene modified electrode [189], and poly(4-aminopyridine) modified electrode [190].

Since the discovery of carbon nanotubes (CNTs) by Iijima in 1991 [191], both single wall (SWCNs) and multiwall carbon nanotubes (MWCNTs) have attracted attention because of their high electrical conductivity, extremely excellent mechanical strength, chemical stability, flexibility, low cost and other extraordinary properties. In recent times, carbon nanotubes have been widely applied in electroanalytical chemistry, particularly in sensors and biosensors, due to their ability to facilitate electron transfer reactions of target molecules when used as an electrode material [188, 192, 193].

Conducting polymer-modified electrodes have been fabricated as electrochemical sensory platforms for the detection of analytes because of their high selectivity, sensitivity, homogeneity, easy preparation, chemical stability and strong adherence of the polymer film [60]. In addition, CPs demonstrated anti-fouling ability, which is an important practical advantage over conventional electrode materials [194]. The selectivity of polymer-modified electrodes as sensors can be attained by different mechanisms such as size exclusion, ion exchange, electrostatic interaction and hydrophobic interaction [195]. Electrochemical sensors modified with electropolymerized organic polymers are reproducible and possess more active sites than conventional electrodes.

Very recently, the use of composite materials based on CPs and CNTs, polymer/CNTs modified electrodes, with the aim of combining the properties of these materials have been intensively studied as reported in the literatures. These composite materials have been shown to possess complementary properties of the individual components with a synergistic effect, demonstrating excellent electrocatalytic ability for some biological molecules. The desirable properties of CPs such as reproducibility, good stability, strong adherence, large number of active sites and homogeneity in electrochemical deposition, together with high surface area and nanoporosity of CNT films, leads to a superior performance of the resulting sensing devices [188, 196]. Thus, this work focuses on the fabrication and use of conducting polymer/functionalized-MWCNTs composite modified electrode for the simultaneous the determination of TP and CF.

5.2.2. FTIR Spectroscopic Characterization

The evidence of chemical functionalisation was confirmed by Fourier transform infrared (FTIR) spectral analyses of the pristine MWCNTs and f-MWCNTs. FTIR spectra of MWCNTs and f-MWCNTs were recorded in the range 4000–400 cm^{-1} using KBr pellets. Figure 19 shows the FTIR spectra of the pristine MWCNTs and f-MWCNTs. As seen in the figure, the increase in the intensity of all the absorption bands and the appearance of a new band at 1081 cm^{-1} for the functionalized MWCNTs compared to pristine MWCNTs is a clear evidence for the functionalisation of the carbon nano tubes. CNTs give a few bands, indicating the presence of small fractions of functional groups most likely incorporated during their synthesis. After chemical oxidation, an increase in the bands at about 3400 cm^{-1}, 1700 cm^{-1} and 1100 cm^{-1} that corresponds to carboxylic acid groups was observed. All the bands that were associated with ether, alcohol and phenol groups increase the IR intensity [38]. The absorption band at 1732 cm^{-1} corresponds to C=O stretching of COOH, while the absorption bands at 1384 cm^{-1} and 1081 cm^{-1} are associated with O–H bending and C–O stretching, respectively. The absorption band at 1583 cm^{-1} is more likely from the C=C stretching mode of carbon nanotubes. Broad absorption band at 3400–3500 cm^{-1} is attributed to –OH stretching. The increase in the intensity of these bands and the appearance of a new band suggests that the chemical functionalization of the MWCNTs have introduced more functional groups on the surface of MWCNTs. Similar observations of the FTIR spectra for f-MWCNTs were reported in the literature [197-199].

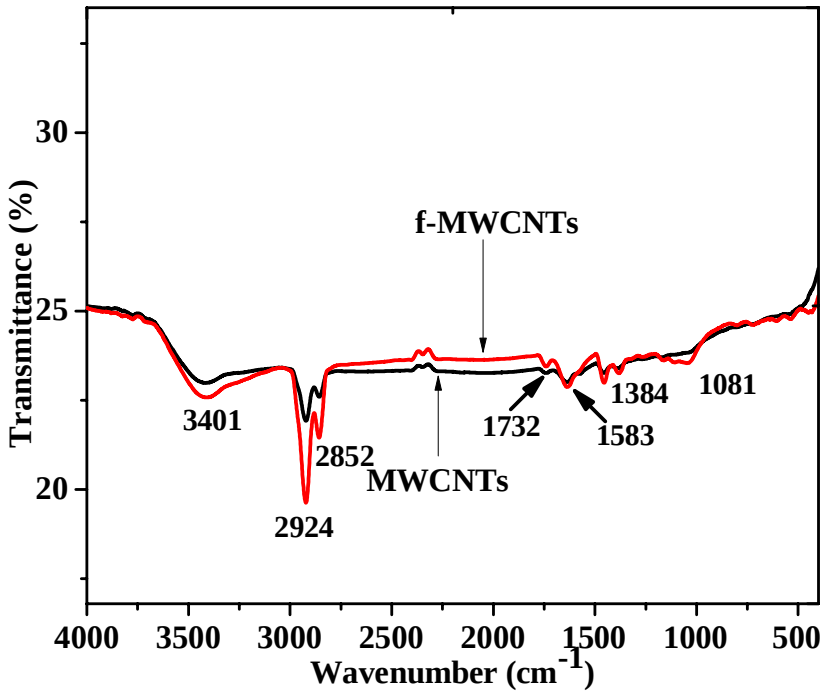

Figure 19. FTIR spectra of the pristine MWCNTs and f-MWCNTs powder samples

5.2.3. Formation of Poly(L-aspartic Acid) Film on f-MWCNTs/GCE

The poly(L-aspartic acid)/f-MWNTs/GCE was prepared according to the procedure described in the experimental section. Cyclic voltammetry (CV) was used for the electropolymerization of L-aspartic acid on bare GCE and f-MWCNTs/GCE. Figure 20 shows the CV obtained during the electropolymerization of L-aspartic acid on f-MWCNTs coated GCE. As shown in the Figure, irreversible oxidation peaks were noticed in the positive potential direction in the first sweep, followed by continuous film growth in the higher positive potential region with successive potential scanning. The growth of the film tends to be stable after 18 scans, which confirmed the formation of the poly(L-aspartic acid) film. Hence, twenty cycles of electropolymerization was selected to get a stable polymer film. Moreover, a uniform blue black film was observed on the GCE surface after modification, which demonstrated that the poly(L-aspartic acid) film was deposited on the surface of f-MWCNTs/GCE. However, for the electropolymerization of L-aspartic acid on bare GCE, no visible anodic peaks were observed in the first cycle.

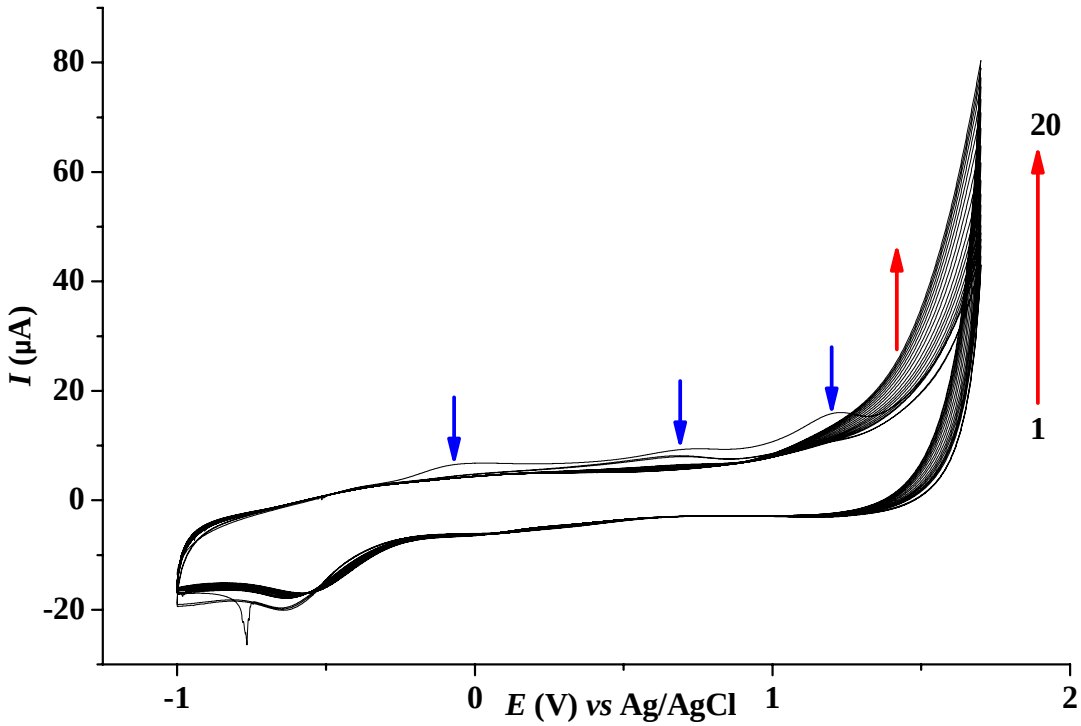

Figure 20. CVs of the electropolymerization of 2.0 mM L-aspartic acid on f-MWCNTs/GCE in 0.1 M PBS (pH 6) at scan rate of 0.1 V s^{-1}

5.2.4. Electrochemical Behavior of TP and CF

The individual electrochemical behaviors of TP and CF were investigated by cyclic voltammetry (CV). Figure 21 A and B show the CV responses of 50 µM TP and 100 µM CF in 0.1 M PBS (pH 4.5) at scan rate of 100 mV s^{-1} at bare GCE (a), P(L-Asp)/GCE (b), f-MWCNTs/GCE (c) and P(L-Asp)/f-MWCNTs/GCE (d), respectively. In all the voltammograms (Figure 21 A and B), a single oxidation peak was observed for both TP and CF with no corresponding reduction peak in the reverse potential scan, suggesting the irreversibility of the electrode reaction. In comparison to the bare glassy carbon electrode, the peak current responses of TP and CF were increased at the modified electrodes with the maximum response observed for the composite modified electrode (curve d), indicating the catalytic activity of the modified electrodes. Obviously, there is a weak peak current response observed at about 1.20 and 1.45 V for TP and CF, respectively at the bare GCE (curve a, Figure 21 A and B), representing the slow rate of electron transfer. The oxidation peak potentials were slightly shifted negatively for both TP and CF at the composite modified P(L-Asp)/f-MWCNTs/GCE.

When the bare GCE surface was coated with P(L-Asp) film, an increase in the anodic peak current of more than 2-fold of the bare electrode response was observed. Further improvement in the oxidation peak current response of about 3-fold of the bare GCE was seen upon modification with functionalized MWCNTs. This indicates the electrocatalytic effect of the polymer and nanotube modifiers used in the electro-oxidation of theophylline and caffeine. The improved electrocatalytic performance of P(L-Asp)/GCE might be attributed to the electrostatic interaction between negatively charged poly(L-aspartic acid) film [34] and the positively charged TP and CF in the slightly acidic pH of 4.5. The higher performance of the CNT modified electrode is due to the catalytic effect of f-MWCNTs which stems from the structure and unique properties they possess such as large specific surface area, strong adsorptive ability and the ability to promote electron transfer reaction. These properties make CNTs to provide enough effective reaction sites to increase the electron exchange rate when used as the electrode material in electrochemical reaction [200-202]. At the composite modified electrode, P(L-Asp)/f-MWCNTs/GCE, the result showed a further enhancement in the peak current response of about 5 fold the current obtained at the bare electrode. This result is also higher than the peak current responses obtained at the individual polymer and nanotubes modified electrodes. This clearly showed the synergic effect of the P(L-Asp) and f-MWCNTs, which effectively enhance the electrocatalytic activity of the composite modified electrode and facilitate the electron transfer rate between the analytes and the GCE. Moreover, the oxidation peak profiles of the composite modified electrode is better than both the peak profiles of the individual polymer and nanotubes modified electrode.

The electrochemical behavior of a mixture of 50 µM TP and 100 µM CF in 0.1 M phosphate buffer (pH 4.5) was investigated simultaneously by CV at scan rate of 100 mV s^{-1} (Figure 21C). The oxidation processes of TP and CF at the bare and modified electrodes are irreversible. As can be seen in Figure 21C, the voltammetric peak current responses of TP and CF are negligible at the bare GCE (curve a), indicating a slow electron transfer kinetics. Therefore, it is impossible to use the bare electrode for the simultaneous determination of the two analytes. However, the oxidation peak current responses of TP and CF were improved at the modified electrodes (Figure 21C, curve b–d) without any interference effects on one another. The maximum current response was observed at the composite modified P(L-Asp)/f-MWCNTs/GCE for both TP and CF in the

simultaneous detection of these drugs. In addition to the significant enhancement of the peak currents, the oxidation peaks of TP and CF were clearly separated, the peak potential of TP being about 250 mV lower than that of CF at the P(L-Asp)/f-MWCNT/GCE, Figure 21C (curve d). These results demonstrate that the two analytes display well separated peak potentials and can be simultaneously and sensitively determined at P(L-Asp)/f-MWCNTs/GCE.

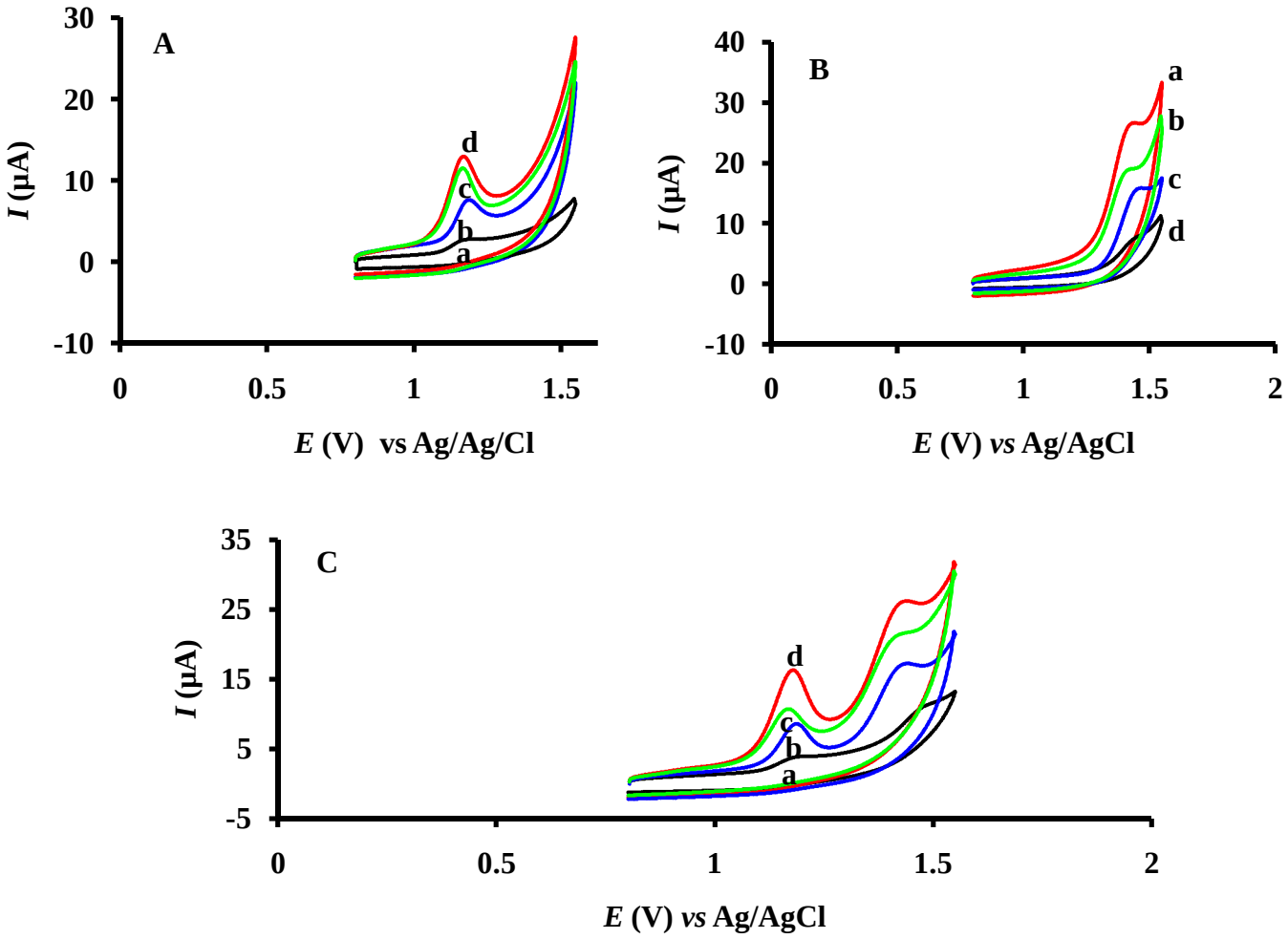

Figure 21. CVs of 50 µM TP (A), 100 µM CF (B) and a mixture of 50 µM TP and 100 µM CF (C) at bare GCE (a), P(L-Asp)/GCE (b), f-MWCNTs/GCE (c) and P(L-Asp)/f-MWCNTs/GCE (d) in pH 4.5 PBS at scan rate of 100 mV s^{-1}

5.2.5. The Effect of Amount of MWCNTs

The effect of varying the amount of f-MWCNTs suspension on the oxidation peak current response of TP and CF was studied. As shown in Figure 22, the current responses increased upon increasing the volume of the f-MWCNTs suspension up to 20 µL for both TP and CF. Above 20 µL, the oxidation current for TP seems to decrease gradually and that of caffeine remains almost constant. Therefore, 20 µL was selected as the optimum amount of f-MWCNTs suspension and was used to modify the glassy carbon electrode in this study.

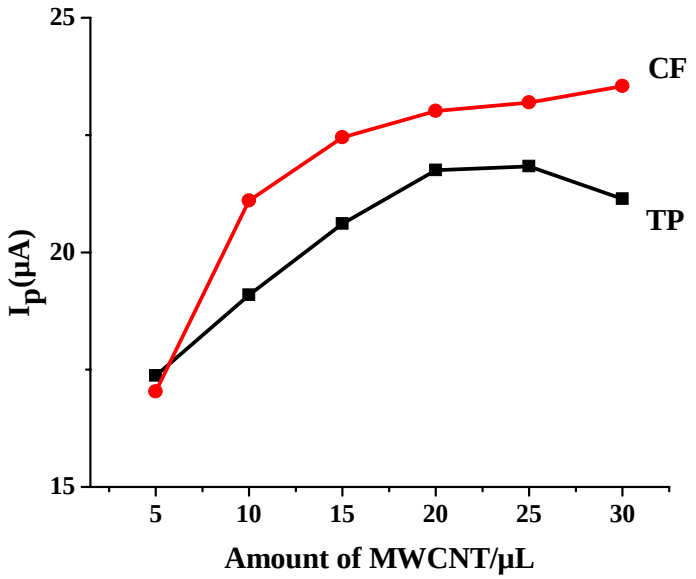

Figure 22. The effect of the amount the f-MWCNTs suspension on the peak current of a mixture of 50 µM TP and 100 µM CF at P(L-Asp)/f-MWCNTs/GCE in pH 4.5 PBS

5.2.6. The Effect of Scan Rate

The effect of scan rate on the simultaneous oxidation of TP and CF at the P(L-Asp)/f-MWCNTs composite film modified electrode was investigated in 0.1 M PBS at different potential scan rates, Figure 23. It can be seen that the oxidation peak currents for both TP and CF linearly increased with the square root of the scan rates ($v^{1/2}$), Figure 24, suggesting that the redox reaction at the electrode surface is predominantly diffusion-controlled process for both TP and CF [188]. The linear regression equation relating I_{pa} with $v^{1/2}$ in the range of 50 to 350 mV s^{-1}, was found to be: I_p (µA) = -3.7(±0.3) + 49.4(±0.6)$v^{1/2}$ ($V^{1/2}$ $s^{-1/2}$) (R^2 = 0.998) for TP and I_p (µA) = -5.2(±0.5) + 82.0(±1)$v^{1/2}$ ($V^{1/2}$ $s^{-1/2}$) (R^2 = 0.998) for CF. Moreover, the oxidation peak

potential (E_p) of both TP and CF shifted in the positive direction with increasing scan rate. The analysis of these data showed that the plot of E_{pa} *vs.* ln *v* gives a linear relation (R^2 of 0.998 and 0.994 for TP and CF respectively), indicating that the oxidation of TP and CF at the composite modified electrode is irreversible [188, 203, 204].

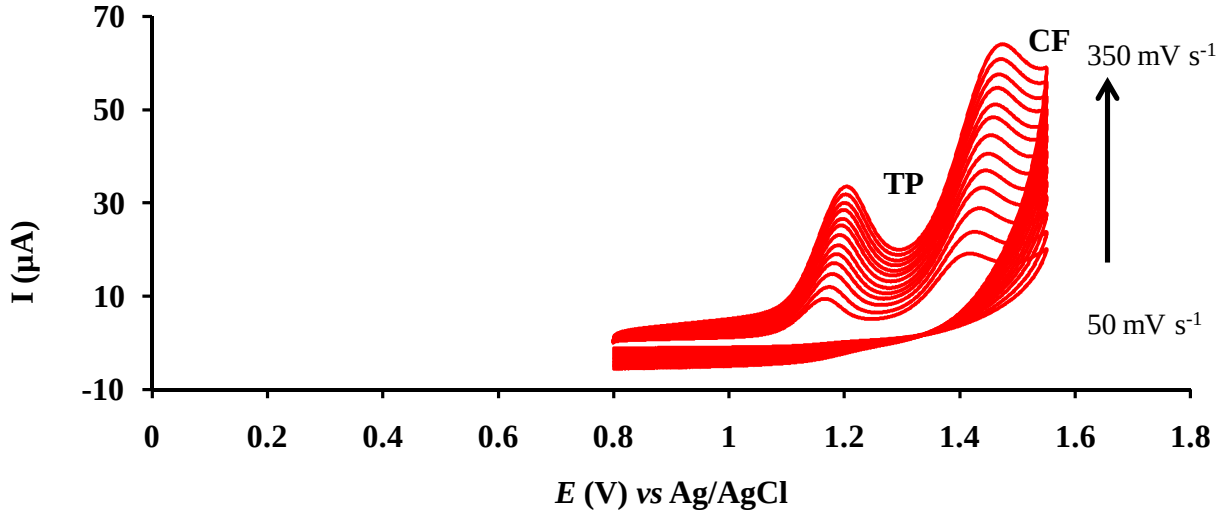

Figure 23. CVs of the mixture containing 50 µM TP and 100 µM CF at P(L-Asp)/f-MWCNTs /GCE in 0.1 M PBS at different scan rates (50–350 mV s^{-1})

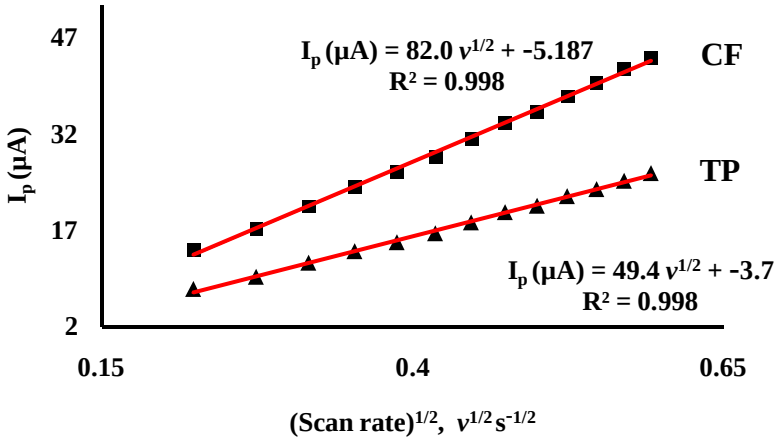

Figure 24. Plot of the dependence of peak current on the square root of scan rate

5.2.7. The Effect of pH

The effect of pH of supporting electrolytes on the redox behavior of electroactive analytes is an important factor. Hence, under the optimized experimental conditions, the effect of pH of common supporting electrolytes used in electrochemical analysis such as Britton-Robinson buffer (BRB), acetate buffer solution (ABS), phosphate buffer solution (PBS) and H_2SO_4 solution were investigated using CV for the simultaneous determination of TP and CF and the results were compared (Figure 25A). Owing to the high peak currents, good peak separation and peak shapes of TP and CF, PBS (pH 4.5) was chosen as the appropriate supporting electrolyte for further work.

The influence of pH on the peak currents and potentials of TP and CF at the composite modified electrode were studied in 0.1 M PBS in the pH range from 3.5 to 8.0 by CV. The peak current of TP decreases as pH increases, Figure 25C. On the contrary, although the oxidation peak current of CF increases slowly with increasing pH value, the peak shape of CF is distorted, Figure 25B. Therefore, the optimum pH value of 4.5 was selected for the simultaneous determination TP and CF to obtain the best response in terms of peak current, peak shape and maximum peak separation.

The dependence of the peak potential (E_p) of TP and CF on the pH of the buffer solution was also studied. The peak potential of TP shifts almost linearly towards negative potentials when the pH is increased (Figure 25C), indicating that protons are directly involved in the rate determination step of the oxidation reaction of TP. A plot of peak potentials *vs* pH values was found to be linear in the range of 4.0 to 8.0 with a regression equation of: E_{pa} (V) = -0.038(±0.0005)pH + 1.3(±0.003), R^2 = 0.998, Inset of Figure 25C. The slope of -0.038/pH, which is about half of the theoretical Nernstian value of 0.059 V/pH, suggests the redox process involves electrons and protons in 2:1 ratio [205]. However, the anodic peak potential (E_{pa}) of CF did not significantly change with increasing pH [188].

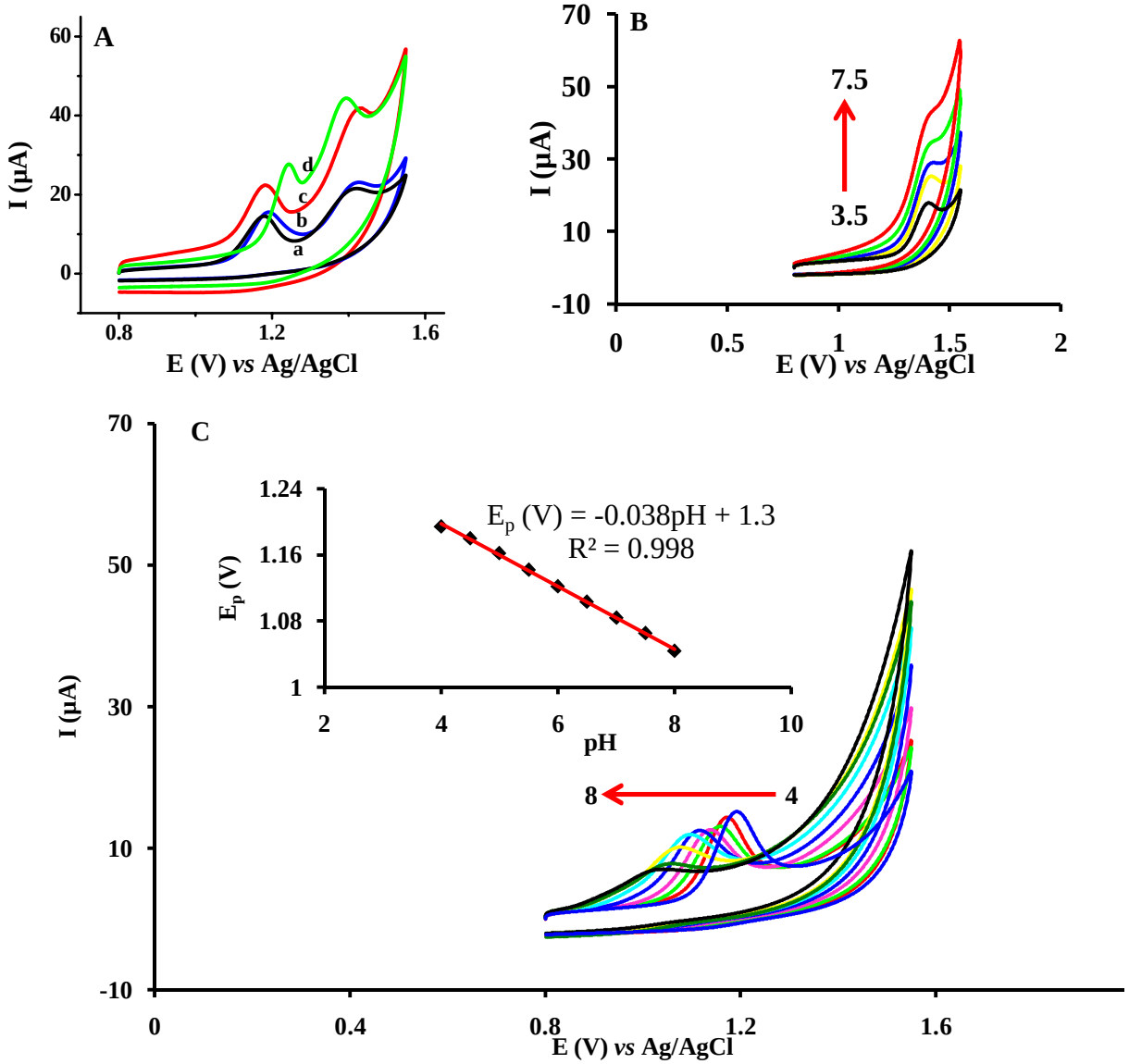

Figure 25. CVs of a mixture of 50 µM TP and 100 µM CF at the P(L-Asp)/f-MWCNTs/GCE in different supporting electrolytes (BRB (a), ABS (b), PBS (c) and H_2SO_4 solution (d)); (B) CVs of 100 µM CF and (C) 50 µM TP at P(L-Asp)/f-MWCNTs/GCE in 0.1 M PBS at various pH. Inset of Figure 5(C): Plot of E_p *vs* pH for TP

5.2.8. The Effect of SWV Parameters for TP and CF Determination

Square wave voltammetry (SWV) was chosen for the simultaneous determination of theophylline and caffeine in the present study as it is a sensitive voltammetric technique. The dependence of peak currents of TP and CF on square wave parameters such as step potential,

amplitude and frequency were investigated and optimized. The ranges studied were 1–16 mV for step potential, 1–120 mV for pulse amplitude and 5–100 Hz for SW frequency and the optimum values are 5 mV, 25 mV and 25 Hz for step potential, amplitude and frequency, respectively.

5.2.9. Determination of TP and CAF at P(L-Asp)/f-MWCNTs/GCE

Using the optimized experimental procedures described above, square wave voltammetry was used for the determination of TP and CF individually and simultaneously at P(L-Asp)/f-MWCNTs/GCE in 0.1 M PBS pH 4.5. First, the individual determination of TP or CAF was performed by keeping the concentration of one of the analyte at a constant value. Figure 26A illustrates the SWV curves for different concentrations of TP at constant concentration of caffeine. The peak currents of TP increased linearly with concentration in the range of 0.1–50 µM and a regression equation of: I_p (µA) = 0.399(±0.006)C (µM) + 0.064(±0.1), R^2 = 0.998, was obtained. The limit of detection was found to be 0.015 µM (*S/N* = 3). Similarly, as shown in Figure 26B, keeping the concentration of TP constant, the peak current of CF increased linearly with increasing concentration in the range of 1–120 µM with a linear regression equation of: I_p (µA) = 0.110(±0.002)C (µM) +0.91 (±0.1), R^2 = 0.995 and a LOD of 0.17 µM (*S/N* = 3).

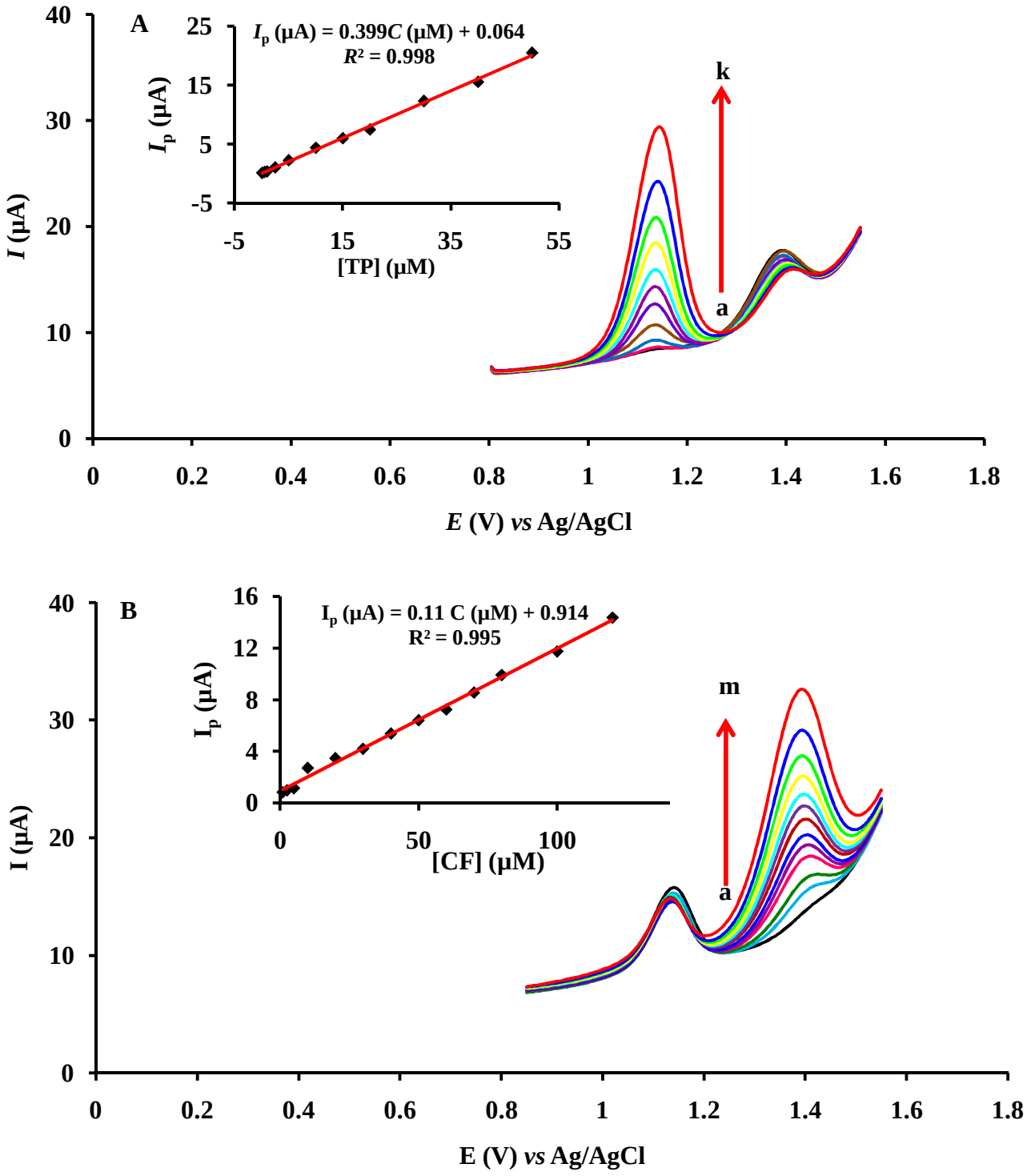

Figure 26. SWVs obtained at P(L-Asp)/f-MWCNTs/GCE for different concentrations of (A) TP (0.1→50 µM) and (B) CF (1→120 µM) in 0.1 M PBS with 10 µM constant concentration of CF and TP, respectively. Inset: Plot of peak current *vs* concentration

One of the main objective of this study was to detect theophylline and caffeine simultaneously using P(L-Asp)/f-MWCNTs/GCE. Under the optimal experimental conditions, SWV of TP and CF mixture with different concentrations were recorded. This was performed by simultaneously changing the concentrations of theophylline and caffeine, Figure 27. It can be seen that the simultaneous determination of TP and CF at P(L-Asp)/f-MWCNTs/GCE provides two well-defined oxidation peaks and the peak current for both are proportional to the corresponding concentrations in the mixture. The peak current response increases linearly with concentration in the range of 0.1–50 µM for TP and 1–150 µM for CF, Figure 28. The linear regression equations are: I_p (µA) = 0.299(±0.005)C (µM) + 0.20(±0.1), R^2 = 0.997 and I_p (µA) = 0.0834(±0.002)C (µM) + 0.51(±0.1), R^2 = 0.994, for TP and CF, respectively. The LOD of TP is found to be 0.020 µM and that of CF is 0.28 µM (*S/N* = 3).

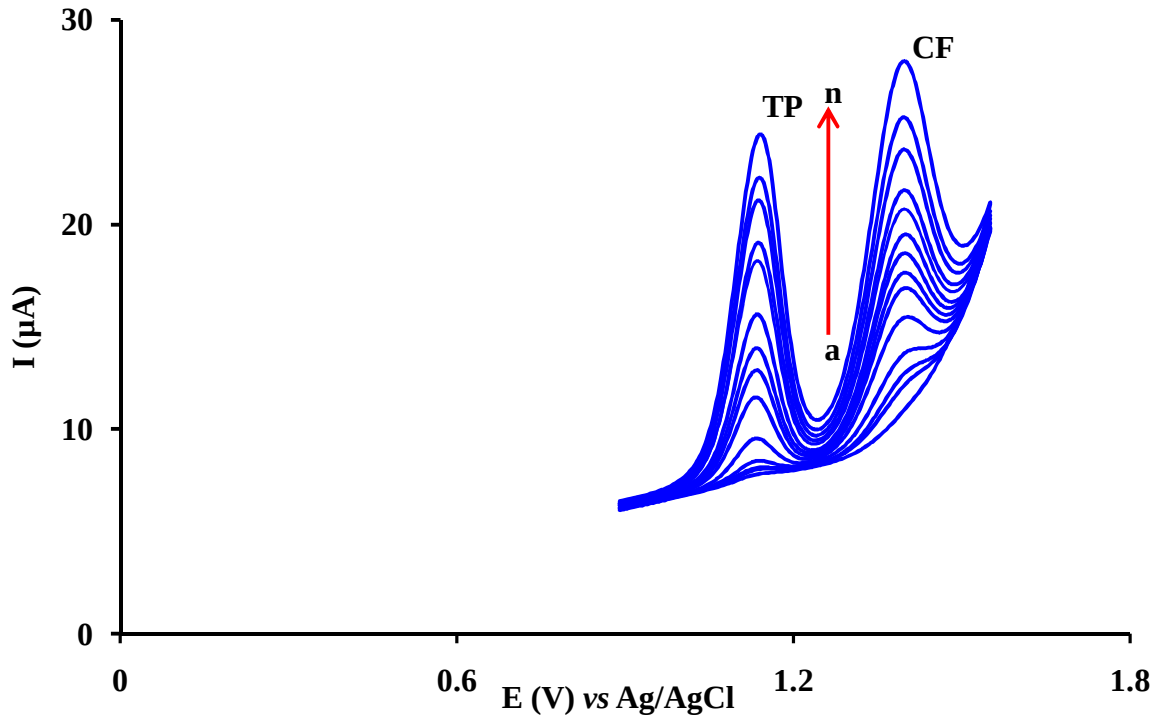

Figure 27. SWVs of a mixture of TP and CF at P(L-Asp)/f-MWCNTs/GCE in 0.1 M PBS for varying concentrations of (TP+CF); (a→n): 0.1+1.0, 0.5+2.5, 1.0+5.0, 2.5+10, 5.0+20, 10+30, 15+40, 20+50, 25+60, 30+70, 35+80, 40+100, 45+120 and 50+150 µM

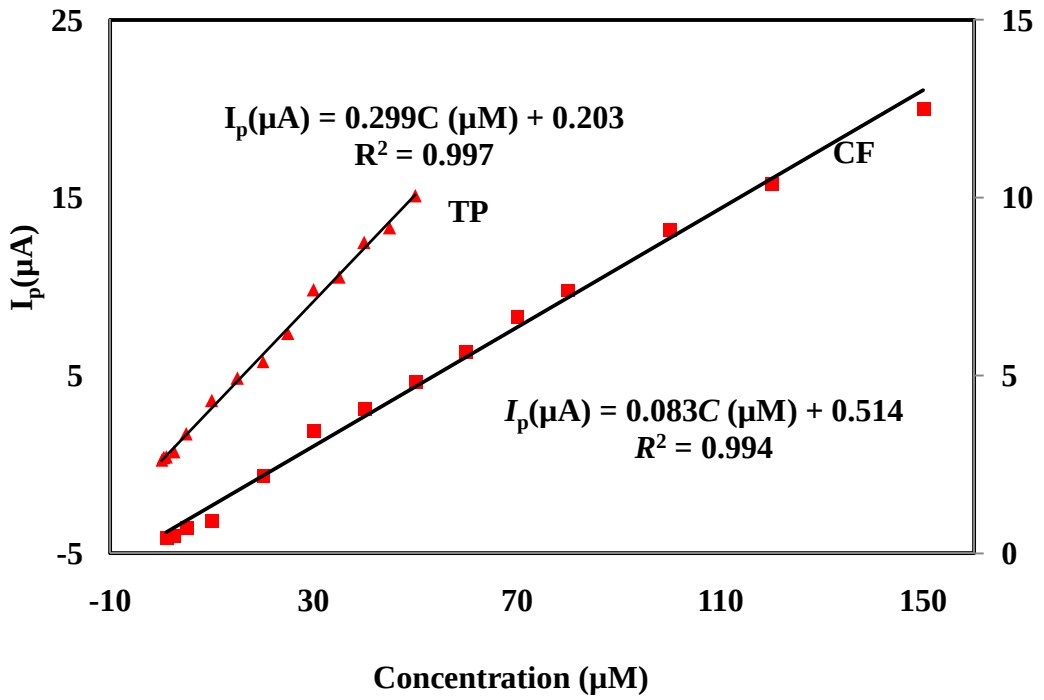

Figure 28. Plot of peak current of TP and CF *vs* concentration in the mixture

A comparison between the analytical performance of the present method and other similar literature reports for the simultaneous and individual determination of TP and CF is given in Table 4. The results suggest that the proposed method shows reasonable linear range and acceptable detection limit. Compared with the other electrochemical methods, the present method has many advantages for the simultaneous determination of TP and CF, such as simplicity of the electrode preparation, good stability and reproducibility. These results reveal that the P(L-Asp)/f-MWCNTs/GCE is highly suitable for the selective determination of one analyte in a wide concentration range in the presence of the other, and the proposed method is reliable for the simultaneous quantitative determination of TP and CF.

Table 4. Comparison of the analytical performance of the present method with other electrochemical methods reported in the literature

Electrode type	Method	Analyte	Linear-range (µM)	LOD (µM)	Reference
[a]ED-GO/GCE	LSV	TP	0.8–60	0.10	[47]
[b]MWCNT/GCE	CV	TP	0.3–10	0.050	[206]
[c]MWCNT–PE	DPV	TP	2–150	0.020	[207]
[d]Poly(AHNSA)/GCE	DPV	TP	1–100	0.047	[208]
[e]MnO_2 NPs/MWNT/GCE	DPV	TP	0.1–20	0.010	[181]
[f]CTAB–Gr/GCE	DPV	CF	0.3–100	0.091	[203]
[g]Nafion–Gr/GCE	DPV	CF	0.4–600	0.12	[204]
[h]BDDE	DPV	CF	0.4–25	0.15	[183]
[i]Nafion /SPG electrode	DPV	CF	3.1–247	1.0	[209]
[j]SWCNT/CCE	DPV	CF	0.25–100	0.12	[210]
[k]LMC/Nafion/GCE	DPV	TP	0.8–180	0.37	[161]
		CF	1.3–230	0.47	
[l]Poly(AV_3B)/MWCNT–GR/GCE	DPV	TP	0.5–120	0.020	[188]
		CF	1.0–120	0.10	
[m]Anisotropic GNP/CHIT/IL/ rGO /GCE	DPV	TP	0.025–2.1	0.0013	[189]
		CF	0.025–2.49	0.0044	
P (L-Asp)/f-MWCNT/ GCE	SWV	TP	0.1–50	0.020	[This
		CF	1–150	0.28	work]

[a]Electrodeposited graphene oxide onto a glassy carbon electrode; [b]multi-wall carbon nanotube modified glassy carbon electrode; [c]multi-wall carbon nanotube paste electrode; [d]poly(4-amino-3-hydroxynaphthalene sulfonic acid) modified glassy carbon electrode; [e]manganese oxide nanoparticles/multiwalled carbon nanotube nanocomposite modified glassy carbon electrode; [f]cetyltrimethylammonium bromide–dispersed graphene; [g]nafion–graphen modified glassy carbon electrode; [h]boron-doped diamond electrode; [i]nafion-modified disposable screen-printed graphite electrodes; [j]single-walled carbon nanotubes on carbon-ceramic electrode; [k]large mesoporous carbon and nafion composite modified electrode; [l]poly(alizarin violet 3B), multiwalled carbon nanotubes and graphene modified electrode; [m]anisotropic gold nanoparticle-chitosan-ionic liquid modified electrode.

5.2.10. Interference Study

The influence of various potentially interfering substances on the simultaneous determination of TP and CF was investigated. The tolerance limit was taken as the maximum concentration of the foreign substances that caused an approximately ±5% relative error in the determination. The results (Table 5) show that 50 fold of lactose, D-glucose, citric acid, oxalic acid, glycine, Ca^{2+}, Mg^{2+}, Na^{+}, K^{+}, NO_3^{-}, CO_3^{2-} and 20 fold theobromine and ascorbic acid did not interfere in the simultaneous determination of TP and CF. However, uric acid begins to interfere when present at concentrations greater than two fold of TP and equimolar amounts with CF. The results of the

interference experiment study shows that the proposed method is selective enough and can be applied for the simultaneous detection of TP and CF in real samples. Moreover, the interference study suggests the possibility of the simultaneous determination of theophylline, caffeine and theobromine at the composite modified electrode.

Table 5. Effect of potential interfering species on the simultaneous determination of 50 µM TP and 100 µM CF (n = 3)

Interferent	Conc. (µM)	Change in response (%)	
		TP	CF
Lactose	2,500	3.4	5.3
D-glucose	2500	3.7	2.9
Citric acid	2500	2.8	4.8
Oxalic acid	2500	4.7	3.0
Glycine	2500	4.0	5.0
Ca^{2+}	2500	1.4	3.6
Mg^{2+}	2500	4.8	2.0
Na^{+}	2500	2.6	3.9
K^{+}	2500	1.7	2.2
NO_3^{-}	2500	2.6	3.9
CO_3^{2-}	2500	1.5	3.8
Theobromine	1000	4	3.5
Ascorbic acid	1000	2.9	3.3
Uric acid	100	1.9	3.9

5.2.11. Analytical Applications

To investigate matrix effects in the analysis of real samples and examine the analytical application of the composite modified electrode, SWV was used under the optimized experimental conditions for the simultaneous determination of TP and CF. TP often coexists with CF in real samples, such as biological samples and tea products. Thus, green tea, blood serum and pharmaceutical formulation (Panadol extra) were used to investigate the practical application of the modified electrode in this study. The sample preparation is described in the experimental section. The standard addition technique was used to determine TP and CF simultaneously by the proposed SWV method. The obtained results are summarized in Table 6. The accuracy and precision of the proposed method was checked by spiking the samples with known amounts of standard TP and CF. It can be seen that good recovery results (92.0 to 106%) were obtained,

which indicates the practical applicability of the modified electrode for the simultaneous determination of TP and CF in the real samples.

Table 6. Simultaneous determination of TP and CF in green tea, human serum and Panadol extra samples (n = 3)

Sample	Analyte	Labeled mg/tablet	Found ±RSD	Detected (%)	Detected (μM)	Added (μM)	Found (μM)	Recovery (%)
Green Tea	TP				10.5	15	25.2	98.0
						40	47.4	92.3
	CF				135	10	144	92.0
						40	172	93.3
Blood Serum	TP				–	20	21.1	106
						30	28.6	95.3
	CF				–	40	38.2	95.5
						60	60.4	101
Panado Extra	TP	–	–	–	–	30	29.7	99.0
						50	47.8	95.6
	CF	65.0	60.7±4	93.4	40.0	75	112	96.0
						100	137	96.5

5.2.12. Repeatability, Reproducibility and Stability of the P(L-Asp)/f-MWCNTs/GCE

To test the repeatability of the modified electrode, the responses of a mixture of TP and CF were measured successively eight times at three different concentration ratios of TP:CF, 10:40, 50:100 and 75:150 μM. The relative standard deviations (RSD) of the peak currents were found to be 1.4%, 0.96% and 2.8% for TP and 0.97%, 1.8% and 1.7% for CF, respectively. Similarly, the reproducibility of the P(L-Asp)/f-MWCNTs/GCE was studied by measuring the peak current response of three different electrodes prepared under identical conditions for a mixture of 50 μM TP and 100 μM CF. The interelectrode relative standard deviations were determined to be 2.6% and 2.1% for TP and CF, respectively. These results demonstrate excellent precision and good reproducibility of the electrode. The long-term stability was also evaluated by keeping the electrode in 0.1 M PBS for 4 weeks at room temperature. The results showed the modified electrode retained 95.8% and 91.4% of the initial response with respect to TP and CF, respectively, which suggests that the proposed sensor has very good stability.

5.3. Sensitive Electrochemical Determination of Epinephrine in Pharmaceutics at Poly(L-Aspartic Acid)/Electrochemically Reduced Graphene Oxide Modified Electrode by Square Wave Voltammetry

5.3.1. Background

Epinephrine [1-(3,4-dihydroxyphenyl)-2-methyloaminoethanol], often called adrenaline (Scheme 6), is one of the most important and well-known catecholamine neurotransmitters in mammalian central nervous systems and plays an important role in the transmission of nerve impulses. It is biosynthesized in the adrenal medulla and sympathetic nerve terminals and is associated with a large variety of physiological processes and illnesses [211-213]. Pharmaceutically, epinephrine is extensively used for the treatment of neural disorders. Clinically, it exists as an organic cation in the nervous tissue and biological fluids. Epinephrine (EP) is used in the treatment of cardiac arrest, heart block, asthma, nasal congestion, hypertension, etc. It increases heart rate, constricts blood vessels, and dilates air passages. It is known to cause what is called the ‘‘fight or flight response’’ which energizes various biological systems by giving glucose to the body, and plays a central role during physical or mental stress. Epinephrine is also important for athletes to improve strength and speed. These important effects of EP also make it a potent stimulant; as a result, it has been banned in athletics competition by World Anti-Doping Agency [214-216]. Moreover, monitoring the concentration of EP in biological body fluid is often useful for diagnosis and evaluation of therapeutic and pharmacodynamic effects for psychiatric, neurological and cardiovascular disorders [211]. High concentrations of EP may cause many diseases such as Parkinsonism, Schizophrenia, Huntington’s disease, etc [213, 217].

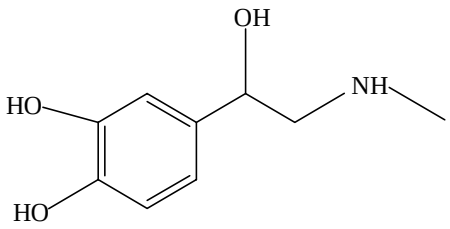

Scheme 6. The chemical structure of epinephrine

Therefore, the development of quantitative methods for the sensitive and selective determination of EP is of great significance. Different methods are available for the determination of EP in real samples such as biological samples and pharmaceutical formulations, including high

performance liquid chromatography coupled with mass spectroscopy (HPLC-MS) or chemiluminescence (HPLC-CL) [218, 219], capillary electrophoresis direct chemiluminescence [211], flow injection analysis coupled with chemiluminescence [220], spectrophotometry [214, 221] and electrochemical methods [212, 222-227]. Although these methods are effective in the determination of EP, most of the above mentioned methods require expensive instrumentation with typical experimental conditions and cumbersome sample preparation protocols [225]. However, due to simple procedures, high sensitivity, reproducibility, economic and ease of miniaturization, electrochemical sensors were explored for the determination of EP [211, 217].

Epinephrine often coexists with ascorbic acid (AA) and uric acid (UA) in biological samples and they can all be oxidized at similar potential regions at most conventional bare solid electrodes, resulting in overlapping of the voltammetric response. Moreover, the final oxidation products of EP would block the electrode surface when it is oxidized directly on a bare electrode, causing electrode passivation [212]. Therefore, the sensitive and selective electrochemical detection of EP in the presence of AA and UA is a real challenge. Chemically modified electrodes have been exploited and proven to be one of the most powerful tools and routes for solving the above problems and many chemical substances, such as nanomaterials, conducting polymers and biomolecules, are extensively studied as modifiers in this regard [228].

Graphene (GR), a single-atom-thick and two-dimensional sp^2 carbon material, has received considerable attention recently owing to its remarkable electrical conductivity, mechanical strength, chemical stability, and thermal properties [229]. The use of GR based electrochemical sensors has been reported in a large number of literatures [62, 94, 230-234]. However, the application of graphene is limited as GR tends to aggregate back to graphite because of the strong π-π and *Van der Waals* interactions. As the most important precursor of GR, graphene oxide (GO) has also attracted significant interests due to its good solubility and interaction with many functional groups. GO is the result of acid exfoliation of natural graphite, which exhibits properties such as facile surface modification, good water dispersibility and high mechanical strength. Due to the presence of epoxide and hydroxyl functional groups on the base plane and carboxyl groups on the edge sites, GO can be used for the preparation of graphene-based composites and the resulting novel hybrid materials of graphene-based composites can form

relatively stable aqueous suspensions [235, 236]. As GO is less conductive in nature compared to pristine graphene [237], reduction of GO is required for the enhancement of conductivity.

Nevertheless, the synthesis of graphene from graphene oxide using the chemical reduction method involves the use of excessive toxic chemicals, and the formation of graphene film on the electrode surface requires a multistep coating process. A promising strategy for graphene synthesis based on electrochemical method to produce electrochemically reduced graphene oxide (ERGO) has been reported [62, 94, 231-234]. This method provides several advantages over other graphene fabrication techniques, as it is green, efficient, inexpensive, and rapid. More importantly, the ERGO can form a stable film on the electrode surface without any further treatment [238]. Additionally, the electrochemically prepared graphene sheets are more conducting than that prepared from chemical reduction, and the oxygen to carbon ratio of electrochemically reduced GO was less than that of chemical methods [239].

Polymer-modified electrodes have shown to be a powerful tool, as characteristics like film thickness, permeation and charge transport can be controlled by adjusting the electrochemical parameters. Therefore, polymer-modified electrodes have many advantages such as improved electrocatalysis, absence of surface fouling and prevention of undesirable reactions competing kinetically with the desired electrode process [240]. Amino acids such as L-aspartic acid have received considerable attention for electrode modification owing to their availability, ease of preparation and good biocompatibility. L-aspartic acid can be electrochemically polymerized on the surface of GCE by cyclic voltammetry and forms a membrane rich with surface negative charge that can catalyze the oxidation of EP and eliminate the interference of AA and UA [34].

Nanocomposites combining two or several different components are expected to further improve the deficient characteristics of each component, a concept which has led to the development of various electrochemical sensors [241]. In this context, to date, several studies have been reported in the area of conducting polymer–graphene nanocomposites. For instance, Kang *et al*. reported the electrochemical detection of epinephrine using an L-glutamic acid functionalized graphene modified electrode [215]. Fan *et al*. also reported an electrochemical sensor based on graphene–polyaniline nanocomposite for the voltammetric determination of 4-aminophenol [59]. A

sensitive stannum film/poly(*p*-aminobenzene sulfonic acid)/electrochemically reduced graphene composite modified electrode for trace Cd determination was reported [94]. Filik and coworkers studied square-wave stripping voltammetric determination of caffeic acid (CA) on electrochemically reduced graphene oxide–nafion composite film and the proposed method was successfully used to determine CA in white wine samples [234]. Palanisamy *et al*. reported a novel and sensitive amperometric sensor for chlorpromazine based on reduced graphene oxide and polydopamine composite modified glassy carbon electrode [62]. Recently, the simultaneous detection of dopamine and uric acid at poly(L-lysine)/graphene oxide modified electrode (PLL/GO) was studied by Zhan and his groups. The prepared PLL/GO platform exhibited high effective surface area, more active sites and enhanced electrochemical activity [60].

Electrocatalysis of epinephrine has been investigated at direct graphene [228] and poly(L-aspartic acid) [34] modified glassy carbon electrode independently. Here, we have exploited the electrocatalytic properties of poly(L-aspartic acid) (P(L-Asp) and electrochemically reduced graphene oxide (ERGO) composite with synergetic effect for the determination of EP. The resulting hybrid composite material takes full advantage of the respective properties without losing any of the electrochemical performance.

5.3.2. Preparation of P(L-Asp)/ERGO/GCE

The P(L-Asp)/ERGO/GCE was formed in situ by cyclic scanning of GO coated GCE in a monomer solution of L-aspartic acid in the range of –1.0–1.8 V at a scan rate of 100 mV s^{-1} for 20 cycles in pH 6.0 PBS, Figure 29. The resulting cyclic voltammogram showed a weak and strong oxidation peaks at about 0.6 and 1.4 V, respectively, which shows anodic oxidation of surface functional groups of GO. In the reverse scan, a sharp irreversible reduction peak was observed at approximately -0.6 V, attributed to the reduction of oxygen moieties at the GO basal plane [231]. The GO sheets are mostly decorated with epoxy and hydroxyl groups on the basal plane, while carbonyl and carboxyl groups are located at the edges [231, 239]. The strong oxidation peak of GO at about 1.4 V decreases gradually and disappears after the fifth cycle and was followed by the growth of poly(L-aspartic acid) film on the ERGO/GCE at the higher

potential region. The reduction peak at about -0.6 V also decreases continuously with cyclic scanning ascribed to the reduction of oxygenated functional groups on the surface of GO [241].

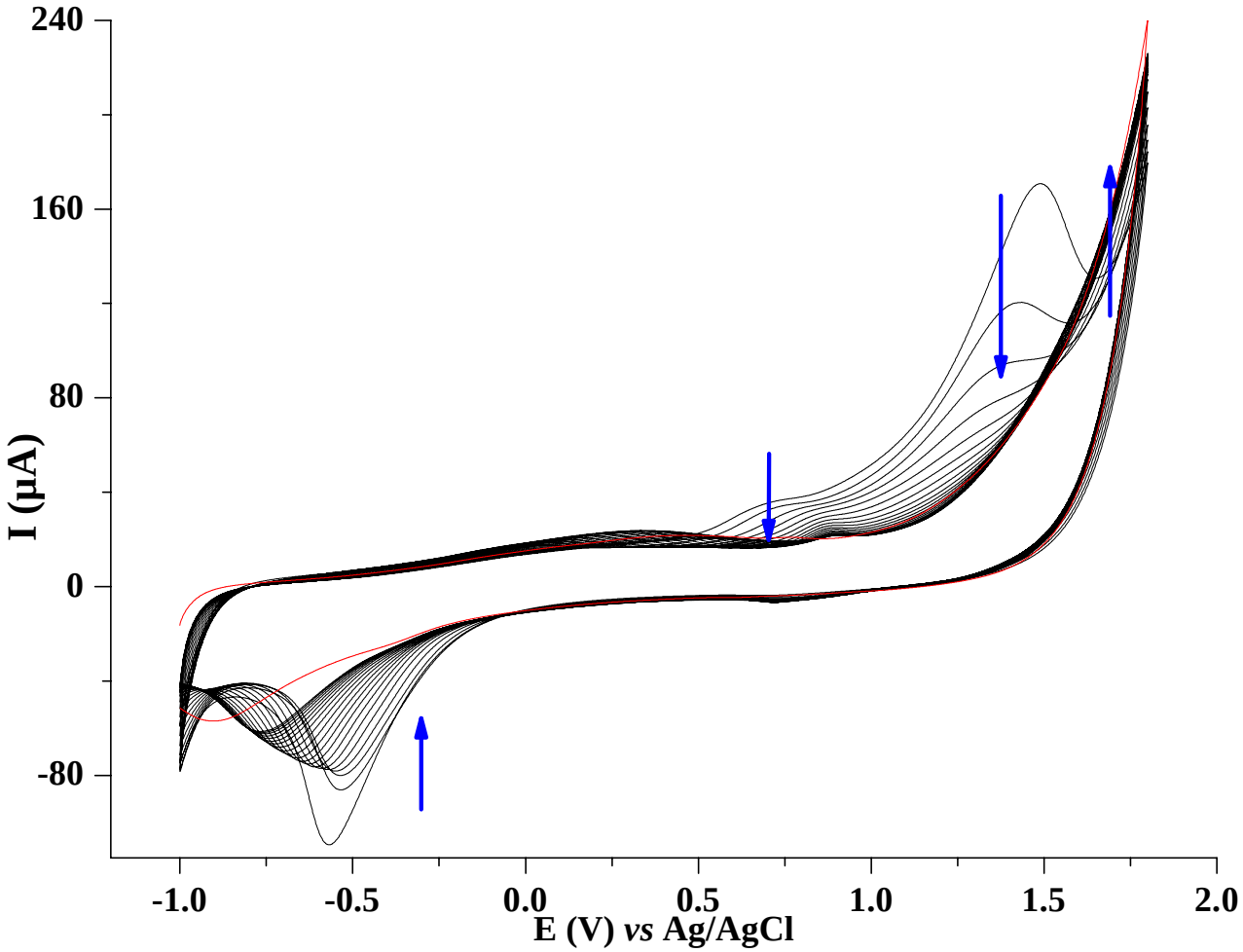

Figure 29. Electropolymerization of 2.0 mM L-aspartic acid in 0.1 M PBS (pH 6) on GO coated GCE between the potentials -1.0 and 1.8 V for 20 cycles at scan rate of 100 mV s^{-1}

5.3.3. FTIR and UV Characterization

The FTIR spectra were recorded for the finely grounded compound in KBr. Figure 30 shows the FTIR spectra of GO, ERGO, P(L-Asp) and P(L-Asp)/ERGO composite. The most intense and broad peaks occur in the range of 3320–3500 cm^{-1} attributed to O–H stretching vibrations of OH groups on the surface of GO and P(L-Asp) and N–H stretching vibrations of amines on P(L-Asp). The relative intensity of O–H stretching band for ERGO has decreased as compared to GO, which indicates that C–OH still exists, but in lower proportion [242, 243]. Two weak peaks

located at approximately 2923 and 2857 cm^{-1} are characteristic for asymmetric and symmetric stretching vibrations of the C-H bond in CH_2 and CH_3 groups. Absorption peaks at about 1632 cm^{-1} is ascribed to C=C skeletal vibrations for GO and C–N stretching for P(L-Asp). This peak is slightly shifted to a lower value, 1628 cm^{-1}, for ERGO with reduced intensity. The electrochemical reduction of GO is confirmed by disappearance of the bands of C=O stretching vibrations of the carbonyl group of GO at ~1737 cm^{-1} (Inset of Figure 32) [57, 242, 244]. The bands at about 1384 and 1282 cm^{-1} are due to C–H bending and C–N stretching vibrations, respectively. The absorption band at about 1078 cm^{-1} can be ascribed to the C–O stretching vibrations. The peak at about 932 cm^{-1} is ascribed to C–C stretching + CO stretching + NH_2 bending vibrations, whereas the spectral band observed at about 525 cm^{-1} is due to COO– bending vibrations of carboxyl functional groups of P(L-Asp) and P(L-Asp)/ERGO [57, 242, 243, 245, 246].

The FTIR spectra of P(L-Asp)/ERGO hybrid material exhibited all the characteristic peaks described for ERGO and P(L-Asp) though they appear with less intensity. Apparently, these peaks appeared because of the co-existence of ERGO along with P(L-Asp) in the composite. The characteristic peaks of P(L-Asp)/ERGO composite were reduced in intensity as compared to the individual peaks observed for GO and P(L-Asp), indicating partial reduction of the oxygen functionalities upon electrochemical reduction during in situ electropolymerization of L-aspartic acid on top of GO coated GCE. All the above results confirmed the formation of P(L-Asp)/ERGO on the surface of GC electrode.

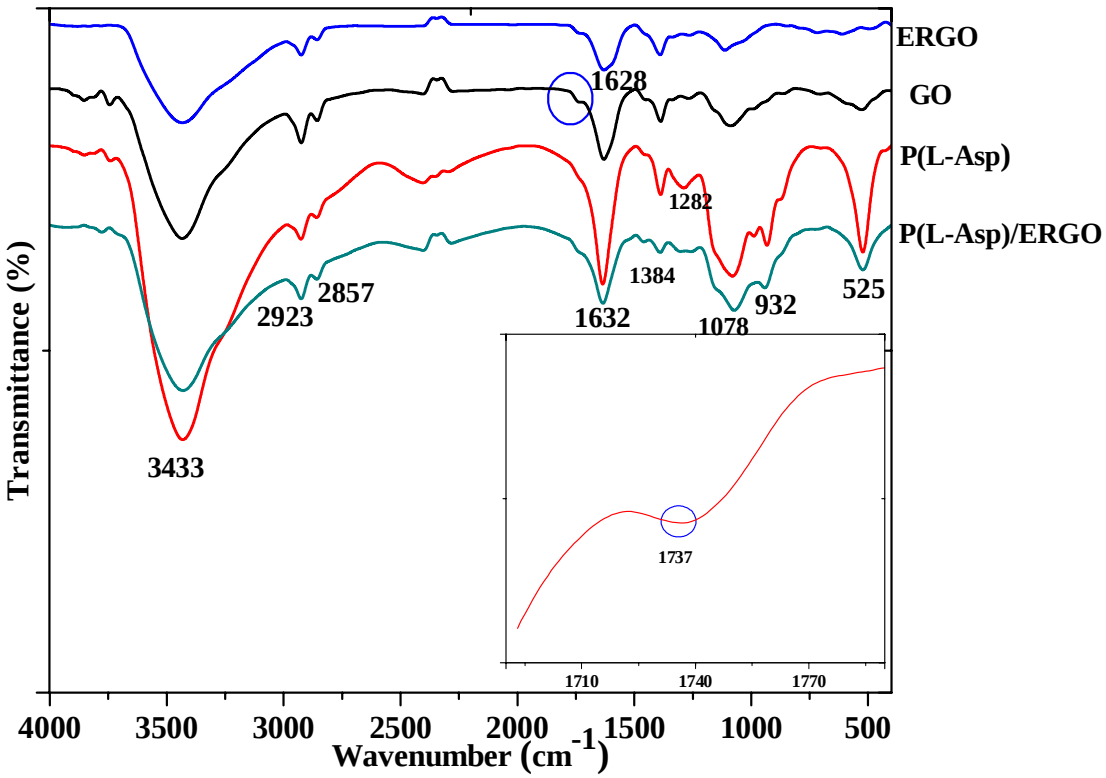

Figure 30. FT-IR spectra (KBr disc) of GO, ERGO, P(L-Asp) and P(L-Asp)/ERGO composite

The reduction process was also confirmed by UV-Vis spectroscopic analysis, Figure 31. The spectral band of L-aspartic acid is observed at 202 nm. The spectrum of GO shows characteristic peak at 226 nm, assigned to π–π* transitions of aromatic C=C bonds and a shoulder at ~290–310 nm, which corresponds to the n–π* transition of the C=O. After the reduction of GO, its maximum peak at 226 nm was slightly red shifted to 230 nm for ERGO and the shoulder peak of GO at 290–310 nm due to n–π* transition of the C=O bond almost disappears, indicating partial reduction of oxygen moieties of GO [244, 247]. For the P(L-Asp)/ERGO composite an intermediate absorption maxima at 228 nm was registered. The results suggest the electrochemical reduction of GO and the successful formation of P(L-Asp)/ERGO on the surface of GCE. However, the FTIR and UV-Vis results were not conclusive enough and hence we have characterized the electrodes further by the Raman spectroscopy which clearly revealed the electrochemical reduction of graphene oxide (GO).

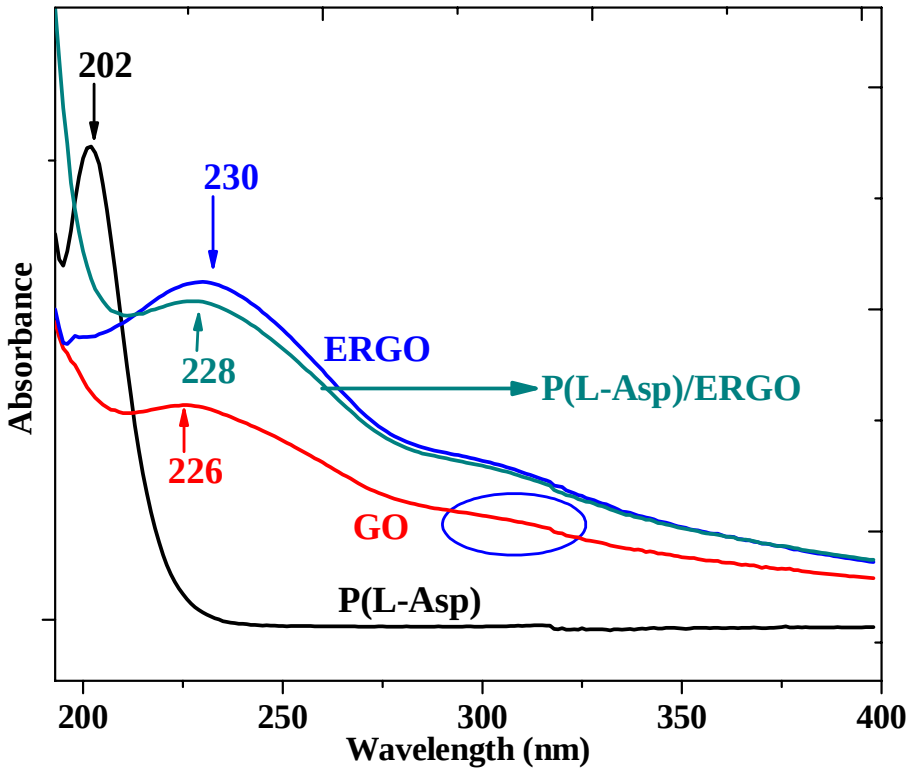

Figure 31. UV absorption spectra of GO, ERGO, L-Asp and P(L-Asp)-ERGO composite (in pH 6 PBS)

5.3.4. Raman Spectroscopy

Raman spectroscopy is a useful tool for studying disorder and defects in crystal structures, and it is often employed to characterize graphite and its derivatives. The formation of electrochemically reduced graphene oxide on GCE within the potential window under investigation was further verified via Raman analysis. Figure 32 shows the Raman spectra of GO and ERGO, where the prominent D and G bands were observed at 1364 and 1598 cm^{-1} for GO and 1356 and 1602 cm^{-1} for ERGO, respectively. The G band represents the first-order scattering of the E_{2g} vibrational mode whereas the D band has been attributed to the in-plane sp^2 C atoms. The D to G band intensity ratio (I_D/I_G) expresses the atomic ratio of sp^2/sp^3 carbons, and is a measure of the extent of disorder [94, 216, 233]. After electrochemical reduction of GO on GC electrode surface, the position of the two bands were almost the same but the intensity ratio (I_D/I_G) increased for ERGO (1.2) compared to that of GO (0.99). This confirms the electro-reduction of oxygen-containing groups on GO and the network restoration within the carbon

structure. This result is consistent with previous reports [62, 94, 233], suggesting the successful preparation of ERGO by this method.

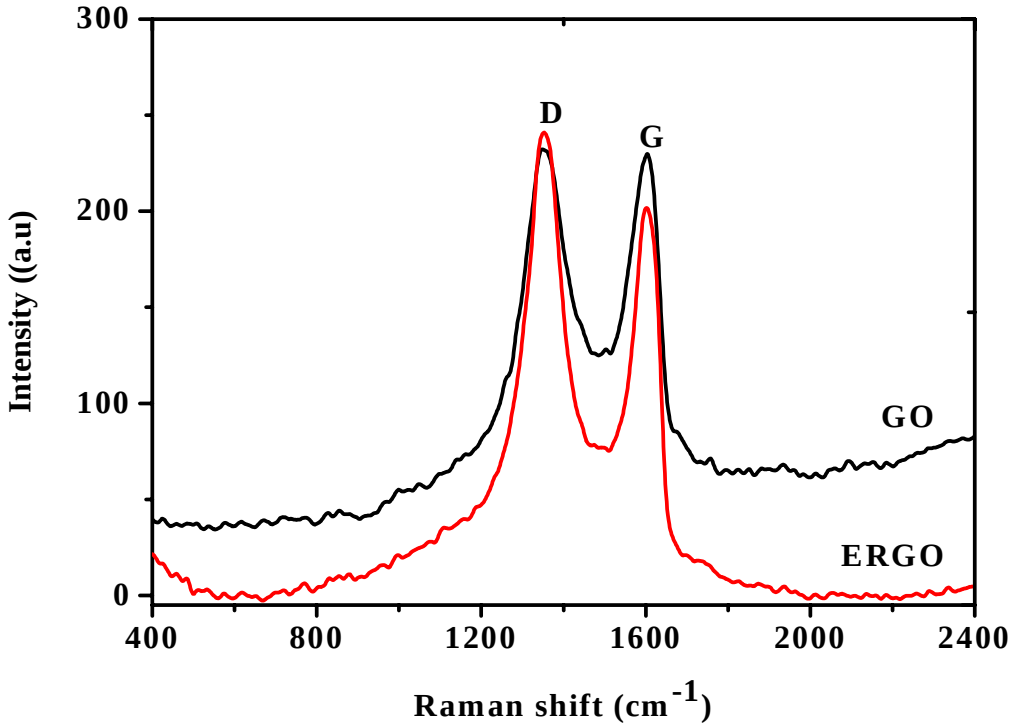

Figure 32. Raman spectra of GO and ERGO

5.3.5. Electrochemical Characterization of the Modified Electrode

In order to confirm whether the modification of the bare GC electrode has brought an improvement in the electrochemical properties and thus the electrical conductivity, the electro-active surface area of bare GCE was compared with that of P(L-Asp)/ERGO composite modified GC electrode by cyclic voltammetry in 1.0 mM $K_3Fe(CN)_6$ as a redox probe at different scan rates. The electro-active surface areas were estimated according to Randles–Sevcik equation (1) [248]. For 1.0 mM $K_3Fe(CN)_6$ in 0.1 M KCl electrolyte, the peak currents were proportional to the square root of the scan rates. From the slope of the plot of I_p *vs* $v^{1/2}$, using the Randles–Sevcik equation, the effective surface area was calculated to be 0.07 and 0.11 cm^2 for bare GCE and P(L-Asp)/ERGO/GCE, respectively, which indicates the effective electroactive surface area of the composite modified electrode is improved by ~57%.

Electrochemical impedance spectroscopy (EIS) is an efficient tool for studying the interface properties of surface-modified electrodes. The diameter of the semicircle portion of Nyquist plot of EIS is equivalent to the charge transfer resistance (R_{ct}) [249]. Figure 33 shows the Nyquist plot of different modified electrodes in the presence of 400 µM EP in 0.1 M PBS (pH 4). The R_{ct} values are in the order of: bare GCE (curve a) > GO/GCE (b) > ERGO/GCE (c) > P(L-Asp)/ERGO/GCE (d). The highest R_{ct} value at conventional bare glassy carbon represents slow electron transfer rate. Similarly, the GO/GCE (curve b) appears to have a large electron transfer resistance (R_{ct}) value because of the presence of excessive oxygenated moieties, which produced an insulating behavior and obstructed its electrochemical characteristics [250]. However, upon electrochemical reduction, ERGO/GCE, the charge transfer resistance has significantly decreased to a lower value due to the regeneration of sp^2 backbone of graphene sheets by the removal of electrochemically unstable oxygen functional groups which enhances the electrical conductivity [239, 249]. The P(L-Asp)/ERGO/GCE composite modified electrode has exhibited the lowest semicircle diameter (inset of Figure 33), which confirm the successful formation of P(L-Asp)-ERGO hybrid material on the surface of GCE that enhances the rate of electron transfer with synergetic effect.

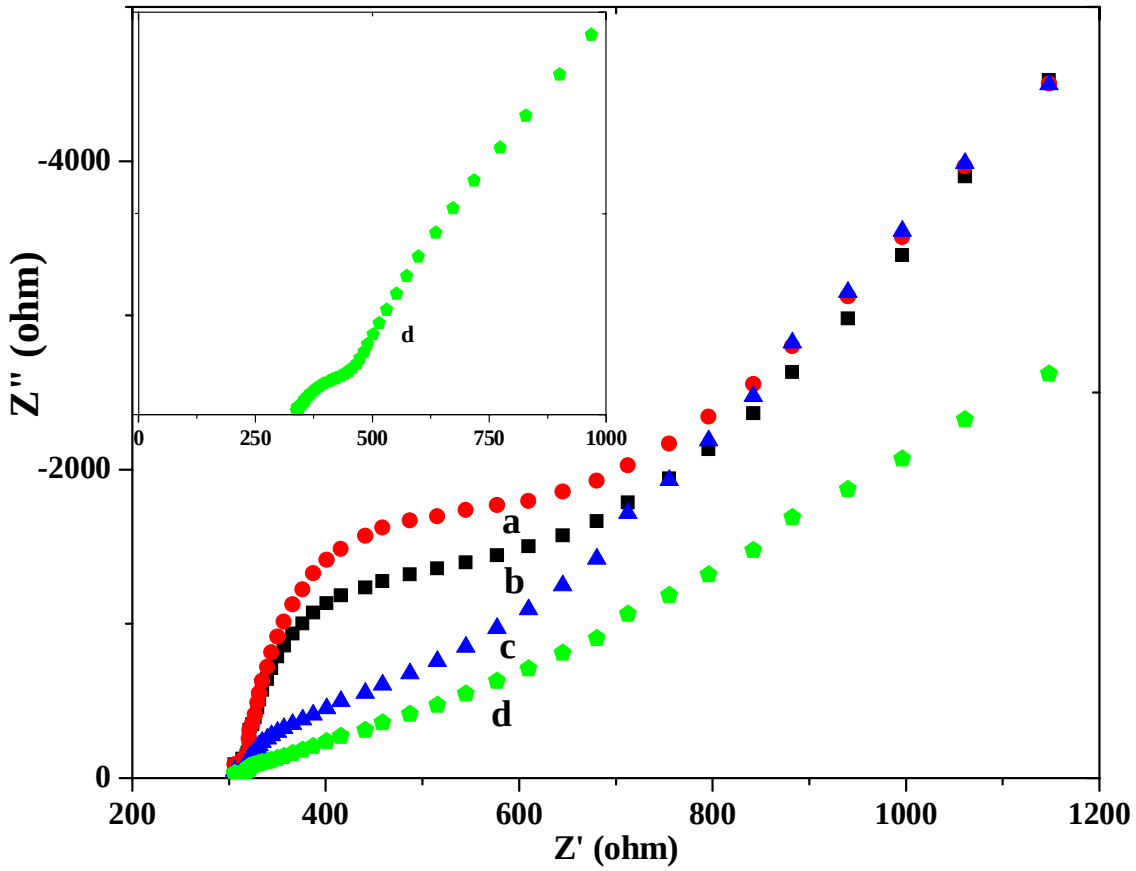

Figure 33. Nyquist plots of EIS obtained at bare GCE (a), GO/GCE (b), ERGO/GCE (c) and P(L-Asp)/ERGO/GCE (d) in 400 µM of EP in 0.1 M PBS of pH 4. Frequency: 100 kHz–0.1 Hz; perturbation amplitude: 10 mV

5.3.6. Electrochemical Behavior of Epinephrine

The electrochemical behavior of EP was examined by cyclic voltammetry (CV) within a potential window of 0.0–0.8 V at a scan rate of 100 mV s^{-1}. Figure 34 compares the CVs recorded at the bare and modified electrodes in 0.1 M PBS (pH 4) in the absence (a) and presence (b–f) of 50 µM EP. No apparent redox peaks appeared in the supporting electrolyte (curve a). At the bare GCE a weak anodic peak was observed at a relatively higher potential region of 0.495 V. The absence of an obvious reduction peak in the reverse direction confirms the electrode reaction of EP is totally irreversible at the conventional bare GCE. However, under the same conditions, the CVs of EP is characterized by the corresponding cathodic peaks at all the modified electrodes (curve c–f). At GO/GCE the oxidation peak shifted negatively to 0.444

V with an improvement in the peak current of about 2 fold of the bare electrode response. A weak reduction current is also observed in the reverse scan at 0.35 V. However, at the P(L-Asp)/GCE and ERGO/GCE the oxidation peak current is increased by 3.6 and 5.1 fold, respectively, compared to the bare electrode. Moreover, the oxidation peaks are negatively shifted to 0.378 and 0.361 V with the corresponding reduction peaks at 0.346 and 0.330 V, respectively. The remarkable peak current enhancement and the negative shift of the oxidation peak potential are undoubtedly attributed to the unusual structure and properties of graphene such as high aspect ratio and excellent electrocatalytic activity [232] as well as the three-dimensional structure and the rich carboxyl groups on the membrane surface of poly(L-aspartic acid) [34], which facilitates the rate of the electron transfer. The result at the P(L-Asp)/ERGO/GCE shows a considerable enhancement in the anodic peak current of about 6.5 fold of the current obtained at bare GCE. This value is much higher than the response obtained at the individual polymer and electrochemically reduced graphene oxide modified electrode. This clearly shows the synergetic effect of the polymer and electrochemically reduced graphene oxide in the electrocatalytic redox reaction of epinephrine at the composite modified electrode. The anodic peak and cathodic peak potentials of EP at the P(L-Asp)/ERGO/GCE are 0.384 and 0.326 V, respectively. The peak-to-peak separation (ΔE_p) and the formal potential (E^0) of EP at the composite modified electrode is 0.058 and 0.355 V, respectively, with I_{pa}/I_{pc} value of approximately 1. The above results confirm that the electrochemical reactions of EP at the P(L-Asp)/ERGO/GCE are a quasi-reversible reaction process [34]. It is interesting to note that the CV results support the formation of the composite material and are in agreement with those obtained from surface area and EIS characterization.

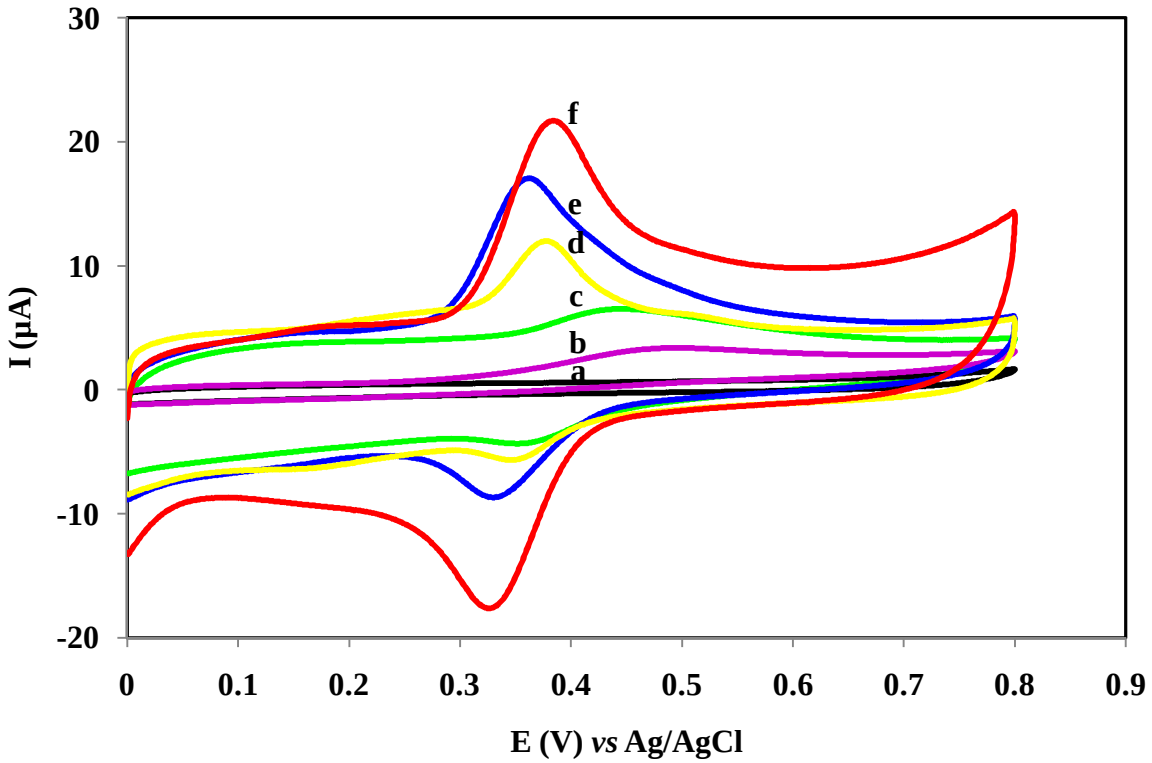

Figure 34. CVs obtained at bare GCE (a, b), GO/GCE (c), P(L-Asp)/GCE (d), ERGO/GCE (e) and P(L-Asp)/ERGO/GCE (f) in the supporting electrolyte (a) and 50 µM EP (b-f) in 0.1 M phosphate buffer (pH 4) at scan rate of 100 mV s^{-1}

5.3.7. The Effect of Scan Rate

The influence of potential scan rate (v) on the peak current response for 50 µM EP at the P(L-Asp)/ERGO/GCE was studied by CV at various scan rates (Figure 35). As shown in the Figure, both the anodic and cathodic peak currents of EP increase with scan rate and there are good linear relationships between the oxidation and reduction peak currents and scan rate (v) in the range of 0.025 to 0.275 V s^{-1} with a linear regression equations: I_{pa} (µA) = 137.7v (V s^{-1}) + 0.35; R^2 = 0.998 and I_{pc} (µA) = –89.6v (V s^{-1}) – 1.1; R^2 = 0.994, respectively. The result suggests that the electrochemical behavior of epinephrine at the P(L-Asp)/ERGO/GCE is predominantly a surface adsorption-controlled process [224, 228]. Besides, the relationship between E_{pa} and E_{pc} *vs* the logarithm of the scan rates were studied and a linear regression equations of: E_{pa} = 0.17 + 0.12log$v$ (R = 0.998) and E_{pc} = 0.43 – 0.041log$v$ (R = 0.991), was obtained. According to

Laviron's equation [59], the slopes are equal to 2.3RT/(1–α)nF and -2.3RT/αnF for anodic and cathodic peak, respectively. Thus, the electron transfer coefficient (α) and the electron transfer number (n) are calculated to be 0.75 and 1.97 (~2), respectively. Accordingly, the redox reaction of EP at the composite modified electrode involves a two electron transfer process.

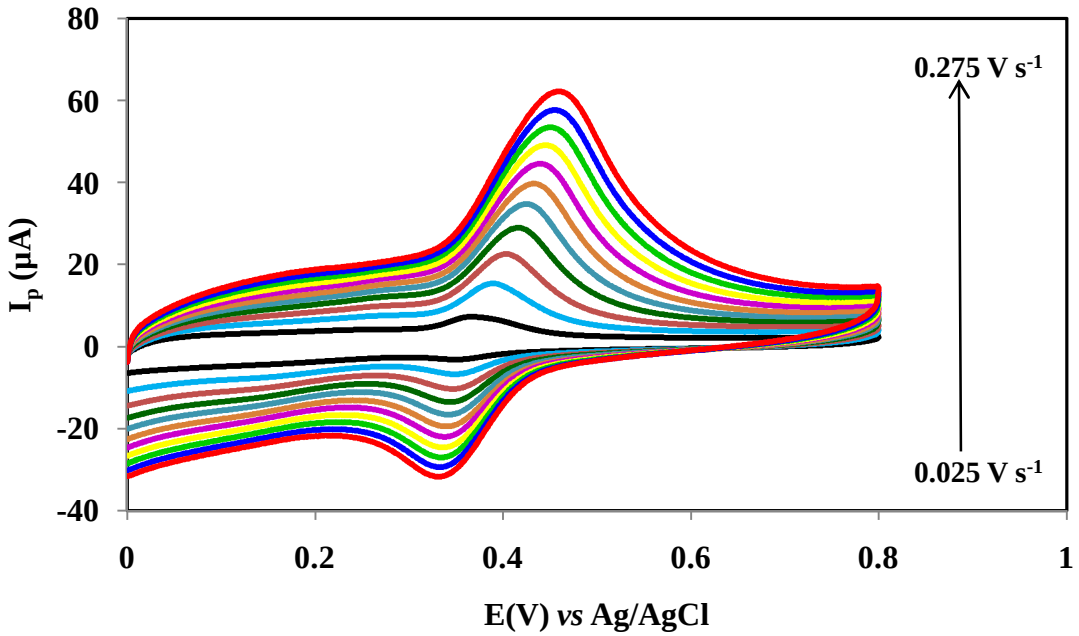

Figure 35. CVs of 50 µM EP at P(L-Asp)/ERGO/GCE in 0.1 M PBS (pH 4.0) at different scan rates (0.025-0.275 V s^{-1})

5.3.8. The Effect of pH

The effect of pH of the buffer solution on the electrochemical response for 50 µM EP was studied in 0.1 M PBS in the range of 3.0–7.5. Cyclic voltammetry was used to investigate the influence of solution pH on the electrochemical behavior of EP at the P(L-Asp)/ERGO/GCE. Figure 386 shows the increase in the oxidation peak current response for EP at first as the pH value increases from 3.0 to 4.0 and then gradually decreases from 4.0–7.5. Moreover, the corresponding cathodic peak current disappears after pH 5.5, Figure 36. Therefore, PBS of pH 4.0 was chosen as the optimum pH for the subsequent investigation of the electrochemical reaction of EP at P(L-Asp)/ERGO/GCE. The effect of the pH of the buffer solution on the oxidation peak potential of EP was also investigated. It shows that both E_{pa} and E_{pc} shifted negatively and were dependent linearly on pH (Figure 37). The negative shift in the oxidation

peak potential due to the change in pH from acidic to basic solution indicates proton participation in the oxidation process. The relationship between the anodic and cathodic peak potentials and pH was linear with the regression equation: E_{pa} (V) = –0.047pH + 0.65 (R^2 = 0.997) and E_{pc} (V) = –0.055pH + 0.59 (R^2 = 0.996), respectively. The fact that E_{pa} and E_{pc} are dependent linearly on pH with slopes of –47.0 and –55.0 mV/pH indicates that the proportion of the electrons and protons involved in the redox reaction of EP are in 1:1 ratio. Therefore, the oxidation of EP at the P(L-Asp)/ERGO-composite modified electrode had been inferred to be a two electron-two proton transfer process to produce adrenalinequinone and the proposed redox mechanism is represented as in Scheme 7. This is in agreement with the previous reports [222, 224, 227].

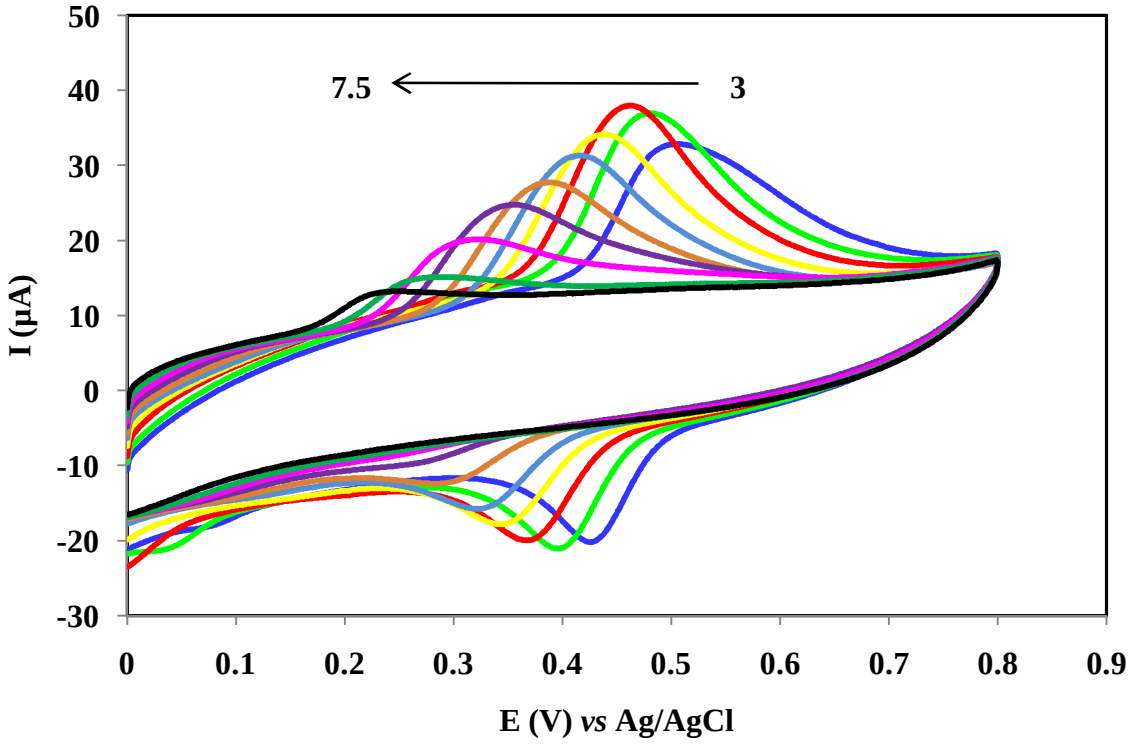

Figure 36. CVs of 50 µM EP at P(L-Asp)/ERGO/GCE in 0.1 M PBS of different pH values (3, 3.5, 4.0, 4.5, 5.0, 5.5, 6.0, 6.5, 7.0, 7.5)

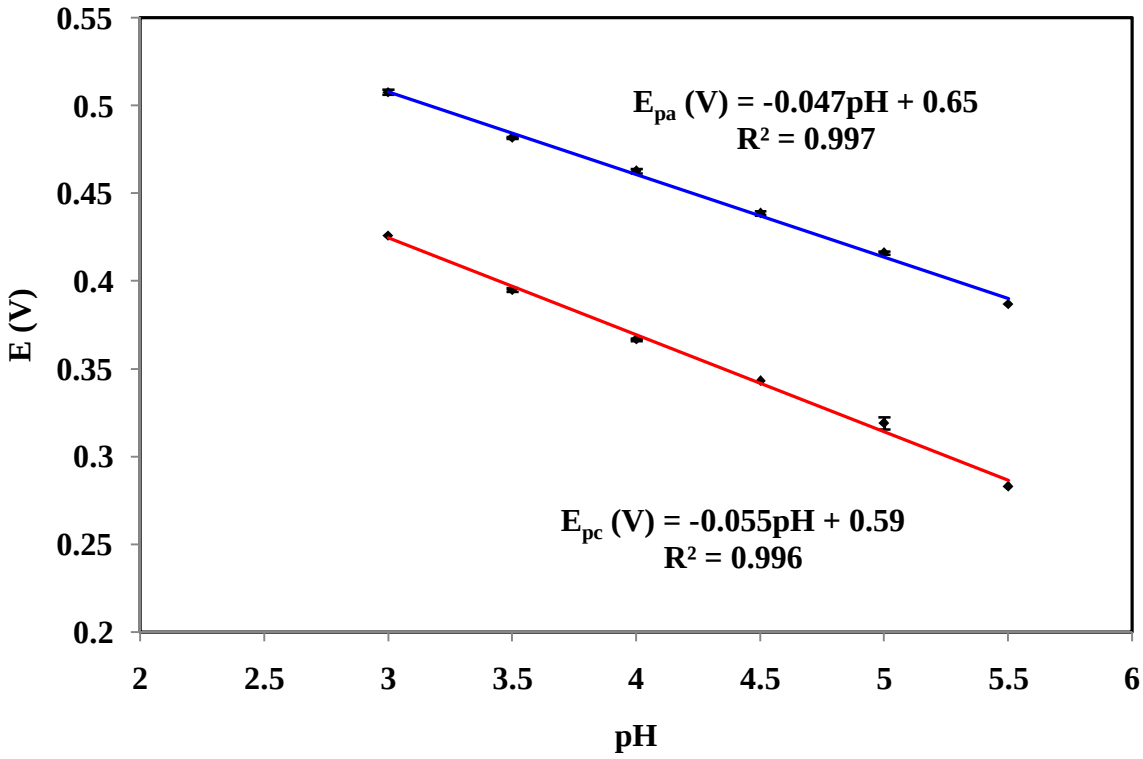

Figure 37. Plot of the effect of pH on peak potentials of 50 µM EP

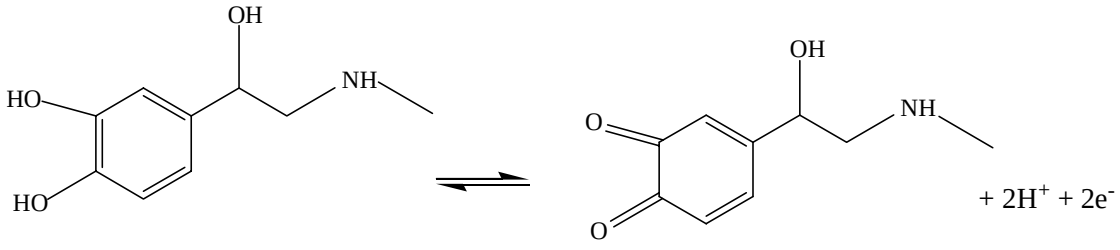

Scheme 7. Reaction mechanism of epinephrine

5.3.9. The Effect of the Amount of GO

The amount of graphene oxide deposited on GCE affects the peak current response of EP. Therefore, the effect of the volume of GO on the current response of 50 µM EP was considered from 2.5 to 15.0 µL. The peak current of EP increased with increasing volume of GO and reached a plateau around 7.5 µL. Above 7.5 µL, the peak current almost remains constant because high loading induced a large increase of capacitive background current [228], which

may lead to a decrease of the peak current. As a result, 7.5 µL was taken as the maximum volume of GO in this experiment.

5.3.10. The Effect of Accumulation Potential and Time

Since the electrode reaction at the composite modified electrode is an adsorption controlled process, the influence of accumulation potential and time on the peak current response of 50 µM EP was investigated by using the SWV. The effect of accumulation potential was studied in the range of +0.6 to –0.2 V with 30 s accumulation time. However, a non-uniform variation in the peak current response of EP with change in accumulation potential was observed within the studied range and the impact was not significant to be considered. Thus, the effect of accumulation time was examined under an open circuit accumulation by varying the accumulation time in the range of 15 to 210 s. As can be seen from Figure 38, the peak current of EP increased considerably from 15 to 120 s and further increase in accumulation time beyond 120 s has resulted in gradual increase of the peak current, suggesting that the P(L-Asp)/ERGO/GCE can effectively accumulate EP. Therefore, 120 s was adopted as the optimum accumulation time for subsequent analyses in this work.

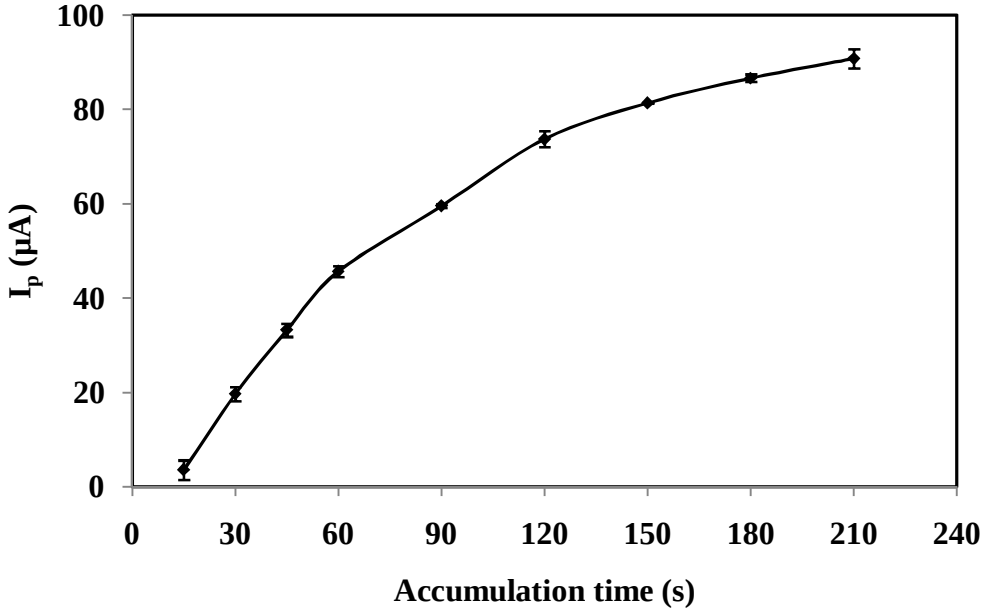

Figure 38. Effect of open circuit accumulation time on the peak current response of 50 µM EP at P(L-Asp)/ERGO/GCE

5.3.11. Optimization of SWV Parameters

Square-wave voltammetry (SWV) was chosen for the determination of EP as it is superior to other pulse-voltammetric techniques, attributed to its excellent analytical sensitivity [251]. The experimental parameters (frequency; pulse amplitude; and potential increment) that affect the SWV response for 50 µM EP were investigated. By considering the shape of the square wave voltammogram and the magnitude of the peak current, the optimum SWV parameters selected for subsequent measurements are frequency of 50 Hz, amplitude of 0.06 V and step potential of 0.008 V.

5.3.12. Voltammetric Determination of EP

Determination of EP was performed under the optimized conditions using square-wave voltammetry. Figure 39 shows the SW voltammograms at the potential of +0.335 V (versus Ag/AgCl) with increasing concentration of EP in 0.1 M PBS (pH 4) using the P(L-Asp)/ERGO/GCE as the working electrode. The peak current *versus* concentration plot for EP is linear in the range of 0.1 to 110 µM, Figure 40. The linear relationship gave the regression equation: I_p (µA) = 1.2C (µM) + 14.0 and R^2 = 0.999. The limit of detection (LOD) and limit of quantification (LOQ) calculated using the relation *3s/m* and *10s/m*, where *s* is the standard deviation of the blank measurements (n = 6) and *m* is the slope of the analytical calibration curve, were found to be 0.025 and 0.083 µM, respectively.

Table 7 presents the analytical parameters (detection limit and linear range of the analytical curve) of different modified electrodes and techniques that have been previously reported in the literature for the detection of EP. The performance of the present sensor is superior to most of the previous sensors reported in the literature in terms of sensitivity and linear dynamic range (Table 7), which can be attributed to the synergic effect of the nanocomposites. Besides, the modification of the present sensor is very simple and does not require much time.

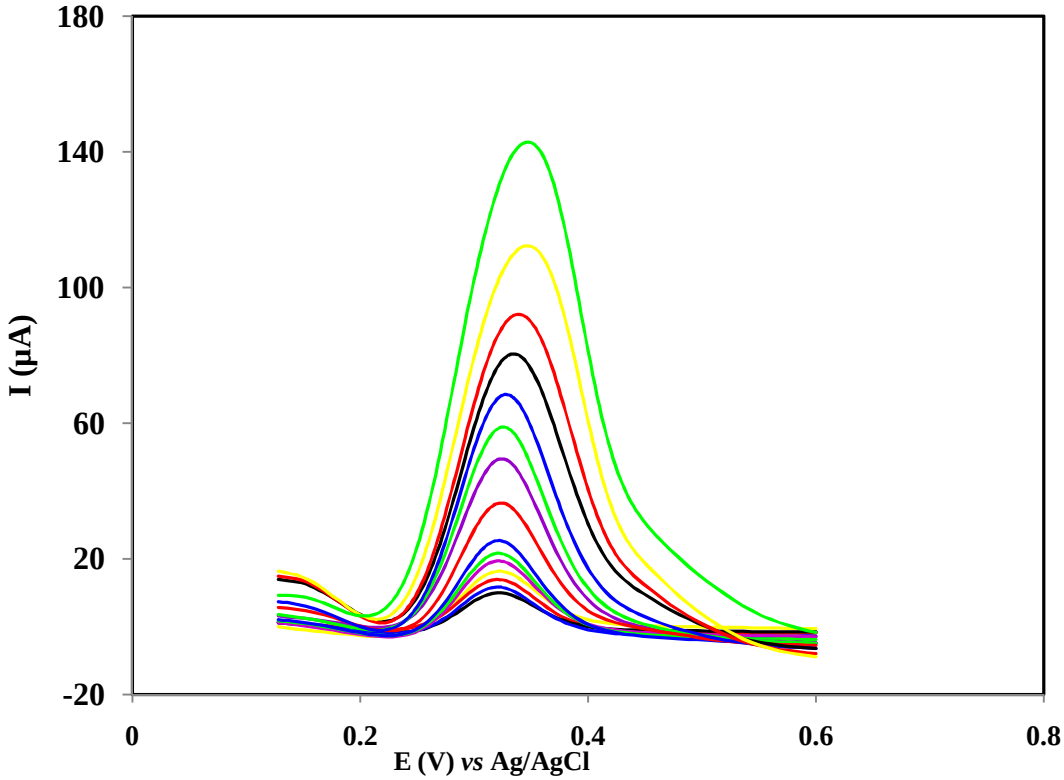

Figure 39. SWVs for varying concentrations of EP: 0.1, 0.5, 1.0, 2.5, 5.0, 10, 15, 20, 30, 40, 50, 60, 70, 90 and 110 µM in 0.1 M PBS pH 4 at P(L-Asp)/ERGO/GCE

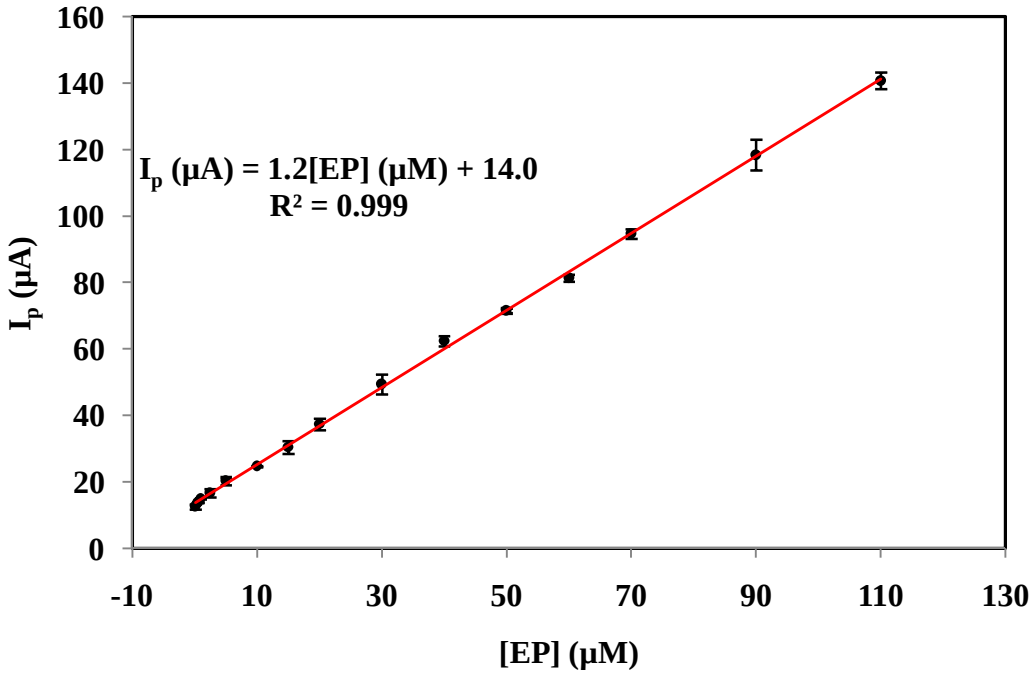

Figure 40. The plot of peak current *vs* EP concentrations

Table 7. Comparison of the performance of the proposed method with other electrochemical sensors used for the determination of EP

Electrode	Method	Linear range (µM)	LOD (µM)	References
[a]GR/GCE	CV	0.385–13.1 and 13.1–109	0.089	[228]
[b]P(L-Asp)/GCE	CV	0.12–11 and 11–110	0.046	[34]
[c]MPA/Au	CV	0.2–1 and 1–500	0.1	[223]
[d]GR/Au/GCE	CV	0.05–8	0.007	[224]
[e]Hcy/Au	CV	50–800	0.1	[226]
[f]L-Glu/GR/GCE	DPV	0.1–1000	0.03	[215]
[g]IL/CNTPE	DPV	0.3–450	0.09	[222]
[h]PTh/AuNPs/GCE	DPV	5.5–220	1.6	[225]
[i]L-Cys SAMs/Au electrode	DPV	0.1–2	0.01	[252]
[j]2,7-BFGR/CPE	SWV	0.05–550	0.027	[253]
P(L-Asp)/ERGO/GCE	SWV	0.1–110	0.025	This work

[a]Graphene-modified glassy carbon electrode (GCE); [b]Poly(l-aspartic acid) modified GCE; [c]3-mercaptopropionic acid self-assembled monolayer modified gold electrode; [d]Graphene/gold nanocomposites modified GCE; [e]Homocysteine self-assembled gold electrode; [f]L-glutamic acid functionalized graphene nanocomposite modified GCE; [g]Novel ionic liquid modified carbon nanotubes paste electrode; [h]Polythionine/gold nanoparticles composites modified GCE; [i]L-cysteine self-assembled monolayers modified gold electrode; [j]2,7-bis(ferrocenylethyl) fluoren-9-one-graphene nano sheets modified carbon paste electrode.

5.3.13. Repeatability, Reproducibility and Stability of P(L-Asp)/ERGO/GCE

The repeatability of the P(L-Asp)/ERGO/GCE was investigated by measuring the SW voltammetric signals in 0.1 M PBS solution (pH 4.0) containing 50 µM EP. The relative standard deviation (RSD) of the peak currents obtained with the same electrode for ten consecutive measurements was 2.3%. On the other hand, the reproducibility of P(L-Asp)/ERGO/GCE was examined by comparing the responses of three different glassy carbon electrodes prepared following the same experimental procedure. The RSD of the peak currents between three different electrodes measured independently was found to be 1.6%. The long term stability of P(L-Asp)/ERGO/GCE was also studied by keeping the electrode in 0.1 M PBS (pH 6) at ambient condition when not in use. The peak current response of 50 µM EP was measured every 7 days for 3 three weeks using SWV in pH 4 PBS. After 15 and 21 days the electrode retained 95.5% and 92.0% of its initial response, respectively. The results show that the developed composite modified GC electrode provided excellent repeatability, reproducibility, and stability towards the electro-oxidation of EP.

5.3.14. Interference Study

The influence of various foreign species on the determination of 50 µM epinephrine was investigated under the optimum experimental conditions. The potentially interfering substances were chosen from the group of substances commonly found with EP in pharmaceutical formulations and biological fluids. The tolerance limit was defined as the maximum concentration of the foreign substances that cause an approximately ±5% relative error in the determination of epinephrine. According to the results, ascorbic acid, citric acid, D-glucose, lactose, glycine, Mg^{2+}, Ca^{2+}, Na^{+}, and K^{+} did not show any interference effect in the determination of epinephrine, Table 8. However, uric acid starts to interfere in the determination of EP when present at concentration of greater than two fold of EP. Thus, the P(L-Asp)/ERGO films not only increase the sensitivity but also successfully differentiates the signals of EP in the presence of common potential interferents.

Table 8. Interference effect of some foreign species on the peak current response of 50 µM epinephrine at P(L-Asp)/ERGO/GCE

Interferent	Concentration (µM)	Change in peak current response (%)
Uric acid	100	4.3
Ascorbic acid	1000	0.81
Citric acid	1000	4.2
D-Glucose	1000	1.5
Lactose	1000	5.3
Glycine	1000	3.0
Mg^{2+}	1000	-1.6
Ca^{2+}	1000	4.4
Na^{+}	1000	-0.57
K^{+}	1000	-3.6

5.3.15. Real Sample Analysis

In order to evaluate the applicability of the proposed electrochemical sensor for the determination of EP in real samples, pharmaceutical formulation of epinephrine hydrochloride injection was analyzed. Standard addition method was used to determine EP in the sample. The pretreatment and determination procedures for epinephrine hydrochloride injection were described in Section 4.4.1.3. The analytical results are summarized in Table 9. The epinephrine content was calculated to be 0.941 mg mL^{-1} with 3.7% RSD, showing good agreement with the content of EP declared by the manufacturer (1 mg mL^{-1} per epinephrine injection). In addition, the accuracy of this method was examined by comparison with the result from the UV assay (the UV absorbance of epinephrine at 278 nm in 0.1 M PBS solution pH 4) [214]. By means of t-test and F-test, the calculated t-value (2.9) and F-value (7.4) were both smaller than the theoretical values (4.3 and 19.0, respectively), at 95% confidence level. This implies that the proposed method could be reliably used for routine analysis.

Furthermore, the accuracy of the present method and UV assay were verified using recovery study by spiking the epinephrine hydrochloride injection with standard EP solution. The obtained recovery values were in the range: 94–109%, Table 9. The results indicate that the P(L-Asp)/ERGO composite modified GC electrode can be effectively used for the selective determination of epinephrine in pharmaceutical samples.

Table 9. Detection of epinephrine in epinephrine hydrochloride injections and the recovery results at P(L-Asp)/ERGO/GCE using SWV and UV assay

Labeled value (mg mL^{-1})	[a]Determined ± RSD (mg mL^{-1})		Detected (%)		Added (μM)	[a]Found ± RSD (μM)		Recovery (%)	
	SWV	UV	SWV	UV		SWV	UV	SWV	UV
					10	10.9 ± 1.5	10.6 ± 0.2	109	106
1	0.941 ± 3.7	0.996 ± 1.1	94.1	99.6	20	19.0 ± 4.7	19.6 ± 0.1	95.0	98.0
					30	30.7 ± 4.2	31.2 ± 0.2	102	104
					50	47.0 ± 4.0	–	94.0	–

[a]*Mean value (n = 3)*

5.4. Synthesis, Characterization and Preparation of Nickel Nanoparticles Decorated Electrochemically Reduced Graphene Oxide Modified Electrode for Electrochemical Sensing of Diclofenac

5.4.1. Background

Nonsteroidal anti-inflammatory drugs (NSAIDs) block the cyclooxygenase enzymes and reduce the production of prostaglandins that promote inflammation, pain and fever throughout the body [254]. Diclofenac sodium, 2-[(2,6-dichlorophenyl)amino]benzeneacetic acid sodium, Scheme 8, is a well known non-steroidal anti-inflammatory drug (NSAID) used for the treatment of a number of diseases such as rheumatoid arthritis, ankylosing spondylitis, osteoarthritis, and sport injuries [255]. It has a strong antipyretic, analgesic and anti-inflammatory properties. The efficacy of diclofenac (DIC) equals many newer and established NSAIDs, with a fast onset and a long duration of action as an analgesic. Diclofenac is well tolerated and rarely produces gastrointestinal ulcerations or other serious side effects compared to other NSAIDs and can be considered as one of the few non-steroidal anti-inflammatory drugs of first choice used in the treatment of acute and chronic inflammatory conditions [255, 256]. It is used as tablets, capsules, suppositories, intravenous solutions and gels for dermal application [257]. Despite its efficient activity, DIC has several drawbacks, mainly a short biological half-life due to its very rapid metabolism, a high percentage of protein binding and a very high pre-systemic metabolism. This makes the need for using high doses, simultaneously leading to severe dose-limiting side effects including cardiac, gastrointestinal, hepatic and renal adverse events [254]. Therefore, it is vital to develop a simple, fast, selective and cost-effective method for the determination of trace amounts of DIC in different pharmaceutical formulations and biological fluids for pharmaceutical and clinical needs where it is used for the treatment of various diseases.

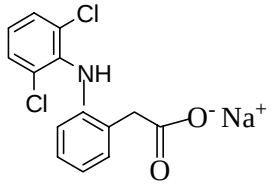

Scheme 8. The chemical structure of diclofenac sodium

Owing to the remarkable use of diclofenac in clinical applications, various methods have been developed for the determination of diclofenac in biological fluids and pharmaceutical preparations including chromatography [258-263], spectrophotometry [264-266], spectrofluorimetry [267] and electrochemical methods [268-272]. Chromatographic and spectrophotometric methods are expensive, use excessive organic solvents and require well trained personnel and exhaustive sample preparation which is time consuming compared to electroanalytical techniques. Therefore, electrochemical techniques are the method of choice due to their fast response, high sensitivities, simple operation, and the possibilities of miniaturization. Besides no sample preparation/preconcentration step requirement, the suitability for real-time monitoring using low-cost instrumentation provides another very important advantage of the electrochemical methods that favors their use and development [271, 272].

The success of electrochemical techniques depends on the performance of the working electrode material since the analytical parameters depend on the response of the working electrodes. Various working electrode materials with different modification protocols were reported in the literature for diclofenac determination including room-temperature ionic liquid-modified carbon nanotubes paste electrode [255], gold nanoparticle/multi-walled carbon nanotubes modified glassy carbon electrode (GCE) [256], bare graphite electrode [257], Tyrosine modified carbon paste electrode (CPE) [268], edge plane pyrolytic graphite electrode [269], carboxyl-functionalized graphene oxide-modified GCE [270], copper ions immobilized on MWCNTs-chitosan thin film modified GCE [271], spinel-structured magnesium ferrite nanoparticles ($MgFe_2O_4$) graphite paste electrode modified with MWCNTs [273], multiwalled carbon nanotubes and ionic liquid modified carbon ceramic electrode [274], novel ionic liquid multiwall carbon nanotubes paste electrode [275], bismuth film electrode [276], and boron-doped diamond electrode [277]. Thus, the development of modified electrodes is certainly one of the most extensive areas of research due to the gradual passivation or contamination of unmodified solid working electrodes due to adsorption of the electrochemically generated products.

Recently, immobilization of mediating nanomaterials on an electrode surface as a catalyst for electrochemical sensor application is a hot topic owing to large specific surface area, excellent conductivity and electrocatalytic activity. Nanomaterials can be directly used as electrode

materials or as catalytic labels for amplified electrochemical detection [51]. Various metal nanoparticles (MNPs) have gained increasing attention because of their unique nanoscale physical and chemical properties. They possess high chemical stability and electrocatalytic activity. Despite the fact that noble metal nanoparticles exhibit good electrocatalytic activities, the scarcity and high cost of noble metal nanocatalysts limits their wider use and commercial applications. Therefore, alternative catalysts consisting of non-precious metals have been of high demand. Transition metal nanoparticles of Ni and Co have attracted extensive interest in this regard due to their low cost and easy availability and have shown outstanding performances for electroanalytical applications [50, 278]. For example, Hassan *et al*. reported the electrochemical and analytical applications of nickel nanoparticles dispersed on poly(1,5-diaminonaphthalene) modified glassy carbon electrode for NADH detection [279], Guo, Yu and Hu described nickel nanoparticles for the efficient electrocatalytic oxidation of methanol in an alkaline medium [280], Zhang and his group illustrated electrochemical deposition of nickel nanoparticles on reduced graphene oxide film for non-enzymatic glucose sensing [281], Long *et al*. described cobalt-nickel bimetallic nanoparticles decorated graphene sensitized imprinted electrochemical sensor for the determination of octylphenol [282], fabricated nickel-cobalt nanostructures coated reduced graphene oxide nanocomposite electrode for non-enzymatic glucose biosensing was also described by Wang *et al*. [283], and Asgari and his group reported electrocatalytic oxidation of methanol on nickel-cobalt modified glassy carbon electrode in alkaline medium [284].

However, though they present high catalytic performance, aggregation was found for this kind of materials because of the effects of magnetic force and smaller particle size, leading to lower catalytic efficiency in long-term applications. Thus, the development of active and stable MNPs-based catalysts is highly desirable. To overcome the above drawback, it is necessary to disperse metal nanoparticles on a suitable solid support with low cost, high surface area, and superior chemical and physical properties. Recently, carbon nanomaterials such as graphene are widely used as the solid support to disperse and stabilize metal nanoparticles in catalytic process [50].

Graphene, a single layer of carbon atoms in a closely packed honeycomb two-dimensional lattice, has attracted tremendous attention because of its excellent physical and chemical properties. The remarkable surface area, excellent conductivity and wide electrochemical

window have made it an ideal material for electrochemical sensing applications [51]. Graphene is a promising matrix to support metal nanoparticles in the realization of new catalysts due to its unique physical, chemical and remarkable tunability. Compared with the unsupported metal nanoparticles, graphene can enhance the stability and improve the electrocatalytic properties of the MNPs [50]. Interestingly, it was also found that the incorporation of nanomaterials into 2D graphene play a role as a bridge for accelerating electron transfer between graphene sheets and hence prevent face-to-face agglomeration or irreversible aggregation of graphene sheets [282].

This work describes a new electrochemical sensor based on nickel nanoparticles (NiNPs) decorated electrochemically reduced graphene oxide (ERGO) modified glassy carbon electrode for the detection of diclofenac. The electrochemical behavior of the sensor was investigated using cyclic voltammetry (CV), square wave voltammetry (SWV) and electrochemical impedance spectroscopy (EIS). The synthesis and characterization of nickel nanoparticles (NiNPs) and graphene oxide (GO) are also presented.

5.4.2. UV–Visible Spectroscopic Characterization

The UV–Visible spectroscopy was studied in the range 200-700 nm. UV-Vis spectroscopic result of NiNPs depicts high absorbance peak at 265 nm, Figure 41 (curve a), confirming the formation of NiNPs. Elango *et al*. reported UV-Vis absorbance at 252 nm for biosynthesized nickel nanoparticles [285]. Singh *et al*. described the synthesis of nickel nanoparticles by pulsed laser induced fragmentation method and reported an intense absorption band at 213 nm with an intense broad absorption band at 263 nm with the later band attributed to surface plasmon resonance of nickel [286]. Chandra, Kumar, and Tomar also reported UV-Vis spectrum of Ni nanoparticles in characterizing the metallic nature with a broad absorbance peak in the range of 250–370 nm [287].

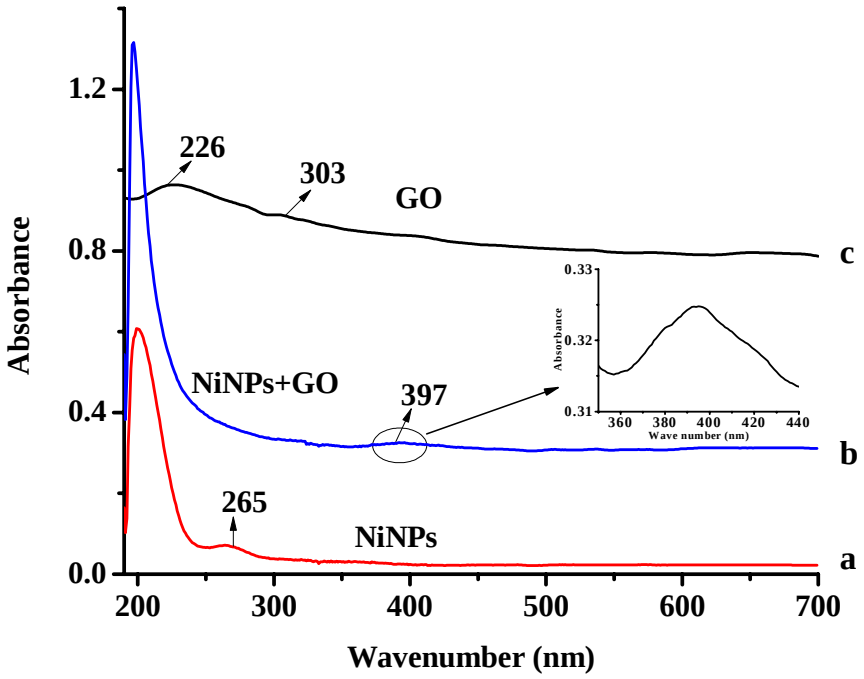

Figure 41. UV-Vis spectra of NiNPs, GO and NiNPs/GO in ethanol

The UV–Visible spectroscopic results of GO is shown in Figure 41 (curve c). Two characteristic absorption peaks are observed in this spectrum with a broad absorption band at 226 nm and weak shoulder peak at about 303 nm corresponding to π-π* transitions for C=C bonds and n-π transitions of carbonyl groups, respectively [288, 289]. The spectrum of NiNPs/GO composite shows a single weak broad absorption band at about 397 nm, Figure 41, (curve b), the inset presents the magnified absorption peak of the region. The red-shift in the absorption band to a higher wavelength in the composite as compared to the individual NiNPs and GO absorption peaks might be attributed to the shift of the π-electron density of graphene oxide to the d-orbital of Ni metal.

5.4.3. FTIR Characterization

Figure 42 presents the FTIR spectra of (a) graphite oxide, GO, and (b) a mixture of nickel nanoparticles and graphite oxide, NiNPs/GO. For comparison the FTIR spectra of pristine graphite and nickel nanoparticles were also presented in the Inset of Figure 42, spectra a and b, respectively. Obviously, no absorbance peak is observed for pure graphite. Similarly, no absorbance band is found for the nickel nanoparticles indicating the absence of oxide formation.

The formation of GO was confirmed by the presence of several bands attributed to oxygen functionalization, Figure 42a. The FTIR spectra of GO shows characteristic peaks at about 3400, 1633, 1431, 1284, 1174, 1069 cm^{-1}, corresponding to O–H-stretching vibration of hydroxyl group, C=C-stretching of non oxidized aromatic ring in the GO, deformation vibration peaks of terminal hydroxyl groups, C–O–C-stretching vibrations, epoxy C–O-stretching vibration and alkoxy C–O-stretching vibration, respectively. C=C–skeletal vibration of the graphene planes was also observed at about 1573 cm^{-1} [242, 290-292]. At NiNPs and GO composite, Figure 42b, the peak at 3400 in GO become broadened and shifted by about 100 cm^{-1} to a lower wave number of 3306 cm^{-1}. The band at about 1633 and 1284 cm^{-1} for GO almost disappeared in the composite while the absorption peaks at 1174 and 1069 cm^{-1} shifted to 1141 and 1090 cm^{-1}. The disappearance and shift of these peaks confirm the interaction between delocalized π-electrons of the GO with the d-orbital of the metal nanoparticles [293]. Nickel is among strongly interacting metals with graphene based materials with a special case of a lattice matched system. It has been reported that the physical properties of GO is significantly altered when decorated with nickel nanoparticles because of the chemical interaction between GO and nickel, attributed to the hybridizations of the metal d-electrons with the π-electrons of graphene [294].

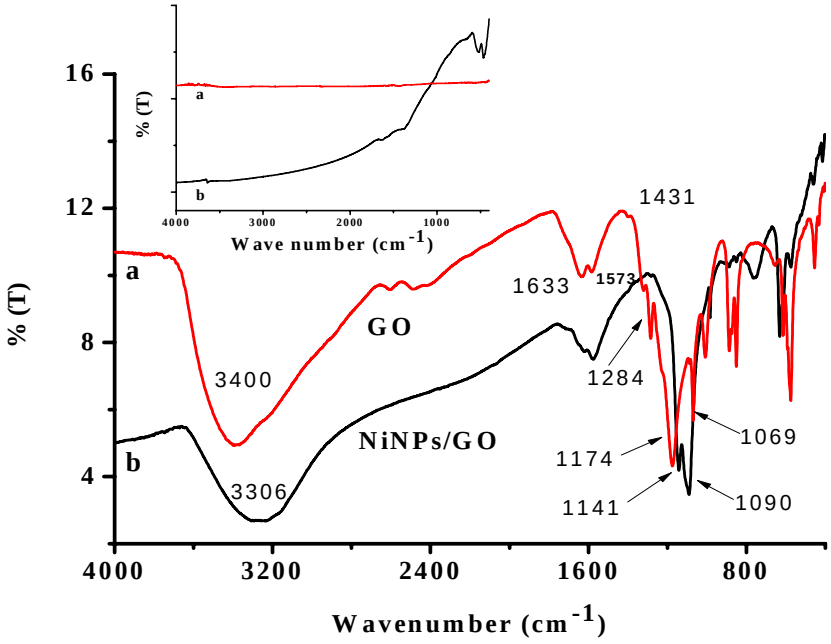

Figure 42. FTIR spectrum of GO (a) and NiNPs/GO; Inset: FTIR spectra of graphite (a) and NiNPs (b)

5.4.4. Morphological and Structural Characterization

The surface morphology, microstructure and size of the synthesized materials were characterized by HR-TEM and HR-SEM techniques. The TEM image of the graphene oxide (Figure 43a and b) clearly shows well exfoliated ultra-thin graphene sheets indicating the successful formation of GO from graphite powder. Figure 43d and e display TEM micrographs of NiNPs at lower and higher magnification. The result shows homogenous distribution of spherically shaped nickel nanoparticles with average particle diameter of about 5 nm as shown in histogram of Figure 44. Generally, Ni nanoparticles tend to aggregate in order to minimize the total surface energy of the system due to the large surface to volume ratio and strong magnetic forces [295]. However, the formation of agglomerates was controlled due to the presence of ethylene glycol used during the synthesis step. On the other hand, Figure 43g and h illustrate the HRTEM image of the composites of NiNPs and GO which obviously presents the incorporation of the metal nanoparticle into the graphene oxide sheets. It has been reported that graphene can aid the nucleation and growth of metal nanoparticles owing to its large surface area [54]. Selected area electron diffraction (SAED) pattern of GO, NiNPs and NiNPs/GO were investigated and the results are shown in Figure 43 (c, f and i), respectively. The diffuse small spots making the rings in Figure 43c indicate the polynanocrytalline nature of GO. However, for the NiNPs, the bright spots making continuous concentric ring patterns over a longer distance is apparent showing the prepared NiNPs are crystalline in nature, Figure 43f. The SAED result of NiNPs/GO also shows ring patterns of a semi-crystalline material, Figure 43i.

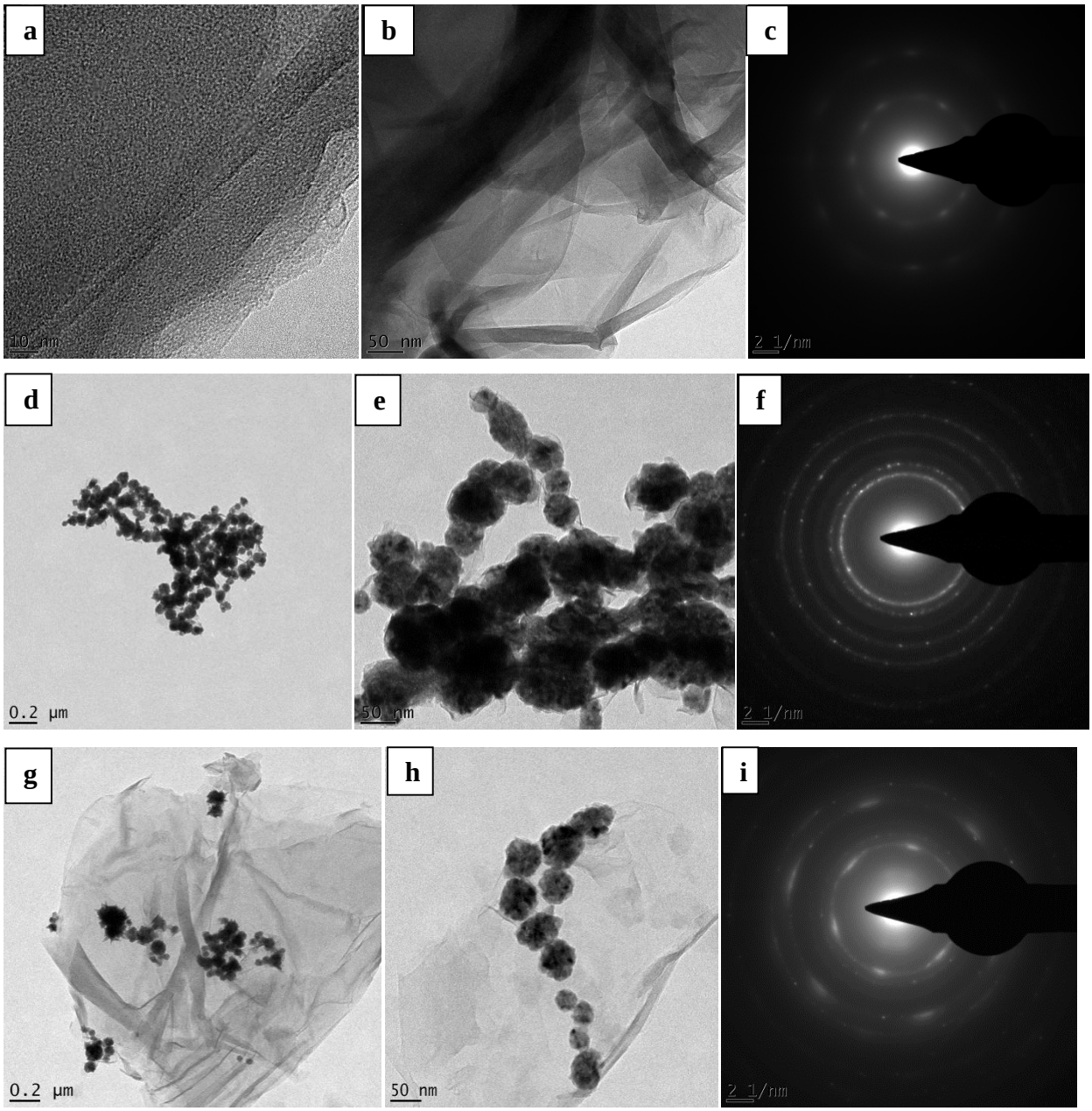

Figure 43. HRTEM micrographs of GO (a and b), NiNPs (d and e) and NiNPs/GO (g and h) and SAED results of GO (c), NiNPs (f) and NiNPs/GO (i)

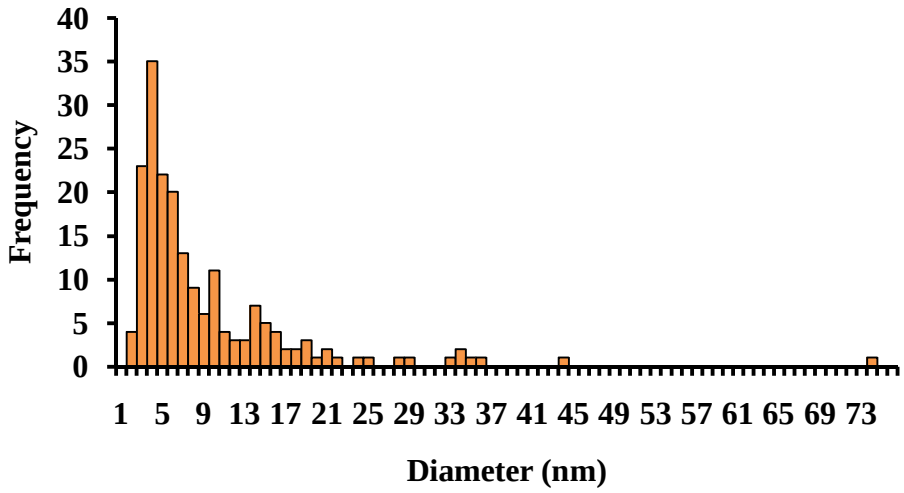

Figure 44. Histogram showing the size distribution of NiNPs

Figure 45(a–c) shows the TEM-EDS data for the elemental composition of the three materials, GO, NiNPs and the mixture of the two, GO and NiNPs. The EDS result confirms the presence of carbon and oxygen atoms in GO as major components, Figure 45a. The EDS peaks of the Ni nanoparticles (Figure 45b) proved the presence of nickel, with energy lines at about 8–9 and 0.8–1 keV which represents the K and L lines, respectively [296]. Figure 45c, illustrates the EDS spectrum of NiNPs/GO composite which confirms the presence of C, O and Ni as expected. The peak at about 8 keV in all the spectra corresponds to the copper grid used to support the sample.

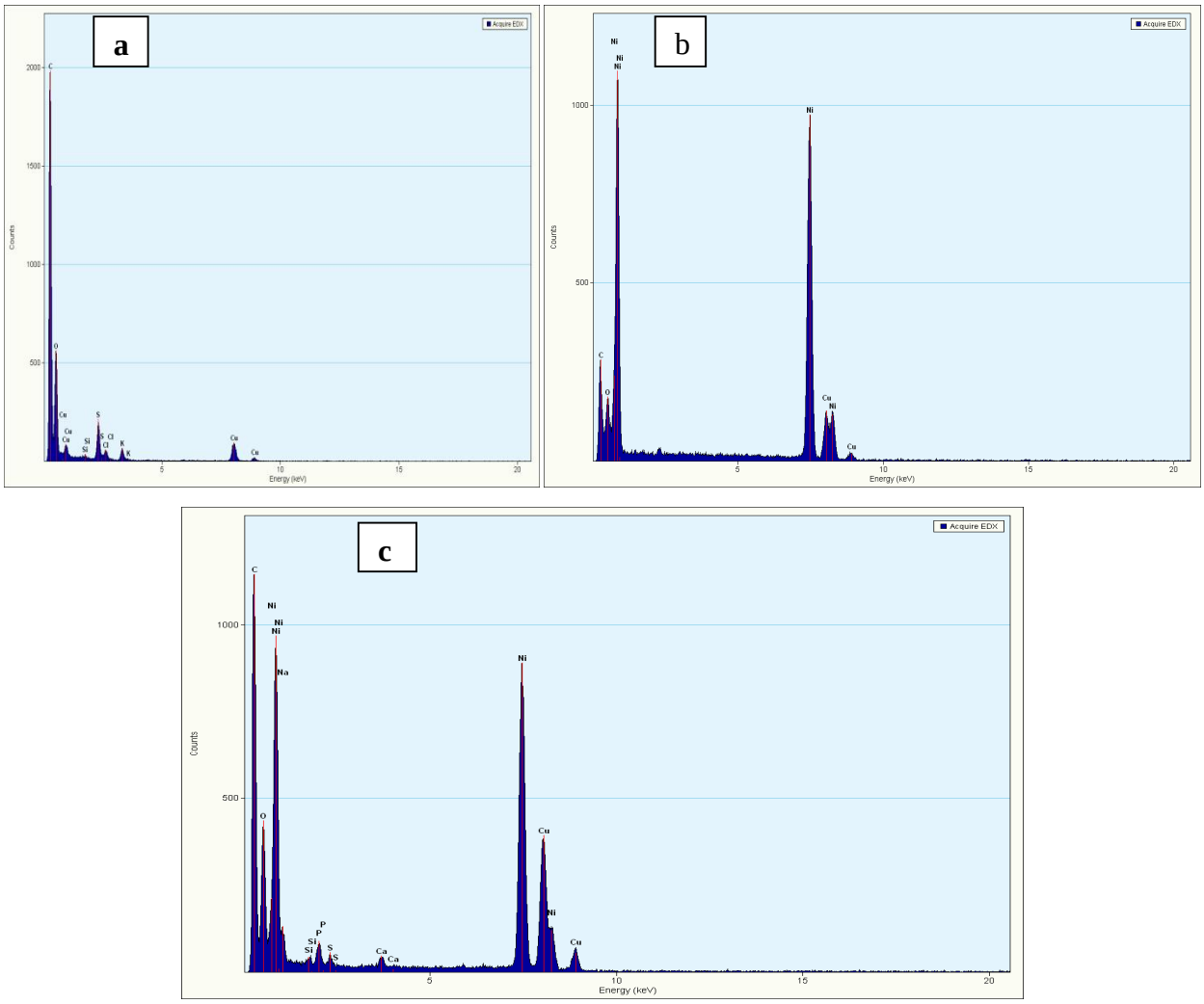

Figure 45. EDS spectrum of GO (a), NiNPs (b) and NiNPs/GO (c)

Figure 46 illustrates the SEM micrographs of graphite (a), graphite oxide (b), NiNPs (c and d), ERGO (e and f) and NiNPs/ERGO (g and h). As can be seen from the image Figure 46a, stacked layers of graphene sheets are observed because of the strong interlayer π-π interaction in the pristine graphite [297]. On the other hand the microstructure of graphite oxide (Figure 46b) clearly demonstrates layered platelets composed of curled and wrinkled graphene sheets. It is clear that the graphene sheets are agglomerated and overlapped [298]. Figure 46c present the HRSEM micrograph images of NiNPs which show densely and uniformly distributed NiNPs.

Figure 46d illustrate the SEM microstructures of electrochemically deposited GO which presents the successful formation of a thin layer of graphene sheets on the working electrode surface with

some small cracks observed. The SEM image of NiNPs/ERGO clearly demonstrates the electrodeposition of both ERGO and the NiNPs on the surface of the electrode which is an evidence for the incorporation of the NiNPs in to graphene, Figure 46e. A closer observation of the image at higher magnification for the composite modified electrode indicates uniform distribution of the nanoparticles within the graphene structure, which is in agreement with the HRTEM results.

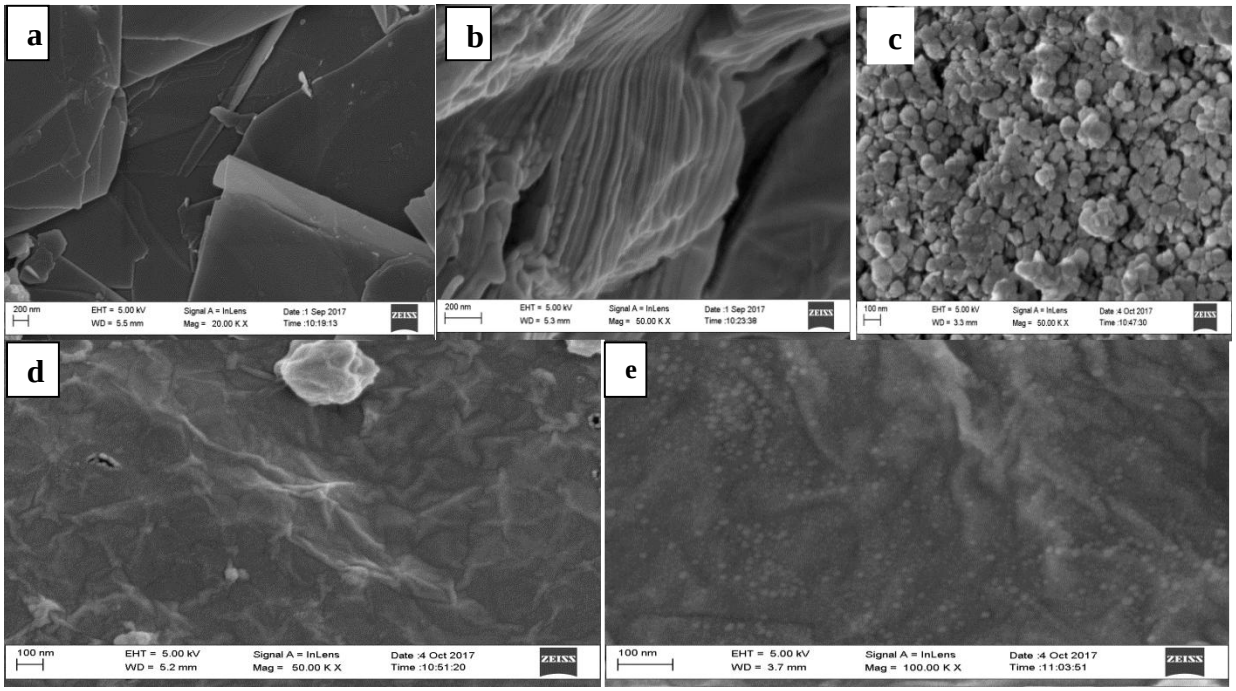

Figure 46. SEM micrographs of graphite (a), graphite oxide (b), NiNPs (c), ERGO (d) and NiNPs/ERGO (e)

5.4.5. Electrochemical Characterization of NiNPs/GCE and NiNPs/ERGO/GCE

The electrochemical behavior of the NiNPs/GCE and NiNPs/ERGO/GCE was investigated by cyclic voltammetry in 0.1 M of NaOH solution at various scan rates (v) in the ranges of 20–200 mV s^{-1}, Figure 47 and Figure 48. As shown in the Figures, a pair of well defined redox peaks is observed in all the cyclic voltammograms in the potential range of 0.2–0.7 V, which can be attributed to the electron transfer between Ni(II) and Ni(III) redox couple. It is well-known that metallic nickel nanoparticles, Ni(0), can react with OH^- ions in alkaline media to produce Ni(II). The Ni(II) can be oxidized to Ni(III) in the anodic scanning cycle which can be followed by the reduction of the Ni(III) to Ni(II) in the reverse cathodic scan. The oxidation peak in the anodic

direction is observed at about 0.53 V arising from the oxidation of $Ni(OH)_2$ to NiOOH at the electrode surface and the corresponding reduction peak in the reverse direction at 0.43 V is ascribed to the reduction of NiOOH to $Ni(OH)_2$, equation (10) and (11) [299, 300]. With increase in potential scan rate, the anodic and cathodic peak currents grow steadily. As shown in the Figure 47 and 48, it can be observed that both the anodic and cathodic peak currents are proportional to the scan rate (Inset of Figure 47 and 48) with a linear regression equation of I_{pa} (µA) = 0.04 *v* (mV s^{-1}) + 0.4, R^2 = 0.998 and I_{pc} (µA) = -0.02 *v* (mV s^{-1}) + -0.2, R^2 = 0.998 for NiNPs modified GCE and I_{pa} (µA) = 0.2 *v* (mV s^{-1}) + 2, R^2 = 0.997 and I_{pc} (µA) = -0.1 *v* (mV s^{-1}) + -0.5, R^2 = 0.998 for NiNPs/ERGO/GCE, respectively, which implies that the electrode reactions are mainly controlled by surface adsorption process. Besides, the anodic peak potential shift positively whereas the cathodic peak potential remain almost constant with increasing scan rate, demonstrating a quasi-reversible electron transfer of the electrochemical reaction at the electrode surface. The anodic and cathodic peak current response at the composite of NiNPs and ERGO was stable and higher as compared to the electrode modified with NiNPs only, showing the graphene has played a role in stabilizing the NiNPs by anchoring to the glassy carbon electrode surface. Additionally, in the absence of graphene, the size of the nickel nanoparticles may grow which may lead to a decrease in the surface area.

$$Ni(s) + 2OH^- \longrightarrow Ni(OH)_2 + 2e^- \quad (10)$$

$$Ni(OH)_2 + OH^- \rightleftharpoons NiOOH + H_2O + e^- \quad (11)$$

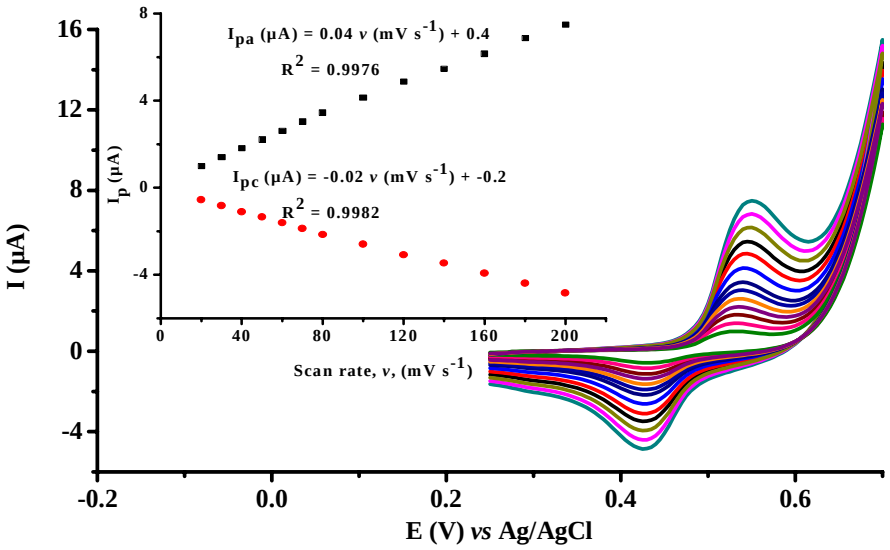

Figure 47. CV of NiNPs/GCE in 0.1 M NaOH solution at different scan rates (20-200 mV s^{-1}); Inset: plot of anodic and cathodic peak currents *vs* the scan rates

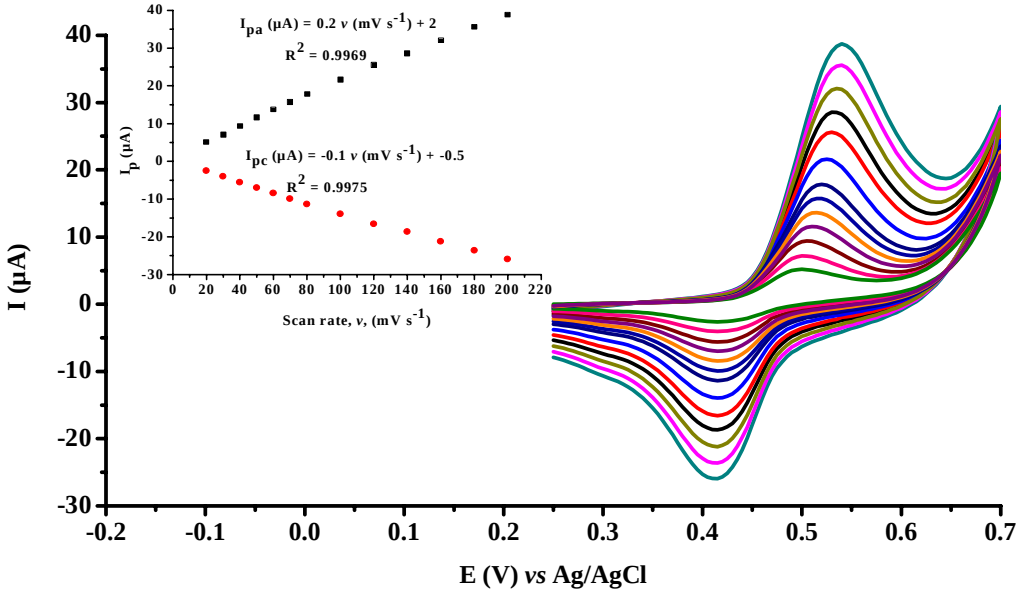

Figure 48. CV of NiNPs/ERGO/GCE in 0.1 M NaOH solution at different scan rates (20-200 mV s^{-1}); Inset: plot of anodic and cathodic peak currents *vs* the scan rates

5.4.6. Electrochemical Impedance Spectroscopy (EIS)

Electrochemical impedance spectroscopy (EIS) is an efficient technique to study the interfacial properties of modified electrodes [301]. The Nyquist plot of EIS consists of a semicircle portion

which represents the charge-transfer resistance (R_{ct}) in the high-frequency range, while the linear part corresponds to the low-frequency range, where diffusion-controlled process occurs [302]. As depicted by the Nyquist plot in Figure 49, the highest diameter of the semicircle which represents the charge transfer resistance, R_{ct}, was observed for bare GCE (curve a), indicating slow electron transfer behavior for the electrochemical probe. At the NiNPs/GCE (curve b) the charge transfer resistance was slightly decreased as compared to the bare electrode which confirms the NiNPs improves the charge transfer process. In the spectra recorded for ERGO (c) and NiNPs/ERGO (d) composite modified electrodes the semicircle region were not observed at high frequency, probably due to the low faradic charge-transfer resistance, instead characterized by high capacitive lines, specific to graphene materials. This represents restricted finite diffusion within the graphene layer [303, 304].

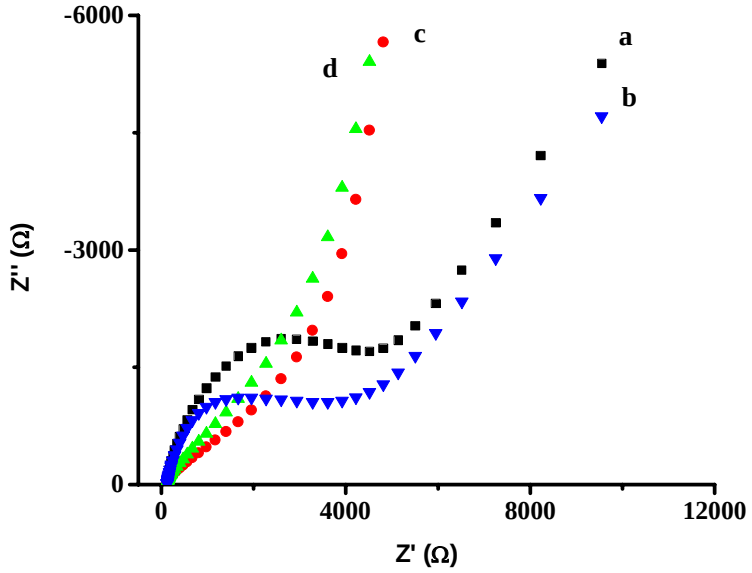

Figure 49. Nyquist plots of electrochemical impedance spectra of bare (a), NiNPs (b), ERGO (c) and NiNPs/ERGO (d) modified GCEs in 1 mM $Fe(CN)_6^{3-}/Fe(CN)_6^{4-}$ in 0.1 M KCl. Applied voltage: 0.23 V, amplitude: 5 mV; frequency: 100 mHz to 100 kHz

5.4.7. Cyclic Voltammetry and Square Wave Voltammetry Study

The electrochemical behavior of DCF at the surface of bare and modified glassy carbon electrodes was investigated by cyclic voltammetry in the potential range of 0.0 to 1.0 V at scan rates of 50 mV s^{-1}. Figure 50 shows the cyclic voltammograms of bare and modified electrodes

containing 0.1 M PBS in the absence (a) and presence (b–e) of 50 µM DIC. No obvious redox peak appeared in the buffer solution, PBS (curve a). At the bare GCE (curve b) a weak anodic peak was observed at a relatively higher potential region of 0.75 V. When the bare glassy carbon electrode was modified with electrochemically reduced graphene oxide, ERGO/GCE (curve c) and nickel nanoparticles, NiNPs (curve d), the peak current response of DIC was increased by nearly two and four fold of the bare electrode response, respectively. The significant enhancement of the peak current response of diclofenac provides clear evidence of the catalytic effect of nickel nanoparticles and the electrochemically reduced graphene oxide. At the ERGO/GCE, the increase in the peak current response was accompanied with high capacitive current which is characteristic of graphene based materials due to the high electrical conductivity and surface area. However, at the NiNPs/GCE and composite of NiNPs/ERGO/GCE the capacitive current significantly drops, indicating the electrocatalytic role played by the metallic nickel nanoparticles. The maximum current response was observed for the NiNPs/ERGO composite modified glassy carbon electrode (curve e) with an anodic peak response of about five fold compared to the glassy carbon electrode which suggests the synergetic effect of the nickel nanoparticles and the electrochemically reduced graphene oxide.

Careful investigation of the cyclic voltammogram of DIC shows an irreversible anodic peak (peak Ia) when scanned in the positive direction. In the reverse scan a cathodic peak (peak IIc) was observed which gave a second reversible oxidation peak (peak IIa) in the subsequent scans towards positive potentials. Figure 51A illustrates the CVs of DIC for the first three scans (1, 2 and 3). Similar observation was obtained using square wave voltammetry, Figure 51B.

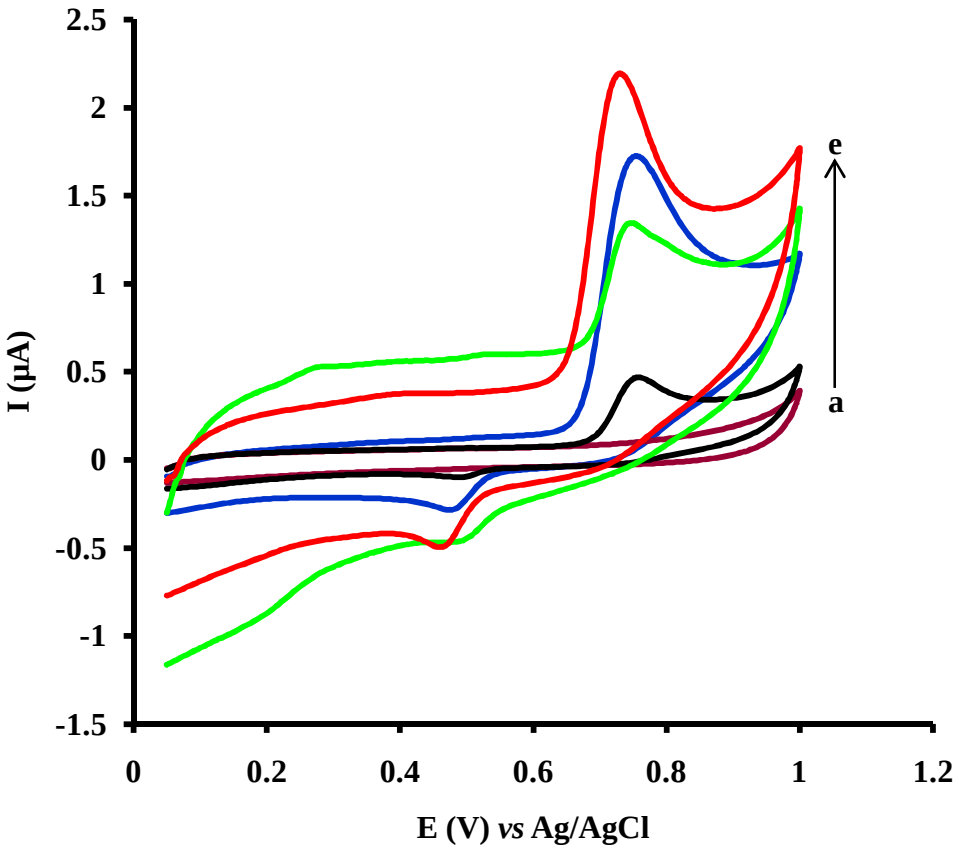

Figure 50. CVs recorded in pH 4 PBS in the absence (curve a) and presence of 50 µM DIC at bare GCE (b), ERGO/GCE (c), NiNPs/GCE (d) and NiNPs/ERGO/GCE (e) at 50 mV s^{-1}

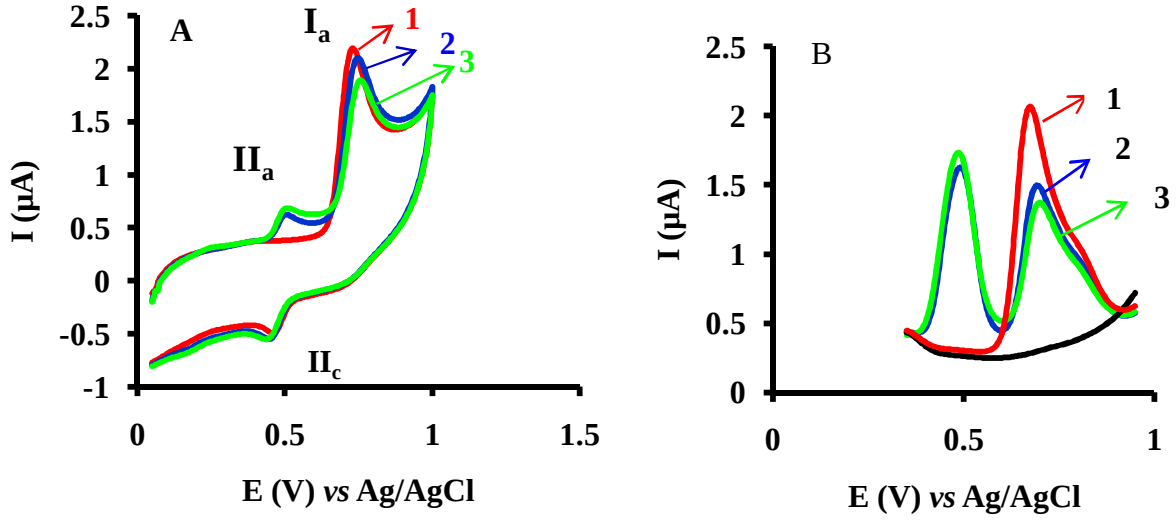

Figure 51. CVs (A) and SWVs (B) of 50 µM DIC in pH 4 PBS for the first three consecutive scans at NiNPs/ERGO/GCE at 50 mV s^{-1}

The redox reaction mechanism of diclofenac is presented in Scheme 9 [269, 270]. The first step involves abstraction of an electron (**1**), which leads to a nitrogen centered radical cation formation (**2**). The radical cation undergoes rearrangement and deprotonation leading to a carbon centered radical *para* to the amino group (**3**), which was followed by a second electron abstraction leading to a carbocation (4). The carbon cation then reacts with water and by aromatization of the intermediate to form 5-OH diclofenac (**5**). Hence, diclofenac is oxidized to 5-OH diclofenac by a process involving the loss of $2e^-$ and $2H^+$. The 5-OH diclofenac intermediate formed further undergoes a reversible electrode reaction involving $2e^-$, $2H^+$ to form quinone imine (**6**). This mechanistic reaction pathway is in agreement with the cyclic voltammetric result of diclofenac, Figure 51a. As shown in the cyclic voltammogram, diclofenac gives a single irreversible oxidation peak at about 0.73 V in the first scan cycle which can be attributed to the oxidation of diclofenac to 5-OH diclofenac. In the reverse scan a reduction peak was observed at about 0.45 V which has a corresponding reversible oxidation peak at about 0.51 V. This reversible redox couple can be due to the conversion of the 5-OH diclofenac to diclofenac 2,5-quinone imine [269].

Another interesting observation in both the cyclic voltammetric and square wave voltammetric study was that the first oxidation peak (peak I_a) was unstable and rapidly decreases during successive scan cycles while the reversible redox pairs give very stable redox peaks (Figure 51 curve 1, 2, 3). This further confirms that the first anodic peak is the result of the formation of unstable 5-hydroxy diclofenac intermediate whereas the stability of the redox pair can be ascribed to the formation of stable equilibration between 5-OH diclofenac and diclofenac 2,5-quinone imine. Therefore, the voltammetric responses corresponding to the second anodic peak current (peak II_a) were generally recorded for the quantification of diclofenac in the present work.

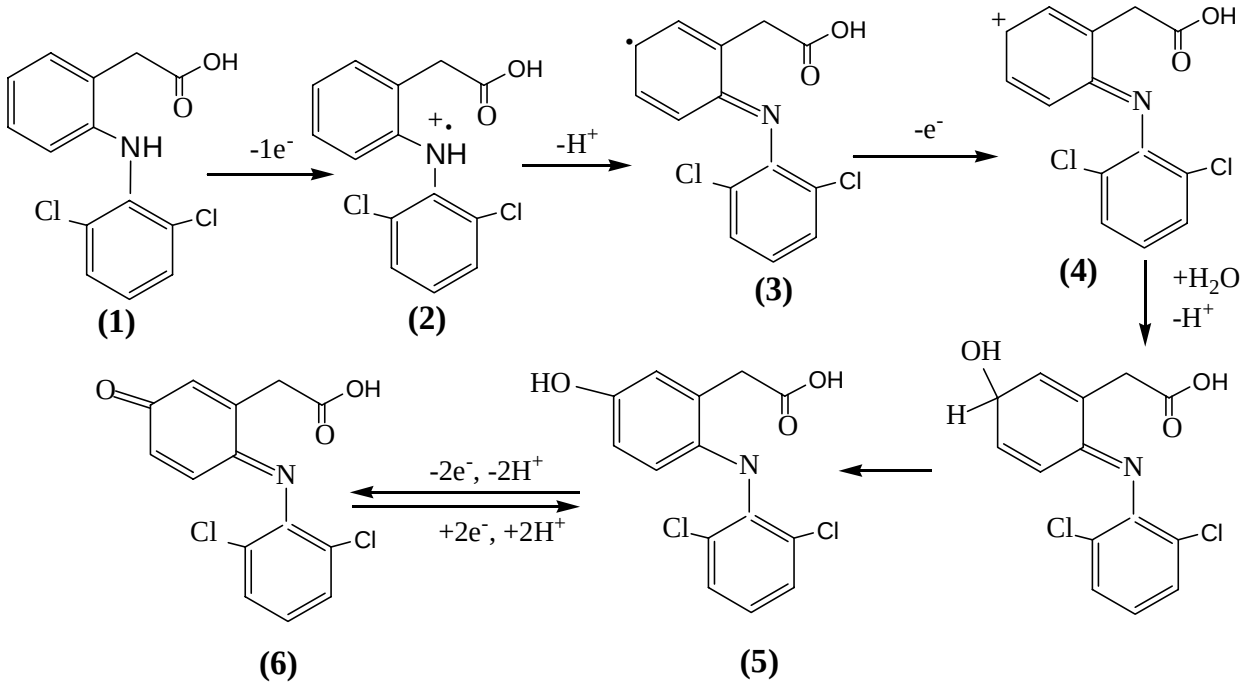

Scheme 9. A proposed mechanism for the electrooxidation of diclofenac

5.4.8. The Effect of Potential Scan Rate

The influence of potential scan rate on the performance of NiNPs/ERGO/GCE in the determination of 50 µM DIC in 0.1 M PBS pH 4 was evaluated at different scan rates using cyclic voltammetry. The scan rate studies were carried out to evaluate whether the processes at NiNPs/ERGO/GCE were under diffusion or adsorption control. As shown in Figure 52, the peak current response of diclofenac increases with scan rate and there is a good linear relationship between the peak currents of DIC and the scan rates in the range of 30–250 mV s^{-1}, Figure 53. The linear regression equation was given as: I_p (µA) = 0.009 *v* (mV s^{-1}) + 0.2, R^2 = 0.999. This relationship suggests that the electrochemical behavior of diclofenac sodium at the NiNPs/ERGO/GCE was predominantly an adsorption-controlled electrode process rather than diffusion-controlled process in the studied scan rates [256, 269, 271]. Moreover, the analysis of the relationship between logarithm of peak current (log Ip) and logarithm of scan rate (log *v*) in the range of 30–250 mV s^{-1} showed a straight line with linear relationship of log I_p (µA) = 0.82 log v (mV s^{-1}) – 1.6, R^2 = 0.993. The slope value of 0.82 is close to the theoretical value of 1.0 for a surface adsorption controlled electrode process [256].

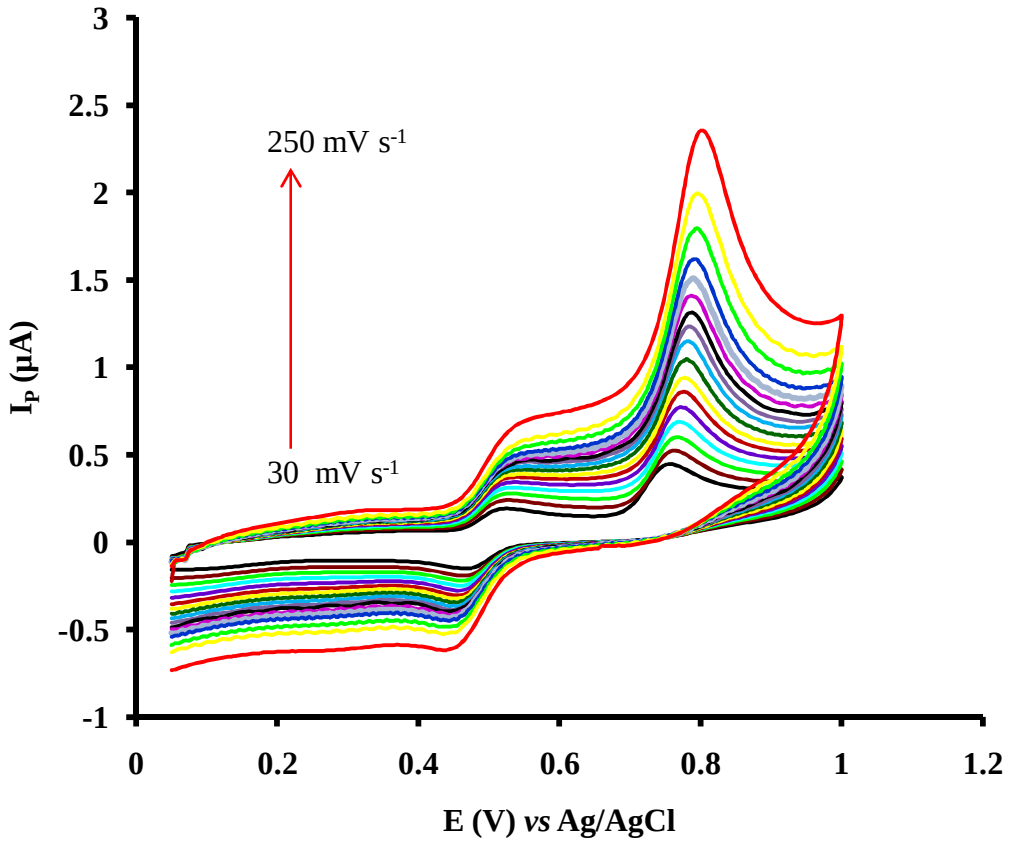

Figure 52. CVs for 50 µM DIC in PBS (pH 4) at NiNPs/ERGO/GCE at various scan rates (30–250 mV s^{-1})

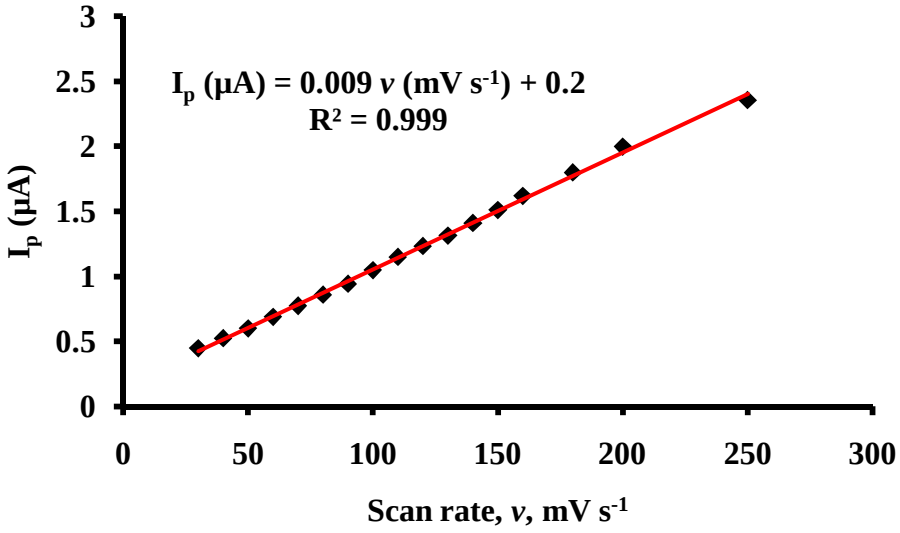

Figure 53. Plot of the peak current *vs* scan rates for 50 µM DIC in 0.1 M PBS

5.4.9. The Effect of pH

The effect of pH on the electrochemical responses of diclofenac at NiNPs/ERGO/GCE was studied using cyclic voltammetry for 50 µM DIC in 0.1 M PBS at a scan rate of 50 mV s^{-1}. Figure 54 shows the cyclic voltammograms of DIC at varying pH in the range 4.0-9.0. It is clearly observed that the peak current of DIC decreased with increasing pH. The maximum peak current was obtained at a lower pH value of 4.0. Hence, 0.1 M phosphate buffer solution of pH 4.0 was used as the supporting electrolyte for subsequent voltammetric experiments in this work.

The dependence of peak potential for 50 µM DIC on the pH of the supporting electrolyte was also investigated, Figure 55. The anodic peak potential (E_{pa}) of diclofenac shifted towards less positive potentials with increasing pH, indicating the involvement of proton/s in the redox reaction of diclofenac at the electrode surface. The linear dependence of the peak potential on pH at the NiNPs/ERGO/GCE is given by the equation: E (V) = 0.052 pH + 1.0, R^2 = 0.999. The slope of 52 mV/pH, is closer to the theoretical Nernstian slope of 59 mV/pH. Thus, it can be concluded that equal number of electrons and protons are transferred in the electrochemical oxidation reaction of diclofenac at the NiNPs/ERGO/GCE surface. This is also in accordance with the oxidation mechanism of diclofenac reported in the literature [255, 269, 275].

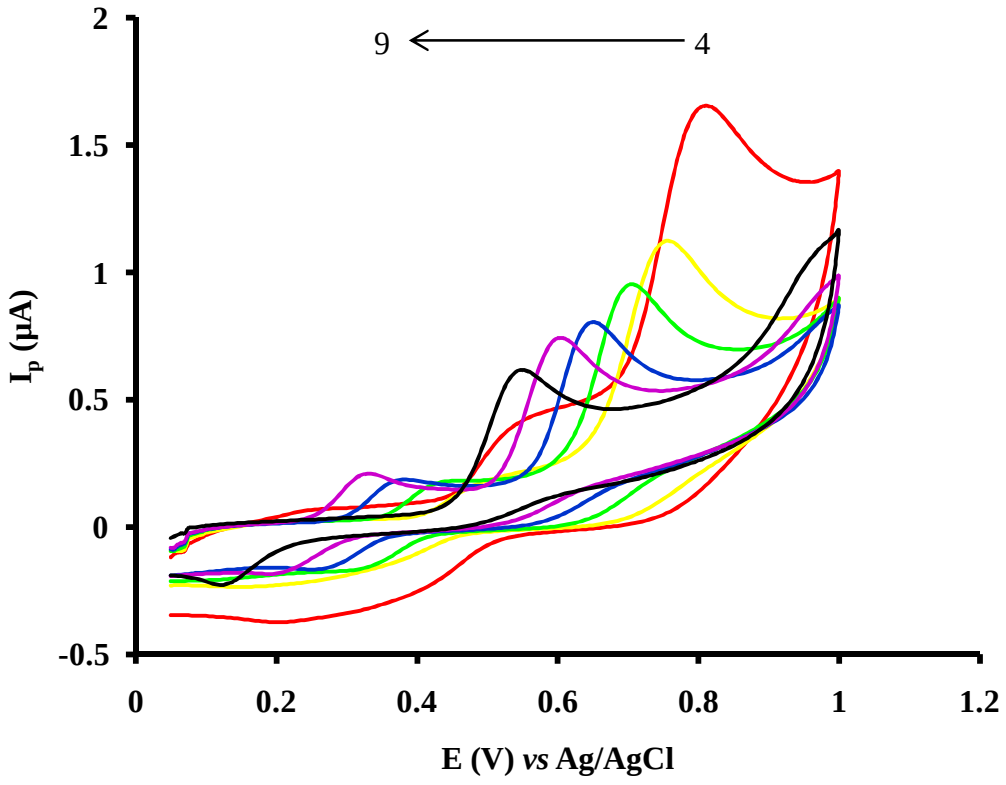

Figure 54. Effect of pH of 0.1 M PBS on the peak current of 50 µM DIC at NiNPs/ERGO/GCE

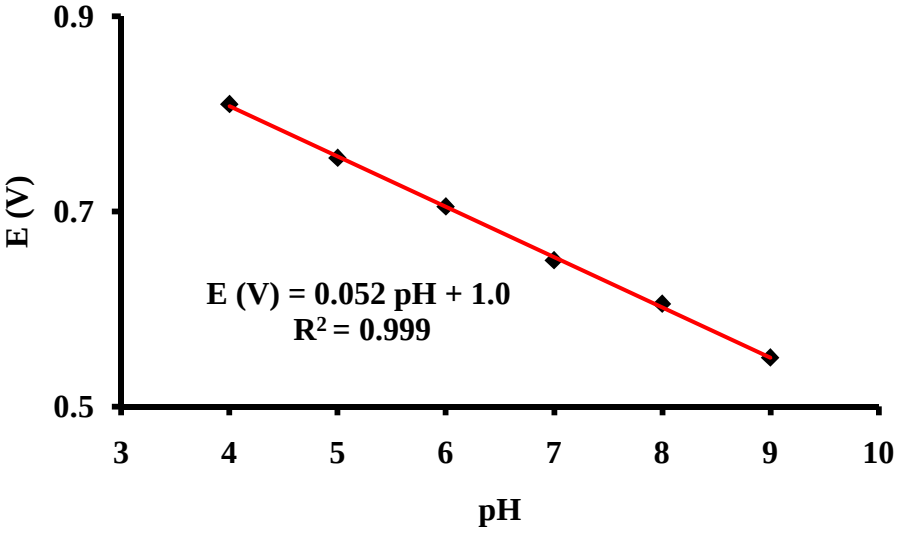

Figure 55. Plot of peak potential *vs* pH for 50 µM DIC at NiNPs/ERGO/GCE

5.4.10. Optimization of Parameters

Since the electrode reaction at the NiNPs/ERGO composite modified electrode is predominantly an adsorption controlled process, the effect of accumulation potential and time on the square wave voltammetric peak current response of 25 µM DIC was examined by using the SWV. The effect of accumulation potential was studied in the range of +0.4 to -0.6 V at 30 s accumulation time. The oxidation peak current response for DIC increased from -0.6 to -0.2 V and becomes almost constant in the subsequent region (Figure 56A). Therefore, accumulation potential of -0.2 V was selected as an optimum accumulation potential for further study. The influence of accumulation time on the peak current for 25 µM DIC was also studied in the range 5–120 s. The square wave anodic peak current increased with increasing accumulation time in the range 15–60 s and then a gradual decrease in the peak current was observed with further increase in accumulation time, which might be attributed to saturation of the electrode surface, Figure 56B. Therefore, 60 s was chosen as the optimal accumulation time for the determination of DIC for subsequent measurements in this study. The influence of square wave voltammetric parameters such as frequency, pulse amplitude and step potential on the response for 50 µM DIC was also studied. By taking into account the shape of the square wave voltammogram and the magnitude of the peak current, the optimum SWV parameters selected for subsequent measurements were frequency of 5 Hz, amplitude of 0.05 V and step potential of 0.005 V.

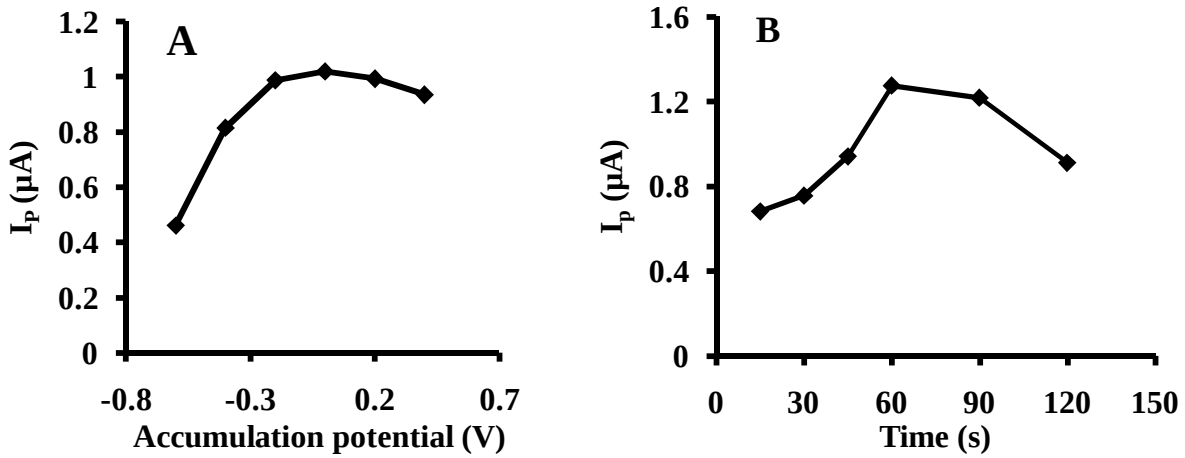

Figure 56. Effect of accumulation potential (A) and accumulation time (B) on the responses for 50 µM DIC

5.4.11. Calibration Curve

Square wave voltammetry (SWV) was used for the analytical determination of diclofenac owing to its high sensitivity and better peak resolution. Using the optimized measurement parameters, a calibration curve was constructed. Figure 57 demonstrates the square wave voltammograms obtained for varying concentrations of DIC in the range of 0.25–125 µM. The peak current increased linearly with concentration of DIC in the range of 0.25–125 µM with a linear regression equation: I_p (µA) = 0.02 [DIC] (µM) + 0.3, R^2 = 0.998. Figure 58 illustrates the linear dependence of the peak currents on the concentration of diclofenac sodium. The measurements were performed in triplicate and an average value of the current was reported with error bars for the three determinations. The calculated limit of detection (LOD) and limit of quantification (LOQ) using the formula *3s/m* and *10s/m*, where *s* is the standard deviation of the blank (n = 10) and *m* is the slope of the analytical calibration curve, was found to be 0.09 and 0.3 µM, respectively. The analytical parameters, limit of detection and linear dynamic range of the analytical calibration curve of this method are compared with similar voltammetric methods for DIC determination reported in the literature, as summarized in Table 10. The result shows that our sensor is better than most of those reported ones in terms of simultaneously providing both sensitivity and wide linear dynamic range.

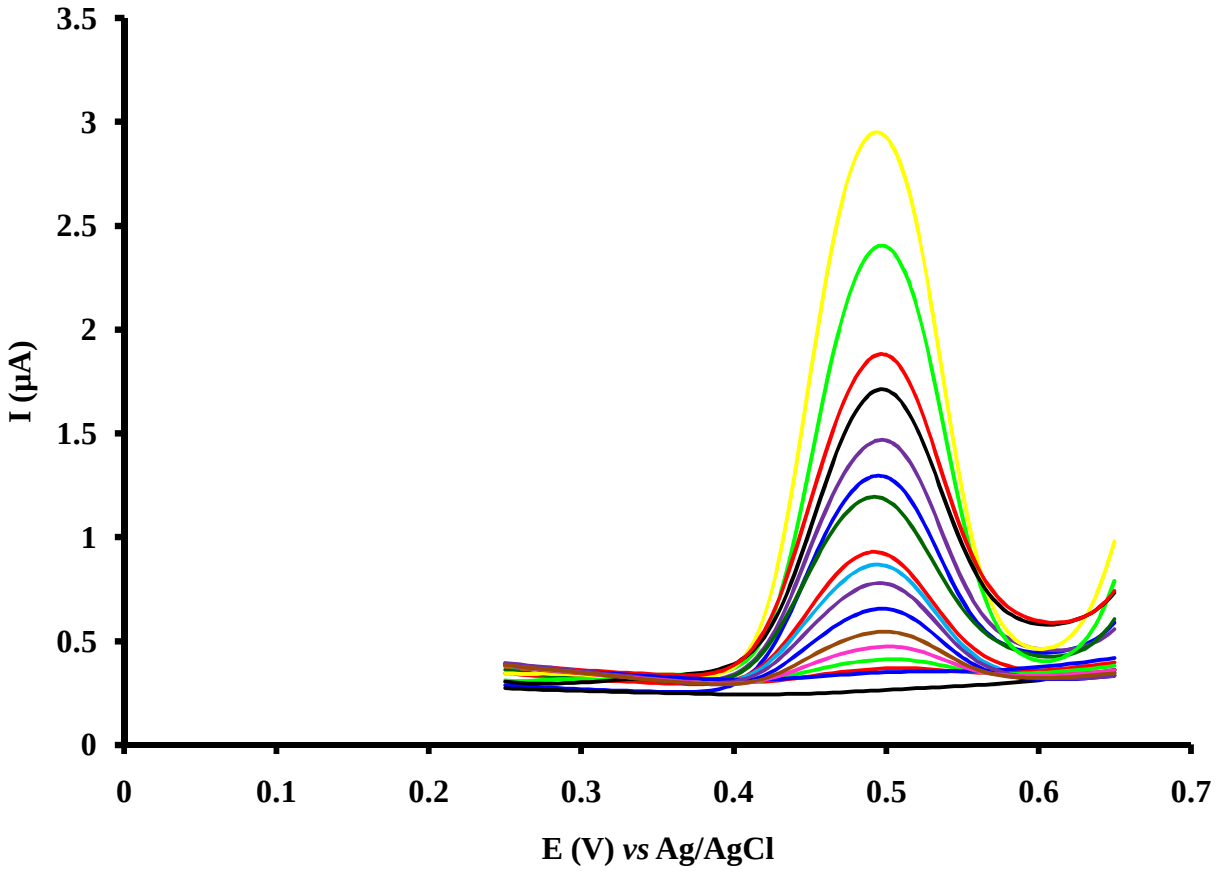

Figure 57. SWVs recorded at NiNPs/ERGO/GCE in PBS pH 4 for various concentrations of diclofenac: 0.25,1, 2.3, 5.2, 8.6, 15, 20, 25, 30, 40, 50, 60, 70, 80, 100 and 125 µM

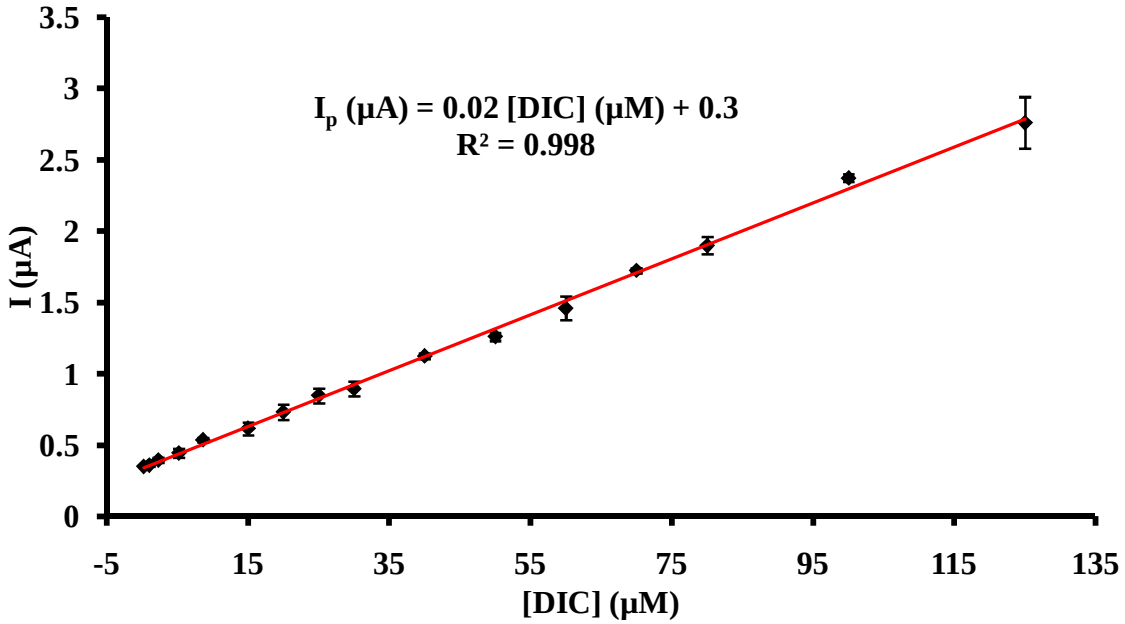

Figure 58. Calibration plot of peak current concentrations of DIC at NiNPs/ERGO/GCE

Table 10. Comparison of the analytical parameters obtained at NiNPs/ERGO/GCE with different electrodes reported in the literature for the electrochemical determination of DIC

Electrode type	Technique	Linear range (μM)	LOD (μM)	References
[a]SWCNT/EPPGE	SWV	0.001–0.5	0.00082	[254]
		0.025–1.5	0.0225	
[b]IL/CNTPE	DPV	0.5–300	0.2	[255]
[c]AuNP/MWCNT/GCE	SWV	0.03–200	0.02	[256]
Graphite	DPV	2.6–9.5	0.76	[257]
[d]Ty/CPE	DPV	10–140	3.28	[268]
EPPG	SWV	0.01–1	0.0062	[269]
[e]GO-COOH/GCE	LSV	1.2–400	0.09	[270]
[f]MWCNTs/CTS-Cu/GCE	SWV	0.3–200	0.021	[271]
[g]MWCNT-IL/CCE	DPV	0.05–50	0.018	[274]
NiNPs/ERGO/GCE	SWV	0.25–125	0.09	[This work]

[a]single-wall carbon nanotubes/edge-plane pyrolytic graphite electrode, [b]ionic liquid-modified carbon nanotubes paste electrode, [c]gold nanoparticle/multi-walled carbon nanotube modified glassy carbon electrode, [d]tyrosine-modified carbon paste electrode, [e]carboxyl-functionalized graphene oxide-modified electrode, [f]multi-walled carbon nanotubes/chitosan-copper complex modified glassy carbon electrode, [g]multiwalled carbon nanotube and ionic liquid modified carbon ceramic electrode

5.4.12. Repeatability, Reproducibility and Stability

The repeatability of the sensor was investigated by measuring the square wave voltammetric response for 50 μM DIC in 0.1 M PBS solution (pH 4.0). The relative standard deviation (RSD) of the peak currents obtained for the same electrode for sixteen consecutive measurements was found to be 4.6%, showing a very good repeatability response at the composite modified electrode. The reproducibility of NiNPs/ERGO/GCE was also examined by comparing the responses of four different glassy carbon electrodes prepared following the same experimental procedure. The RSD of the peak currents of the four electrodes for 50 μM DIC was found to be 4.0%. The long term stability of NiNPs/ERGO/GCE was also tested by keeping the electrode in 0.1 M PBS (pH 7) at ambient condition when not in use. The square wave voltammetric peak current responses for 50 μM DIC at 50 mV s^{-1} were examined. After one week the electrode retained 94.7% of its initial response. The results show that the developed composite modified GC electrode showed very good repeatability, reproducibility, and stability towards the detection of DIC.

5.4.13. Interference Study

The anti-interference ability of the sensor in diclofenac determination was evaluated by adding different concentrations of potential interfering compounds that might be present in real samples together with the analyte. The change in SWV responses for 50 µM diclofenac sodium in 0.1 M PBS (pH 4) was monitored at the optimum experimental conditions after addition of each of the interferents. Possible species that may interfere with the diclofenac determination, such as glucose, urea, L-ascorbic acid, citric acid, Ca^{2+}, Mg^{2+}, K^{+}, SO_4^{2-}, CO_3^{2-} and Cl^{-} were evaluated. The tolerance limit was defined as the maximum concentrations of foreign species which gave an error less than ±5% in the detection of diclofenac. The results indicated that 500-fold concentration of glucose, urea, citric acid, Ca^{2+}, Mg^{2+}, K^{+}, SO_4^{2-}, CO_3^{2-} and Cl^{-} and ten-fold L-ascorbic acid had little or no effect on the determination of DIC, Table 11, showing that the sensor had very high selectivity.

Table 11. Effect of potential interferents on the peak current response of 50 µM DIC at NiNPs/ERGO/GCE, (n = 3)

Interferences	[Interferent]/[DIC]	Signal change (%)
Glucose	500	2.3
Urea	500	-1.1
Citric acid	500	2.3
L-Ascorbic acid	10	-4.4
Ca^{2+}, Mg^{2+}, K^{+}, SO_4^{2-}, CO_3^{2-}, Cl^{-}	500	0.9

5.4.14. Analytical Application

The practical applicability of the proposed sensor, NiNPs/ERGO/GCE, was investigated by using the sensor in the determination of diclofenac sodium in real samples of commercially available pharmaceutical tablets and human urine samples. The sample preparation procedures were according to section 4.4.1.4. The amount of DCF in the pharmaceutical formulation was determined using standard addition method. The quantified amount of DIC (50.2±3 mg) is very close to the claimed amount (50 mg) for the diclofenac sodium tablet. Furthermore, the accuracy and reliability of the proposed sensor was investigated by spiking the real samples with known

concentrations of standards. The recovery results were in the range 94.7–101% and 98.7–104% for the tablet formulation and urine samples, respectively (Table 12), indicating the good reliability of the developed method. Therefore, the proposed sensor is promising for direct determination of diclofenac in real samples.

Table 12. Analysis of DIC in diclofenac sodium tablet and urine samples and the recovery results at NiNPs/ERGO/GCE using SWV assay

Real sample	Labeled content (mg)	[a]Amount determined ± RSD (mg)	Added (μM)	[a]Found ± RSD (μM)	Recovery (%)
Tablet	50	48.3 ± 4.1	5	5.0 ± 4.0	100
			10	9.8 ± 6.1	98.0
			15	15.2 ± 2. 0	101
			30	28.4 ± 1.7	94.7
Urine	–	–	15	14.8 ± 6.8	98.7
			30	30.6 ± 6.5	102
			60	62.2 ± 2	104

[a] *Mean value (n = 3)*

5.5. Sensitive Electrochemical Determination of Ethambutol in Pharmaceutical Formulation and Human Urine at Nickel Nanoparticles/Electrochemically Reduced Graphene Oxide Modified Electrode

5.5.1. Background

Tuberculosis (TB) is an infectious disease caused by *Mycobacterium tuberculosis* (MB-TB) and remains one of the most common infectious diseases of a major public health concern [305, 306]. It is the ninth leading cause of death worldwide and the leading cause from a single infectious agent, with 10.4 million cases and 1.674 million deaths in 2016 according to 2017 global WHO TB report [307, 308]. The treatment of latent TB infection is usually done by a single antibiotic; however in the treatment of active TB therapy, the combinations of several antibiotics would be the best way to reduce the risk of antibiotic resistance by the bacteria [309]. More than twenty antituberculosis drugs exist for the treatment of TB infection which can be categorized into three lines of treatment and five groups on the basis of different efficacy levels, drug class, potency and usability. Ethambutol (ETB), Scheme 10, together with pyrazinamide, isoniazid and rifampicin, are the first-line drugs for the treatment of tuberculosis [306, 310]. ETB is a *Mycobacterium*-specific drug recommended for the treatment of the diseases caused by MB-TB and opportunistic infections of AIDS patients caused by the *Mycobacterium avium* complex [309].

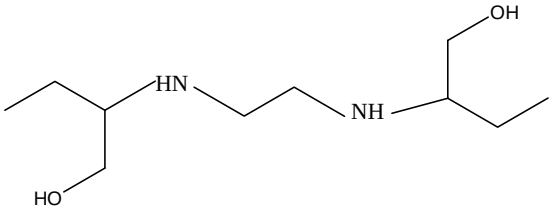

Scheme 10. The chemical structure of ethambutol

Continuous intake of antituberculosis drugs causes severe side effects; for example, an excess intake of isoniazid and pyrazinamide causes hepatic failure, leading to a fatal condition due to the excess formation of hydrazine during the isoniazid metabolism. Similarly, overconsumption of ETB causes ophthalmic problems [311]. In contrast to rifampicin, isoniazid or pyrazinamide which are essentially eliminated by the liver, ETB is renally excreted, with two-thirds of the

administered dose being recovered unchanged in urine. Renal failure is associated with significantly higher risks of toxicity, notably with retrobulbous optical nevritis [312]. Moreover, as the drug is used practically in higher doses for a longer periods (6-9 months) continuous monitoring of the drug quality is crucial to reduce the risk of toxicity.

Therefore, it is very important to develop a simple, sensitive, reliable and environmentally friendly method for the determination of ethambutol. So far, several analytical techniques were reported including, potentiometry [313, 314], Fourier-transform infrared spectroscopy (FTIR) [315], UV spectrophotometry [316], fluorescence spectroscopy [317], capillary electrophoresis (CE) [318-320], supercritical fluid chromatography mass spectrometry (SFC-MS) [321], high performance liquid chromatography (HPLC) [306, 322, 323] and electroanalytical methods [309, 311, 324-327]. However, emphasis has been given to electrochemical techniques recently owing to their operational simplicity, sensitivity, cost effectiveness, absence of exhaustive sample pretreatment and suitability for onsite analysis due to their portability. Among the electrochemical methods voltammetry based on chemically modified electrodes has got significant attention because of the possibility to deliberately control and design the surface of the electrode for the intended application.

Graphene–metal nanocomposite modified electrodes are one of the most widely studied electrodes for electrochemical sensing. Metal nanoparticles (MNPs) incorporated in graphene exhibited outstanding properties such as high electrocatalytic activity, excellent conductivity and selectivity which makes metal nanostructures decorated graphene an ideal choice to be used as an active material in electrochemical sensors [328, 329]. The favorable behavior of the graphene supports may be ascribed to a number of advantages, such as a high dispersion of noble metals catalyst resulting from an improved interaction between functionalized graphene or graphene oxide surface and the noble metals nanoparticles and a large surface area of the graphene sheet support. Besides, abundant functional groups on the surfaces of GO can be used as anchoring sites for metal nanoparticles, which makes it possible to use them as a support to produce graphene-nanoparticle hybrid nanostructures [330]. Furthermore, the incorporation of MNPs to high-surface-area materials like two-dimensional graphene structures provides enormous advantages for catalytic applications in terms of controlling the nucleation and growth of MNPs,

protecting them from aggregation and harvesting the synergistic effects of the MNPs and the supports [331].

This work is based on extending further application of NiNPs/ERGO/GCE for the determination of ETB in pharmaceutical dosage forms and biological fluids. The synthesis of NiNPs and GO and the preparation of the NiNPs/ERGO/GCE is according to the procedure described in the experimental section. The synthesized NiNPs and GO and the prepared NiNPs/ERGO/GCE were characterized and successfully applied for the determination of diclofenac in section 5.4.

5.5.2. Electrochemical Behavior of ETB

The electrochemical behavior of ethambutol was examined by cyclic voltammetry. As it can be seen in Figure 59, no obvious redox peaks appeared for the buffer solution at the NiNPs/ERGO/GCE (curve a). However, a single oxidation peak was observed at the bare (b) and the modified glassy carbon electrodes (c–e) without any corresponding reduction peak in the reverse direction, indicating the irreversibility of the reaction of ethambutol at all the electrode surfaces. A weak oxidation peak of ETB appeared at a relatively higher potential region of about 1.2 V at the bare glassy carbon electrode (curve b). However, the peak current response of ethambutol was increased accompanied with a negative shift in peak potential at both nickel nanoparticles (curve c) and electrochemically reduced graphene oxide (curve d) modified electrodes. The observed result confirms further improvement in the electrochemical response of ETB at the composite modified electrode (NiNPs/ERGO/GCE) (curve e) with about 2.25 times increments in the peak current compared to the response of the bare electrode and a negative shift of the peak potential by nearly about 200 mV. This observation can be attributed to the increase in the surface area of the electrode and the catalytic role played by the nickel nanoparticles and electrochemically reduced graphene oxide with a synergetic effect.

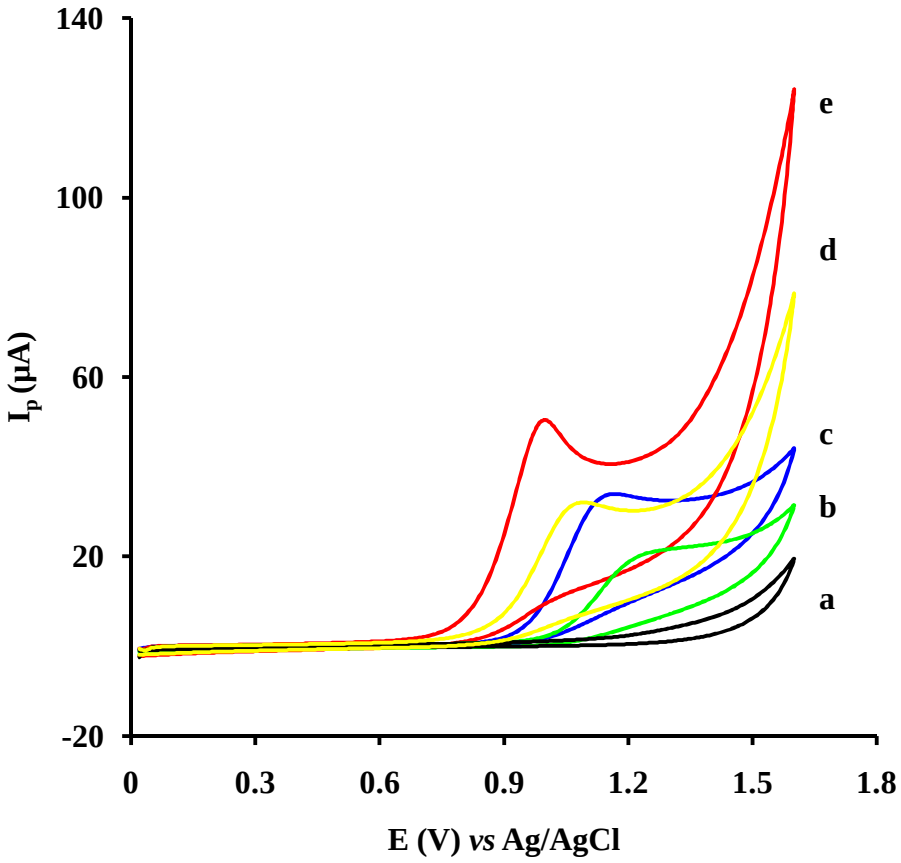

Figure 59. CVs recorded at bare GCE (b), NiNPs/GCE (c), ERGO/GCE (d) and NiNPs/ERGO/GCE (a, e) in the absence (a) and presence (b–e) of 50 µM ETB in 0.1 M PBS pH 7

5.5.3. Electrochemical Impedance Spectroscopy (EIS)

Electrochemical impedance spectroscopy (EIS) was employed to investigate the electrochemical characteristics of the bare and modified electrodes towards ETB detection. EIS measurement was carried out in 0.1 M phosphate buffer solution containing 500 µM ETB over a frequency range of 0.1 Hz to 10^5 Hz with the AC signal amplitude of 10 mV, Figure 60. Generally, the Nyquist plot of the EIS is characterized by two important regions: a semicircular region at a higher frequency corresponding to the electron-transfer-limited process and a linear portion at low frequency region featuring diffusion limited process [54, 332]. The diameter of the semicircular portion is equivalent to the charge transfer resistance (R_{ct}). The R_{ct} value obtained using the equivalent circuit fittings of the present study is in the order of: 42.9 > 24.5 > 13.7 > 12.2 kΩ for

the unmodified GCE (a), NiNPs/GCE (b), ERGO/GCE (c) and NiNPs/ERGO/GCE (d), respectively. The smallest semicircle domain obtained at the NiNPs/ERGO modified GCE suggests that the nickel nanoparticles and graphene oxide composite promotes the electron transfer between ethambutol and the underlying electrode surface. The decrease in the diameter of the Nyquist plot at the composite compared to the individually modified electrode with nickel nanoparticles and graphene oxide further confirms the catalytic role played by each with synergistic effect. The result is in good agreement with the cyclic voltammetric characterization.

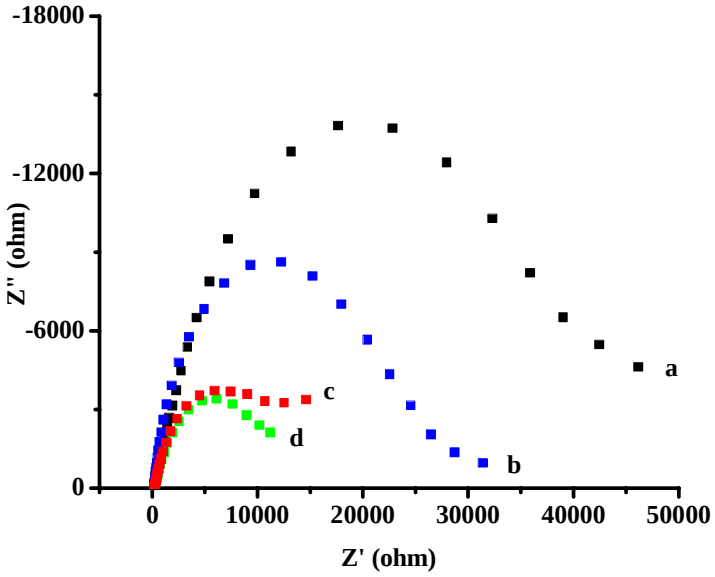

Figure 60. Nyquist Plot of EIS measured for 500 µM ETB recorded at bare GCE (a), NiNPs/GCE (b), ERGO/GCE (c) and NiNPs/ERGO/GCE (d) in 0.1 M PBS pH 7

5.5.4. The Effect of Potential Scan Rate

In order to evaluate whether the electron transfer process of ETB at the composite modified electrode is diffusion or adsorption controlled, cyclic voltammetry was employed in the range of 10–500 mV s^{-1}, Figure 61. The result showed that the peak current for 50 µM ETB in 0.1 M PBS pH 7 linearly increases with the square root of scan rates in the range of 10–500 mV s^{-1} with the linear regression equation of I_p (µA) = 5.5 $v^{1/2}$ (mV s^{-1})$^{1/2}$ + -2.8, R^2 = 0.994, Figure 62. This relationship suggests that the electrochemical reaction of ethambutol at the NiNPs/ERGO modified electrode is mainly diffusion-controlled electrode process [333-335]. The relationship between the logarithm of the peak current and the logarithm of the scan rate (log I_p *vs* log *v*) is also linear with the regression equation of log I_p (µA) = 0.56 log *v* (mV s^{-1}) + 0.60, R^2 = 0.990.

The slope value of 0.56 for the linear plot is very close to the theoretical value of 0.5 for diffusion controlled electrode process [69, 336].

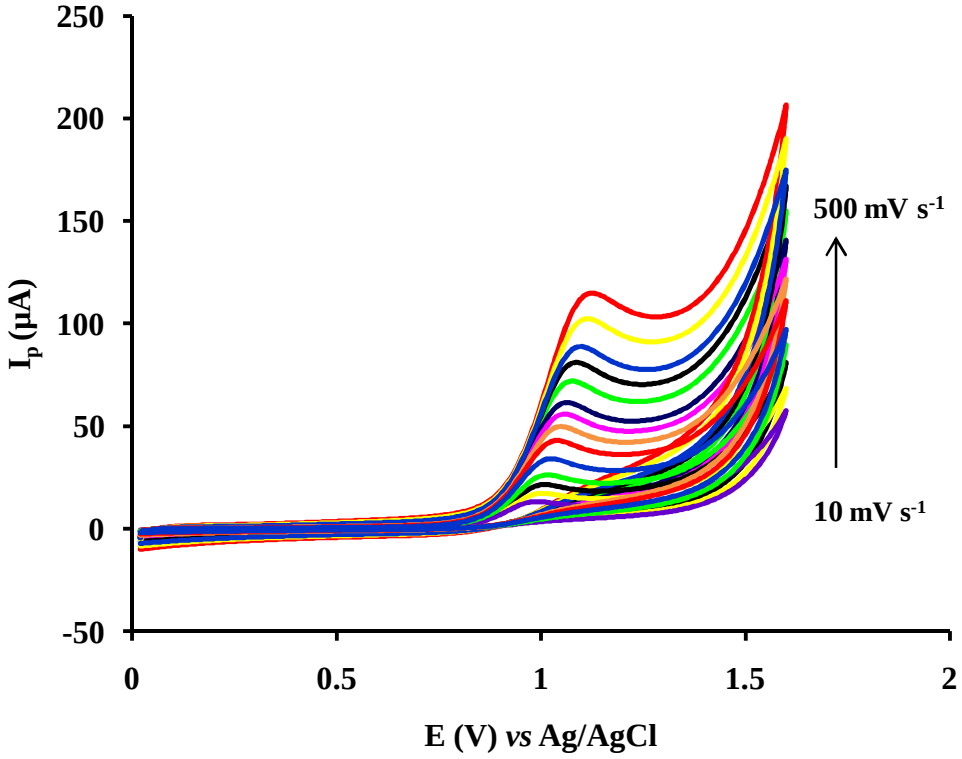

Figure 61. CVs recorded for 50 µM ETB in PBS (pH 7) at NiNPs/ERGO/GCE at various scan rates (100–500 mV s^{-1})

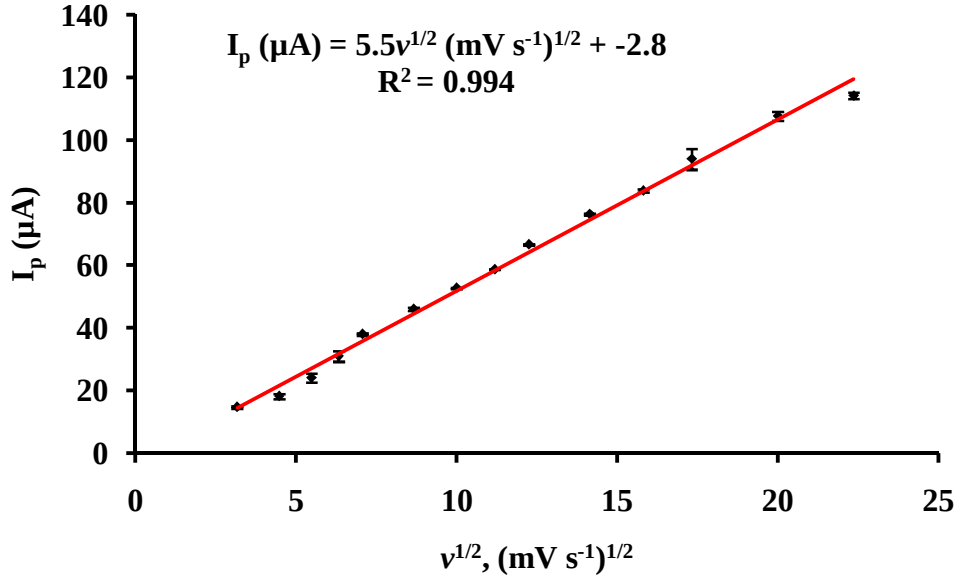

Figure 62. Plot of I_p *vs* $v^{1/2}$ for 50 µM ETB in PBS (pH 7) at NiNPs/ERGO/GCE

The correlation between peak potential and scan rate was also investigated. It was observed that the oxidation peak potential depends on scan rate and gradually shifted to more positive values on increasing the scan rate, which confirms the irreversibility of the oxidation process of ethambutol at the electrode surface. According to Laviron's, for an irreversible electrode process the peak potential is defined by equation (12) [69, 337]:

$$E_p = E^{0'} + \left(\frac{2.303RT}{\alpha nF}\right) \log \left(\frac{RTk^0}{\alpha nF}\right) + \left(\frac{2.303RT}{\alpha nF}\right) log\ v \qquad (12)$$

where $E^{0'}$ is the formal redox potential, n the number of electron transferred, *v* the scan rate, α the transfer coefficient, k^o the standard heterogeneous rate constant and the other symbols have their usual meanings. The relationship between the peak potential and the logarithm of the scan rate is gave a linear equation: E_p (V) = 0.071 log *v* + 1.12, R^2 = 0.965. Hence, from the slope of E_p *vs* log *v* in the above equation, the value of αn can be calculated. The result was found to be 0.833 by taking R = 8.314 J K^{-1} mol^{-1}, T = 298 K and F = 96480 C mol^{-1}.

According to Bard and Faulkner [11], the transfer coefficient α is given by equation (13):

$$\left|E_p - E_{p/2}\right| = \frac{1.857RT}{\alpha nF} = \frac{47.7}{\alpha n}\ \text{mV at 25 °C} \qquad (13)$$

where $E_p/2$ is the potential where the current is at half of the peak value. Based the above equation, the calculated α value is found to be 0.47 and the number of electrons transferred during the oxidation of ETB was estimated to be 1.8 ~ 2.

5.5.5. The Effect of pH

The influence of pH of the supporting electrolyte solution on the electrochemical response for 50 µM ETB was examined in 0.1 M PBS in the pH ranges of 5.0–10 using cyclic voltammetry. Figure 63 depicts the CVs of 50 µM ETB for varying pH (5.0–10) at NiNPs/ERGO/GCE. The result shows the increase in the oxidation peak current response of ETB as the pH increases from 5.0 to 7.0 and reaches a maximum value at pH 7. Further increase in the pH from 7 to 10 resulted in a gradual decrease of the peak current responses, Figure 64. Therefore, PBS of pH 7.0 was employed as the optimum pH for the subsequent analysis at NiNPs/ERGO/GCE. The effect of the pH of the buffer solution on the oxidation peak potential of ETB was also evaluated. It was found that the oxidation peak potential shifted negatively with increasing pH (Figure 65). The negative shift in the oxidation peak potential due to the change in pH from acidic to basic

solution indicates proton participation in the oxidation process. The relationship between the anodic peak potentials and pH was linear with the regression equation: E_{pa} (V) = -0.034pH + 1.3, R^2 = 0.991. The slope of –34 mV/pH is nearly half of the theoretical Nernstian slope of 59 mV/pH. This indicates that the proportion of the electrons and protons involved in the oxidation reaction of ETB at NiNPs/ERGO/GCE are in 2:1 ratio. This is in agreement with previous reports [311].

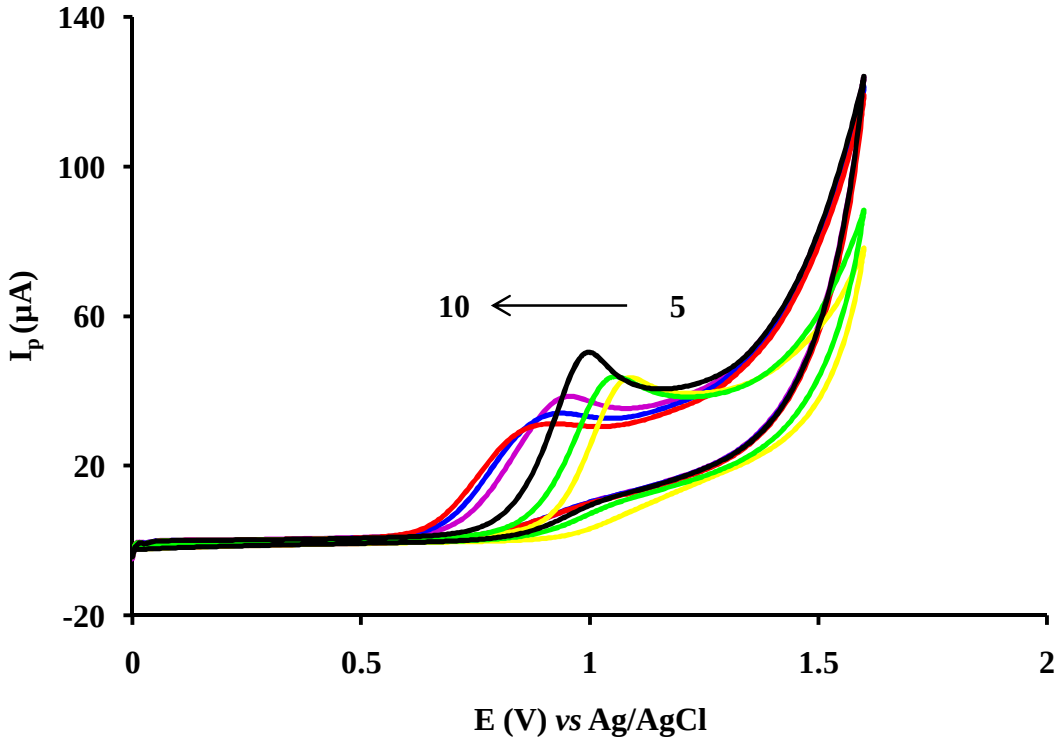

Figure 63. CVs of 50 µM ETB recorded in 0.1 M PBS of varying pH at NiNPs/ERGO/GCE

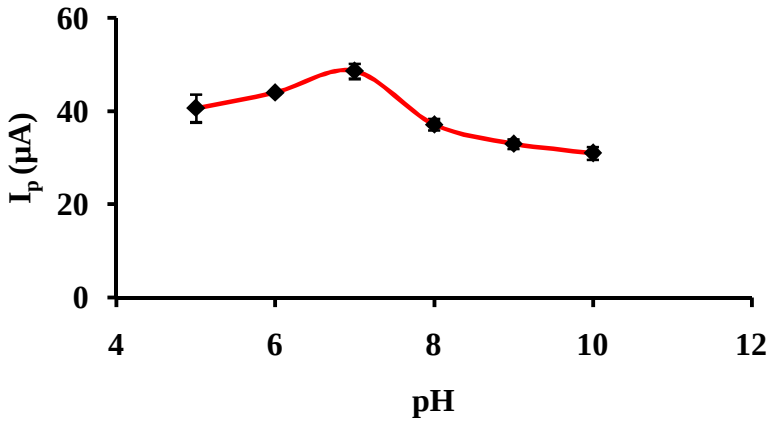

Figure 64. The effect of pH on the peak current response of 50 µM ETB at NiNPs/ERGO/GCE

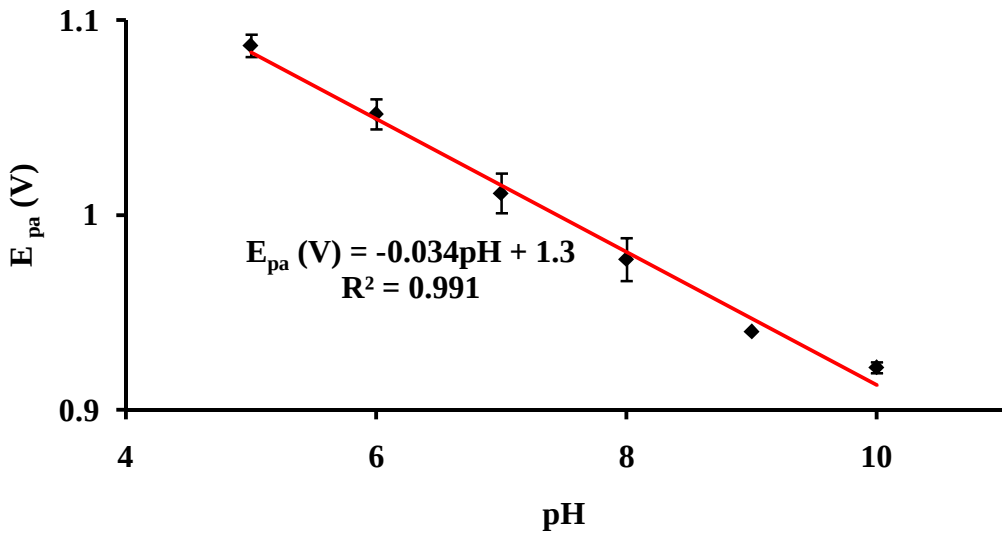

Figure 65. Peak potential *vs* pH for 50 µM ETB at NiNPs/ERGO/GCE

5.5.6. Calibration Curve

Square wave voltammetry was used to study the relationship between peak current and concentrations of ethambutol due to its high sensitivity. Under the optimal experimental conditions, the peak current response varied linearly with concentration of ETB in range of 0.05–100 µM with a linear regression equation of I_p (µA) = 0.4 [ETB] (µM) + 1.7, R^2 = 0.998, Figure 66 and 67. The limit of detection (S/N = 3) and limit of quantification (S/N = 10) were found to be 0.023 and 0.075 µM, respectively. The analytical parameters of the present method were compared with other electrochemical methods reported in the literature for the determination ETB which is summarized in Table 13. The obtained results confirm that the present sensor exhibited a better performance than the previously reported electrochemical methods in terms of achieving lower limit of detection and acceptable linear dynamic range.

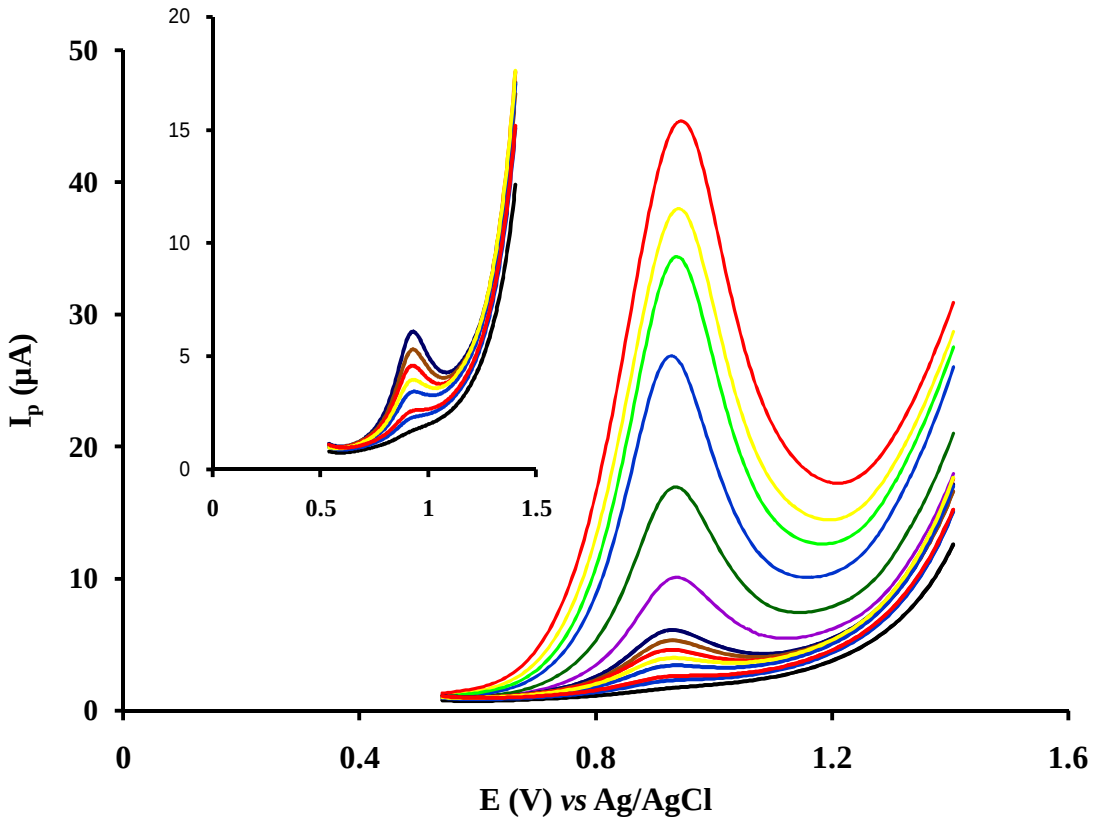

Figure 66. SWVs at NiNPs/ERGO/GCE in 0.1 M PBS pH 7 for different concentrations of ETB: 0, 0.05, 2, 4, 6, 8, 10, 12, 20, 40, 60, 75, 90 and 100 µM. Inset: magnified CV curve for lower concentrations (0–12 µM)

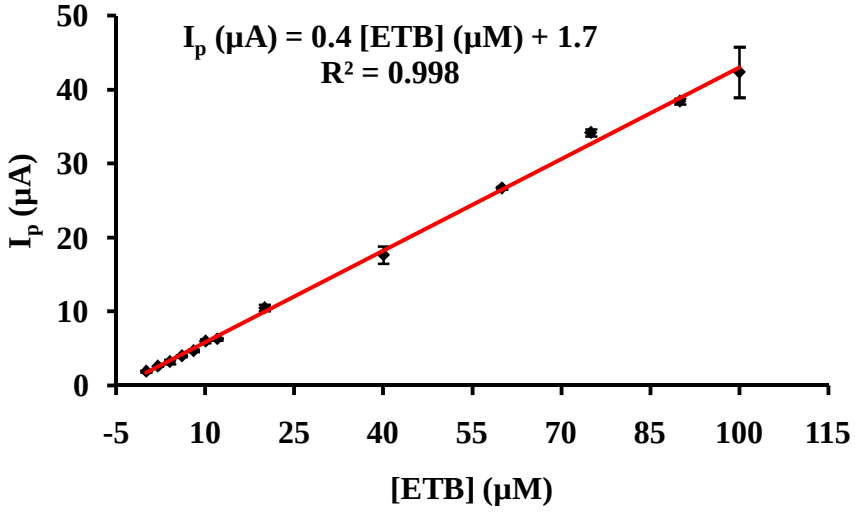

Figure 67. Calibration plot of peak current *vs* concentration of ETB at NiNPs/ERGO/GCE

Table 13. Comparison of the analytical performance of the NiNPs/ERGO/GCE with other electrodes previously reported in the literature for the determination of ETB

Electrode type	Technique	Linear range (µM)	LOD (µM)	[Ref.]
Graphite-paraffin composite electrode	Amperometric	250–1500	100	[257]
Graphite-polyurethane composite electrode	Amperometric	500–1100	63.4	[270]
Gold microelectrode array	Amperometric	50–2000	0.155	[269]
[a]Au/PVP-Ag-PANSA/CYP2E1	Chronoamperometric	2–12	0.7	[271]
Nafion/MWCNT/SPCEs	SWV	1.4×10^5–1.4×10^6	4000	[268]
Tyrosine/GCE	DPV	20–100	9.61	[254]
MWCNT/GCE	DPV	8–2500	0.76	[274]
[b]P_{Mel}-Au_{nano}/GCE	DPV	0.5–150	0.21	[256]
NiNPs/ERGO/GCE	SWV	0.05–100	0.023	[This work]

[a]cytochrome C immobilised on poly(8-anilino-1-napthalene sulphonic acid) and silver nanoparticles stabilized in polyvinylpyrrolidone (PVP) modified gold electrode, [b]poly-melamine/electrodeposited gold nanoparticles modified pre-anodized GCE.

5.5.7. Repeatability, Reproducibility and Stability

The precision of the method was evaluated as a degree of repeatability by measuring the square wave voltammetric response of 50 µM ETB. Figure 67 depicts the SWVs recorded for 50 µM ETB for twenty consecutive measurements for the same electrode. The relative standard deviation (RSD) of the peak currents measured for the same electrode for twenty consecutive measurements was found to be 1.0% (n = 20), showing excellent repeatability of the composite modified electrode. The reproducibility of the sensor was evaluated by comparing the responses of three NiNPs/ERGO/GCE electrodes independently prepared under similar experimental conditions. The relative standard deviation (RSD) of the current responses was 1.9%. The long-term stability of this sensor was also tested. The electrode was kept at ambient conditions when not in use. The oxidation current response for 50 µM ETB was measured by SWV for the same electrode every day for two weeks. The current response was only slightly reduced after two weeks and maintains greater than 92% of its initial current response. In general, the developed composite modified GC electrode showed excellent repeatability, reproducibility, and long-term stability towards the detection of ethambutol.

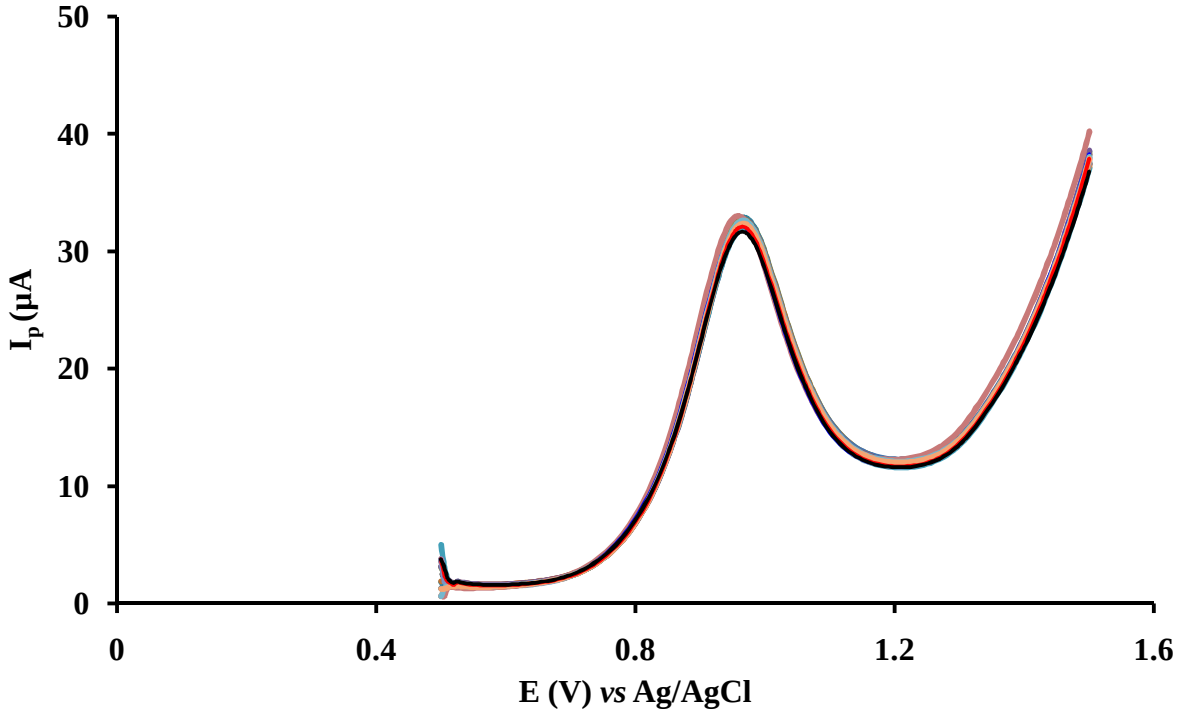

Figure 68. SWVs recorded for 50 µM ETB for twenty consecutive measurements

5.5.8. Effect of Interferences

In order to evaluate the potential analytical application of the proposed method, the interference effect of some common inorganic and organic substances that might coexist in pharmaceutical formulation and/or biological fluids were examined. The tolerance limit was defined as the maximum concentration of the potentially interfering substances that caused an error of less than 5% in the determination of ethambutol. The effect of these interfering compounds on the square wave voltammetric response was studied by measuring the response for a solution containing a fixed amount of ethambutol (50 µM) spiked with varying concentrations of the interferents under the same experimental conditions. The results are presented in Table 14, which shows the selectivity of the method towards ethambutol detection. Figure 69 shows the CVs recorded for 50 µM ETB before (a) and after (b–d) addition of 50 µM of isoniazid (ISZ) (b), L-ascorbic acid (AA) (c) and acetaminophen (ACP) (d) at NiNPs/ERGO/GCE at 50 mV s^{-1}. These results suggest the possibility of simultaneous determination of these substances with ethambutol without any interference effect.

Table 14. The influence of potential interfering substances on the peak current response of 50 µM ETB at NiNPs/ERGO/GCE, (n = 3).

Interferents	Concentration (µM)	Signal change (%)
Ca^{2+}, Mg^{2+}, K^{+}, SO_4^{2-}, CO_3^{2-}, Cl^{-1}	10000	-0.91
L-Ascorbic acid	10000	-1.0
Glucose	6600	4.3
Urea	6600	-1.8
Citric acid	3000	2.0
Isoniazid	3000	-2.9
Acetaminophen	800	2.2

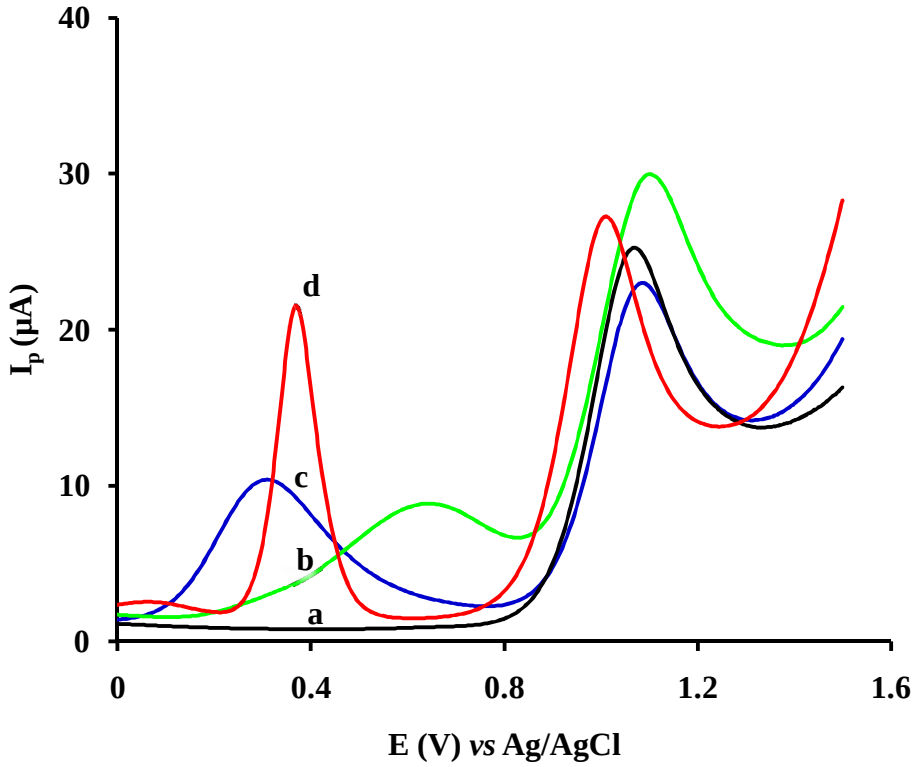

Figure 69. CVs recorded for 50 µM ETB before (a) and after (b–d) addition of 50 µM of ISZ (b), AA (c) and ACP (d) at NiNPs/ERGO/GCE at 50 mV s^{-1}

5.5.9. Analytical application

The feasibility and reliability of the proposed method for practical application was evaluated by analyzing commercial pharmaceutical tablet of Rifafour containing ethambutol and human urine. The procedure followed for sample preparation is described in Section 4.4.1.5. Square wave voltammetric measurements were carried out in triplicate and the standard addition method was employed to quantify the amount of ethambutol present. In addition, the accuracy of the method was tested by spiking the real sample with known concentrations of standards and calculating the recovery values. The results are summarized in Table 15. The amount of ethambutol determined is in close agreement with the specified amounts in the drug information leaflet and the recovery results for both real samples are also very good. Moreover, the other drugs present in the Rifafour formulation did not interfere with the determination of ethambutol. Figure 70 shows the SWV response of Rifafour in PBS pH 7 in the potential window of -0.2 V to 1.6 V, showing two peaks: the first one attributed to isoniazid and the second peak for ethambutol. Uric acid was detected at about 0.3 V in the urine samples analyzed but did not interfere with the determination of ethambutol. Figure 71 shows the SWVs of the urine sample before (a) and after spiking (b-h) with different concentrations of ETB.

Table 15. Determination of ETB in Rifafour tablet formulation and human urine samples and the recovery results at NiNPs/ERGO/GCE using SWV

Real sample	Specified content (mg)	Determined ± RSD (mg)	Added (µM)	[a]Found ± RSD (µM)	Recovery (%)
Rifafour	275	267 ± 5	0	15.4 ± 0.6	-
			15	32.3 ± 1.4	106
			50	65.7 ± 1.4	101
			0	8 ± 2.5	-
			20	27.9 ± 1.8	99.6
			50	58.0 ± 0.9	100
Urine			0	-	-
			15	15.6 ± 5.4	104
			40	43.7 ± 2.2	109
			75	74.8 ± 1.2	99.7

[a] *Mean value (n = 3)*

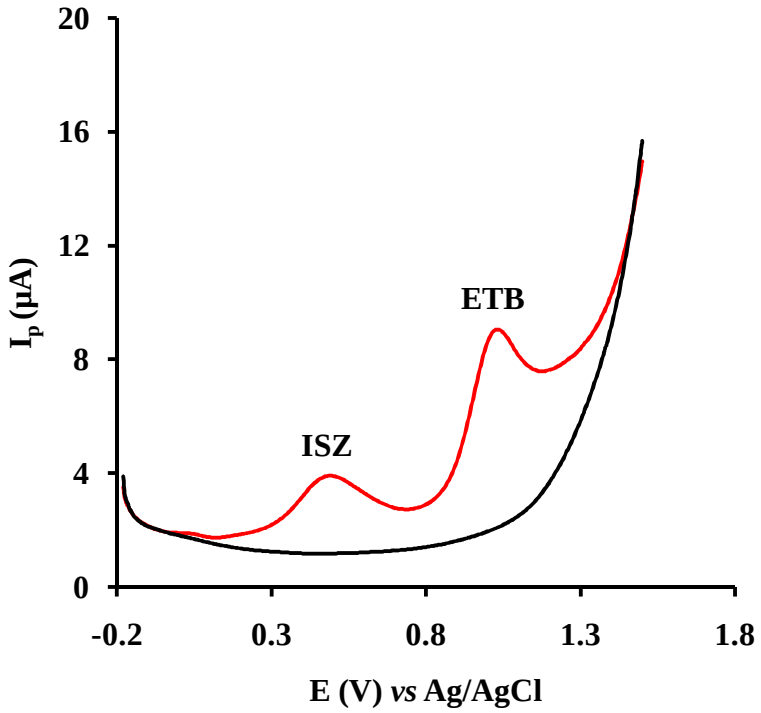

Figure 70. CVs recorded for Rifafour in PBS of pH 7 at scan rate of 50 mV s^{-1}

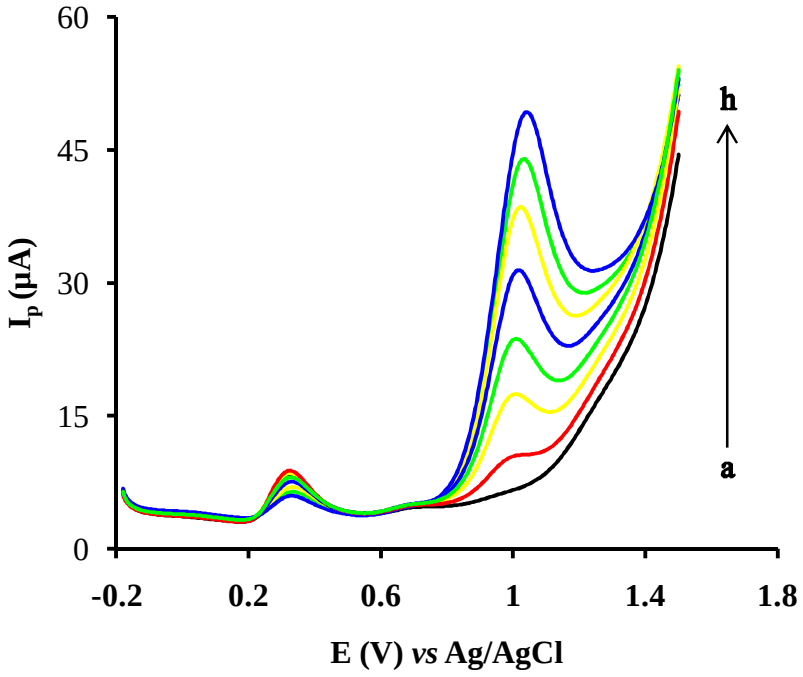

Figure 71. SWVs of the urine sample after spiking with different concentrations of ETB (a→h: 0, 15, 30, 40, 60, 70, 90, 100 µM)

6. Conclusion

Various types of chemically modified electrodes were developed in the present study for the electrochemical determination of selected pharmaceutical drugs (ibuprofen, caffeine, theophylline, epinephrine, diclofenac and ethambutol) in biological fluids and pharmaceutical formulations. Poly(L-aspartic acid), f-MWCNTs, ERGO and NiNPs were used to modify the conventional bare glassy carbon electrode and has proven to show improved sensitivity, selectivity to suppress interference and acted as a support matrix for the catalyst molecules. They also enhanced the resistance to electrode fouling, decreased the overpotential and improved the reversibility of the electrode reactions.

Firstly, L-aspartic acid was successfully electrodeposited on bare GCE by CV and used for IBP detection. The modified electrode showed excellent electrocatalytic activity in lowering the overpotential and significant enhancement of peak current as compared to the bare GCE. The developed P(L-Asp)/GCE was successfully validated for determining IBP in pharmaceutical preparations and biological fluids. The sensor showed good performance characteristics with regard to stability, sensitivity and selectivity..

A poly(L-Asp)/f-MWCNTs/GCE has been prepared and used successfully for the simultaneous determination of TP and CF. The modified electrode provides advantages such as ease of preparation, low cost, excellent peak-to-peak separation between theophylline and caffeine, good stability, reproducibility and repeatability. It also exhibits satisfactory sensitivity and high selectivity in voltammetric measurement of TP and CF simultaneously. Furthermore, the method was successfully used to detect TP and CF in green tea, human blood, and Panadol extra real samples with satisfactory recovery results, 92.0–106%. In general, the proposed method provides a useful tool for the simultaneous determination of TP and CF in food, biological, pharmaceutical analysis and clinical applications.

A new composite modified electrode based on ERGO and poly(L-Asp), poly(L-Asp)/ERGO/GCE, was also developed for the determination of EP. The proposed electrode demonstrates enhanced electrocatalytic activity towards the oxidation of epinephrine and lowers

the overpotential compared to the bare electrode response, attributed to the synergetic effect of reduced graphene oxide and poly(L-aspartic acid). The developed P(L-Asp)/ERGO/GCE also shows excellent analytical characteristics such as high sensitivity, repeatability, reproducibility, and stability. The selectivity of the electrode towards potential interferents is good. The real sample analyses reveal that the modified electrode can be suitable for the determination of EP in pharmaceutical injections.

Finally, a facile NiNPs/ERGO/composite modified glassy carbon electrode was prepared and successfully applied for the determination of diclofenac and ethambutol. The composite modified electrode showed an improved sensing activity towards diclofenac and ethambutol compared to the bare glassy carbon electrode and individual NiNPs or ERGO modified GCE due to the synergistic effect of the modifiers. The use of nickel nanoparticle decorated graphene oxide promoted the electron transfer process between the analytes and the underlying electrode, attributed to the catalytic activity of the nanomaterials and improved surface area. The prepared sensor displayed excellent response towards DIC and ETB determination in terms achieving wide linear range and lower limit of detections. The NiNPs/ERGO/GCE was effectively used for diclofenac and ethambutol detection in real sample analysis, with good recovery results. In general, the proposed electrode showed good sensitivity, selectivity, stability and is a promising material for electrochemical sensing of similar drugs and biologically active compounds in real samples.

7. References

1. Castillo J, Gaspar S, Leth S, Niculescu M, Mortari A, Bontidean I, Soukharev V, Dorneanu SA, Ryabov AD, Csoregi E: Biosensors for life quality. *Sensors and Actuators B: Chemical* **2004**, 102:179–194.
2. Stoytcheva M: Pesticides in the modern world - trends in pesticides analysis. *wwwIntechopencom* **2011**:453–464.
3. Rahman MA, Kumar P, Park D-S, Shim Y-B: Electrochemical sensors based on organic conjugated polymers. *Sensors* **2008**, 8:118–141.
4. Ozkan SA: Principles and techniques of electroanalytical stripping methods for pharmaceutically active compounds in dosage forms and biological samples. *Current Pharmaceutical Analysis* **2009**, 5:127–143.
5. Otles S: Handbook of food analysis instruments. Turkey: CRC Press; **2008**.
6. Munoz RAA, Almeida ES, Angnes L: Sample preparation techniques for the electrochemical determination of metals in environmental and food samples. *Molecular Sciences and Chemical Engineering* **2013**:1–10.
7. Esfandiari Baghbamidi S, Beitollahi H, Karimi-Maleh H, Soltani-Nejad S, Soltani-Nejad V, Roodsaz S: Modified carbon nanotube paste electrode for voltammetric determination of carbidopa, folic acid, and tryptophan. *Journal of Analytical Methods in Chemistry* **2012**, 2012:1–8.
8. Uslu B, Ozkan SA: Solid electrodes in electroanalytical chemistry: present applications and prospects for high throughput screening of drug compounds. *Combinatorial Chemistry and High Throughput Screening* **2007**, 10:495–513.
9. Stradiotto NR, Yamanaka H, Zanoni MVB: Electrochemical sensors: a powerful tool in analytical chemistry. *Journal of Brazilian Chemical Society* **2003**, 14:159–173.
10. Wang J: Analytical electrochemistry. Canada: John Wiley & Sons, Inc, **2006**:29–190.
11. Bard AJ, Faulkner LR: Electrochemical methods fundamentals and applications. New York: John Wiley & Sons, Inc.; **2001**.
12. Alexandru Ciucu A: Chemically modified electrodes in biosensing. *Journal of Biosensors and Bioelectronics* **2014**, 05:1–10.

13. Radi A-E: Recent updates of chemically modified electrodes in pharmaceutical analysis. *Combinatorial Chemistry and High Throughput Screening* **2010**, 13:728–752.
14. Sajid M, Nazal MK, Mansha M, Alsharaa A, Jillani SMS, Basheer C: Chemically modified electrodes for electrochemical detection of dopamine in the presence of uric acid and ascorbic acid: A review. *Trends in Analytical Chemistry* **2016**, 76:15–29.
15. Zen J-M, Kumar AS, Tsai D-M: Recent updates of chemically modified electrodes in analytical chemistry. *Electroanalysis* **2003**, 15:1073–1087.
16. Durst RA, Baumner AJ, Murray RW, Buck RP, Andrieux CP: Chemically modified electrodes: Recommended terminology and definitions. *Pure and Applied Chemistry* **1997**, 69:1317–1323.
17. Guo W, Geng M, Zhou L, Chao S, Yang R, An H, Cui C: Multi-walled carbon nanotube modified electrode for sensitive determination of an anesthetic drug: Tetracaine hydrochloride. *International Journal of Electrochemical Science* **2013**, 8:5369–5381.
18. Saleh Ahammad AJ, Lee JJ, Rahman MA: Electrochemical sensors based on carbon nanotubes. *Sensors* **2009**, 9:2289–2319.
19. Tiwari I, Singh KP, Singh M, Banks CE: Polyaniline/polyacrylic acid/multi-walled carbon nanotube modified electrodes for sensing ascorbic acid. *Analytical Methods* **2012**, 4:118–124.
20. Yanez-Sedeno P, Pingarron JM, Riu J, Rius FX: Electrochemical sensing based on carbon nanotubes. *Trends in Analytical Chemistry* **2010**, 29:939–953.
21. Kumar S, Vicente-Beckett V: Glassy carbon electrodes modified with multiwalled carbon nanotubes for the determination of ascorbic acid by square-wave voltammetry. *Beilstein Journal of Nanotechnology* **2012**, 3:388–396.
22. Abuilaiwi FA, Laoui T, Al-Harthi M, Atieh MA: Modification and functionalization of multiwalled carbon nanotube (MWCNT) via Fischer esterification. *The Arabian Journal for Science and Engineering* **2010**, 35:37–38.
23. Wang J: Carbon-nanotube based electrochemical biosensors: A review. *Electroanalysis* **2005**, 17:7–14.
24. Sikkander AM, Vedhi C, Manisankar P: Electrochemical stripping studies of amlodipine using MWCNT modified glassy carbon electrode. *Chemistry and Materials Research* **2011**, 1:1–9.

25. Dhand C, Arya SK, Datta M, Malhotra BD: Polyaniline-carbon nanotube composite film for cholesterol biosensor. *Analytical Biochemistry* **2008**, 383:194–199.
26. Li J, Zhang X: Fabrication of poly(L-aspartic acid)-nanogold modified electrode and its application for simultaneous determination of dopamine, ascorbic acid, and uric acid. *American Journal of Analytical Chemistry* **2012**, 03:195–203.
27. Ali SR, Parajuli RR, Balogun Y, Ma Y, He H: A nonoxidative electrochemical sensor based on a self-doped polyaniline/carbon nanotube composite for sensitive and selective detection of the neurotransmitter dopamine: A review. *Sensors* **2008**, 8:8423–8452.
28. Pilan L, Raicopol M: Highly selective and stable glucose biosensors based on polyaniline/carbon nanotubes composites. *UPB Scientific Bulletin, Series B* **2014**, 76:155–166.
29. Sabzi E, Rezapour K, Samadi N: Polyaniline-multi-wall-carbon nanotube nanocomposites as a dopamine sensor. *Journal of Serbian Chemical Society* **2010**, 75:537–549.
30. Dhand C, Solanki PR, Pandey MK, Datta M, Malhotra BD: Electrophoretically deposited polyaniline nanotubes based film for cholesterol detection. *Electrophoresis* **2010**, 31:3754–3762.
31. Gerwig R, Fuchsberger K, Schroeppel B, Link GS, Heusel G, Kraushaar U, Schuhmann W, Stett A, Stelzle M: PEDOT-CNT composite microelectrodes for recording and electrostimulation applications: Fabrication, morphology, and electrical properties. *Frontiers in Neuroengineering* **2012**, 5:1–11.
32. Sun X, Qiao L, Wang X: A novel immunosensor based on Au nanoparticles and polyaniline/multiwall carbon nanotubes/chitosan nanocomposite film functionalized interface. *Nano-Micro Letters* **2013**, 5:191–201.
33. Shahrokhian S, Kamalzadeh Z, Saberi R-S: Application of glassy carbon electrode modified with a bilayer of multiwalled carbon nanotube and polypyrrole doped with nitrazine yellow for voltammetric determination of naltrexone. *Electroanalysis* **2011**, 23:2925–2934.
34. Zhang-yu Y, Xiao-chun L, Xue-liang W, Jinjin L, Ke-wei C: Studies on the electrochemical behaviors of epinephrine at a poly(L-aspartic acid) modified glassy

carbon electrode and its analytical application. *International Journal of Electrochemical Science* **2011**, 6:3890–3901.

35. Babaei A, Sohrabi M: Selective simultaneous determination of levodopa and acetaminophen in the presence of ascorbic acid using a novel TiO_2 hollow sphere/multi-walled carbon nanotube/poly-aspartic acid composite modified carbon paste electrode. *Analytical Methods* **2016**, 8:1135–1144.
36. Guo S, Zhu Q, Yang B, Wang J, Ye B: Determination of caffeine content in tea based on poly(safranine T) electroactive film modified electrode. *Food Chemistry* **2011**, 129:1311–1314.
37. Dutta S, Sarkar S, Ray C, Pal T: Benzoin derived reduced graphene oxide (rGO) and its nanocomposite: Application in dye removal and peroxidase-like activity. *RSC Advances* **2013**, 3:21475–21483.
38. Gao Y, Wang L, Zhang Y, Zou L, Li G, Ye B: Highly sensitive determination of gallic acid based on a Pt nanoparticle decorated polyelectrolyte-functionalized graphene modified electrode. *Analytical Methods* **2016**, 8:8474–8482.
39. Jaiswal N, Tiwari I: Recent build outs in electroanalytical biosensors based on carbon-nanomaterial modified screen printed electrode platforms. *Analytical Methods* **2017**, 9:3895–3907.
40. Li S, Yang B, Wang J, Bin D, Wang C, Zhang K, Du Y: Nonenzymatic electrochemical detection of rutin on Pt nanoparticles/graphene nanocomposite modified glassy carbon electrode. *Analytical Methods* **2016**, 8:5435–5440.
41. Yao S, Cai W, Liu L, Liao X, Tao K, Feng F, Yang G: Electrochemical behavior of eriocitrin and highly sensitive determination based on an electrochemically reduced graphene oxide modified glassy carbon electrode. *Analytical Methods* **2016**, 8:3722–3729.
42. Kim S, Wang N, Li Y, He X: Electrochemical determination of mesalazine by using graphene oxide coated with a molecularly imprinted sol–gel. *Analytical Methods* **2016**, 8:7780–7788.
43. Hu Y, Liu Z, Zhan H, Hu L, Cui L, Wang K: A novel electrochemiluminescence sensor for bisphenol A determination based on graphene–palladium nanoparticles/polyvinyl alcohol hybrids. *Analytical Methods* **2017**, 9:3870–3875.

44. Luo X, Morrin A, Killard AJ, Smyth MR: Application of nanoparticles in electrochemical sensors and biosensors. *Electroanalysis* **2006**, 18:319–326.
45. Oyama M: Recent nanoarchitectures in metal nanoparticle-modified electrodes for electroanalysis. *Analytical Science* **2010**, 26:1–12.
46. Muraviev DN, Ruiz P, Muñoz M, Macanás J: Novel strategies for preparation and characterization of functional polymer-metal nanocomposites for electrochemical applications. *Pure and Applied Chemistry* **2008**, 80:2425–2437.
47. Maduraiveeran G, Jin W: Nanomaterials based electrochemical sensor and biosensor platforms for environmental applications. *Trends in Environmental Analytical Chemistry* **2017**, 13:10–23.
48. Sharma G, Kumar A, Sharma S, Naushad M, Prakash Dwivedi R, Alothman ZA, Mola GT: Novel development of nanoparticles to bimetallic nanoparticles and their composites: A review. *Journal of King Saud University-Science* **2017**:1–13.
49. Azad UP, Ganesan V: Influence of metal nanoparticles on the electrocatalytic oxidation of glucose by poly(Ni^{II}teta) modified electrodes. *Electroanalysis* **2010**, 22:575–583.
50. Ji Z, Wang Y, Yang J, Shen X, Yu Q, Kong L, Zhou H: Reduced graphene oxide uniformly decorated with Co nanoparticles: Facile synthesis, magnetic and catalytic properties. *RSC Advances* **2016**, 6:107709–107716.
51. Song Y, He Z, Zhu H, Hou H, Wang L: Electrochemical and electrocatalytic properties of cobalt nanoparticles deposited on graphene modified glassy carbon electrode: Application to some amino acids detection. *Electrochimica Acta* **2011**, 58:757–763.
52. Rassaei L, Marken F, Sillanpää M, Amiri M, Cirtiu CM, Sillanpaa M: Nanoparticles in electrochemical sensors for environmental monitoring. *Trends in Analytical Chemistry* **2011**, 30:1704–1715.
53. Nasrollahzadeh M, Babaei F, Fakhri P, Jaleh B: Synthesis, characterization, structural, optical properties and catalytic activity of reduced graphene oxide/copper nanocomposites. *RSC Advances* **2015**, 5:10782–10789.
54. Li X, Zhong A, Wei S, Luo X, Liang Y, Zhu Q: Polyelectrolyte functionalized gold nanoparticles-reduced graphene oxide nanohybrid for electrochemical determination of aminophenol isomers. *Electrochimica Acta* **2015**, 164:203–210.

55. Chen D, Feng H, Li J: Graphene oxide: Preparation, functionalization, and electrochemical applications. *Chemical Reviews* **2012**, 112:6027–6053.
56. Han T, Jin J, Wang C, Sun Y, Zhang Y, Liu Y: Ag nanoparticles-modified 3D graphene foam for binder-free electrodes of electrochemical sensors. *Nanomaterials* **2017**, 7:40–51.
57. Hossain MF, Park JY: Fabrication of sensitive enzymatic biosensor based on multi-layered reduced graphene oxide added PtAu nanoparticles-modified hybrid electrode. *PLoS One* **2017**, 12:1–16.
58. Lv Y, Wang F, Zhu H, Zou X, Tao C-A, Wang J: Electrochemically reduced graphene oxide-Nafion/Au nanoparticle modified electrode for hydrogen peroxide sensing. *Nanomaterials and Nanotechnology* **2016**, 6:30–36.
59. Fan Y, Liu J-H, Yang C-P, Yu M, Liu P: Graphene–polyaniline composite film modified electrode for voltammetric determination of 4-aminophenol. *Sensors and Actuators B: Chemical* **2011**, 157:669–674.
60. Zhang Y, Lei W, Xu Y, Xia X, Hao Q: Simultaneous detection of dopamine and uric acid using a poly(l-lysine)/graphene oxide modified electrode. *Nanomaterials* **2016**, 6:1–17.
61. Yin H, Ma Q, Zhou Y, Ai S, Zhu L: Electrochemical behavior and voltammetric determination of 4-aminophenol based on graphene–chitosan composite film modified glassy carbon electrode. *Electrochimica Acta* **2010**, 55:7102–7108.
62. Palanisamy S, Thirumalraj B, Chen SM, Wang YT, Velusamy V, Ramaraj SK: A facile electrochemical preparation of reduced graphene oxide at polydopamine composite: A novel electrochemical sensing platform for amperometric detection of chlorpromazine. *Scientific Reports* **2016**, 6:1–9.
63. Weia X, Xua X, Qic W, Wuc Y, Wang L: Molecularly imprinted polymer/graphene oxide modified glassy carbon electrode for selective detection of sulfanilamide. *Progress in Natural Science: Materials International* **2017**, 27:374–379.
64. Karimi-Maleh H, Tahernejad-Javazmi F, Atar N, Yola ML, Gupta VK, Ensafi AA: A novel DNA biosensor based on a pencil graphite electrode modified with polypyrrole/functionalized multiwalled carbon nanotubes for determination of 6-mercaptopurine anticancer drug. *Industrial and Engineering Chemistry Research* **2015**, 54:3634–3639.

65. Xu XL, Huang F, Zhou GL, Zhang S, Kong JL: A novel electrochemical sensor for probing doxepin created on a glassy carbon electrode modified with poly(4-amino-benzoic acid)/multi-walled carbon nanotubes composite film. *Sensors* **2010**, 10:8398–8410.

66. Zhu X, Tong J, Bian C, Gao C, Xia S: The polypyrrole/multiwalled carbon nanotube modified Au microelectrode for sensitive electrochemical detection of trace levels of Pb^{2+}. *Micromachines* **2017**, 8:86–94.

67. Kumar D, Prasad BB: Multiwalled carbon nanotubes embedded molecularly imprinted polymer-modified screen printed carbon electrode for the quantitative analysis of C-reactive protein. *Sensors and Actuators B: Chemical* **2012**:1141–1150.

68. Yogeswaran U, Chen SM: Recent trends in the application of carbon nanotubes–polymer composite modified electrodes for biosensors: A review. *Analytical Letters* **2008**, 41:210–243.

69. Gowda JI, Nandibewoor ST: Electrochemical behavior of paclitaxel and its determination at glassy carbon electrode. *Asian Journal of Pharmaceutical Sciences* **2014**, 9:42–49.

70. Sanchez Rojas F, Bosch Ojeda C: Recent development in derivative ultraviolet/visible absorption spectrophotometry: 2004–2008. *Analytica Chimica Acta* **2009**, 635:22–44.

71. Gorog S: The changing face of pharmaceutical analysis. *Trends in Analytical Chemistry* **2007**, 26:12–17.

72. Hasanzadeh M, Pournaghi-Azar MH, Shadjou N, Jouyban A: Magnetic nanoparticles incorporated on functionalized mesoporous silica: an advanced electrochemical sensor for simultaneous determination of amiodarone and atenolol. *RSC Advances* **2014**, 4:4710–4717.

73. Sanghavi BJ, Wolfbeis OS, Hirsch T, Swami NS: Nanomaterial-based electrochemical sensing of neurological drugs and neurotransmitters. *Microchimica Acta* **2015**, 182:1–41.

74. Farghaly OA, Abdel Hameed RS, Abu-Nawwas A-AH: Analytical application using modern electrochemical techniques. *International Journal of Electrochemcal Science* **2014**, 9:3287–3318.

75. Gupta VK, Jain R, Radhapyari K, Jadon N, Agarwal S: Voltammetric techniques for the assay of pharmaceuticals: A review. *Analytical Biochemistry* **2011**, 408:179–196.

76. Ozkan SA, Kauffmann J-M, Zuman P: Electroanalysis in biomedical and pharmaceutical sciences: Voltammetry, amperometry, biosensors, applications. New York: Springer-Verlag; **2015**.
77. Mirceski VRG, Lovric M, Bogeski I, Kappl R, Hoth M: Square-wave voltammetry: A review on the recent progress. *Electroanalysis* **2013**, 25:2411–2422.
78. Inzelt G: Conducting polymers: A new era in electrochemistry. Berlin: Springer-Verlag; **2008**.
79. Barsoukov E, Macdonald JR: Impedance spectroscopy theory, experiment, and applications. Canada: John Wiley & Sons, Inc.; **2005**.
80. Ramya R, Sivasubramanian R, Sangaranarayanan MV: Conducting polymers-based electrochemical supercapacitors–progress and prospects. *Electrochimica Acta* **2013**, 101:109–129.
81. Xu H, Wu J-X, Li C-L, Zhang J-L, Wang X-X: Investigation of polyaniline films doped with Co^{2+} as the electrode material for electrochemical supercapacitors. *Ionics* **2015**, 21:1163–1170.
82. Bumbrah GS, Sharma RM: Raman spectroscopy–Basic principle, instrumentation and selected applications for the characterization of drugs of abuse. *Egyptian Journal of Forensic Sciences* **2016**, 6:209–215.
83. Egerton RF: Physical principles of electron microscopy: An introduction to TEM, SEM, and AEM. New York: Springer Science + Business Media, Inc.; **2005**.
84. Skoog DA, West DM, Holler FJ, Crouch SR: Fundamentals of analytical chemistry. United States: Mary Finch; **2014**.
85. Owen T: Fundamentals of UV-visible Spectroscopy. Germany: Hewlett-Packard Company; **1996**.
86. Khandpur RS: Handbook of analytical instruments, Third Edition. India: McGraw Hill Education; **2015**.
87. Amir RM, Anjum FM, Khan MI, Khan MR, Pasha I, Nadeem M: Application of Fourier transform infrared (FTIR) spectroscopy for the identification of wheat varieties. *Journal of Food Science and Technology* **2013**, 50:1018–1023.
88. Tobina MJ, Puskara L, Barberb RL, Harveyb EC, Heraudc P, Woodd BR, Bamberyd KR, Dillone CT, Munroe KL: FTIR spectroscopy of single live cells in aqueous media by

synchrotron IR microscopy using microfabricated sample holders. *Vibrational Spectroscopy* **2010**, 53:34–38.

89. Birarda G, Grenci G, Businaro L, Marmiroli B, Pacor S, Piccirilli F, Vaccari L: Infrared microspectroscopy of biochemical response of living cells in microfabricated devices. *Vibrational Spectroscopy* **2010**, 53:6–11.
90. Xu Y, Mahmood M, Li Z, Dervishi E, Trigwell S, Zharov V, Ali N, Saini V, Biris AR, Lupu D *et al*: Cobalt nanoparticles coated with graphitic shells as localized radio frequency absorbers for cancer therapy. *Nanotechnology* **2008**, 19:435102–435110.
91. Kudin KN, Ozbas B, Schniepp HC, Prud'homme RK, Aksay IA, Car R: Raman spectra of graphite oxide and functionalized graphene sheets. *Nano Letters* **2008**, 8:36–41.
92. Ferrari AC: Raman spectroscopy of graphene and graphite: Disorder, electron–phonon coupling, doping and nonadiabatic effects. *Solid State Communications* **2007**, 143:47–57.
93. Kaniyoor A, Ramaprabhu S: A Raman spectroscopic investigation of graphite oxide derived graphene. *AIP Advances* **2012**, 2:032183–032196.
94. Wang Z, Wang H, Zhang Z, Yang X, Liu G: Sensitive electrochemical determination of trace cadmium on a stannum film/poly(*p*-aminobenzene sulfonic acid)/electrochemically reduced graphene composite modified electrode. *Electrochimica Acta* **2014**, 120:140–146.
95. Schwoeble AJ, Exline DL: Current methods in forensic gunshot residue analysis. Washington, D.C.: CRC Press LLC; **2000**.
96. Hodoroaba V-D, Rades S, Unger WES: Inspection of morphology and elemental imaging of single nanoparticles by high-resolution SEM/EDX in transmission mode. *Surface and Interface Analysis* **2014**, 46:945–948.
97. Liu F, Wu J, Chen K, Xue D: Morphology study by using scanning electron microscopy. *Microscopy: Science, Technology, Applications and Education* **2010**:1781–1792.
98. Ma H, Shieh K-J, Qiao TX: Study of transmission electron microscopy (TEM) and scanning electron microscopy (SEM). *Nature and Science* **2006**, 4:14–22.
99. Rades S, Hodoroaba V-D, Salge T, Wirth T, Lobera MP, Labrador RH, Natte K, Behnke T, Grossa T, Unger WES: High-resolution imaging with SEM/T-SEM, EDX and SAM as a combined methodical approach for morphological and elemental analyses of single engineered nanoparticles. *RSC Advances* **2014**, 4:49577–49587.

100. Klementova M: Electron diffraction–SAED, CBED, PED. *http://wwwxraycz/xray/csca/-kol2009/abst/klementovahtm:* accessed on 10, 1, **2018**:1–2.
101. Li Y, Yang S-Y, Chen S-M: Biosensing approach for glutathione detection using glutathione reductase (GR) with multi-walled carbon nanotubes on gold electrode. *International Journal of Electrochemical Science* **2011**, 6: 3982–3996
102. Chen W-C, Unnikrishnan B, Chen S-M: Electrochemical oxidation and amperometric determination of isoniazid at functionalized multiwalled carbon nanotube modified electrode. *International Journal of Electrochemical Science* **2012**, 7:9138–9149
103. Wu S-H, Chen D-H: Synthesis and characterization of nickel nanoparticles by hydrazine reduction in ethylene glycol. *Journal of Colloidal and Interface Science* **2003**, 259:282–286.
104. Hummers WS, Offema RE: Preparation of graphitic oxide. *Journal of American Chemical Society* **1958**, 80.
105. Yu Z, Li X, Wang X, Ma X, Li X, Cao K: Voltammetric determination of dopamine and norepinphrine on a glassy carbon electrode modified with poly(L-aspartic acid). *Journal of Chemical Sciences* **2012**, 124:537–544.
106. Wang X-G, Fan Y-J, Hao Z-X, Gan L-H: Voltammetric determination of 2,4-dinitrophenol and 2,5-dinitrophenol using a poly-aspartic acid modified electrode. *Russian Journal of Electrochemistry* **2011**, 46:1402–1407.
107. Zhang L, Lin X: Electrochemical behavior of a covalently modified glassy carbon electrode with aspartic acid and its use for voltammetric differentiation of dopamine and ascorbic acid. *Analytical and Bioanalytical Chemistry* **2005**, 382:1669–1677.
108. Khan I, Mulpuri K, Das B, Mohiuddin M, Rahman MHU: Analytical techniques (chromatography, spectroscopy, electrophorosis) in pharmaceutical analysis: A review. *International Journal of Research in Pharmaceutical and Nano Sciences* **2015**, 4:19–27.
109. Alsirawan MB, Mohammad MA, Alkasmi B, Alhareth K, El-Hammadi M: Development and validation of a simple HPLC method for the determination of ibuprofen sticking onto punch faces. *International Journal of Pharmacy and Pharmaceutical Sciences* **2013**, 5:227–231.

110. Peikova L, Georgieva M, Tsvetkova B: RP-HPLC method for simultaneous determination of ibuprofen and famotidine in pharmaceutical dosage form. *Pharmacia* **2014**, 61:3–6.
111. Kesur BR, Salunkhe VR, Magdum CS: Development and validation of UV spectrophotometric method for simultaneous estimation of ibuprofen and famotidine in bulk and formulated tablet dosage form. *International Journal of Pharmacy and Pharmaceutical Sciences* **2012**, 4:271–274.
112. Gondalia R, Mashru R, Savaliya P: Development and validation of spectrophotometric methods for simultaneous estimation of ibuprofen and paracetamol in soft gelatin capsule by simultaneous equation method. *International Journal of ChemTech Research* **2010**, 2:1881–1885.
113. Eraga SO, Arhewoh MI, Chibuogwu RN, Iwuagw MA: A comparative UV-HPLC analysis of ten brands of ibuprofen tablets. *Asian Pacific Journal of Tropical Biomedicine* **2015**, 5:880–884.
114. Motoc S, Manea F, Pop A, Pode R, Burtica G: Determination of ibuprofen in water using Ag-doped zeolite-expanded graphite composite electrode. *Advanced Science, Engineering and Medicine* **2011**, 3:7–12.
115. Roushani M, Shahdost-fard F: Fabrication of an ultrasensitive ibuprofen nanoaptasensor based on covalent attachment of aptamer to electrochemically deposited gold-nanoparticles on glassy carbon electrode. *Talanta* **2015**, 144:510–516.
116. Sabri N, Hanna K, Yargeau V: Chemical oxidation of ibuprofen in the presence of iron species at near neutral pH. *Science of the Total Environment* **2012**, 427–428:382–389.
117. Matrovic SR, Valle GM, Briand LE: Quantitative analysis of ibuprofen in pharmaceutical formulations through FTIR spectroscopy. *Latin American Applied Research* **2005**, 35:189–195.
118. Ebeshi BU, Oseni KE, Ahmadu AA, Oluwadiyay JO: Comparative utilization of visual, potentiometric titrations and UV spectrophotometric methods in the determination of ibuprofen. *African Journal of Pharmacy and Pharmacology* **2009**, 3:426–431.
119. Mallah MA, Sherazi STH, Mahesar SA, Khaskheli AR: Simultaneous quantification of ibuprofen and paracetamol in tablet formulations using transmission Fourier transform infrared spectroscopy. *American Journal of Analytical Chemistry* **2012**, 03:503–511.

120. Rifai N, Sakamoto M, Law T, Galpchian V, Harris N, Colin AA: Use of a rapid HPLC assay for determination of pharmacokinetic parameters of ibuprofen in patients with cystic fibrosis. *Clinical Chemistry* **1996**, 42:1812–1816.

121. Ziylan A, Ince NH: The occurrence and fate of anti-inflammatory and analgesic pharmaceuticals in sewage and fresh water: Treatability by conventional and non-conventional processes. *Journal of Hazardous Materials* **2011**, 187:24–36.

122. Pattanaik S, Mukhi S, Pattnaik G, Panda J: Assay method development and validation of ibuprofen tablets by HPLC. *Der Pharmacia Sinica* **2013**, 4:91–96.

123. Rahman A, Sarowar SJ, Jahirul JI, Rehana RB, Kayesh RK: A study of method development, validation, and forced degradation for simultaneous quantification of paracetamol and ibuprofen in pharmaceutical dosage form by RP-HPLC method. *Analytical Chemistry Insights* **2014**, 9:75–81.

124. Lockwood GF, Wagner JG: High-performance liquid chromatographic determination of ibuprofen and its major metabolites in biological fluids. *Journal of Chromatography* **1982**, 232:335–343.

125. Shaalan RA, Haggag RS, Belal SF, Agami M: Simultaneous determination of hyoscine, ketoprofen and ibuprofen in pharmaceutical formulations by HPLC-DAD. *Journal of Applied Pharmaceutical Science* **2013**, 3:038–047.

126. El Haj BM, Al Ainri AM, Hassan MH, Bin Khadem RK, Marzouq MS: The GC/MS analysis of some commonly used non-steriodal anti-inflammatory drugs (NSAIDs) in pharmaceutical dosage forms and in urine. *Forensic Science International* **1999**, 105:141–153.

127. Hashim NH, Khan SJ: Enantioselective analysis of ibuprofen, ketoprofen and naproxen in wastewater and environmental water samples. *Journal of Chromatography A* **2011**, 1218:4746–4754.

128. Huber G, Garg U: Quantitation of ibuprofen in blood using gas chromatography-mass spectrometry (GC-MS). *Methods in Molecular Biology* **2010**, 603:289–296.

129. Shihabi ZK, Hinsdale ME: Analysis of ibuprofen in serum by capillary electrophoresis. *Journal of Chromatography B* **1996**, 683:115–118.

130. Hamoudova R, Pospisilova M: Determination of ibuprofen and flurbiprofen in pharmaceuticals by capillary zone electrophoresis. *Journal of Pharmaceutical and Biomedical Analysis* **2006**, 41:1463–1467.
131. Glowka FK, Karazniewicz M: High performance capillary electrophoresis method for determination of ibuprofen enantiomers in human serum and urine. *Analytical Chimica Acta* **2005**, 540:95–102.
132. Sunaric S, Petkovic M, Denic M, Mitic S, Pavlovic A: Determination of ibuprofen in combined dosage forms and cream by direct UV spectrophotometry after solid-phase extraction. *Acta Poloniae Pharmaceutica–Drug Research* **2013**, 70:403–411.
133. Issa YM, Zayed SIM, Habib IHI: Simultaneous determination of ibuprofen and paracetamol using derivatives of the ratio spectra method. *Arabian Journal of Chemistry* **2011**, 4:259–263.
134. Turk SC, Satana E, Basan H, Goger NG: Determination of ibuprofen and paraben in pharmaceutical formulations using flow-injection and derivative spectrophotometry. *Journal of Analytical Chemistry* **2014**, 70:50–54.
135. Hassan WS: Determination of ibuprofen and paracetamol in binary mixture using chemometric-assisted spectrophotometric methods. *American Journal of Applied Sciences* **2008**, 5:1005–1012.
136. Hergert LA, Escandar GM: Spectrofluorimetric study of the β-cyclodextrin–ibuprofen complex and determination of ibuprofen in pharmaceutical preparations and serum. *Talanta* **2003**, 60:235–246.
137. Amin S, Soomro MT, Memon N, Solangi AR, Sirajuddin, Qureshi T, Behzad AR: Disposable screen printed graphite electrode for the direct electrochemical determination of ibuprofen in surface water. *Environmental Nanotechnology, Monitoring & Management* **2014**, 1–2:8–13.
138. Farghaly OA, Abdel Hameed RS, Abu-Nawwas A-AH: Analytical application using modern electrochemical techniques. *International Journal of Electrochemical Science* **2014**, 9:3287–3318.
139. Lima AB, Torres LMFC, GuimarAes CFRC, Verly RM, Silva LMd, Carvalho Júnior AD, Santos WTPd: Simultaneous determination of paracetamol and ibuprofen in

pharmaceutical samples by differential pulse voltammetry using a boron-doped diamond electrode. *Journal of the Brazilian Chemical Society* **2014**, 25:478–483.

140. Lima AB, Faria EO, Montes RHO, Cunha RR, Richter EM, Munoz RAA, dos Santos WTP: Electrochemical oxidation of ibuprofen and its voltammetric determination at a boron-doped diamond electrode. *Electroanalysis* **2013**, 25:1585–1588.
141. Motoc S, Remes A, Pop A, Manea F, Schoonman J: Electrochemical detection and degradation of ibuprofen from water on multi-walled carbon nanotubes-epoxy composite electrode. *Journal of Environmental Sciences* **2013**, 25:838–847.
142. Manea F, Motoc S, Pop A, Remes A, Schoonman J: Silver-functionalized carbon nanofiber composite electrodes for ibuprofen detection. *Nanoscale Research Letters* **2012**, 7:331–334.
143. Riquelme MA, Lucero MA, Villagran M, Arevalo MC, Hernández-Creus A, Aguirre MJ, Arce R, Ramirez G: Glassy carbon modified electrode: Polymer and supramolecular assembly of Co(II)-[tetra(*o*-aminophenyl) porphyrin] new material for electrocatalytic assays. *International Journal of Electrochemical Science* **2012**, 7:9738–9747.
144. Geto A, Amare M, Tessema M, Admassie S: Polymer-modified glassy carbon electrode for the electrochemical detection of quinine in human urine and pharmaceutical formulations. *Analytical and Bioanalytical Chemistry* **2012**, 404:525–530.
145. Chowdhury A-N, Ferdousi S, Islam MM, Okajima T, Ohsaka T: Arsenic detection by nanogold/conducting-polymer-modified glassy carbon electrodes. *Journal of Applied Polymer Science* **2007**, 104:1306–1311.
146. Wang L, Huang P-F, Wang H-J, Bai J-Y, Zhang L-Y, Zhao Y-Q: Covalent modification of glassy carbon electrode with aspartic acid for simultaneous determination of hydroquinone and catechol. *Analytical Chemistry* **2007**, 97:365–404.
147. Iwasaki Y, Niwa O, Morita M: Electrochemical reaction of Cytochrome C on polyaspartic acid modified gold electrodes. *Sensors and Materials* **1996**, 11:051–056.
148. Gamero-Quijano A, Huerta F, Salinas-Torres D, Morallón E, Montilla F: Electrocatalytic performance of SiO_2-SWCNT nanocomposites prepared by electroassisted deposition. *Electrocatalysis* **2013**, 4:259–266.
149. Fotouhi L, Fatollahzadeh M, Heravi MM: Electrochemical behavior and voltammetric determination of sulfaguanidine at a glassy carbon electrode modified with a multi-

walled carbon nanotube. *International Journal of Electrochemical Science* **2012**, 7:3919–3928.

150. Rezaei B, Damiri S: Voltammetric behavior of multi-walled carbon nanotubes modified electrode-hexacyanoferrate(II) electrocatalyst system as a sensor for determination of captopril. *Sensors and Actuators B* **2008**, 134:324–331.
151. Stefano JS, de Lima AP, Montes RHO, Richter EM, Munoz RAA: Fast determination of naproxen in pharmaceutical formulations by batch injection analysis with pulsed amperometric detection. *Journal of Brazilian Chemical Society* **2012**, 23:1834–1838.
152. Sarhangzadeh K: Application of multi wall carbon nanotube–graphene hybrid for voltammetric determination of naproxen. *Journal of the Iranian Chemical Society* **2015**, 12:2133–2140.
153. Suravajhala R, Suri N, Bhagat M, Saxena AK: Biological evaluation of 8-alkyl xanthines as potential cytotoxic agents. *Advances in Biological Chemistry* **2013**, 03:314–319.
154. Landaeta VR, Rodríguez-Lugo RE, Rodríguez-Arias EN, Coll-Gómez DS, González T: Studies on the coordination chemistry of methylated xanthines and their imidazolium salts. Part 1: benzyl derivatives. *Transition Metal Chemistry* **2009**, 35:165–175.
155. Bispo MS, Veloso MCC, Pinheiro HLC, De Oliveira RFS, Reis JON, De Andrade JB: Simultaneous determination of caffeine, theobromine, and theophylline by high-performance liquid chromatography. *Journal of Chromatographic Science* **2002**, 40:45-48.
156. Coco FL, Lanuzza F, Micali G, Cappellano G: Determination of theobromine, theophylline, and caffeine in by-products of cupuacu and cacao seeds by high-performance liquid chromatography. *Journal of Chromatography Science* **2007**, 45:273–275.
157. Srdjenovic B, Djordjevic-Milic V, Grujic N, Injac R, Lepojevic Z: Simultaneous HPLC determination of caffeine, theobromine, and theophylline in food, drinks, and herbal products. *Journal of Chromatography Science* **2008**, 46:144–149.
158. Patil PN: Caffeine in various samples and their analysis with HPLC–A review. *International Journal of Pharmaceutical Sciences and Research* **2012**, 16:76-83.

159. Kan X, Liu T, Li C, Zhou H, Xing Z, Zhu A: A novel electrochemical sensor based on molecularly imprinted polymers for caffeine recognition and detection. *Journal of Solid State Electrochemistry* **2012**, 16:3207–3213.

160. Allwood MB, Cannan B, van Aalten DMF, Eggleston IM: Efficient synthesis of 1,3,7-substituted xanthines by a safety-catch protection strategy. *Tetrahedron* **2007**, 63:12294–12302.

161. Gao Y, Wang H, Guo L: Simultaneous determination of theophylline and caffeine by large mesoporous carbon/nafion modified electrode. *Journal of Electroanalytical Chemistry* **2013**, 706:7–12.

162. Charehsaz M, Gürbay A, Aydin A, Sahin G: Simple, fast and reliable liquid chromatographic and spectrophotometric methods for the determination of theophylline in urine, saliva and plasma samples. *Iranian Journal of Pharmaceutical Research* **2014**, 13:431–439.

163. Ojoe E, Miyauchi EM, Viviani TC, Consiglieri VO: Formulation and in vitro evaluation of theophylline-eudragit sustained-release tablets. *Brazilian Journal of Pharmaceutical Sciences* **2005**, 41:377–384.

164. Svorc L: Determination of caffeine: A comprehensive review on electrochemical methods *International Journal of Electrochemical Science* **2013**, 8:5755–5773.

165. Nawrot P, Jordan S, Eastwood J, Rotstein J, Hugenholtz A, Feeley M: Effects of caffeine on human health. *Food additives and contaminants* **2003**, 20:1–30.

166. Arinobu T, Hattori H, Kumazawa T, Lee X-P, Mizutani Y, Katase T, Kojima S, Omori T, Kaneko R, Ishii A *et al*: High-throughput determination of theophylline and caffeine in human serum by conventional liquid chromatography-mass spectrometry. *Forensic Toxicology* **2008**, 27:1–6.

167. Buyuktuncel E: Simultaneous determination of theobromine, paraxanthine, theophylline, and caffeine in urine by reversed-phase high-performance liquid chromatography with diode array UV detection. *Analytical Letters* **2010**, 43:2518–2524.

168. Sereshti H, Khosraviani M, Samadi S, Amini-Fazl MS: Simultaneous determination of theophylline, theobromine and caffeine in different tea beverages by graphene-oxide based ultrasonic-assisted dispersive micro solid-phase extraction combined with HPLC-UV. *RSC Advances* **2014**, 4:47114–47120.

169. Brunetto MR, Gutiérrez L, Delgado Y, Gallignani M, Zambrano A, Gómez Á, Ramos G, Romero C: Determination of theobromine, theophylline and caffeine in cocoa samples by a high-performance liquid chromatographic method with on-line sample cleanup in a switching-column system. *Food Chemistry* **2007**, 100:459–467.

170. Emara S: Simultaneous determination of caffeine, theophylline and theobromine in human plasma by on-line solid-phase extraction coupled to reversed-phase chromatography. *Biomedical Chromatography* **2004**, 18:479–485.

171. Zou J, Li N: Simple and environmental friendly procedure for the gas chromatographic-mass spectrometric determination of caffeine in beverages. *Journal of Chromatography A* **2006**, 1136:106–110.

172. Shrivas K, Wu HF: Rapid determination of caffeine in one drop of beverages and foods using drop-to-drop solvent microextraction with gas chromatography/mass spectrometry. *Journal of Chromatography A* **2007**, 1170:9–14.

173. Song (Sherry) S, Ashley DL: Sample purification for the analysis of caffeine in tobacco by gas chromatography–mass spectrometry. *Journal of Chromatography A* **1998**, 814:171–180.

174. Singh DK, Sahu A: Spectrophotometric determination of caffeine and theophylline in pure alkaloids and its application in pharmaceutical formulations. *Analytical Biochemistry* **2006**, 349:176–180.

175. Aktas AH: Chemometric methods for the simultaneous spectrophotometric determination of caffeine, theobromine and theophylline in tea. *Asian Journal of Chemistry* **2013**, 25:8333–8338.

176. Paradkar MM, Irudayaraj J: Rapid determination of caffeine content in soft drinks using FTIR–ATR spectroscopy. *Food Chemistry* **2002**, 78:261–266.

177. López-Martínez L, López-de-Alba PL, García-Campos R, De León-Rodríguez LM: Simultaneous determination of methylxanthines in coffees and teas by UV-Vis spectrophotometry and partial least squares. *Analytica Chimica Acta* **2003**, 493:83–94.

178. Belay A, Ture K, Redi M, Asfaw A: Measurement of caffeine in coffee beans with UV/Vis spectrometer. *Food Chemistry* **2008**, 108:310–315.

179. Xia Z, Ni Y, Kokot S: Simultaneous determination of caffeine, theophylline and theobromine in food samples by a kinetic spectrophotometric method. *Food Chemistry* **2013**, 141:4087–4093.

180. Talebpour Z, Maesum S, Jalali-Heravi M, Shamsipur M: Simultaneous determination of theophylline and caffeine by proton magnetic resonance spectroscopy using partial least squares regression techniques. *Analytical Sciences* **2003**, 19:1079–1082.

181. Yang YJ, Li W: High sensitive determination of theophylline based on manganese oxide nanoparticles/multiwalled carbon nanotube nanocomposite modified electrode. *Ionics* **2014**, 21:1121–1128.

182. Spaftaru N, Sarada BV, Tryk DA, Fujishima A: Anodic voltammetry of xanthine, theophylline, theobromine and caffeine at conductive diamond electrodes and its analytical application. *Electroanalysis* **2002**, 14:721–728.

183. Svorc L, Tomcik P, Svitkova J, Rievaj M, Bustin D: Voltammetric determination of caffeine in beverage samples on bare boron-doped diamond electrode. *Food Chemistry* **2012**, 135:1198–1204.

184. Shubietah RM, Zuhri AA: Adsorptive cathodic stripping voltammetric determination of theophylline at a hanging mercury drop electrode. *Analyst* **1994**, 119:1967–1970.

185. Wang T, Randviir EP, Banks CE: Detection of theophylline utilising portable electrochemical sensors. *Analyst* **2014**, 139:2000–2003.

186. Campean A, Tertis M, Sandulescu R: Electrochemical behavior of some purine derivatives on carbon based electrodes. *Central European Journal of Chemistry* **2011**, 9:466–473.

187. Wang Y, Bi C: Simultaneous electrochemical determination of ascorbic acid, dopamine and uric acid using poly(tyrosine)/functionalized multi-walled carbon nanotubes composite film modified electrode. *Journal of Molecular Liquids* **2013**, 177:26–31.

188. Wang Y, Wu T, Bi C-y: Simultaneous determination of acetaminophen, theophylline and caffeine using a glassy carbon disk electrode modified with a composite consisting of poly(alizarin violet 3B), multiwalled carbon nanotubes and graphene. *Microchimica Acta* **2015**, 183:731–739.

189. Yang G, Zhao F, Zeng B: Facile fabrication of a novel anisotropic gold nanoparticle-chitosan-ionic liquid/graphene modified electrode for the determination of theophylline and caffeine. *Talanta* **2014**, 127:116–122.
190. Zhenhui W, Zhiguo L, Shuping Z: Voltammetric behavior of caffeine and theophylline at poly(4-aminopyridine) modified electrode and their simultaneous determination. *Chinese Journal of Analytical Chemistry* **2004**, 32:305–308.
191. Iijima S: Helical microtubules of graphitic carbon. *Nature* **1991**, 354:56–58.
192. Sun W, Hu J: Voltammetric determination of theophylline in pharmaceutical formulations using aligned carbon nanotubes (ACNTs) film modified electrode. *Journal of Analytical Chemistry* **2013**, 68:694–699.
193. Filik H, Avan AA, Aydar S: Simultaneous detection of ascorbic acid, dopamine, uric acid and tryptophan with Azure A-interlinked multi-walled carbon nanotube/gold nanoparticles composite modified electrode. *Arabian Journal of Chemistry* **2016**, 9:471–480.
194. March G, Nguyen TD, Piro B: Modified electrodes used for electrochemical detection of metal ions in environmental analysis. *Biosensors* **2015**, 5:241–275.
195. Vasantha VS, Chen S-M: Effect of reaction conditions on electropolymerization of melatonin on bare electrodes and PEDOT-modified electrodes. *Journal of Electrochemical Society* **2005**, 152:151–159.
196. Shahrokhian S, Kamalzadeh Z, Saberi R-S: Glassy carbon electrode modified with a bilayer of multi-walled carbon nanotube and polypyrrole doped with new coccine: Application to the sensitive electrochemical determination of sumatriptan. *Electrochimica Acta* **2011**, 56:10032–10038.
197. Her S-C, Lai C-Y: Dynamic behavior of nanocomposites reinforced with multi-walled carbon nanotubes (MWCNTs). *Materials* **2013**, 6:2274–2284.
198. Ujjain SK, Bhatia R, Ahuja P, Attri P: Highly conductive aromatic functionalized multi-walled carbon nanotube for inkjet printable high performance supercapacitor electrodes. *PloS One* **2015**, 10:1–12.
199. Guo W, Geng M, Zhou L, Chao S, Yang R, An H, Cui C: Multi-walled carbon nanotube modified electrode for sensitive determination of an anesthetic drug: Tetracaine hydrochloride. *International Journal of Electrochemical Science* **2013**, 8:5369–5381

200. Liu J, Zhou D, Liu X, Wu K, Wan C: Determination of kojic acid based on the interface enhancement effects of carbon nanotube/alizarin red S modified electrode. *Colloids and surfaces B, Biointerfaces* **2009**, 70:20–24.

201. Xie X, Gan T, Sun D, Wu K: Application of multi□walled carbon nanotubes/nafion composite film in electrochemical determination of Pb^{2+}. *Fullerenes, Nanotubes and Carbon Nanostructures* **2008**, 16:103–113.

202. Moghaddam AB, Mohammadi A, Fathabadi M: Application of carbon nanotube-graphite mixture for the determination of diclofenac sodium in pharmaceutical and biological samples. *Pharmaceutica Analytica Acta* **2012**, 03:1–6.

203. Sun J-Y, Huang K-J, Wei S-Y, Wu Z-W: Application of cetyltrimethylammonium bromide – graphene modified electrode for sensitive determination of caffeine. *Canadian Journal of Chemistry* **2011**, 89:697–702.

204. Sun JY, Huang KJ, Wei SY, Wu ZW, Ren FP: A graphene-based electrochemical sensor for sensitive determination of caffeine. *Colloids and surfaces B, Biointerfaces* **2011**, 84:421–426.

205. Li Y, Wu S, Luo P, Liu J, Song G, Zhang K, Ye B: Electrochemical behavior and voltammetric determination of theophylline at a glassy carbon electrode modified with graphene/nafion. *Analytical Sciences* **2012**, 28:497–502.

206. Zhu Y-H, Zhang Z-L, Pang D-W: Electrochemical oxidation of theophylline at multi-wall carbon nanotube modified glassy carbon electrodes. *Journal of Electroanalytical Chemistry* **2005**, 581:303–309.

207. Malode SJ, Shetti NP, Nandibewoor ST: Voltammetric behavior of theophylline and its determination at multi-wall carbon nanotube paste electrode. *Colloids and Surfaces B, Biointerfaces* **2012**, 97:1–6.

208. Amare M, Admassie S: Differential pulse voltammetric determination of theophylline at poly(4-amino-3-hydroxyl naphthalene sulfonic acid) modified glassy carbon electrode. *Bulletin of the Chemical Society of Ethiopia* **2012**, 26:73–84.

209. Valassi L, Tsimpliaras D, Katseli V, Economou A, Svancara I, Stoces M, Mikysek T, Prodromidis M: Disposable nafion-modified screen printed graphite electrodes for the rapid voltammetric assay of caffeine. *Insights in Analytical Chemistry* **2015**, 1:1–8.

210. Habibi B, Abazari M, Pournaghi-Azar MH: A carbon nanotube modified electrode for determination of caffeine by differential pulse voltammetry. *Chinese Journal of Catalysis* **2012**, 33:1783–1790.

211. Su Y, Chen C, Hou X, Zhang J: A new capillary electrophoresis-direct chemiluminescence system for the determination of epinephrine and mechanism study. *Analytical Methods* **2011**, 3:2893–2897.

212. Wang H-S, Huang D-Q, Liu R-M: Study on the electrochemical behavior of epinephrine at a poly(3-methylthiophene)-modified glassy carbon electrode. *Journal of Electroanalytical Chemistry* **2004**, 570:83–90.

213. Fouad DM, El-Said WA: Selective electrochemical detection of epinephrine using gold nanoporous film. *Journal of Nanomaterials* **2016**, 2016:1–8.

214. Al-Ameri SAH: Spectrophotometric determination of adrenaline in pharmaceutical preparations. *Arabian Journal of Chemistry* **2016**, 9:1000–1004.

215. Kang H, Jin Y, Han Q: Electrochemical detection of epinephrine using an l-glutamic acid functionalized graphene modified electrode. *Analytical Letters* **2014**, 47:1552–1563.

216. Li J, Wang X, Duan H, Wang Y, Luo C: Ultra-sensitive determination of epinephrine based on TiO2-Au nanoclusters supported on reduced graphene oxide and carbon nanotube hybrid nanocomposites. *Material Science and Engneering C* **2016**, 64:391–398.

217. Barman K, Jasimuddin S: Simultaneous electrochemical detection of dopamine and epinephrine in the presence of ascorbic acid and uric acid using a AgNPs–penicillamine–Au electrode. *RSC Advances* **2016**, 6:99983–99988.

218. Mishra A: Simultaneous determination of epinephrine and norepinephrine by high performance liquid chromatography. *Scientia Pharmaceutica* **2009**, 77:367–374.

219. Wu D, Xie H, Lu H, Li W, Zhang Q: Sensitive determination of norepinephrine, epinephrine, dopamine and 5-hydroxytryptamine by coupling HPLC with [$Ag(HIO_6)_2$](5-)-luminol chemiluminescence detection. *Biomedical Chromatography* **2016**, 30:1458–1466.

220. Liu Y, Liu Z, Shi Y: Sensitive determination of epinephrine in pharmaceutical preparation by flow injection coupled with chemiluminescence detection and mechanism study. *Luminescence* **2011**, 26:59–64.

221. Al Abachi MQ, Hadi H: A new kinetic and thermodynamic study of spectrophotometric method for determination of adrenaline in its pharmaceutical formulations. *Pharmaceutical Chemistry Journal* **2014**, 48:558–563.

222. Tavana T, Khalilzadeh MA, Karimi-Maleh H, Ensafi AA, Beitollahi H, Zareyee D: Sensitive voltammetric determination of epinephrine in the presence of acetaminophen at a novel ionic liquid modified carbon nanotubes paste electrode. *Journal of Molecular Liquids* **2012**, 168:69–74.

223. Zeng B, Yang Y, Zhao F: Voltammetric determination of epinephrine with a 3-mercaptopropionic acid self-assembled monolayer modified gold electrode. *Electroanalysis* **2003**, 15:1054–1059.

224. Cui F, Zhang X: Electrochemical sensor for epinephrine based on a glassy carbon electrode modified with graphene/gold nanocomposites. *Journal of Electroanalytical Chemistry* **2012**, 669:35–41.

225. Huang J: Selective and reliable electrochemical sensor based on polythionine/AuNPs composites for epinephrine detection in serum. *International Journal of Electrochemical Science* **2016**:8193–8203.

226. Zhang H-M, Zhou X-L, Hui R-T, Li N-Q, Liu D-P: Studies of the electrochemical behavior of epinephrine at a homocysteine self-assembled electrode. *Talanta* **2002**, 56:1081–1088.

227. Sun Y-X, Wang S-F, Zhang X-H, Huang Y-F: Simultaneous determination of epinephrine and ascorbic acid at the electrochemical sensor of triazole SAM modified gold electrode. *Sensors and Actuators B: Chemical* **2006**, 113:156–161.

228. Li X, Chen M, Ma X: Selective determination of epinephrine in the presence of ascorbic acid using a glassy carbon electrode modified with graphene. *Analytical Sciences* **2012**, 28:147–151.

229. Haque AM, Park H, Sung D, Jon S, Choi SY, Kim K: An electrochemically reduced graphene oxide-based electrochemical immunosensing platform for ultrasensitive antigen detection. *Analytical Chemistry* **2012**, 84:1871–1878.

230. Li J, Kuang D, Feng Y, Zhang F, Xu Z, Liu M: A graphene oxide-based electrochemical sensor for sensitive determination of 4-nitrophenol. *Journal of Hazardous Materials* **2012**, 201–202:250–259.

231. Devadas B, Rajkumar M, Chen S-M, Saraswathi R: Electrochemically reduced graphene oxide/neodymium hexacyanoferrate modified electrodes for the electrochemical detection of paracetamol. *International Journal of Electrochemical Science* **2012**, 7:3339–3349.

232. Xi X, Ming L: A voltammetric sensor based on electrochemically reduced graphene modified electrode for sensitive determination of midecamycin. *Analytical Methods* **2012**, 4:3013–3018.

233. Mutyala S, Mathiyarasu J: A reagentless non-enzymatic hydrogen peroxide sensor presented using electrochemically reduced graphene oxide modified glassy carbon electrode. *Material Science and Engineering C* **2016**, 69:398–406.

234. Filik H, Cetintas G, Avan AA, Aydar S, Koc SN, Boz I: Square-wave stripping voltammetric determination of caffeic acid on electrochemically reduced graphene oxide-nafion composite film. *Talanta* **2013**, 116:245–250.

235. Yan L, Niu X, Wang W, Li X, Sun X, Zheng C, Wang J, Sun W: Electrochemical sensor for rutin detection with graphene oxide and multi-walled carbon nanotube nanocomposite modified electrode. *International Journal of Electrochemical Science* **2016**, 11:1738–1750.

236. Liu S, Tian J, Wang L, Luo Y, Sun X: Production of stable aqueous dispersion of poly(3,4-ethylenedioxythiophene) nanorods using graphene oxide as a stabilizing agent and their application for nitrite detection. *Analyst* **2011**, 136:4898–4902.

237. Sharma D, Kanchi S, Sabela MI, Bisetty K: Insight into the biosensing of graphene oxide: Present and future prospects. *Arabian Journal of Chemistry* **2016**, 9:238–261.

238. Ping J, Wang Y, Ying Y, Wu J: Application of electrochemically reduced graphene oxide on screen-printed ion-selective electrode. *Analytical Chemistry* **2012**, 84:3473–3479.

239. Raj MA, John SA: Fabrication of electrochemically reduced graphene oxide films on glassy carbon electrode by self-assembly method and their electrocatalytic application. *The Journal of Physical Chemistry C* **2013**, 117:4326–4335.

240. Zhou YZ, Zhang LJ, Chen SL, Dong SY, Zheng XH: Electroanalysis and simultaneous determination of dopamine and epinephrine at poly(isonicotinic acid)-modified carbon paste electrode in the presence of ascorbic acid. *Chinese Chemical Letters* **2009**, 20:217–220.

241. Wu B, Zhao N, Hou S, Zhang C: Electrochemical synthesis of polypyrrole, reduced graphene oxide, and gold nanoparticles composite and its application to hydrogen peroxide biosensor. *Nanomaterials* **2016**, 6:1–11.

242. Drewniak S, Muzyka R, Stolarczyk A, Pustelny T, Kotyczka-Moranska M, Setkiewicz M: Studies of reduced graphene oxide and graphite oxide in the aspect of their possible application in gas sensors. *Sensors* **2016**, 16:103–118.

243. Mohamed ME, Mohammed AMA: Experimental and computational vibration study of amino acids. *International Letters of Chemistry, Physics and Astronomy* **2013**, 10:1–17.

244. Kakaei K, Hasanpour K: Synthesis of graphene oxide nanosheets by electrochemical exfoliation of graphite in cetyltrimethylammonium bromide and its application for oxygen reduction. *Journal of Materials Chemistry A* **2014**, 2:5428–15436.

245. Li J, Wang Y, Sun Y, Ding C, Lin Y, Sun W, Luo C: A novel ionic liquid functionalized graphene oxide supported gold nanoparticle composite film for sensitive electrochemical detection of dopamine. *RSC Advances* **2017**, 7:2315–2322.

246. Nguyen VH, Lamiel C, Kharismadewi D, Tran VC, Shim J-J: Covalently bonded reduced graphene oxide/polyaniline composite for electrochemical sensors and capacitors. *Journal of Electroanalytical Chemistry* **2015**, 758:148–155.

247. Mani V, Devadas B, Chen SM: Direct electrochemistry of glucose oxidase at electrochemically reduced graphene oxide-multiwalled carbon nanotubes hybrid material modified electrode for glucose biosensor. *Biosensors and Bioelectronics* **2013**, 41:309–315.

248. Muhammad A, Yusof NA, Hajian R, Abdullah J: Construction of an electrochemical sensor based on carbon nanotubes/gold nanoparticles for trace determination of amoxicillin in bovine milk. *Sensors* **2016**, 16:1–13.

249. Peik-See T, Pandikumar A, Nay-Ming H, Hong-Ngee L, Sulaiman Y: Simultaneous electrochemical detection of dopamine and ascorbic acid using an iron oxide/reduced graphene oxide modified glassy carbon electrode. *Sensors* **2014**, 14:15227–15243.

250. Ibrahim I, Lim HN, Huang NM, Pandikumar A: Cadmium sulphide-reduced graphene oxide-modified photoelectrode-based photoelectrochemical sensing platform for copper(II) ions. *PLoS One* **2016**, 11:1–18.

251. Mirceski V, Gulaboski R: Recent achievements in square-wave voltammetry: A review. *Macedonian Journal of Chemistry and Chemical Engineering* **2014**, 33:1–12
252. Wang S-F, Du D, Zou Q-C: Electrochemical behavior of epinephrine at L-cysteine self-assembled monolayers modified gold electrode. *Talanta* **2002**, 57:687–692.
253. Mahmoudi Moghaddam H, Beitollahi H, Tajik S, Soltani H: Fabrication of a nanostructure based electrochemical sensor for voltammetric determination of epinephrine, uric acid and folic acid. *Electroanalysis* **2015**, 27:2620–2628.
254. Goyal RN, Chatterjee S, Rana ARS: The effect of modifying an edge-plane pyrolytic graphite electrode with single-wall carbon nanotubes on its use for sensing diclofenac. *Carbon* **2010**, 48:4136– 4144.
255. Ensafi AA, Izadi M, Karimi-Maleh H: Sensitive voltammetric determination of diclofenac using room-temperature ionic liquid-modified carbon nanotubes paste electrode. *Ionics* **2013**, 19:137–144.
256. Afkhami A, Bahiraei A, Madrakian T: Gold nanoparticle/multi-walled carbon nanotube modified glassy carbon electrode as a sensitive voltammetric sensor for the determination of diclofenac sodium. *Material Science and Engineering C* **2016**, 59:168–176.
257. Aguilar-Lira GY, Álvarez-Romero GA, Zamora-Suárez A, Palomar-Pardavé M, Rojas-Hernández A, Rodríguez-Ávila JA, Páez-Hernández ME: New insights on diclofenac electrochemistry using graphite as working electrode. *Journal of Electroanalytical Chemistry* **2017**, 794:182–188.
258. Yilmaz B, Ciltas U: Determination of diclofenac in pharmaceutical preparations by voltammetry and gas chromatography methods. *Journal of pharmaceutical analysis* **2015**, 5:153–160.
259. Elkady EF: Simultaneous determination of diclofenac potassium and methocarbamol in ternary mixture with guaifenesin by reversed phase liquid chromatography. *Talanta* **2010**, 82:1604–1607.
260. Kaphalia L, Kaphalia BS, Kumar S, Kanz MF, Treinen-Moslen M: Efficient high performance liquid chromatography/ultraviolet method for determination of diclofenac and 4-hydroxydiclofenac in rat serum. *Journal of Chromatography B* **2006**, 830:231–237.
261. Roskar R, Kmetec V: Liquid chromatographic determination of diclofenac in human synovial fluid. *Journal of Chromatography B* **2003**, 788:57–64.

262. Yilmaz B: GC–MS determination of diclofenac in human plasma. *Chromatographia* **2010**, 71:549–551.
263. Shah I, Barker J, Naughton DP, Barton SJ, Ashraf SS: Determination of diclofenac concentrations in human plasma using a sensitive gas chromatography mass spectrometry method. *Chemistry Central Journal* **2016**, 10: (52) 1–10.
264. Kramancheva I, Dobrev I, Brakalov L, Andreeva A: Spectrophotometric determination of diclofenac sodium in gel-ointment. *Analytical Letters* **1997**, 30:2235–2249.
265. Zh.O.Kormosh, Hunka IP, Bazel YR: Extraction and spectrophotometric determination of diclofenac in pharmaceuticals. *Journal of Chinese Chemical Society* **2008**, 55:356–361.
266. Souza RLd, Tubino M: Spectrophotometric determination of diclofenac in pharmaceutical preparations. *Journal of the Brazilian Chemical Society* **2005**, 16:1068–1073.
267. Arancibia JA, Boldrini MA, Escandar GM: Spectrofluorimetric determination of diclofenac in the presence of β-cyclodextrin. *Talanta* **2000**, 52:261–268.
268. Chethana BK, Basavanna S, Naik YA: Voltammetric determination of diclofenac sodium using tyrosine modified carbon paste electrode. *Industrial and Engineering Chemistry Research* **2012**, 51:10287–10295.
269. Goyal RN, Chatterjee S, Agrawal B: Electrochemical investigations of diclofenac at edge plane pyrolytic graphite electrode and its determination in human urine. *Sensors and Actuators B* **2010**, 145:743–748.
270. Karuppiah C, Cheemalapati S, Chen S-M, Palanisamy S: Carboxyl-functionalized graphene oxide-modified electrode for the electrochemical determination of nonsteroidal anti-inflammatory drug diclofenac. *Ionics* **2015**, 21:231–238.
271. Shalauddin M, Akhter S, Bagheri S, Karim MSA, Kadri NA, Basirun WJ: Immobilized copper ions on MWCNTS-Chitosan thin film: Enhanced amperometric sensor for electrochemical determination of diclofenac sodium in aqueous solution. *International Journal of Hydrogen Energy* **2017**, 42:19951–19960.
272. Motoc S, Manea F, Iacob A, Martinez-Joaristi A, Pop A, Schoonman J: Electrochemical selective and simultaneous detection of diclofenac and ibuprofen in aqueous solution

using HKUST-1 metal-organic framework-carbon nanofiber composite electrode. *Sensors* **2016**, 16:1719–1730.

273. Basiri F, Taei M: Application of spinel-structured $MgFe_2O_4$ nanoparticles for simultaneous electrochemical determination diclofenac and morphine. *Microchimica Acta* **2017**, 184:155–162.
274. Sarhangzadeh K, Khatami AA, Jabbari M, Bahari S: Simultaneous determination of diclofenac and indomethacin using a sensitive electrochemical sensor based on multiwalled carbon nanotube and ionic liquid nanocomposite. *Journal of Applied Electrochemistry* **2013**, 43:1217–1224.
275. Goodarzian M, A.Khalilzade M, Karimi F, Gupta VK, Keyvanfard M, Bagheri H, Fouladgar M: Square wave voltammetric determination of diclofenac in liquid phase using a novel ionic liquid multiwall carbon nanotubes paste electrode. *Journal of Molecular Liquids* **2014**, 197:114–119.
276. Rodrıguez JA, Barrado E, Castrillejo Y, Santos JR, Lima JLFC: Validation of a tubular bismuth film amperometric detector determination of diclofenac sodium by multi-syringe flow injection analysis. *Journal of Pharmaceutical and Biomedical Analysis* **2007**, 45:47–53.
277. Gimenes DT, Freitas JMd, Munoz RAA, Richter EM: Flow-injection amperometric method for determination of diclofenac in pharmaceutical formulations using a boron-doped diamond electrode. *Electroanalysis* **2011**, 23:2521–2525.
278. Song Y, He Z, Zhu H, Hou H, Wang L: Electrochemical and electrocatalytic properties of cobalt nanoparticles deposited on graphene modified glassy carbon electrode: Application to some amino acids detection. *Journal of Materials Chemistry B* **2015**, 3:556–561.
279. Hassan KM, Hathoot AA, Ashour WFD, Abdel-Azzem M: Electrochemical and analytical applications for NADH detection at glassy carbon electrode modified with nickel nanoparticles dispersed on poly 1,5-diaminonaphthalene. *Journal of Solid State Electrochemistry* **2015**, 19:1063–1072.
280. Guo M, Yu Y, Hu J: Nickel nanoparticles for the efficient electrocatalytic oxidation of methanol in an alkaline medium. *Electrocatalysis* **2017**, 8:392–398.

281. Zhang Y, Xiao X, Sun Y, Shi Y, Dai H, Ni P, Hu J, Li Z, Song Y, Wang L: Electrochemical deposition of nickel nanoparticles on reduced graphene oxide film for nonenzymatic glucose sensing. *Electroanalysis* **2013**, 25:959–966.

282. Long F, Zhang Z, Wang J, Yan L, Zhou B: Cobalt-nickel bimetallic nanoparticles decorated graphene sensitized imprinted electrochemical sensor for determination of octylphenol. *Electrochimica Acta* **2015**, 168:337–345.

283. Wang L, Lu X, Ye Y, Sun L, Song Y: Nickel-cobalt nanostructures coated reduced graphene oxide nanocomposite electrode for nonenzymatic glucose biosensing. *Electrochimica Acta* **2013**, 114: 484–493.

284. Asgari M, Maragheh MG, Davarkhah R, Lohrasbi E, Golikand AN: Electrocatalytic oxidation of methanol on the nickel–cobalt modified glassy carbon electrode in alkaline medium. *Electrochimica Acta* **2012**, 59:284–289.

285. Elango G, Roopan SM, Dhamodaran KI, Elumalai K, Al-Dhabi NA, Arasu MV: Spectroscopic investigation of biosynthesized nickel nanoparticles and its larvicidal, pesticidal activities. *Journal of Photochemistry & Photobiology, B: Biology* **2016**, 162:162–167.

286. Singh MK, Agarwal A, Gopal R, Swarnkar RK, Kotnala RK: Dumbbell shaped nickel nanocrystals synthesized by a laser induced fragmentation method. *Journal of Material Chemistry* **2011**, 21:11074–11079.

287. Chandra S, Kumar A, Tomar PK: Synthesis of Ni nanoparticles and their characterizations. *Journal of Saudi Chemical Society* **2014**, 18:437–442.

288. Ogino I, Yokoyama Y, Iwamura S, Mukai SR: Exfoliation of graphite oxide in water without sonication: bridging length scales from nanosheets to macroscopic materials. *Chemistry of Materials* **2014**, 26:3334–3339.

289. Emiru TF, Ayele DW: Controlled synthesis, characterization and reduction of graphene oxide: A convenient method for large scale production. *Egyptian Journal of Basic and Applied Sciences* **2017**, 4:74–79.

290. Zhang J, Yang H, Shen G, Cheng P, Zhang J, Guo S: Reduction of graphene oxide via L-ascorbic acid. *Chemical Communications* **2010**, 46:1112–1114.

291. Xu C, Shi X, Ji A, Shi L, Zhou C, Cu Y: Fabrication and characteristics of reduced graphene oxide produced with different green reductants. *PLoS ONE* **2015**, 10:144842–144856.

292. Abdolhosseinzadeh S, Asgharzadeh H, Kim HS: Fast and fully-scalable synthesis of reduced graphene oxide. *Scientific Reports* **2015**, 5:10160–10166.

293. Ghanbari K, Hajheidari N: Simultaneous electrochemical determination of dopamine, uric acid and ascorbic acid using silver nanoparticles deposited on polypyrrole nanofibers. *Journal of Polymer Research* **2015**, 22:152–160.

294. Dahal A, Batzill M: Graphene–nickel interfaces: A review. *Nanoscale* **2014**, 6:2548–2562.

295. Maringa A, Mugadza T, Antunes E, Nyokong T: Characterization and electrocatalytic behavior of glassy carbon electrode modified with nickel nanoparticles towards amitrole detection. *Journal of Electroanalytical Chemistry* **2013**, 700:86–92.

296. Phelane L, Muya FN, Richards HL, Baker PGL, Iwuoha EI: Polysulfone nanocomposite membranes with improved hydrophilicity. *Electrochimica Acta* **2014**, 128:326–335.

297. Liu W, Tanna VA, Yavitt BM, Dimitrakopoulos C, Winter HH: Fast production of high-quality graphene via sequential liquid exfoliation. *Applied Materials Interfaces* **2015**, 7:27027–27030.

298. Liu L, An M, Yang P, Zhang J: Superior cycle performance and high reversible capacity of SnO/graphene composite as an anode material for lithium-ion batteries. *Scientific Reports* **2015**, 5:9095–9064.

299. Ji Z, Wang Y, Yu Q, Shen X, Li N, Ma H, Yang J, Wang J: One-step thermal synthesis of nickel nanoparticles modified graphene sheets for enzymeless glucose detection. *Journal of Colloidal and Interfaces Science* **2017**, 506:678–684.

300. Lin Q, Wei Y, Liu W, Yu Y, Hu J: Electrocatalytic oxidation of ethylene glycol and glycerol on nickel ion implanted-modified indium tin oxide electrode. *International Journal of Hydrogen Energy* **2017**, 42:1403–1411.

301. Mani V, Vilian ATE, Chen S-M: Graphene oxide dispersed carbon nanotube and iron phthalocyanine composite modified electrode for the electrocatalytic determination of hydrazine. *International Journal of Electrochemcal Science* **2012**, 7:12774–12785.

302. Sang S, Li D, Zhang H, Sun Y, Jian A, Zhang Q, Zhang W: Facile synthesis of AgNPs on reduced graphene oxide for highly sensitive simultaneous detection of heavy metal ions. *RSC Advances* **2017**, 7:21618–21624.

303. Prathish KP, Barsan MM, Geng D, Sun X, Brett CMA: Chemically modified graphene and nitrogen-doped graphene: Electrochemical characterization and sensing applications. *Electrochimica Acta* **2013**, 114:533–542.

304. Neiva EGC, Souza VHR, Huang K, Pénicaud A, Zarbin AJG: Graphene/nickel nanoparticles composites from graphenide solutions. *Journal of Colloidal and Interfaces Science* **2015**, 453:28–35.

305. Zumla A, Nahid P, Cole ST: Advances in the development of new tuberculosis drugs and treatment regimens. *Nature Reviews: Drug Discovery* **2013**, 12:388–404.

306. Gong Z, Basir Y, Chu D, McCort-Tipton M: A rapid and robust liquid chromatography/tandem mass spectrometry method for simultaneous analysis of anti-tuberculosis drugs–ethambutol and pyrazinamide in human plasma. *Journal of Chromatography B* **2009**, 877:1698–1704.

307. Organization WH: Global tuberculosis report 2017. In: *Global tuberculosis report 2017 Geneva: World Health Organization; 2017 Licence: CC BY-NCSA 30 IGO*. Switzerland; **2017**: 1–249.

308. Wallis RS, Maeurer M, Mwaba P, Chakaya J, Rustomjee R, Migliori GB, Marais B, Schito M, Churchyard G, Swaminathan S *et al*: Tuberculosis—advances in development of new drugs, treatment regimens, host-directed therapies, and biomarkers. *The Lancet Infectious Diseases* **2016**, 16:34–46.

309. Sepehri Z, Bagheri H, Ranjbari E, Amiri-Aref M, Amidi S, Rouini MR, Ardakani YH: Simultaneous electrochemical determination of isoniazid and ethambutol using poly-melamine/electrodeposited gold nanoparticles modified pre-anodized glassy carbon electrode. *Ionics* **2017**.

310. Ferraz BR, Leite FR, Malagutti AR: Simultaneous determination of ethionamide and pyrazinamide using poly(L-cysteine) film-modified glassy carbon electrode. *Talanta* **2016**, 154:197–207.

311. Cheemalapati S, Devadas B, Chen S-M, Ali MA, Al-Hemaid FMA: Electrochemical determination of selected antihypertensive and antituberculosis drugs at a tyrosine-modified electrode. *Analytical Methods* **2014**, 6:6774–6782.

312. Chenevier P, Massias L, Gueylard D, Farinotti R: Determination of ethambutol in plasma by high-performance liquid chromatography after pre-column derivatization. *Journal of Chromatography B* **1998**, 708:310–315.

313. Hassan SSM, Shalaby A: Determination of ethambutol in pharmaceutical preparations by atomic absorption spectrophotometry. *Mikrochimica Acta* **1992**, 109:193–199.

314. Gupta V: Preparation of ethambutol–copper(II) complex and fabrication of PVC based membrane potentiometric sensor for copper. *Talanta* **2003**, 60:149–160.

315. Kurniati Z, Riyanto S, Rohman A: Determination of rifampicin, isoniazid, pyrazinamide and ethambutol hydrochloride in 4fdc tablet by FTIR spectrophotometry in combination with multivariate calibration. *Journal of Food and Pharmaceutical Sciences* **2016**, 4:25–30.

316. Faria AF, Marcellos LF, Vasconcelos JP, de Souza MVN, Junior ALS, do Carmo WR, Diniz R, de Oliveir MAL: Ethambutol analysis by copper complexation in pharmaceutical formulations: Spectrophotometry and crystal structure. *Journal of the Brazilian Chemical Society* **2011**, 22:867–874.

317. Wu WY, Yang JY, Du LM, Wu H, Li CF: Determination of ethambutol by a sensitive fluorescent probe. *Spectrochimica Acta Part A: Molecular and Biomolecular Spectroscopy* **2011**, 79:418–422.

318. da Silva JA, de Castro NV, de Jesus DP, Faria AF, De Souza MV, de Oliveira MA: Fast determination of ethambutol in pharmaceutical formulations using capillary electrophoresis with capacitively coupled contactless conductivity detection. *Electrophoresis* **2010**, 31:570–574.

319. Hsieh YC, Whang CW: Analysis of ethambutol and methoxyphenamine by capillary electrophoresis with electrochemiluminescence detection. *Journal of Chromatography A* **2006**, 1122:279–282.

320. Faria AF, de Souza MVN, Bruns RE, de Oliveira MAL: Optimization of an electrolyte system for analysis of ethambutol in pharmaceutical formulations by capillary zone

electrophoresis using complexation with copper(II). *Journal of Chromatography A* **2008**, 1202:224–228.

321. Prajapati P, Agrawal YK: SFC-MS for the identification and estimation of ethambutol in its dosage form and in human urine samples. *Analytical Methods* **2016**, 8:4895–4902.
322. Chellini PR, Lages EB, Franco PH, Nogueira FH, Cesar IC, Pianetti GA: Development and validation of an HPLC method for simultaneous determination of rifampicin, isoniazid, pyrazinamide, and ethambutol hydrochloride in pharmaceutical formulations. *Journal of AOAC International* **2015**, 98:1234–1239.
323. Yan M, Guo T, Song H, Zhao Q, Sui Y: Determination of ethambutol hydrochloride in the combination tablets by precolumn derivatization. *Journal of Chromatogric Science* **2007**, 45:269–272.
324. Bellei Perantoni C, Soares Carbogim LG, Silva Semaan F, Camargo Matos R, Lowinsohn D: Flow injection analysis of ethambutol in antituberculosis drugs using a graphite-paraffin electrode as amperometric detector. *Electroanalysis* **2011**, 23:2582–2585.
325. Lima AEB, Luz GE, Batista NC, Longo E, Cavalcante LS, Santos RS: Determination of ethambutol in aqueous medium using an inexpensive gold microelectrode array as amperometric sensor. *Electroanalysis* **2016**, 28:985–989.
326. Ngece RF, West N, Ndangili PM, A. OR, Williams A, Hendricks N, Mailu S, Baker P, Iwuoha E: A silver nanoparticle/poly(8-anilino-1-naphthalene sulphonic acid) bioelectrochemical biosensor system for the analytical determination of ethambutol. *International Journal of Electrochemcal Science* **2011**, 6:1820–1834.
327. Couto RA, Quinaz MB: Development of a Nafion/MWCNT-SPCE-based portable sensor for the voltammetric analysis of the anti-tuberculosis drug ethambutol. *Sensors* **2016**, 16:1015–1027.
328. Gutes A, Hsia B, Sussman A, Mickelson W, Zettl A, Carraro C, Maboudian R: Graphene decoration with metal nanoparticles: towards easy integration for sensing applications. *Nanoscale* **2012**, 4:438–440.
329. Pandikumar A, Soon How GT, See TP, Omar FS, Jayabal S, Kamali KZ, Yusoff N, Jamil A, Ramaraj R, John SA *et al*: Graphene and its nanocomposite material based electrochemical sensor platform for dopamine. *RSC Advances* **2014**, 4:63296–63323.

330. Ioni Y, Buslaeva E, Gubin S: Synthesis of graphene with noble metals nanoparticles on its surface. *Materials Today: Proceedings* **2016**, 3:209–213.

331. Zhu Q-L, Xu Q: Immobilization of ultrafine metal nanoparticles to high-surface-area materials and their catalytic applications. *Chem* **2016**, 1:220–245.

332. Gan T, Wang Z, Wang Y, Li X, Sun J, Liu Y: Flexible graphene oxide−wrapped SnO_2 hollow spheres with high electrochemical sensing performance in simultaneous determination of 4−aminophenol and 4−chlorophenol. *Electrochimica Acta* **2017**, 250:1–9.

333. Asadpour-Zeynali K, Mollarasouli F: Novel electrochemical biosensor based on PVP capped $CoFe_2O_4$@CdSe core-shell nanoparticles modified electrode for ultra-trace level determination of rifampicin by square wave adsorptive stripping voltammetry. *Biosensensors and Bioelectronics* **2017**, 92:509–516.

334. Zhao Z, Xia Z, Liu C, Huang H, Ye W: Green synthesis of Pd/Fe_3O_4 composite based on polyDOPA functionalized reduced graphene oxide for electrochemical detection of nitrite in cured food. *Electrochimica Acta* **2017**, 256:146–154.

335. Kaur B, Srivastava R: Simultaneous electrochemical determination of nanomolar concentrations of aminophenol isomers using nanocrystalline zirconosilicate modified carbon paste electrode. *Electrochimica Acta* **2014**, 141:61–71.

336. Gorla FA, Duarte EH, Sartori ER, Tarley CRT: Electrochemical study for the simultaneous determination of phenolic compounds and emerging pollutant using an electroanalytical sensing system based on carbon nanotubes/surfactant and multivariate approach in the optimization. *Microchemical Journal* **2016**, 124:65–75.

337. Lavron E: General expression of the linear potential sweep voltammogram in the case of diffusionless electrochemical systems. *Journal of Electroanalytical Chemistry* **1979**, 101:19–28.

List of Publications

1. **Birhanu Mekassa**, Merid Tessema, Bhagwan Singh Chandravanshi; Simultaneous determination of ca□eine and theophylline using square wave voltammetry at poly(L-aspartic acid)/functionalized multi-walled carbon nanotubes composite modified electrode, *Sensing and Bio-Sensing Research*, **2017**, 16, 46–54.
2. **Birhanu Mekassa**, Merid Tessema, Bhagwan Singh Chandravanshi, Priscilla G.L. Baker, Francis N. Muya; Sensitive electrochemical determination of epinephrine in pharmaceutics at poly(L-aspartic acid)/electrochemically reduced graphene oxide modified electrode by square wave voltammetry, *Journal of Electroanalytical Chemistry*, **2017**, 807, 145–153.
3. **Birhanu Mekassa**, Merid Tessema, Bhagwan Singh Chandravanshi, and Molla Tefera; Square wave voltammetric determination of ibuprofen at poly(L-aspartic acid) modified glassy carbon electrode, *IEEE Sensors Journal*, **2018**, 18, (1), 37–44.
4. **Birhanu Mekassa**, Merid Tessema, Bhagwan Singh Chandravanshi, Priscilla G.L. Baker; Synthesis, characterization and preparation of nickel nanoparticles decorated electrochemically reduced graphene oxide modified electrode for electrochemical sensing of diclofenac; **Ready for submission**.
5. **Birhanu Mekassa**, Merid Tessema, Bhagwan Singh Chandravanshi, Priscilla G.L. Baker; Sensitive electrochemical determination of ethambutol in pharmaceutical formulation and human urine at nickel nanoparticles/electrochemically reduced graphene oxide modified electrode; **Ready for submission**.